2014

Palaeoenvironmental change in the Macquarie Marshes, NSW, Australia

Lili Yu
University of Wollongong

UNIVERSITY OF WOLLONGONG

School of Earth & Environmental Sciences

Palaeoenvironmental Change in the Macquarie Marshes, NSW, Australia

LILI YU

This thesis is presented as part of the requirements for the award of the Degree of DOCTOR OF PHILOSOPHY of University of Wollongong

July 2014

ABSTRACT

The Macquarie Marshes (MM), located in semiarid northwest New South Wales (NSW), are a unique wetland system for its inland location, high biodiversity and important role as "sanctuary" or "refuge" for flora and fauna especially colonially breeding waterbirds. However, the high demand for water in this semiarid area especially to support agriculture has led to the decline of the wetlands and their associated wildlife in particular since the 1950s.

This PhD project analyses surface sediments and modern plant samples from the main areas of the northern and southern marshes to assess the most appropriate proxies to be applied to sediment cores to reveal the 'condition' of the MM. Four cores from the northern marshes where organic matter was better preserved were chosen to reconstruct the palaeoenvironmental history of the marshes. Optically stimulated luminescence (OSL) single-grain dating was applied to obtain the chronology; lipid biomarkers particularly *n*-alkanes and α-phellandrene were analysed to trace the vegetation change in the marshes.

The palaeoenvironmental history of MM in the past ~ 50 ka is reconstructed: the site where the modern Marshes are likely had been inundated since the late Pleistocene and experienced oscillations of dry/wet climate which in turn led to the change of water level and in response the variation of the vegetation types and abundances. The abundance of wetland plants was probably highest during the establishment of the marshes 8-6 ka ago. A dry period at about 2 ka is shown by C_4 drought-tolerant plants. It is not until after European arrival (from the 1880s) that terrestrial plants started intruding and gradually replacing the wetland plants. The most striking shift of aquatic wetland plants to more terrestrial plants in this ecosystem occurred in the 1950s to 1970s due to water diversion after the construction of upstream dams. Compared to natural environmental changes, anthropogenic effects have a greater and irreversible impact on the well-being of the marshes. The fact that the MM are free from anthropogenic pollutants (i.e. pesticides from cotton farming and faecal contaminant from the grazing industry) indicates that water loss, rather than pollutants, is the main cause of the decline of the wetlands.

ACKNOWLEDGEMENTS

I wish to extend sincere gratitude and appreciation to the following people and organisations for helping me to achieve this PhD – a significant milestone in my life.

To Professor Allan R. Chivas, my principal supervisor, for introducing me to the field of Quaternary Geoscience; and for guiding me through, and contributing to my research. I wish to thank him for his support throughout my PhD, and for allowing me the necessary scope and independence to develop as a scientist: through trial and error, and continual learning. I have always admired Professor Chivas' insightfulness and extensive scientific knowledge.

To Dr Adriana García, my co-supervisor and dear friend, for her support and assistance in this thesis. Dr García welcomed me from the first day I arrived in Australia, and was always willing to listen, and provide me with every support, both as an invaluable mentor and confidant.

To Dr Jianfang Hu, for introducing me to Professor Allan R. Chivas and Dr Adriana García; for her supervision and patience; and for her constructive suggestions and numerous discussions in relation to the organic geochemistry aspect of my work.

To New South Wales National Parks for permitting us to access the Macquarie Marshes. To Mr Ray Jones (NSW National Parks) for his invaluable knowledge and help in the field. To Myra and Phillip Tolhurst from Willie Retreat for their warm welcome and kind help during our visits to the Macquarie Marshes.

To Brent Peterson, Dr Tony Nicholas, Dr Paolo Abballe, Dr Paul Hesse, Dr Tim Ralph, Dr Scott Mooney and Daniel Smith for their help in collecting samples during the fieldtrips to Macquarie Marshes.

To Richard Miller, Heidi Brown, Chris Owers and Yi Lu for assisting me with the mappings for this thesis.

To Professor Richard (Bert) Roberts, Dr Zenobia Jacobs, Dr Terry Lachlan, Dr Lee Arnold, Dr Martina Demuro and Dr Bo Li, for their invaluable help with the OSL work.

To AINSE grant 09/P016 to A.R. Chivas for supporting the radiocarbon dating used in this thesis.

To Dr Paolo Abballe, Florian Dux and especially David Wheeler for their solid geochemistry laboratory help; and special thanks to David Wheeler for his help with the EA analysis.

To Dr Jochen Brocks and Janet Hope from the Australian National University, and John Korth from the School of Chemistry at the University of Wollongong for their assistance in GC-MS analysis.

To José Abrantes, Associate Professor Brian Jones and Associate Professor Paul Carr for their help with the XRD, XRF and particle size analysis.

To Dr Jianfang Hu, Dr Jan-Hendrik May, Venera Espanon, Dr Lee Arnold, Dr Martina Demuro and Dr Bo Li, for their help with my data analysis and proofreading; and for their constructive suggestions.

To the Environmental Trust of NSW (Grant 2006/ RD0055 to Chivas and García) for providing me a PhD scholarship and supporting the broader project on the Marshes.

To the School of Earth & Environmental Sciences, University of Wollongong for offering me a job; which allowed me to continue with my research after my scholarship had expired.

To the kind academic and general staff in the School of Earth & Environmental Sciences, for all of their support and help. In particular, I wish to thank Professor Colin Murray-Wallace, Sandra Chapman, Denise Alsop and Wendy Weeks.

To my dearest friends, in particular: Chrissy, Paolo, Tony, Venera, Elena, Sabina, Bec, Bo and Jing, Richard and Emily; for their company, friendship, love and help through all these years.

To my wonderful parents and husband Ted; for their unconditional love; their steadfast belief in me, and for their strong support. Thank you for your understanding and patience throughout the many weekends, holidays and late nights working in the lab or preparing the thesis. None of this would have been possible without you.

To my beautiful baby Paolo; for all of the times I was taken away, writing up this thesis, and could not spend as much time with you as I would have liked.

Lastly, many thanks go also, to my many friends and colleagues; whom I have not listed here, but who have offered their time and support. Thank you for your generosity.

DECLARATION

I, Lili YU, declare that this thesis, submitted in fulfilment of the requirement of the award of Doctor of Philosophy, in the School of Earth & Environmental Sciences, University of Wollongong, is wholly my own work unless otherwise referenced or acknowledged. The document has not been submitted for qualifications at any other academic institution.

Lili YU, July 2014.

TABLE OF CONTENTS

LIST OF FIGURES

LIST OF TABLES

CHAPTER 1 INTRODUCTION

1.1 Introduction

Wetlands are one of the most biologically diverse ecosystems that provide habitat for a wide range of plants and animals. They also play a significant role in the global carbon cycle and climate change. On a global scale, about 50 % of wetland area has been lost since the first half of the twentieth century and wetlands now occupy probably less than 9 % of the Earth's land area (Zedler and Kercher, 2005). The principal forces are human impact and climatic variation, and in particularly since early civilisation, wetlands have been systematically drained and destroyed to support growing, land-hungry populations (Myers et al., 2013). Sediments accumulated sequentially through time in wetlands contain a detailed chronological record of the wetland history. Analysis of these sediments provides information on past environmental conditions and events that have occurred within the wetland ecosystem. This information will assist in the better understanding, management and conservation of the wetlands.

The Macquarie Marshes (MM) are located in a semi-arid area of Australia and are one of the largest floodplain wetlands in the Murray-Darling Basin. Covering a total area of approximately 200,000 hectares, the MM are of international and national significance (listed by the Ramsar Convention 1986; the National Heritage Register and the National Trust Register). They have the largest stand of river red gums (*Eucalyptus camaldulensis*) in northern New South Wales, the largest reed beds (*Phragmites australis*) of any wetlands in New South Wales, and the most southerly occurrence of coolibah woodland (*E. coolibah*) (Shelly, 2005). The semi-permanent wetland vegetation provides habitats for fauna, in particularly colonially-breeding waterbirds (Kingsford and Thomas, 1995).

Along the floodplain, the MM contain 16 waterbird breeding sites, each of which can consist of up to 40,000 birds in the breeding season (Kingsford and Thomas, 1995; Kingsford and Johnson, 1998). Despite the recognition of the conservation importance, the MM are declining (about 40-50 % of the wetlands have been lost in the last 50 years) (Kingsford and Thomas, 1995). The loss of wetlands inevitably has great impact on its biota including colonial waterbirds, whose breeding habits are highly dependent on the water flow and food supply in the wetland ecosystem. As a result, the abundance and species richness of water-birds in the northern marshes declined over an 11-year period (Kingsford and Thomas, 1995).

Factors affecting the health and permanence of the marshes can be considered as:

Natural

- The MM are located in a dry area subjected to irregular climatic patterns, surviving by means of water carried to the MM by the permanent Macquarie River (headwaters to the SE). The rainy season in the Macquarie River headlands and MM area, usually occurred during autumn (although this pattern has also changed in recent years due to climate change). The marshes formed during the mid-Holocene (Climatic Optimum), and apparently have been healthy until human colonisers arrived ~ 170 years ago (Herron et al., 2002), though long-term data show that aridity has been increasing in the Australian continent for the last 500 ka (Bowler, 1978).

Anthropogenic

- The first settlers and livestock grazing arrived in the area around 1840 AD and the flows that originally reached the MM have been diverted in particular after the construction of Burrendong Dam in 1960 and Windamere Dam in the early 1980s;

- Land-use has been converted to agriculture by clearing natural vegetation, creation of artificial channels, and the use of marsh land to cultivate annual crops (cotton). The diverted water is subject to greater evaporation and thus less water reaches the marshes when flooding occurs (Kingsford and Thomas, 1995; Kingsford and Johnson, 1998; Roshier et al., 2002);
- The effect of the use of fertilisers and pesticides in the cotton farming areas adjacent to the marshes, which may have adverse consequences on the health of any waterbody and the biota living within, has barely been explored (Brock, 1998); and,
- Increasing global temperatures by human activities (increased production of CO_2), produces irregular seasonal patterns, irregular periods of drought/floods, which increases the pressure on agricultural methods and threatens the MM.

Previous studies of the MM are mainly based on contemporary and recorded data and can only indicate the recent environmental history (past ~170 years) (e.g. Brock, 1998; Kingsford and Johnson, 1998; Kingsford, 2000; Roshier et al., 2002; Kingsford and Auld, 2003; Kingsford and Auld, 2005; Hogendyk, 2007). This is the timescale when human activities have had a greater impact on the natural environment. In order to obtain information on the natural long-term variability and response mechanisms of the environment beyond historically documented records and to compare the anthropogenic and natural processes of environmental change in the marshes, palaeoenvironmental data are of great importance. However, there are very few studies on the palaeoenvironment of the Macquarie Marshes and these are restricted to the southern marshes and are largely geomorphological (Ralph, 2008; Yonge and Hesse, 2009; Ralph and Hesse, 2010; Ralph et al., 2011).

The work in this thesis complements the work of a multidisciplinary team led by Prof. Allan Chivas and Dr Adriana García, dedicated to reconstruct the past ecology of the MM (using proxies such as macrophytes, charophytes, diatoms, pollen, charcoal, dating, geochemistry and geomorphology). The broader objective is to reconstruct the past environments and disentangle natural versus anthropogenically induced changes that occurred in the area in particular after European arrival in order to contribute information for the preservation and management of the MM. Results in this area are presented in a paper published in *Aquatic Botany* (Appendix B).

1.2 Aims

This thesis seeks

- To obtain an accurate chronology of sediment cores using dating techniques (e.g. optically stimulated luminescence dating) not previously applied to the northern MM;
- To investigate the proxies of lithology, sedimentology, mineralogy and geochemistry (in particular organic geochemical proxies) and to choose the most appropriate palaeoecological proxies for tracing past vegetation types, waterbird colonial events, fires and chemical pollution; and,
- To assemble the experimental results from both chronology and mainly organic geochemistry to elucidate the history of the MM concerning
  - the frequency of drought/flood cycles
  - the changes in water level
  - the changes of biodiversity (i.e. variation of wetland vegetation, establishment and decline of waterbird colonies) with focus on the vegetation
  - the effect of land clearing and farming

– the impact of anthropogenic pollution

The work will provide a palaeoenvironmental reconstruction and explore the changes between the undisturbed and modern environments (i.e. diversion of water for irrigation, deforestation due to large-scale cotton farming, etc.).

1.3 Research approach

Chapter 2 summarises the studies of the MM in the fields of geology and hydrology, ecology and planning, as well as its history. It presents an overall picture of the Macquarie Marshes and their significance as a wetland ecosystem with diversity of flora and fauna. Most importantly, it reviews the techniques applied to study environmental change in the MM and raises the issues that this thesis will try to address with techniques not previously applied to the marshes.

Chapter 3 begins with the sampling campaign and methods. It describes the location, documented history and contemporary environment (including geological setting, vegetation types, etc.) of the sampling sites. A preliminary study of the lithology, sedimentology, mineralogy and general geochemistry of the sediment samples is also presented in this chapter. In addition, the isotope chemistry of modern plants was studied as references to the sediment samples. These data offer general information on: the main source of the sediments (in particular the source of organic matter), the difference between the northern and southern marshes ecosystems, how this wetland ecosystem has responded to environmental changes and how such processes have been recorded in the sediments. The physical and geochemical proxies were also assessed for their robustness to indicate environmental change and for their application as palaeoecological proxies.

Accurate and reliable chronology has always been a key element in palaeoenvironmental studies. Chapter 4 explores the application of optically stimulated luminescence dating technology to date the MM sediments with a broad age span and provide chronological continuity. Detailed information concerning sample preparation, instrumental analysis and age calculation using several age models are presented in this chapter.

Chapter 5 tests and extends the findings of Chapter 3 by applying specific organic markers to obtain more information on the organic sources and assesses their contributions. Specific organic compounds indicative of the biota (i.e. wetland vegetation, colonial waterbirds) were sought in modern plants and surface sediment samples and accordingly applied to sediment cores for a palaeoenvironmental reconstruction of the MM. Some organic compounds indicative of pollution sources were also analysed to assess the contamination (if any) in this Nature Reserve wetland.

Chapter 6 summarises and discusses the findings from Chapters 3, 4 and 5. Suggestions for future work are also presented in this chapter.

CHAPTER 2 REGIONAL SETTING AND EVOLUTION

This chapter reviews previous studies concerning the Macquarie Marshes in the fields of geology and hydrology, ecology and planning, as well as their history. The review presents a picture of the Macquarie Marshes and attributes, and their significance as a wetland ecosystem with diversity of flora and fauna.

2.1 Geomorphic setting

The Macquarie Marshes (Figure 2.1, Page 9) are a wetland covering more than 220,000 ha in north-west NSW within the lower Macquarie River catchment. They are at the lower end of an alluvial fan system -- Macquarie River system which rises above Bathurst in the Central Tablelands area. These Marshes are one of the largest floodplain wetlands in Australia.

The Macquarie Marshes were formed as a result of complete breakdown of the Macquarie River, influenced by the degree of topographic confinement produced by surrounding palaeoalluvial ridges (Yonge and Hesse, 2009). The discontinuous drainage networks occur in two well-defined areas (known as the northern and southern Macquarie Marshes) that lie in sequence and are joined by short natural and reformed channelised reaches (Yonge and Hesse, 2009). The geomorphology of the marshes shows a complex array of divergent, reticulate and convergent channels with a mosaic of perennial, intermittent and ephemeral wetlands which are dominated by variable overbank flows and depositional processes (Ralph, 2008; Yonge and Hesse, 2009; Ralph and Hesse, 2010; Kobayashi et al., 2011). The inundation pattern produced various landforms including

braided swamps, lagoons, channel country and floodplains, which in turn influence the inundation patterns (Paijmans, 1981).

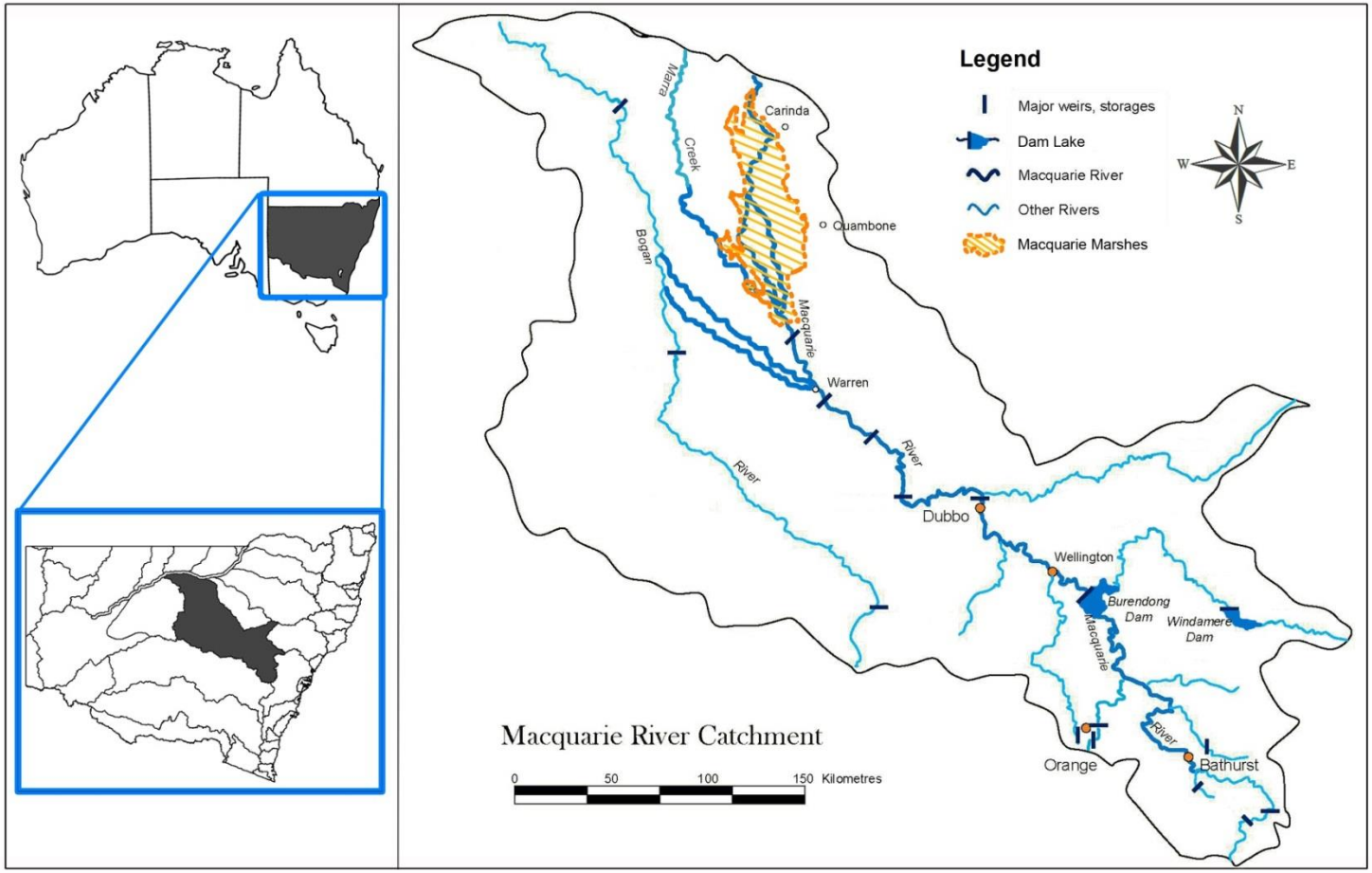

Figure 2.1. Map of the Macquarie Marshes and Macquarie River catchments. Inset map shows the location within Australia and New South Wales. (sourced from http://en.wikipedia.org/wiki/Macquarie_River)

This type of floodplain wetland system undergoes geomorphic and ecological changes that are both directly and indirectly related to natural cycles of flood and drought, and anthropogenic disturbance (Kingsford, 2000; Yonge and Hesse, 2009; Ralph et al., 2011). In particular, avulsion and channel breakdown are driven by the characteristic nature of the dense in-channel vegetation which chokes the streams and leads to in-channel aggradation, reduced fluvial efficiency and frequent overbank flows (Yonge and Hesse, 2009). Geomorphic changes are usually manifest through processes of sediment erosion, reworking and deposition, leading to channel and floodplain evolution that affects flooding and drives wetland vegetation and habitat changes (Ralph et al., 2011). Ralph and Hesse (2010) investigated the downstream hydrogeomorphic changes in the Macquarie Marshes and found that channel width-to-depth ratio decreases in the middle reaches and then increases, while channel sinuosity increases until immediately upstream of the main wetlands and rapidly declines as straight channels enter areas of extensive channel breakdown. The same authors also found that floodplain width is greatest on the alluvial plain, allowing a broader area of floodplain wetlands to develop and that floodplain connection is greatest where floodouts and wetlands form in the marshes.

2.2 Climatic setting

The Macquarie Marshes are located in a semi-arid area with low rainfall, hot summers and cold winters (Wen et al., 2012). The median precipitation for the Macquarie Marshes is 300-400 mm a^{-1} (Kingsford and Thomas, 1995), less than half that of the upper catchment of the Macquarie River (965 mm a^{-1} Bureau of Meteorology 2007). This relatively low rainfall is coupled with a high evaporation rate of 1800 mm a^{-1} which reduces inputs to the lower Macquarie River and favours sediment deposition (Kingsford and Auld, 2003;

Yonge and Hesse, 2009). The temperatures in the Macquarie Marshes recorded in the Water Resources Commission's report in 1979 range from 4 °C (average daily minimum temperature) in winter to 35 °C (average daily maximum temperature) in summer (Kingsford and Thomas, 1995).

On the larger timescale, the interannual and interdecadal climate trends in the Macquarie Marshes are strongly related to El Niño Southern Oscillation (ENSO) and Interdecadal Pacific Oscillation (IPO), and affect the seasonal and annual variability of river discharge (Ralph and Hesse, 2010).

2.3 Hydrologic setting and changes

The Macquarie Marshes depend on water from the Macquarie River, not on local rainfall (Kingsford and Thomas, 1995). The dominant force shaping the current marshes has been the history of water flow (Brock, 1998). However numerous studies show that flows to the marshes have been severely impacted by the construction of Burrendong Dam (storage capacity: $1{,}188 \times 10^9$ L) above Wellington in 1967 and again since the construction of Windamere Dam (storage capacity: 368×10^9 L) near Wellington in 1984 (Brock, 1998; Kingsford and Auld, 2005). Over a 60-year period, annual average flows to the wetlands have decreased by 200,000 ML (ML = 1 million litres = "Olympic-size swimming pool") (Finkel and Normile, 2012). Thomas et al. (2011) applied remote sensing techniques to map inundated areas and found that the marshes became drier between 1979 and 2006, despite no corresponding change in annual catchment or local rainfall. The study also showed that the inundation patterns are highly spatially variable with high frequency of inundation occurring mostly in the northern region of the marshes (Thomas et al., 2011).

The flood regime is also the dominant force influencing the marshes' watertable (Brock, 1998). Brereton (1994) established that the watertable varies from 2-3 m below the surface in near permanent wetlands, and up to 5-7 m in ephemeral wetlands inundated only in large floods.

2.4 Ecological setting and changes

The Macquarie Marshes are typical inland floodplain wetlands that when flooded increase the concentration of inorganic nutrients and dissolved organic matter, and the abundance of plankton in the water column (Robertson et al., 1999; Wetzel, 2001; Kobayashi et al., 2009). Thus they support a diverse aquatic biota (Kingsford and Thomas, 1995; Kingsford, 2000). During dry periods, inundated areas of the floodplains diminish and flow in the river channels may be insufficient to inundate the floodplain (Kobayashi et al., 2011). An ecological modelling study by Wen et al. (2012) also demonstrated that both rainfall and inflow, which were projected to be more intense under potential future climate change, were significantly positively related to ecosystem primary productivity. Kobayashi et al. (2011) conducted a field survey to investigate the longitudinal spatial patterns of variation in ecological conditions in channels of the large floodplain system of the Macquarie Marshes. They found that some parameters tended to increase in a downstream direction. These parameters included conductivity, total nitrogen, total phosphorus, dissolved reactive phosphorus, dissolved silica, dissolved organic carbon, dissolved organic nitrogen, dissolved organic phosphorus and abundance of planktonic bacteria.

Despite water release from the major dams since the 1980s, the ecological recovery of the marshes could take decades. The Murray-Darling Basin Authority (MDBA)'s water

purchases and infrastructure upgrades have returned 1,327 × 10^9 L to the rivers, rejuvenating parched wetland systems. The numbers of nesting waterfowl species have recovered, but *Ruppia tuberosa*, a key aquatic grass species that fish and waterfowl feed upon, has disappeared. Soil acidification still affects wetlands and farm fields (Finkel and Normile, 2012).

2.4.1 Soils and water quality

According to Brock (1998), the soil types found in the Macquarie Marshes include:

- Red-brown earths located on the western side of the marshes, restricted to higher ground, and associated with prior streams;
- Grey-brown soils of heavy texture on the eastern side;
- Black organic loam over a grey clay (150 mm), grey clay with ferruginous mottles (200 mm) and pisolithic ironstone gravel at 450 mm, with watertable at 600 mm; they are usually hydromorphic soils with significant gilgai formation, linear cracks and crab-holes; and,
- Yellow prairie soils with red-brown earths on the elevated areas with a soluble surface salt; they are well documented in some areas of river red gum and lignum.

The study also pointed out the scalding present outside the main wetland areas owing to removal of topsoil and exposure of heavy clay subsoil, especially on the red-brown earths (Brock, 1998). The two main causes are thought to be 1) the drought that occurred from 1894 to the early 1900s, when stock were concentrated around the remaining areas of water supply; 2) the rabbit plagues of the 1900s and 1950s.

The geomorphic study in the southern marshes (Yonge and Hesse, 2009) found a subtle reduction in suspended sediment concentration which occurs in the reach where

reeds (*Phragmites australis*) first occur across the entire channel and about 98 % of the total suspended sediment is deposited at the channel breakdown. These channel and floodplain sediments consist almost entirely of muds (Yonge and Hesse, 2009). The study by Ralph (2008) found a general upward fining textural sequence (70 – 90 % mud to >90 % mud) in the floodplain deposits and a subtle decrease in sediment calibre occurs away from the levees; an increase in sand content (up to 40 %) also occurs in the floodout zone and lower reaches of the marsh, where distinct sandy layers reflect flood-pulse deposition.

The study by Ralph (2008) also found that sediments in the floodout zone have the greatest radionuclide inventories, indicating rapid recent sedimentation (0.4 to 11 mm a^{-1}); relatively high sedimentation rates (2.9 to 5.3 mm a^{-1}) also occur further upstream on the levees in Monkeygar Marsh, while the distal floodplain has lower rates (0.8 to 3.6 mm a^{-1}).

A recent survey of sulfidic sediments in the Murray-Darling Basin reported that the acidity and potential sulfidic acidity of the sediments in the MM were relatively low compared to other sampling sites in the Murray-Darling Basin; and the sediments had relatively high acid-neutralising capacity, indicating net acidification would be prevented even if the sediments were oxidised (Hall et al., 2006).

In the review of Brock (1998), the author stated that by 1998 there had only been minor problems with general water quality: 1) the pesticide endosulfan (used extensively on cotton crops) had been detected in the upper areas of marshes; 2) turbidity and sediment levels had been high in some instances, particularly with small flows which were unable to spread out of channels to receive the full filtering effects of the wetland; 3) high levels of total phosphorus, total nitrogen and copper at Bell's Bridge (Lower Macquarie

River), mainly when the northern marshes Bypass Channel was open; 4) blue-green algae were present on one occasion near Carinda, but a bloom did not occur.

2.4.2 Vegetation

The change in flood regime has been the main cause for changes to vegetation complexes (Paijmans, 1981). Frequently flooded wetlands are characterised by the semi-permanent wetland vegetation communities of river red gum (*Eucalyptus camaldulensis*) forest and woodland, common reed (*Phragmites australis*), cumbungi (*Typha orientalis*), water couch (*Paspalum distichum*), lignum (*Muehlenbeckia florulenta*) and river cooba (*Acacia stenophylla*) (Paijmans, 1981; Jenkins, 2005; Shelly, 2005). Where there is less frequent flooding, vegetation communities are characterised by coolibah (*E. coolibah*) and black box (*Eucalyptus largiflorens*) woodlands, and myall (*Acacia pendula*) and grasslands are distributed at high elevations on the floodplain (Paijmans, 1981; Jenkins, 2005; Shelly, 2005).

Field investigation and remote sensing studies show river red gum (*Eucalyptus camaldulensis*) forests and woodlands historically received flooding every 1-1.5 years, and their distribution coincided with the northern marshes which is the wettest part and flooded 20 times over the 28 years period (1976-2006) (Shelly, 2005; Thomas et al., 2011). Common reed (*Phragmites australis*), a perennial emergent macrophyte relying on frequent flooding, is also found to survive prolonged drought if the soil moisture is retained (Thomas et al., 2011).

The size of the marshes varies depending on the inundated area, with estimates ranging from 200,000 ha (the current size under water resource development and without significant flooding) to up to 1,280,000 ha during the 1955 flood event (one of the largest

floods on record and which pre-dated significant water resource developments in the area) (Kingsford and Thomas, 1995; Morrison et al., 2011). In general, the extent and condition of semi-permanent wetland in the Macquarie Marshes have been declining since the 1930s (DECC, 2009).

2.4.3 Fauna

Wetlands provide habitat, food and breeding areas for insects, crustaceans, amphibians, reptiles, fish, birds and mammals. The Macquarie Marshes have been long recognised for their significance for waterbirds. Of all the fauna, colonial nesting species are most prominent and have been the most studied.

The marshes are home to 200 bird species including threatened species of brolga, Australasian bittern, blue-billed duck, painted snipe, magpie goose and freckled duck. Breeding sites are provided for the straw-necked ibis, glossy ibis, Australian white ibis, intermediate egret and rufous night heron (Kingsford and Thomas, 1995; Kingsford and Johnson, 1998; Kingsford, 2000; Kingsford and Auld, 2003). The MM have the greatest diversity of wetland bird species and the highest nest density rates in Australia (Kingsford and Auld, 2005). Seventy-six waterbird species have been recorded in the marshes, 42 of which have been recorded breeding (DECC, 2009), with between 10,000 and 300,000 waterbirds relying on the marshes each season (Kingsford and Thomas, 1995) for their breeding, feeding and habitat requirements. These birds include the glossy ibis *Plegadis falcinellus*, Australian white ibis *Threskiornis mollucca*, straw-necked Ibis *Threskiornis spinicollis*, intermediate egret *Ardea intermedia* and rufous night heron *Nycticorax caledonicus* (Kingsford and Johnson, 1998).

The study by Kingsford and Auld (2005) found the minimum requirement for colonially nesting waterbirds to breed successfully is flooding of sufficient volume and duration for colony sites and feeding areas to be inundated for a minimum of four to five months between August and March of the following year. They also found colonial waterbird breeding is triggered by flows above 200,000 ML (Kingsford and Auld, 2005). These flows are also critical for both maintaining wetland vegetation and for completion of life cycles of aquatic invertebrates (DECC, 2009). Other factors include timing of flows, water quality and changes to the extent of flooding of colonially-nesting waterbirds in the marshes (Kingsford, 2000). When the marshes dry birds travel north and stay away until flooding reoccurs.

According to the 2009 draft on "Macquarie Marshes Adaptive Environmental Management Plan", between 1986 and 2001, colonially nesting species bred in ten years at 14 sites throughout the marshes; by 2008 several of the known breeding sites were considered to be in poor condition due to lack of water and grazing pressure; since 2001, only one breeding event of colonially nesting waterbirds occurred in the marshes; in 2008, a relatively small flood supported successful nesting and about 2,000 pairs of egrets in river red gum forest on the Bora Channel. This was the first record of colonially nesting waterbirds breeding at only a single location in the marshes. Between 1883 and 1993 the number of species and density of waterbirds on the northern marshes declined as a result of decreased flooding (Kingsford and Thomas, 1995). The essential habitats and nest platforms for waterbird colonies, such as common reed and river coolliba community, were found in poor condition in the marshes (DECC, 2009).

From 2009 to 2013, the Macquarie River has flooded, the cool and clean north-flowing water favours the growth of red fern *Azolla*, *Typha* sp., lignum, yellow-flowering

water primrose and *Ranunculus* sp., which then provide habitats for turtles, fish, ducks and grebes, ibis, brolgas, swamphens, pelicans and herons (Eastwood, 2013).

2.5 Palaeoevolution

Study of the alluvial plain upon which Macquarie Marshes are located found that the plain is predominately Quaternary in age and is built on up to 100 m of Neogene sediments (Watkins and Meakin, 1996). Geomorphic evidence on the surface of the plain indicates numerous phases of palaeochannel activity and the dynamic history of changing fluvial styles throughout the recent geological past (Yonge and Hesse, 2009). Tomkins and Hesse (2004) found three major changes in the depositional regime of the Macquarie River valley: First, erosion of the valley basement in the Late Miocene was followed by (and possibly synchronous with) deposition of a basal clay and sand unit. Second, the valley was filled with a wedge of sediments containing abundant gravel and sand during the Pliocene and the Pleistocene valley incision is mainly due to climate change to drier conditions. Third, the older gravelly unit was eroded and reworked in the Quaternary and a sandy clay unit, which forms the modern floodplain, was deposited. This finding provides a reference for studying the depositional history of the sediments in the Macquarie Marshes. There is no information about the palaeoenvironment of the Macquarie Marshes prior to the Neogene. The main areas of marshes were thought to have formed between 6 and 8 ka ago (Yonge and Hesse, 2009) as a result of the geomorphological, topographic and climatic controls of the area and which have persisted to the present (Ralph et al., 2011).

Because the Macquarie Marshes are so variable, it is difficult to simply draw a baseline at a particular time to compare with the existing conditions. From previous

studies, it is generally considered that the marshes have been in their present location and have maintained their general wetland state for the past 8 to 6 ka, and significant evidence for landscape change commonly refers to pre-European and post-European periods (Ralph, 2008; Yonge and Hesse, 2009). Grazing of domestic animals and establishment of cattle stations began in the 1830s (DECC, 2009). Although irrigated agriculture began in the southern marshes in the 1840s, it was not until the 1950s when large-scale irrigation began (DECC, 2009). Starting from the 1950s, dams and irrigation channels were built one after another and the free-flowing waterways were transformed into a highly managed system. According to a 2008 study by the Commonwealth Scientific and Industrial Research Organisation (CSIRO): before European arrival in the 1800s, more than 40 % of the rainwater (about 12,200 billion litres) entered the system annually; in 2008 the flow in the river's lower reaches had dropped to nearly one-third of historical levels (about 4,700 billion litres). The decade-long Millennium Drought starting in the late 1990s exacerbated the water shortage.

Geomorphological evidence shows new natural marsh channels are initiated by avulsion and incision into the floodplain surface and they then gradually aggrade until a new avulsion results in abandonment, typically over an approximately 100-year time scale (Ralph, 2008; Yonge and Hesse, 2009). These conditions favour the growth of dense riparian and aquatic vegetation around and within the channels, in turn contributing to channel constriction and breakdown (Ralph et al., 2011).

Yonge and Hesse (2009) found that average accumulation rates for the floodplain sediments are low and range from 0.18 mm a^{-1} to 2.92 mm a^{-1} for the last 5,000 years; while over the last 200 years, they increase to between 1.44 mm a^{-1} and 4.39 mm a^{-1}. The ages obtained from the 'Terminus Marshes' core (southern marshes) ranged from ~ 59 ka

at 350 cm below the surface (within the late Pleistocene palaeochannel sediments) to ~ 540 cal. years BP at just 20 cm deep; the estimate of the long-term sedimentation rate at this site is ~ 0.32 mm a^{-1} for the last ~ 4.9 ka, while the accretion rate over the last ~ 540 years is around 0.37 mm a^{-1} (Ralph et al., 2011). Data from another core on lower Monkeygar Creek shows the estimated accretion rate for the last ~ 149 years is ~ 4.09 mm a^{-1} and ~ 5.56 mm a^{-1} for the last ~ 54 years; however, the authors think the age for this core was unreliable as it contained rare sand grains for OSL and no measurable unsupported ^{210}Pb and ^{137}Cs (Ralph et al., 2011). The study by Ralph (2008) found that the mean contemporary sedimentation rate near the main channel in the southern marshes, in particular those in the floodout zone, is around an order of magnitude greater than the longer-term floodplain sedimentation rates (~ 0.18 to 2.92 mm a^{-1}) found in the system.

A pilot study was carried out using palaeoecological techniques to investigate colonial waterbird breeding events in the marshes (Cull, 2007). Assuming that colonial waterbird breeding within the marshes would elevate the nutrient levels of the ambient soil, the study focused on concentrations of phosphorus and bulk organic matter in pigments, but the results were not conclusive. The author suggested nutrients such as bulk organic matter and phosphorus alone, as preserved in the sedimentology record, was not an ideal and reliable technique to verify past breeding populations.

The first evidence of significant changes in wetland communities and ecological successions directly related to the geomorphic processes of avulsion and floodplain evolution in Macquarie Marshes is a multi-proxy study by Ralph et al. (2011) restricted to the southern marshes. It indicates the avulsion in the southern Macquarie Marshes caused the formation of a major new channel (Monkeygar Creek) and the abandonment of a reach of the Macquarie River in the last 200 years. The study also found that the floodplain near

lower Monkeygar Creek was only periodically inundated prior to avulsion (before ~ 149 years ago) and experienced disturbance, with rapid accretion and ecological succession during the avulsion. This part of the floodplain became a substantial wetland, dominated by algae (and/or permanent charophytes and diatoms) and submerged macrophytes, due to a more consistent flood regime following the avulsion. The contemporary marsh on lower Monkeygar Creek has evolved in the last ~ 54 years into a shallower, less frequently flooded wetland, probably due to changes in inundation caused by rapid local floodplain accretion (~ 0.4 to 0. 6 cm a^{-1}) and possibly river regulation (Ralph et al., 2011).

2.6 Management

In order to preserve key ecological assets, the Macquarie Marshes need to have a permanent 125 ML environmental water allocation when upstream storages are full (Morrison et al., 2011). However, this allocation is adjusted downwards according to upstream storage volumes and the marshes rarely receive the maximum allocation (Morrison et al., 2011). To supplement this continuing allocation, the New South Wales State and Federal governments periodically purchase environmental water to supplement these flows particularly by attempting to 'top-up' natural events to add extra water to the system (Morrison et al., 2011). These attempts aim to reach areas that have not been inundated for significant periods of time and maintain water levels for sufficient duration to achieve successful waterbird breeding events (Morrison et al., 2011).

The 'buyback of water' started in the 1980s and in 1980, the first environmental flow release occurred. By 1986, it was clear that a formalised environmental management plan focusing on water for the Macquarie Marshes was essential (DWR and NPWS, 1986). However, by the mid-1990s, this plan was shown to be inadequate (DLWC, 2000) and a

new water management plan was developed (DLWC and NPWS, 1996). The Macquarie-Cudgegong Water Sharing Plan was developed under the NSW *Water Management Act 2000* and has identified the need for 160,000 ML of environmental flow below Burrendong Dam. However, all the water is only available when there is 100 % allocation to water licences in the system. Between November 2005 and January 2006, the Macquarie Marshes received an environmental water release of approximately 84,000 ML, which was triggered by rainfall in the upper catchment and a flood in the Bell River below Burrendong Dam (Driver and Knight, 2007). It has been estimated that a total area of over 24,600 ha of the marshes was inundated from this environmental water release event. However, after January 2006, the flow to the marshes declined again. In June 2010, the Wentworth Group of Concerned Scientists, called for water flows to be returned to two-thirds of historical levels. In response to this, the Murray-Darling Basin Authority (MDBA) issued a plan in November 2010 to return $3{,}200 \times 10^9$ L to the Murray-Darling system by 2024.

2.7 Summary

Previous studies of the Macquarie Marshes mainly focus on the fields of geology (Brock, 1998), biological proxies (Kingsford and Thomas, 1995; Roshier et al., 2002; Ralph et al., 2011), history (Kingsford and Thomas, 1995; Hogendyk, 2007), management and planning (Kingsford and Johnson, 1998; Kingsford, 2000; Lemly et al., 2000; Roshier et al., 2002; Kingsford and Auld, 2005; Ren and Kingsford, 2011).

The techniques used have been mainly remote sensing, hydrology, geomorphology, sedimentology, field surveys and statistically modelling calculations using data based on aerial surveys (Kobayashi et al., 2011; Ren and Kingsford, 2011; Wen et al., 2012) and

biological proxies such as charophytes, diatoms and invertebrates (Ralph et al., 2011). Based on the data available, most of these studies can only indicate a history based on less than the past 100 years. Very few studies have considered the palaeoenvironment of the marshes (Cull, 2007; Ralph, 2008; Yonge and Hesse, 2009; Ralph and Hesse, 2010; Ralph et al., 2011) and these mainly focus on the geomorphology of the southern marshes.

This thesis attempts to obtain more information on palaeoenvironments in the Macquarie Marshes in particular by filling the gap of the northern marshes, which are better preserved and have been more active since the late Quaternary. One of the foci is to trace bio-markers related to vegetation and waterbird guano, whose abundance is sensitive to both climate change and human impact. Characterising the complex and interactive effects of palaeoclimatic and anthropogenic changes requires multi-proxy methods, including proxies sensitive to particular changes.

CHAPTER 3 SAMPLING AND MULTI-PROXY STUDIES OF THE MACQUARIE MARSHES

This chapter discusses the sampling campaign and methods, as well as lithology, sedimentology, mineralogy and general geochemistry of the samples as background to study the Macquarie Marshes. The numerical dates for sediment cores mentioned here are discussed in more detail in Chapter 4.

3.1 Sampling campaign and methods

A preliminary fieldtrip to the Macquarie Marshes was conducted by Professor Allan Chivas and Dr Adriana García in June 2007. Another two fieldtrips, in which the author participated, were conducted in Spring season on 2 to 7 November 2008 and 23 to 27 November 2009, at the peak of an 11-year drought. Even in the Nature Reserve marshes, hardly any wetlands could be seen. The dominant landscapes were drylands of cracked and broken earth, littered with the blanched shells of freshwater mussels and bordered by the skeletons of river red gums whose dead branches no longer supported the nests of migrating birds or sheltered native fish. Shells of molluscs were found on some of the dry river beds. Though it was supposed to be breeding season for most of the waterbirds, none of the common colonial waterbird species was observed. In general, the North Reserve was better preserved than the South Reserve with more water and vegetation coverage.

3.1.1 Sampling sites

During the fieldtrips, 25 cores from 7 sites covering the North and South Reserve areas were collected (Figure 3.1, Page 26). Further information for each sampling site is

presented in Table 3.1 (Page 27) and representative photographs of the coring procedures are in Figures 3.2, 3.3 and 3.4 (Page 31 and 32).

The sampling sites in southern marshes are along Monkeygar Creek and its wetland system, which comprises the central part of the southern marshes. In this system, large reed beds (*Phragmites australis*) comprise 15 % of the area and chenopod and grassland plains dominate the remainder (DLWC, 1996). Degraded river red gum woodland is evident in the north-western component of this system and coolibah and poplar box occur in the north-east (DLWC, 1996). During 1992-1996 (a relatively dry period), these wetlands were severely degraded, primarily due to the erosion occurring in Monkeygar Creek and the formation of a new channel.

The sampling sites in the northern marshes are located near the centre of its wetland where reed beds (*Phragmites australis*) occur. Mixed marsh and *Typha* sp. dominate its eastern edge, close to the northern Marsh Bypass Channel (DLWC, 1996). Surrounding this reedbed are large areas of water couch, river red gum forest, woodland and associated patches of coolibah (DLWC, 1996). A stand of black box and poplar box occurs in the north-eastern corner (DLWC, 1996). The coring sites chosen were mostly in water courses, lagoons or floodplains that were close to the main water channel (to permit recovery of near-continuous sedimentation) and notionally organic-rich to facilitate organic geochemical analysis. However, such strategy may reduce the amount of quartz available for OSL dating (see Chapter 4).

At each sampling site, duplicate cores were taken to ensure sufficient material for investigation and to allow one core for OSL dating and which needed to be opened in a darkened laboratory. Owing to the dry-soil conditions at the time of sampling, most cores were only 50-100 cm long; the longest (at 190.5 cm) was from Loudens Lagoon (LOLA).

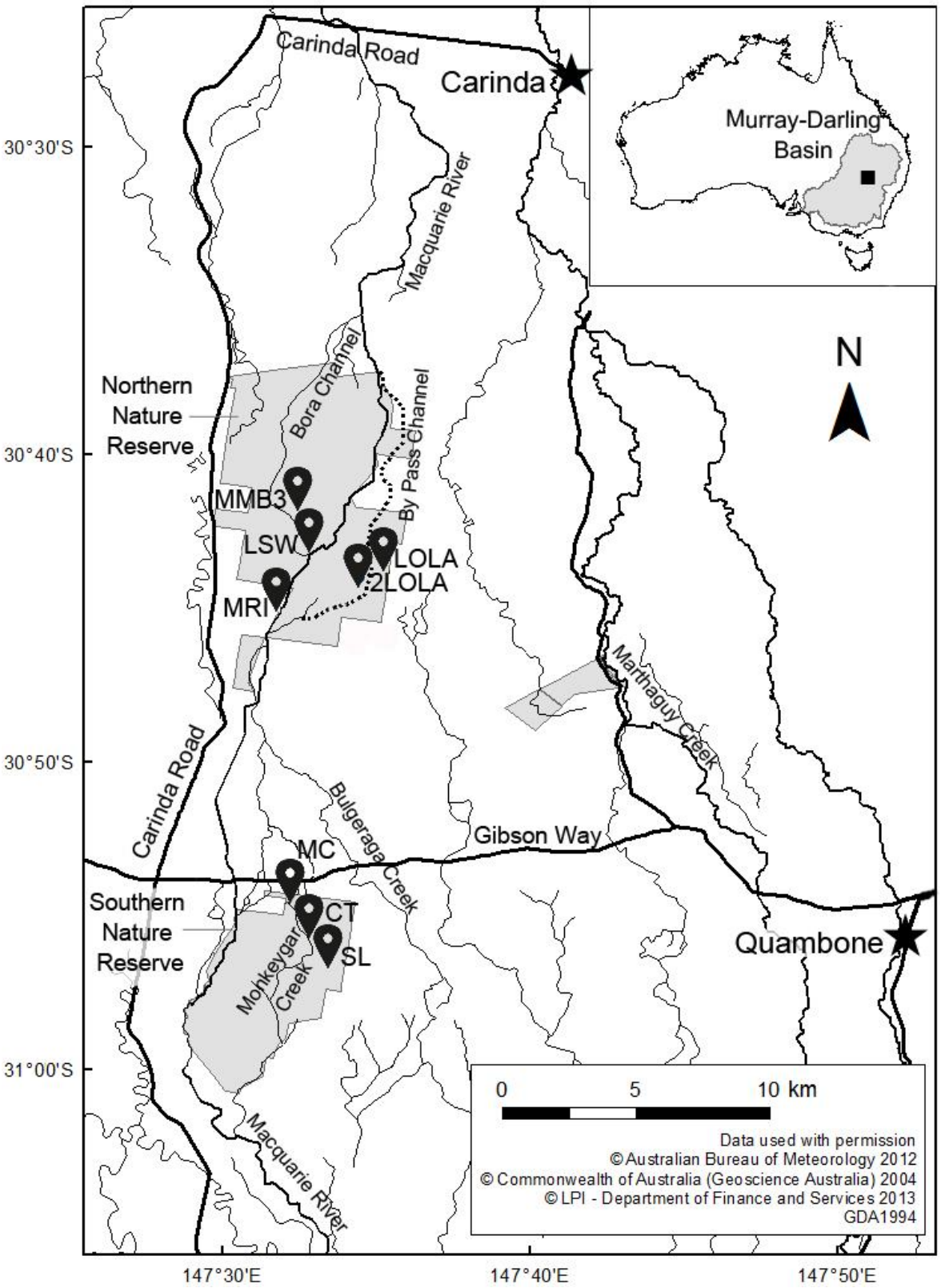

Figure 3.1. Map of the Macquarie Marshes and the sampling sites. (The three shaded areas are Nature Reserve wetlands.)

Table 3.1
General information on samples collected from fieldtrips to Macquarie Marshes (2007-2009).

Sites and Descriptions	Sample Name	GPS Location			Core Length (cm)	Core Depth (cm)	Surface sediments /modern samples
		Lat.	Long.	Alt. (m)			
Southern Marshes South Lagoon	SL1-1	S 30º56.436'	E 147º33.434'	149	82	100	Collected profile samples from surface (SL-C1) to 50 cm.
	SL1-2				155	106	
Southern Marshes Monkeygar Creek on the flood plain	MC1-1	S 30º54.349'	E 147º32.298'	147	79	102	Collected profile samples from surface (MC-C6) to 53 cm.
	MC1-2				75	122	
Southern Marshes Monkeygar Creek in the creek	MC1-3	S 30º54.444'	E 147º32.224'	158	55	63	
	MC1-4				48	60	
Southern Marshes Monkeygar Creek east of the creek, end of Campsite Trail, small depression area, gastropods on the surface, some shells are brown (i.e. not fully bleached)	CT-1	S 30º55.454'	E 147º32.546'	132	112.5	112.5	Collected two bags of surface soil (CT-S1), one bag of *Phragmites* leaves and one bag of *Eucalyptus* sp. leaves.
	CT-2				213	219	
	CT-3				114.5	116.5	
Northern Marshes Bora channel east side of the lagoon, which has remained inundated for a long time	MMB3	S 30° 41.082'	E 147° 31.259'		75	100	Collected surface sediments (MMB3-S1)
Northern Marshes Longstowe Station private property, water depth 15-18 cm; used to be bird colony area	LSW-1	S 30º44.867'	E 147º31.923'	150	56	93	Collected two bags of surface mud at this site (LSW-S1).
	LSW-2				52	83	
Northern Marshes Longstowe Station private property,water depth 90 cm	LSW-3	S 30º44.941'	E 147º31.817'	157	44	73	Collected surface mud (LSW-S3) and surface soil (LSW-S2) from the swamp bank under a red gum tree.
	LSW-4				60	82	
Northern Marshes Loudens Lagoon dry since 1990s (flooded early in 2008)	LOLA-1	S 30º43.957'	E 147º34.458'	148	190.5	210	Collected surface sediments from coring site (LOLA-S1), centre of lagoon (LOLA-S2), and reed beds (LOLA-S3).
	LOLA-2				114	146	
Northern Marshes Loudens Lagoon the reeds (*Phragmites australis*) are dead and the surface is completely dry.	LOLA-3	S 30º43.958'	E 147º34.458'	134	70	122	
	LOLA-4				43		
	LOLA-5				151	153	
Northern Marshes Loudens Lagoon 2nd lagoon to the west with green reeds (*Phragmites australis*) and wet areas, patches of water, one patch burnt	2LOLA-1	S 30º44.080'	E 147º33.810'		111	152	Collected one bag of sediment (2LOLA-S1), one bag of *Phragmites* leaves, one bag of *Ranunculus* leaves with flowers.
	2LOLA-2				135	164	
	2LOLA-3				73	112	
	2LOLA-4				85	134	
	2LOLA-5				79		
Northern Marshes Macquarie River Bank of a channel parallel to Macquarie River, small sections with little water	MRI-1	S 30º45.998'	E 147º31.721'	146	59.5	75.5	Collected surface sediment samples from river mud (MRI-S1), one from surface soil close to coring site (MRI-S2).
	MRI-2				79.5	87	

This thesis focuses on four core sites from the northern marshes (MMB3, LSW, LOLA and 2LOLA) because the sedimentary record was more complete and unaltered, palaeobiota from these low-lying areas or lagoons or marshy sites was better preserved, and have been important waterbird colonial sites for the last 30 years (Kingsford and Johnson, 1998).

Core site MMB3 is located in a lagoon, about 50 m east of the Bora Channel, in one of the few areas which is almost permanently inundated in the MM. This site used to provide woodland nesting vegetation and support bird colonies as large as 3,550 during the breeding season (Kingsford and Auld, 2003). At the time of sampling (June 2007), it was still inundated but breeding in this site had not occurred since 2000 (Kingsford and Auld, 2003), and which was also a small event. Core MMB3, which was 75 cm long and penetrated a depth of 100 cm was obtained from this site.

Core site LSW is located within Longstowe station, on the west side of the Bora Channel and south of MMB3. It used to be a bird colony site (Kingsford and Johnson, 1998; Cull, 2007). At the time of sampling (November 2008), the water was relatively shallow (15-18 cm depth) (Figure 3.2); and it was difficult for the aquatic biota to survive. A small nesting event (egrets) was recorded in the previous months, and fruit-bats were present at the time of coring. LSW-1 and LSW-2 cores (56 and 52 cm long covering 93 and 83 cm depth respectively) were duplicates obtained from a swampy area where the water depth was 15-18 cm. LSW-3 and LSW-4 cores (44 and 60 cm long covering 73 and 82 cm depth respectively) were duplicates nearby where the water depth was 90 cm.

Figure 3.2. Site of LSW (Longstowe station, Northern MM). (Photo taken in November 2008)

Core site LOLA is at Loudens Lagoon, which is located away from the Bora Channel and close to the Bypass Channel. Despite being dry since the 1990s, a small flow reached it early in 2008 (Figure 3.3, left photo). One year later (November 2009), the reeds (*Phragmites australis*) were completely dry (Figure 3.3, right photo). LOLA-1 and LOLA-2 cores (190.5 and 114 cm long covering 210 and 146 cm depth respectively) were duplicates from the dry Loudens Lagoon which had been dry since 1990s and was flooded early in 2008. LOLA-3, LOLA-4 and LOLA-5 cores (70, 43 and 151 cm long covering 122, 60 and 153 cm depth respectively) were triplicates from the other part of the dry Loudens Lagoon where the reeds (*Phragmites australis*) were dead and the surface was completely dry.

Figure 3.3. Site of LOLA (Loudens Lagoon). (Left - photo taken in November 2008; Right – photo taken in November 2009)

The 2LOLA site was close to but just to the west of LOLA site, and is the second lagoon to the west of the Bypass Channel. At the time of sampling (November 2009) (Figure 3.4), the 2LOLA site was green with patches of water and reed beds (*Phragmites australis*). In this site, 5 cores were obtained from west of the Loudens Lagoon with green reeds (*Phragmites australis*) and wet areas. The core lengths are 111, 135, 73, 85, 79 cm individually, covering depths of 152, 164, 112, 134 and 90 cm, respectively.

Figure 3.4. Site of 2LOLA (Loudens Lagoon, Northern MM). (Photo taken in November 2009)

3.1.2 Coring methods

In wet marshy areas, aluminium coring tubes were driven into the underlying sediments by sledge hammer to minimise disturbing the mud-water interface (Figure 3.5). On floodplains and dry lagoons, a hydraulic jack hammer was used for coring (Figure 3.6). However, due to the long-term drought in these areas, the tubes failed to penetrate more than 1 metre excepting at two sites (SL and LOLA). The ends of the coring tubes were sealed with plastic caps and black plastic bags to avoid exposure to light as some cores would be used for OSL dating.

Figure 3.5. Coring at the LSW site. (Photo taken in November 2008; impaling aluminium core barrel by sledge hammer and withdrawing core barrel with strap and horizontal bar)

Figure 3.6. Coring at the LOLA site. (Photo taken in November 2008; Left photo - driving steel core barrel with hydraulic jack hammer; Right photos – extracting core barrel with (a) quadripod and block and tackle, (b) kangaroo jacks.)

Surface (0-5 cm) mud or soils (Table 3.1, Page 27) in and around the coring sites were collected in plastic sampling bags. They were used as 'modern' reference material to which the older samples from the core sections could be compared. Such comparison allows the determination of molecular heritage from the organic sources and estimation of molecular biomarker degradation in the sediment. Sediment from the lowest barrel-layer of each core tube ('core catcher') was also collected for reference. Samples of plants adapted to aquatic (emergent, submerged, littoral) and terrestrial habitats were collected in order to obtain and characterise their geochemical markers. Selected extant species included leaves and stems of river red gum (*Eucalyptus* sp.), reeds (*Phragmites australis*), cumbungi (*Typha* sp.), buttercup (*Ranunculus* sp.) and charophytes (*Chara australis*).

Bird guano was also sought but because bird colonies had not been present immediately before or at the time of sampling there were no deposits of guano (the fieldtrips were done at the peak of the 11-year drought).

Waterbodies within the northern and southern marshes were sampled for water quality and their aquatic biota was investigated, especially charophytes, ostracods, and molluscs.

After collection in the field, the samples were kept at 4 ºC, in the field and later at the University of Wollongong, principally in order to preserve organic compounds.

The cores were cut longitudinally using an electrical saw under subdued orange light in the laboratory. One half was sectioned in 2 cm intervals and subsamples used for the several proxies (biological, organic geochemistry, total organic carbon content (TOC), total nitrogen (TN), $\delta^{13}C_{org}$ analysis, as well as for water-content, particle size analysis, mineralogy (X-ray diffraction, XRD) and elemental analysis (X-ray fluorescence, XRF). The other half was divided into 4-6 cm intervals (in order to obtain enough quartz) for optically stimulated luminescence (OSL) dating. The depth of the core profile was corrected for the compaction factor (core penetration depth divided by the recovered core length). Further details of the sample preparation methods and various analyses are presented in later sections/chapters.

3.2 Sedimentology and geochemistry of the Macquarie Marshes

The Macquarie Marshes are a complicated system with highly variable seasonal climate. Accordingly characterising palaeoclimatic and environmental changes requires multi-proxy methods. The proxies presented in this chapter include lithology, sedimentology, mineralogy, total organic carbon, total nitrogen, C/N, $\delta^{13}C$, as well as some major- and

trace-element data. There is a focus on the proxies that are sensitive to climate and/or indicative of waterbird colonial events and vegetation changes.

3.2.1 Lithology, sedimentology and mineralogy

Visual inspection of the samples was conducted prior to other analysis to describe the colour (Munsell, 1971) and lithology of the samples and to identify significant changes such as the presence of laminations, or other changes along the cores.

The sediment particle size is one of the most commonly used physical characteristics of sediments. It is mainly controlled by the energy condition of a depositional system and can assist in estimating the transportation of sediments (e.g. flow velocity), the depositional environment into which the sediments settled (e.g. sedimentation rate, water depth of palaeo-lake) (e.g. Blatt et al., 1980; Yum et al., 2003; Hatfield et al., 2010) and also the past geomorphology of the region (e.g. Woodroffe, 2002). Sorting gives clues to the energy conditions of the transporting medium from which the sediment was deposited. As a general rule, the more reworking that is applied to sediments, the greater is their degree of sorting. Well-sorted sediments in a site are indicative of frequent or continuous occurrence of hydraulic flow conditions at the site. Conversely, poorly sorted sediments point to rare or intermittent occurrence of hydraulic flow (Visher, 1969; Håkanson and Jansson, 1983). Fluvial deposits are usually poorly sorted because the energy (velocity) in a stream varies with position in the stream and time (Håkanson and Jansson, 1983).

X-ray powder diffraction (XRD) is one of the analytical techniques used to identify and characterize the minerals present in a sediment sample (e.g. Loomis et al., 2011; Sun et al., 2011). The XRD data are usually interpreted with the geochemical data (i.e. major- and trace-element results) to trace the sediment sources, their transportation and

weathering (e.g. Vesk and Allaway, 1997; Loomis et al., 2011; Sun et al., 2011). In this thesis, XRD was used to identify and semi-quantify quartz and feldspar contents for OSL dating purposes (discussed in Chapter 4) and to obtain the mineral composition of selected sediments.

3.2.1.1 Methodology

The colour of the dry core sections was visually inspected by comparing to the Munsell (1971) soil color chart.

The moisture content was measured from an aliquot of the samples used for geochemical analysis. Each sample was weighed before and after drying in an 80 °C oven for 6-8 hours, then the water content of the samples was calculated by dividing the weight of water (the weight difference between the wet and dry sample) by the weight of wet sample.

The particle-size distribution of sediment samples from the cores was analysed at the University of Wollongong using a Malvern Mastersizer 2600/2000 which uses laser diffraction to determine various particle sizes. Approximately 1 g of sediment was added to a beaker containing 1L of water, mixed and dispersed ultrasonically before measurement. Duplicate analyses were performed to ensure that the reproducibility of results was less than 1 %. The proportions of sand (>63 μm), silt (3.9-63 μm) and clay (<3.9 μm) were recorded. The uniformity, asymmetry of the grain-size distribution and the shape of the grain-size frequency distribution were also reflected by the parameters of sorting (StdDev), skewness (G Skew) and kurtosis (Kurt). The surface sediment samples were sieved with a 500 μm mesh to remove plant debris before analysis by the Mastersizer.

The minerals were identified by X-ray diffraction (XRD) using a Philips diffractometer in the School of Earth & Environmental Science, University of Wollongong. Thirteen surface sediment samples were analysed for their mineral composition and two cores (MMB3 and 2LOLA) were analysed to record mineralogical changes during the last 1,000-year time span.

3.2.1.2 Results

3.2.1.2.1 Surface sediment samples

The surface sediment samples were collected mostly from/around the coring sites from both southern and northern marshes (Table 3.1 on Page 27 and Table 3.2 on Page 38). Water content, particle size fractions, sorting, skewness and kurtosis are presented in Table 3.2. The surface sediment samples varied in colour depending on their organic content. Those with higher organic content appeared to be black and the colour was lighter when the organic content reduced. Most of these surface sediment samples contained plant debris.

The water content varied significantly from 4.69 % to 53.18 % depending on the environmental setting. Unsuprisingly, the water content was high at sites that were wet/inundated and decreased at sites that were dry. Sediments from sites where there was a vegetation canopy tended to retain more water than neighbouring exposed sites where the vegetation had died.

The most abundant (>50 %) particle size for most of the samples was silt. Two exemptions were samples from LOLA and MMB3 that were rich in sand. Samples collected from the watercourses (e.g. the MRI and LSW sites) tended to contain more clay

than sand while those collected from dry land (e.g. the LOLA and 2LOLA sites) were the opposite. The sorting parameters for all the surface sediment samples appeared to be close to 2, indicating they were all very poorly sorted. The skewness parameters indicated that except for three samples (MRI-S1, LSW-S3 and MC-C6) that were near symmetrical (G Skew between +0.10 to -0.10), other samples were well skewed to various extents (G Skew between +0.30 to +0.10). The kurtosis parameters varied slightly from 0.83 to 1.06, indicating a bimodal grain size distribution. Unlike typical river sediments which are commonly moderately sorted, the sediments in the Macquarie Marshes were mostly poorly sorted indicating they had not been transported very far and little time had been involved in separating particles of various sizes. This explains why some of the quartz grains in the sediments were not fully-bleached before burial (see the OSL single-grain dating, Chapter 4).

The mineralogical results for the surface sediment samples are presented in Table 3.3 (Page 39). There is little significant variation among the sites, indicating a likely similar source. Among them, quartz (mean 59 %), muscovite (mean 11 %), illite (mean 7.9 %) and kaolinite (mean 7.6 %) constitute more than 85 % while orthoclase (mean 4.3 %), albite (mean 3.3 %), biotite (mean 3.3 %), gypsum (mean 1.8 %) and traces of labradorite (mean 1.0 %), chlorite (mean 0.9 %), ankerite (mean 0.2 %), calcite (mean 0.1 %) and siderite (mean 0.1 %) varied from site to site. Quartz was more abundant than feldspar which was a great advantage for OSL dating.

Table 3.2
Descriptions and some parameters of the surface sediments.

Sample ID	Location	Sample Type	Water (%)	Sand (%)	Silt (%)	Clay (%)	Sorting (Std Dev)	Skewness (G Skew)	Kurtosis (Kurt)
MRI-S1	Bank of a channel parallel to Macquarie River, northern MM	River mud	34.2	13.9	52.4	33.7	2.33	-0.08	0.86
MRI-S2		Surface soil close to coring site	10.1	10.4	64.9	24.8	2.09	0.21	0.85
LOLA-S1	Loudens Lagoon, northern MM	Surface soil from dry land in lagoon centre	6.0	30.3	56.1	13.6	2.17	0.29	1.06
LOLA-S2		Soil near reed beds	13.8	37.6	51.4	11.1	2.22	0.27	1.03
LOLA-S3		Soil at coring site	5.5	46.7	44.9	8.4	2.18	0.24	1.04
2LOLA-S1		Surface sediment	33.3	18.0	56.2	25.9	2.34	0.12	0.83
MMB3-S1	Bora channel east of the lagoon which has remained inudated for a long time, northern MM	Surface sediment	60.9	51.9	36.9	11.2			
LSW-S1	Longstowe Station, northern MM	Coring site mud	35.7	15.3	64.2	20.5	2.09	0.15	0.93
LSW-S2		Soils from swamp bank under a red gum tree	24.5	22.4	57.1	20.5	2.13	0.25	0.86
LSW-S3		Surface sediment	53.2	11.9	62.4	25.7	2.10	0.05	0.89
MC-C6	Monkeygar Creek, southern MM	Surface sediment	21.9	16.0	59.3	24.7	2.07	0.01	0.86
CT-S1	East side of Monkeygar Creek, end of Campsite Trail, southern MM	Surface sediment	4.7	17.6	63.8	18.7	2.15	0.19	0.98
SL-C1	South Lagoon, southern MM	Surface sediment	16.2	16.2	67.7	16.2	1.98	0.37	1.04

Table 3.3
The XRD-determined mineralogy of the surface sediments (Unit %).

Sample ID	Quartz	Muscovite	Illite 1	Kaolin, BISH12	Orthoclase 1	Biotite	Albite(low)	Gypsum	Labradorite	Chlorite	Ankerite	Calcite 1	Siderite (rhomb)
MRI-S1	65.8	9.7	6.2	6.2	7.7	1.0	2.9	0.0	0.5	0.0	0.0	0.0	0.0
MRI-S2	57.5	8.8	7.8	7.9	5.1	2.0	4.4	3.6	0.0	1.9	1.0	0.0	0.0
LOLA-S1	57.8	5.8	10.0	6.4	0.0	9.3	1.1	4.3	4.6	0.0	0.0	0.0	0.6
LOLA-S2	76.7	6.8	7.0	3.6	0.0	1.4	2.4	0.0	1.6	0.0	0.1	0.0	0.0
LOLA-S3	81.0	0.0	7.8	3.1	0.0	1.4	3.8	0.0	1.0	0.0	1.3	0.3	0.3
2LOLA-S1	44.4	17.4	10.2	9.3	5.6	3.5	2.4	2.2	1.9	2.7	0.0	0.3	0.0
MMB3-S1	67.6	12.7	5.0	6.0	5.3	0.7	1.8	0.0	0.8	0.0	0.0	0.0	0.0
LSW-S1	60.1	9.3	8.6	7.6	4.7	3.1	1.5	2.2	1.3	1.1	0.0	0.7	0.0
LSW-S2	50.2	12.9	8.7	9.3	5.3	4.0	2.6	3.8	0.2	3.0	0.2	0.0	0.0
LSW-S3	51.6	12.1	8.5	10.4	7.1	4.4	3.3	2.3	0.0	0.0	0.3	0.0	0.0
MC-C6	47.4	16.3	9.1	11.7	0.0	1.6	12.2	1.7	0.0	0.0	0.0	0.0	0.0
CT-S1	47.1	16.7	6.6	9.8	9.7	4.4	3.0	2.1	0.6	0.0	0.0	0.0	0.0
SL-C1	56.0	11.6	7.6	7.1	5.2	6.3	1.9	1.2	0.4	2.6	0.0	0.0	0.0

3.2.1.2.2 Sediment cores

The four cores studied (MMB3, LSW-2, LOLA-1 and 2LOLA-1) from the northern marshes varied slightly in their colour. Generally the change of colour in the cores was gradual. No laminations were found along the core profiles. It was observed that the deeper parts of the sediment cores were poorly sorted compared to their upper surface sediments. They were also finely skewed and showed bimodal particle size distributions.

The core dates (by OSL) are introduced in this section of Chapter 3 for convenience; the full details of their determinations are presented in Chapter 4.

As shown in Figure 3.7, the lower part of core MMB3 was pale yellow in colour between 100 cm and 96 cm. From 96 cm to 72 cm, the colour of the sediments gradually is progressively darker grey. While the clay fraction remains relatively stable (~30 %) between 96 cm to 72 cm, the sand fraction tends to increase up to 86 cm and decrease from 86 cm to 72 cm. At the depth of 87-88 cm and 77-79 cm, there are pebbles probably indicating a flood at these time intervals. From 72 cm to 40 cm, the colour of the sediments becomes darker. The silt and clay fractions increase from 67 cm to 57 cm and are very abundant between 41 cm and 57 cm. The upper 40 cm of core MMB3 contains young sediments, less than 50 years old, organic-rich with black colour. The sand fraction increases towards the surface while the silt and clay fractions decrease. Plant debris was found at 20-21 cm and 13-17 cm and fragments of wood were found at 27-28 cm. Some charcoal fragments were found between 48-52 cm, 35-39 cm and 13-19 cm. The water content is ~22 % at a depth of 87 cm, slowly increasing to ~ 35 % at the depth of 28 cm, and with a high value of 60 % at 7 cm. The XRD results (Figure 3.8, Page 42) show fluctuations among the dominant and trace minerals between 28 cm to 56 cm (1942-1963

AD), while most of the mineral composition remained steady before and after this 20-year time span.

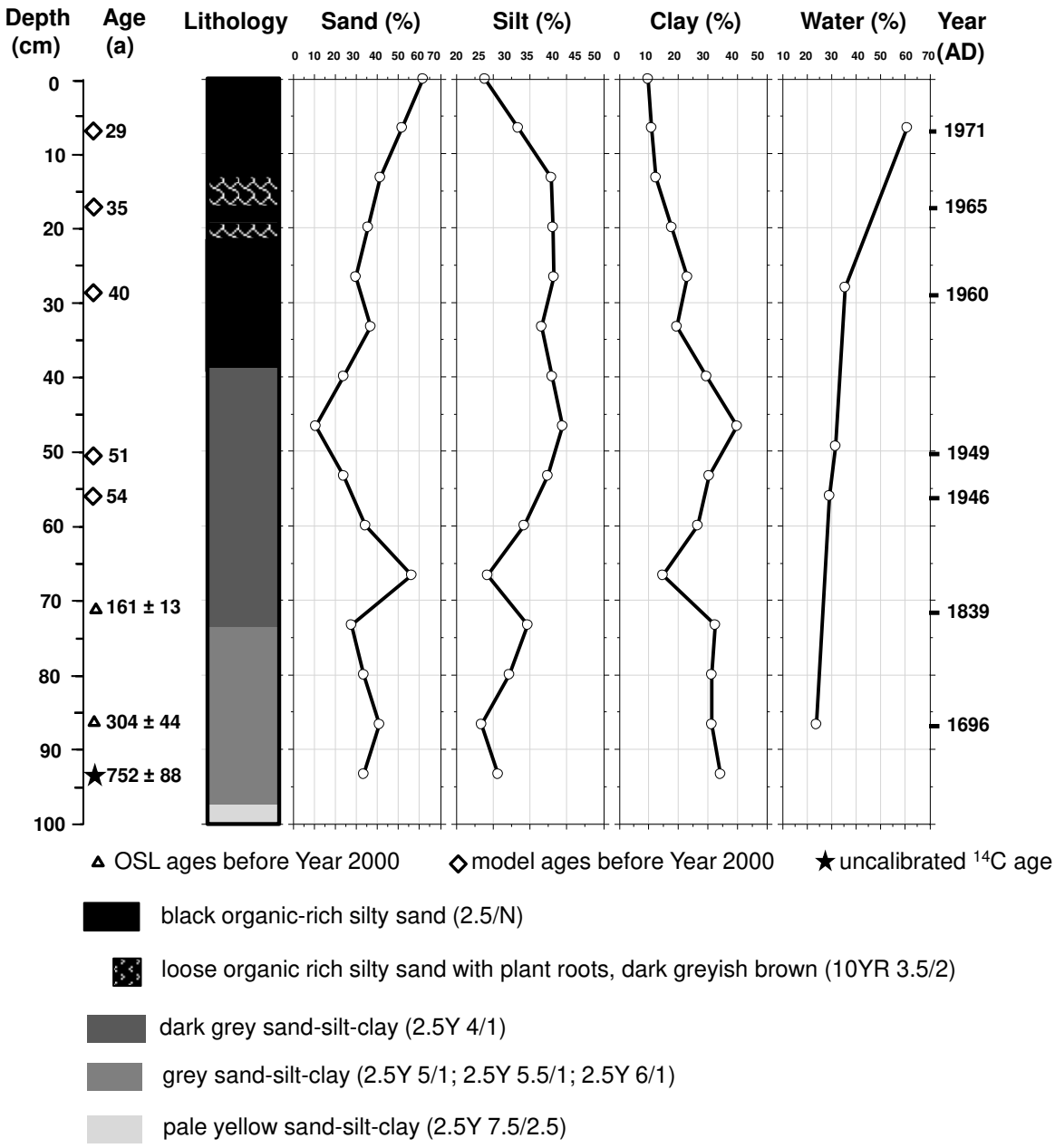

Figure 3.7. Chronology, lithology, particle size and water content of core MMB3.

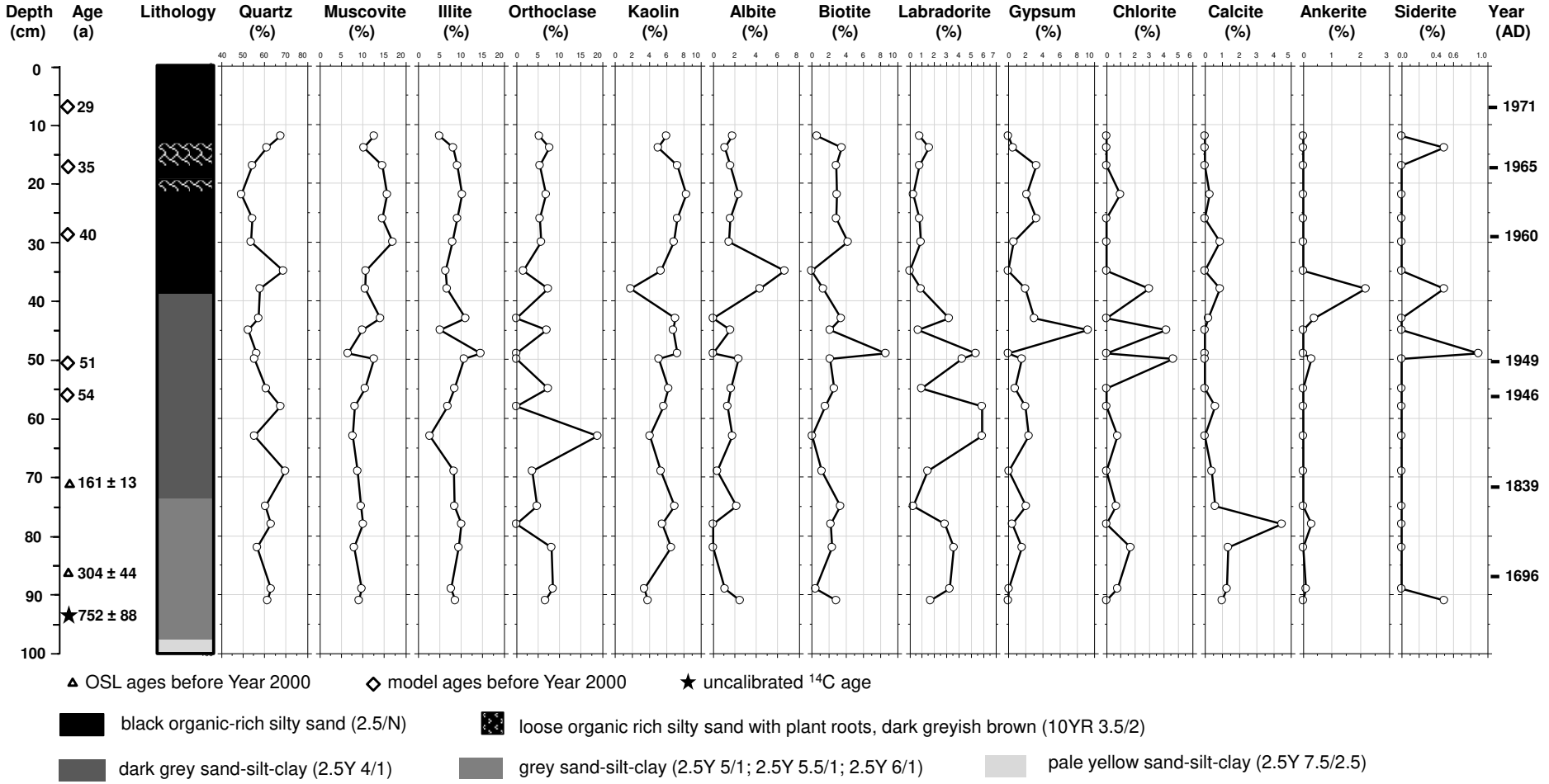

Figure 3.8. Chronology, lithology and XRD results of core MMB3.

The OSL ages from core LSW-1 date to approximately 4,000 years (before 2008 AD) at a depth of 90 cm. Duplicate core LSW-2, which was slightly shorter, penetrated to a depth of 82 cm. As shown in Figure 3.9, the sediment colour of core LSW changed from light grey (93-42 cm), to grey (42-8 cm) and to dark grey (8 cm). The sediments generally appear to be homogeneous except some yellow areas which were found in deeper parts of the core (up to 23 cm deep). Major variations in particle size occur in the deeper section of this core (53-78 cm). The clay fraction shows a peak at 68 cm where the sand fraction is lowest. A significant peak in the sand content occurs at 62 cm (between about 135 and 300 years old); where both the silt and clay fractions are at their lowest. There are small fluctuations in the particle size between 37 cm to 54 cm (23 to ~120 years old). From a depth of 37 cm to the surface (less than 23 years old), the sand and silt fractions tend to increase while the clay fraction decreased. The water content remains relatively stable at 20-22 % from the bottom of the core to a depth of 30 cm and increases to 33 % in the surface.

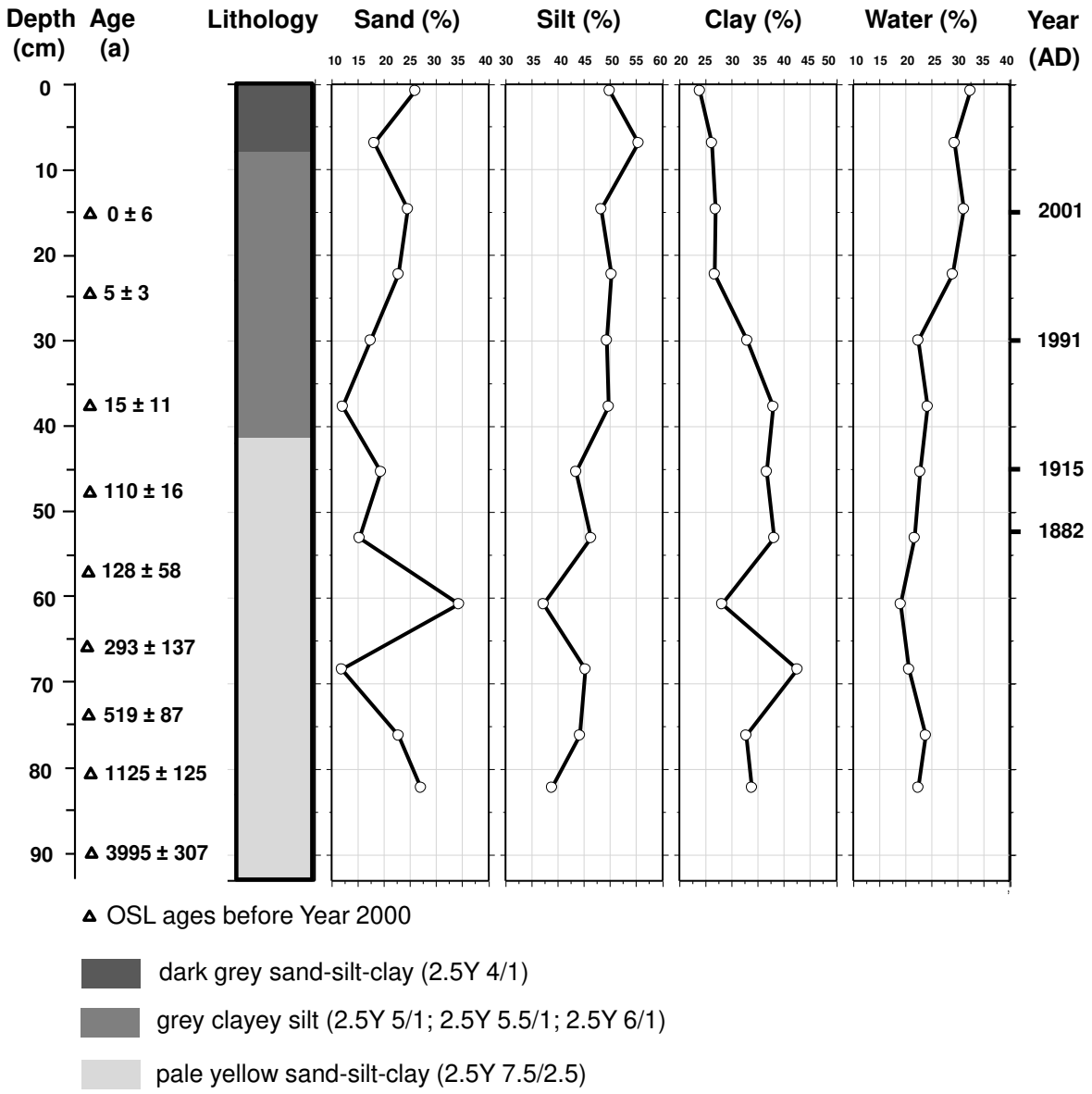

Figure 3.9. Chronology, lithology, particle size and water content of core LSW.

As shown in Figure 3.10 (Page 46), the sediment colour of core LOLA appeared to be lighter than the MMB3 and LSW cores, in particular at the deeper section. The colour is pale yellow from the bottom of the core (204 cm) to 119 cm depth with some minor darker grey areas and iron oxide fragments. From 119 to 67 cm, the colour is light grey, with some pale carbonate nodules between 116 and 54 cm depth, iron oxides between 106 to 90 cm, and hard black fragments between 114 and 106 cm, appearing to be organic debris.

From 67 to 6 cm, the colour is darker, except for the section between 19 and 6 cm in depth, where the sediments are less consolidated. Between 67 cm and 29 cm depth, particularly at 41-38 cm, some iron oxide concretions were found. The upper 6 cm is loose grey soil and some iron oxide fragments. The sediment particle-size fractions varied along the core. Three significant peaks of sand occur at 66 cm (~0.95 ka), 52 cm (~0.74 ka) and 19 cm (~0.23 ka). The silt fraction ranges from around 40 % to 55 %. The clay fraction remains fairly constant at around 30-40 % from 210 to 80 cm depth and decreases to 10 % at the surface. The water content fluctuates along the core and generally decreases from 17-20 % at the deeper part of the core to 12 % at the surface.

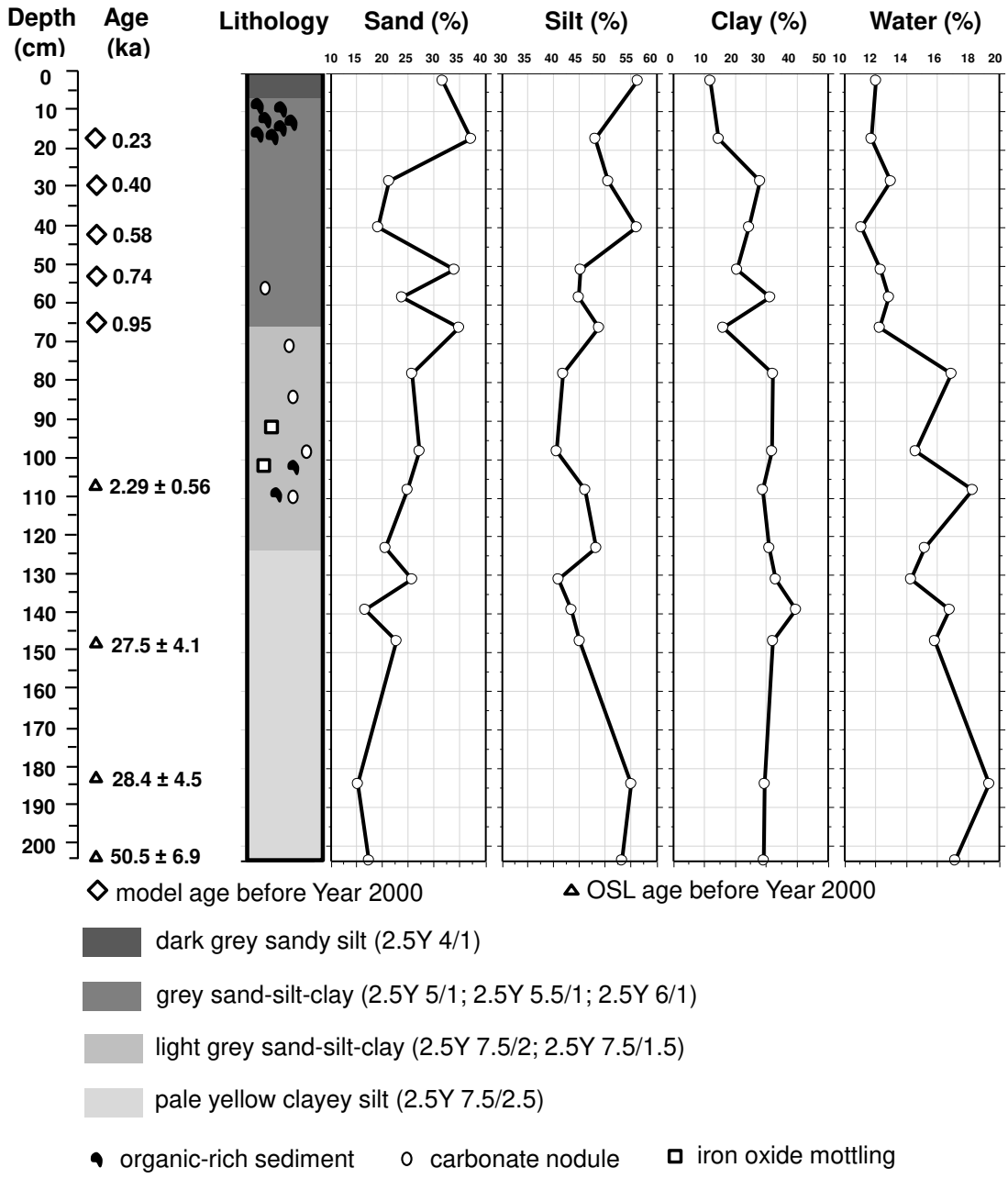

Figure 3.10. Chronology, lithology, particle size and water content of core LOLA.

As shown in Figure 3.11, the colour of core 2LOLA is similar to that of cores MMB3 and LSW at the upper surface but more like LOLA in the deeper layers. From the base of the core (163 cm) to 47 cm depth, the colour is mostly grey but the textures change slightly. From 72 to 64 cm, there are more organic-rich areas. Iron oxides are more abundant between 164 to 116 cm and 91 to 70 cm depth, while carbonate occurs from 164

to 116 cm. From 47 to 28 cm, the colour is dark grey and changes to grey from 28 to 4 cm, with the top 7 cm being dark organic-rich sediment with loose rootlets. The water content approximates 15 % in the deeper part of the core (163 cm to 65 cm) and increases to 40 % at the surface. Compared to core MMB3, the mineral composition of 2LOLA (Figure 3.12) shows less fluctuation during the last 1,000 years and quartz (55 ± 10 %) is the dominant mineral. However, at a depth of ~100 cm (~980 a), there is a significant decrease in the content of quartz, albite, chlorite and an increase in labradorite and calcite content.

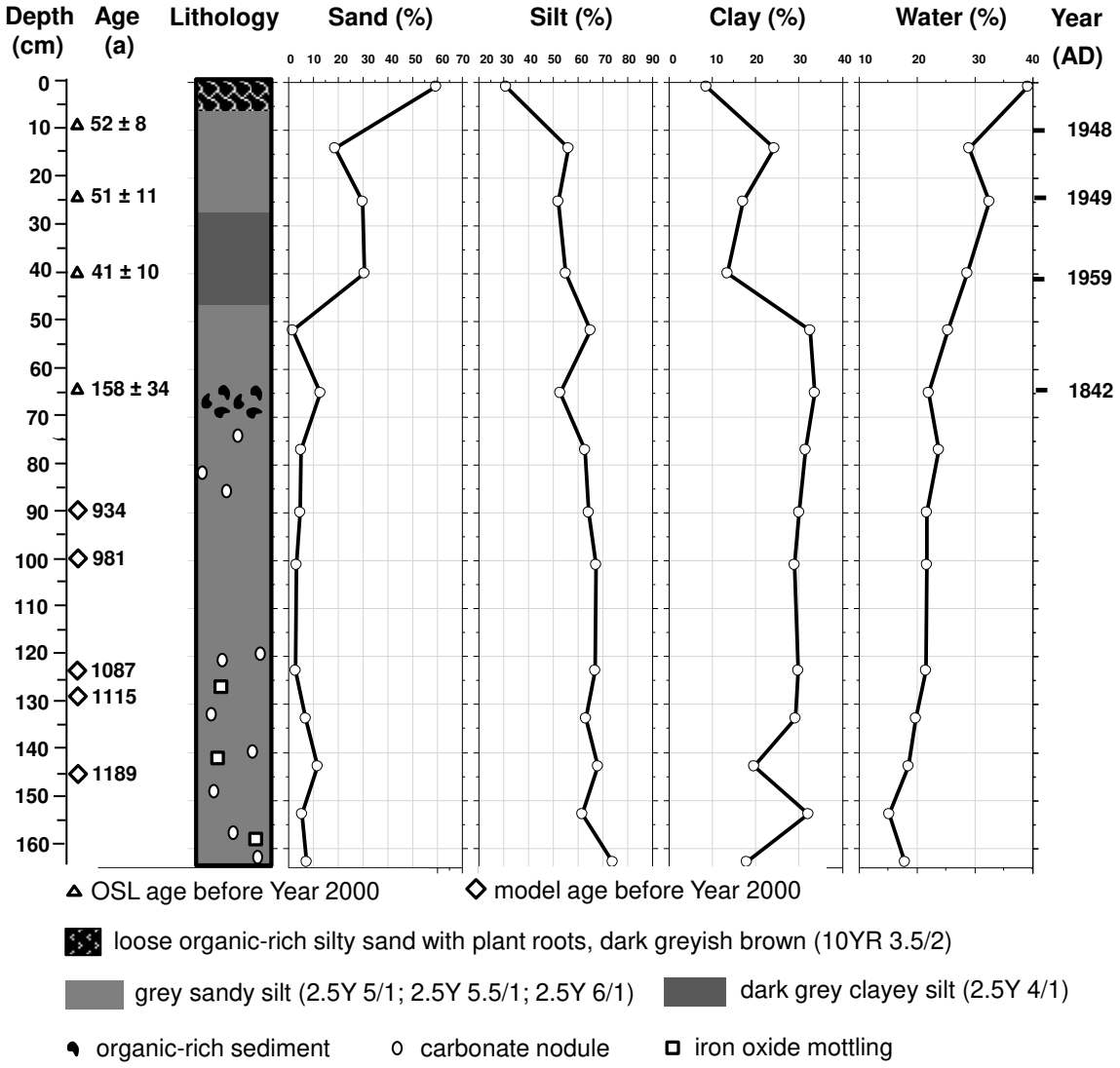

Figure 3.11. Chronology, lithology, particle size and water content of core 2LOLA.

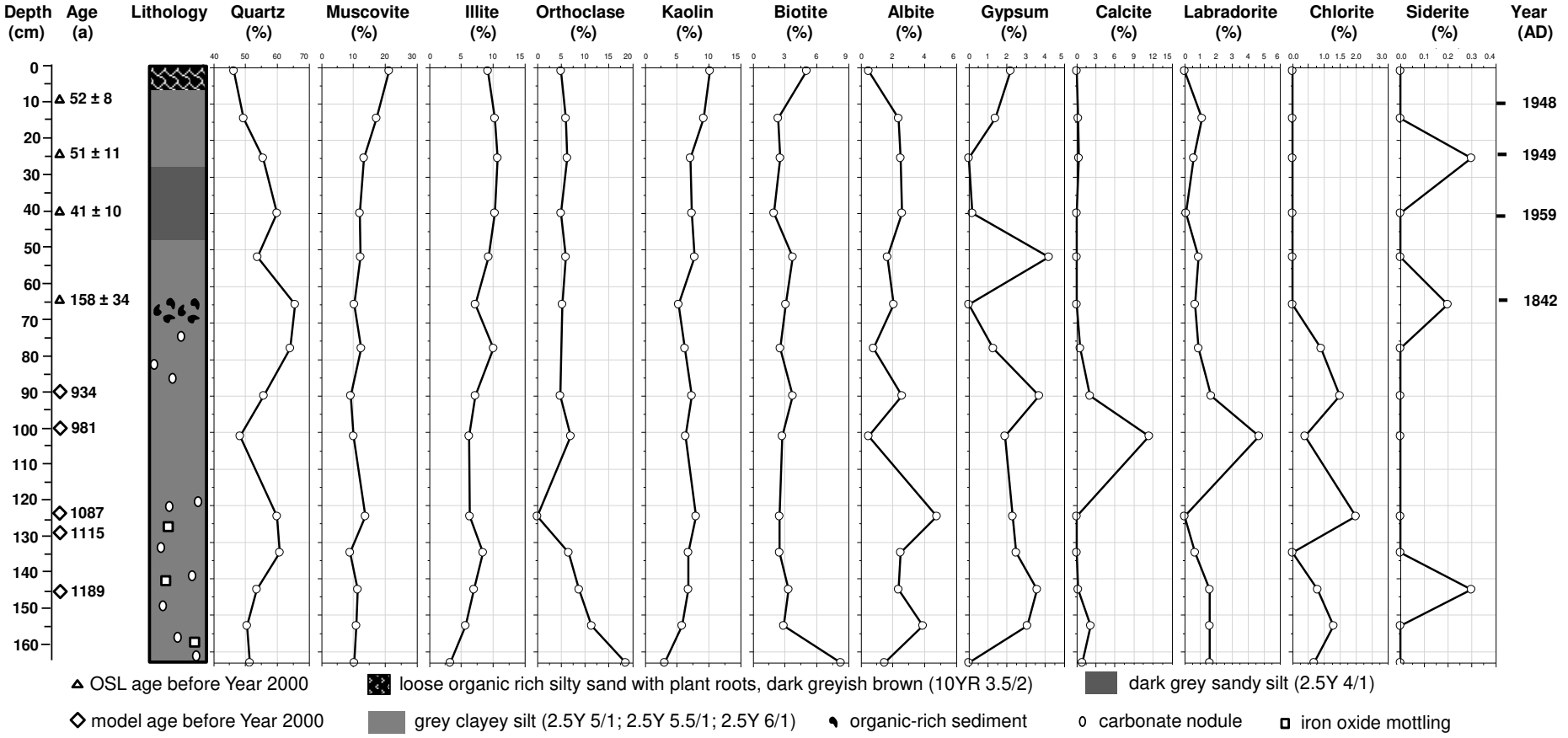

Figure 3.12. Chronology, lithology and XRD results for core 2LOLA.

3.2.2 Geochemistry – bulk carbon, nitrogen, stable carbon-isotope and elemental analysis

Carbon, nitrogen and their isotopes are important for studying ecosystem function and ecology as they can provide information on the origin, formation and pathways of biological materials (Blatt et al., 1980). Bulk organic matter (OM) in lacustrine sediments is a mixture of organic materials derived from aquatic (autochthonous OM, e.g. phytoplankton, macrophytes) and/or terrestrial sources from the surrounding catchment (allochthonous OM, e.g. trees, shrubs, grasses, animals) (Meyers and Ishiwatari, 1993; Fisher et al., 2003; Brodie et al., 2011).

Total organic carbon content (TOC) is a widely used bulk sedimentary parameter that represents the fraction of OM that survived degradation during deposition and early diagenesis in the sediments. It is influenced by both initial authochtonous and allochthonous production and subsequent exposure to degradation, so reveals the different origins of OM, delivery routes, depositional processes, and consequent degree of preservation. In lake systems, the TOC concentration can serve as an indirect indicator of the type and biomass of local vegetation and potentially reflects changes in regional precipitation (Zheng et al., 2007); higher TOC concentration can also reflect improved preservation of OM under conditions of limited oxygen availability or colder temperature (Meyers and Ishiwatari, 1993).

The bulk stable carbon-isotope composition ($\delta^{13}C$ value) is commonly applied to trace the photosynthesic pathways of various plants and thus their contribution to OM in soils/sediments. There are three biochemical mechanisms in carbon fixation, known as C_3 (also known as Calvin cycle), C_4 (also known as Hatch-Slack pathway) and CAM (Crassulacean acid metabolism) photosynthesis (Craig, 1953; Bender, 1971; Kluge & Ting,

1985). They differ in the amount of energy used, the reactions and steps during the carbon fixation process and the by-products generated therein (O'Leary, 1988 and reference therein). The C_3 pathway is the most common and operates among most plants, with nearly 90 % of the estimated 250,000 land plant species using this photosynthetic pathway (Craig, 1953); the C_4 pathway is an elaboration of the more common C_3 carbon fixation and evolved more recently (Bender, 1971); and the CAM resembles the C_4 pathway in their efficiency of concentrating CO_2, differing temporally and spatially in synthesis and respiration (Kluge & Ting, 1985). Due to their efficiency in carbon fixation, CAM and C_4 plants are more tolerant of conditions like drought, high temperature and nitrogen or CO_2 limitations. CAM plants are commonly cacti and yucca from arid environments, consisting of 7 % of plants (Dodd et al., 2002). Common C_4 plants are grass species (Poaceae) (46 % of grasses belong to C_4 plants) which are concentrated in the tropics (below latitude of 45°) (Rowan and Monson, 1999), consisting 5 % of plants (Bond et al., 2005). Virtually all trees, most shrubs, and cool-season grasses and sedges use the C_3 carbon fixation (Schefuß et al., 2003). The photosynthesic pathways are reflected by the $\delta^{13}C$ value of plant material from -21 ‰ to -35 ‰ in C_3 plants and from -9 ‰ to -20 ‰ in C_4 plants (Hesse et al., 2004). As noted by Brodie et al. (2011), the $\delta^{13}C$ value of OM has also been used for various investigations, including: (1) assessment of carbon reservoir turnover times and soil C dynamics, (2) determination of trophic levels in environmental systems, (3) primary productivity reconstructions and estimation of carbon burial rates, and (4) to understand soil mineralisation processes.

The difference between the composition of C_3 and C_4 plants can also be reflected by C/N values, which is calculated by dividing TOC to total nitrogen content (TN) in this thesis. Protein-rich C_3 plants (e.g. algae) generate OM with C/N values between 4 and 8;

whereas cellulose-rich/vascular C_3 and C_4 land plants usually create OM that has C/N ratios of 20 and more (Meyers, 1994; Sifeddine et al., 2011). This distinction arises from the absence of cellulose in algae and its abundance in vascular plants. The difference between algal and land-plant C/N source signatures is largely preserved in sedimentary OM (Meyers, 1994).

There are numerous successful applications of carbon, nitrogen, their ratios and isotopes to reconstruct the palaeoenvironment (e.g. Schwartz et al., 1986; Boutton et al., 1998; Bai et al., 2009; Russell et al., 2009; Kobayashi et al., 2011; Bai et al., 2012). For example, these parameters have been successfully used for interpreting savannah grassland (C_4) vs woodland (C_3) successions (Schwartz et al., 1986; Boutton et al., 1998; Bai et al., 2009; Bai et al., 2012). In some studies, the nitrogen pool is found to be more sensitive to changes than carbon, resulting in relatively large changes of nitrogen isotopic values. For example, Liu et al. (2006a) found the enrichment of $\delta^{15}N$ in closed lake sediments that were rich in penguin guano.

Inorganic elements are robust geochemical parameters to study many sedimentary processes. The major elements are the primary rock-forming elements Ca, Fe, K, Mg, Na with Al, O, and Si in silicate minerals and minor amounts of Mn , P, and Ti (Li, 2000). Some ratios of the major elements are good indicators of pedogenic processes and weathering (Sheldon and Tabor, 2009). Most of the trace elements are directly related to the concentrations in the soils and rocks and therefore can be applied for examining the weathering intensity, evaluating leaching and estimating their transportation from the source. Trace element modelling of sedimentary processes can offer a degree of sensitivity not typically afforded by other methods (Hatfield et al., 2010). However the author also pointed out that it is critically dependent on precise analysis of the trace element

composition of sediments. Some trace elements (e.g. Pb) have several potential sources, including natural sources (atmospheric deposition, weathering of local soil and rocks, transport from sea salt, volcanic activities and forest fires) and anthropogenic sources (smelting of ores, burning of coal and use of petroleum products containing lead) (Tomkins and Hesse, 2004). These trace elements therefore may be used to 'fingerprint' pollutants.

One of the applications of inorganic elements as bio-elements was seen in the study by Liu et al. (2006b) on a close freshwater lake in an isolated island of Dongdao Islands. The authors found the concentrations of As, Cd, Cu, Se, Zn, P and S are significantly correlated with seabird droppings and vary with their population. They also found that such geochemical characteristics were not observed in the upper sediment layer affected by cattle excrement (Liu et al., 2006b). Another study of ornithogenic sediments from Antarctica (Liu et al., 2006a) was largely unsuccessful in using such bio-elements to indicate the palaeoecology processes of penguins. A previous study of the Macquarie Marshes found that P levels were elevated in response to waterbird breeding (Cull, 2007). However the author pointed out that the sediments were not well-preserved so that P levels could not be a reliable technique to verify past breeding habits. Accordingly, the application of bio-elements for the Macquarie Marshes did not appear very promising because they are located in an arid/semi-arid area where the frequent change of water availability and flow enhances the erosion of sediments. In this study, selected core sections were analysed for K, U and Th contents as required for OSL dating (Chapter 4). Only core MMB3 was studied at higher resolution, and for a variety of major and trace elements, to aid in understanding the sediment source(s).

3.2.2.1 Methods

The isotopic composition and concentration of TOC were determined using a Carlo Erba NA1500 elemental analyzer coupled to a PRISM III or Finnigan Delta Plus mass spectrometer. All results are reported in the $\delta^{13}C$ notation in per mil relative to the Vienna Pee Dee Belemnite (V-PDB) standard. TOC was calculated on a carbonate-free basis with samples (~ 2 g each) treated with 1M HCl to remove carbonates, prior to analysis.

Major- and trace-element analysis of whole-sediment samples was conducted by X-ray fluorescence (XRF). Samples were dried and crushed to fine homogeneous powders using a TEMA chromium-steel gyratory ring mill at the University of Wollongong. For trace-elements determinations, ~ 5 g of powdered sample with 5 to 6 drops of an organic binder solution (PVC) were pressed into aluminium cups to produce pellets. The pellets were dried in an oven at ~ 60 ºC overnight. For major-element determinations, ~ 2.4 g of 1222 flux (35.3 % lithium tetraborate and 64.7 % lithium metaborate) and 400 mg of each sample were added to Pt/Au crucibles. These samples were fused in a furnace with ramping temperature from 600 ºC to 970 ºC at 7 ºC/min. Once the temperature reached 970 ºC, a pellet of ammonium iodide (NH_4I) was added to each of the crucibles to reduce the melt's viscosity. The resulting liquid of each sample was poured onto a graphite disc and pressed to make a glass disc.

The major elements determined and expressed in their oxide forms were Si, Ti, Al, Fe, Mn, Mg, Ca, Na, K and P. The trace elements determined were Ba, Ce, Co, Cu, Ga, La, Nb, Rb, S, Sc, Sr, Rh, U, Y, Zr, Hg and Zn. The detection limit was typically1 ppm for the later group. Both the major and trace elements were analysed by a Spectro Xepos XRF spectrometer at the University of Wollongong.

3.2.2.2 Results

3.2.2.2.1 Modern biota

The TOC values of the plants ranged between 41.9 to 53.8 %, varying among plants species and locations (Table 3.4). Comparatively, TN values differed much more among samples from different species and locations, from 1.1 to 4.0 %. The highest TN value was found in *Chara australis* and aquatic plants generally show higher TN values than terrestrial plants.

The $\delta^{13}C$ values of the plants were relatively similar within the same species, and were comparable to values found in assorted watershed plants and lacustrine sediments (Meyers and Ishiwatari, 1993) . However, the $\delta^{13}C$ values showed a range from about -30 ‰ in terrestrial plants to -26 ‰ in algae.

In this study, there is an increasing trend in C/N values from algae such as *Chara australis* (C/N=11) to vascular terrestrial plants such as *Phragmites australis* (C/N=30) and *Eucalyptus* sp. (C/N=48). These results are consistent with the generalised data published (Meyers and Ishiwatari, 1993; Meyers, 2003). A combination of the C/N values and the $\delta^{13}C$ values can provide more discrimination and assist in OM source identification of the sediments, as will be discussed later.

Table 3.4
TOC, TN, $\delta^{13}C$ and C/N values of modern plants.

Type of plants	Location	TOC (%)	TN (%)	$\delta^{13}C$ (‰)	C/N
Typha sp. (cumbungi)	Monkeygar Creek, Macquarie Marshes	41.9	-	-31.5	-
Eucalyptus sp.	Monkeygar Creek, Macquarie Marshes	53.8	1.12	-30.1	48
unknown sp. (buttercup)	Loudens Lagoon, Macquarie Marshes	44.0	-	-29.9	-
Ranunculus sp. (buttercup)	Killalea Lagoon, Shellharbour	47.4	2.53	-29.5	19
Phragmites australis (reeds)	Loudens Lagoon, Macquarie Marshes	47.4	-	-28.7	-
Phragmites australis (reeds)	Monkeygar Creek, Macquarie Marshes	43.0	1.45	-27.4	30
Chara australis (charophyte)	Monkeygar Creek, Macquarie Marshes	46.1	4.03	-26.6	11
Azolla filiculoides (fern)	Killalea Lagoon, Shellharbour	44.7	2	-27.0	24

3.2.2.2.2 Surface sediment samples

Samples from Loudens Lagoon and Longstowe station (Table 3.5), both of which are from the northern Macquarie Marshes, contain relatively higher OM than samples from other sites. These two sites are from the few areas where vegetation cover was retained during the drought and which were the main breeding sites for colonial waterbirds (Cull, 2007; Hogendyk, 2007). As a single breeding colony can consist of up to 40,000 birds (Kingsford and Auld, 2003; Kingsford and Auld, 2005), the potential for birds to influence the nutrient status of the soil might be large. The highest TOC value (8.55 %) is found in a soil sample from a swamp bank under a red gum tree, where the input of leaves and debris was another main contributor to the total organic matter. As organic matter tends to be better preserved in anoxic conditions (Meyers and Ishiwatari, 1993; Meyers, 2003; Peters et al., 2005), in environmental settings such as lagoons, where the sediments are covered by water and remain relatively undisturbed, the TOC will be higher. This can be seen by comparing the TOC of samples from dry lagoon/land (MRI-S2, LOLA-S1, CT-S1 and SL-C1) with sites that have remained inundated (LOLA-S2, 2LOLA-S1, LSW-S3, MC-C6). It is worth noticing that some of the mud samples (MRI-S1 and LSW-S1) collected from shallow river beds still contained relatively low level of OM. It is likely that degradation might have been accelerated due to bioturbation and by exposure to oxidation among these sediments (Meyers and Ishiwatari, 1993). Generally, the TOC values were higher in the northern marshes than in the southern marshes, indicating more organic input and/or preservation.

Table 3.5
Descriptions and some parameters of the surface sediments.

Sample ID	Location	Sample Type	TOC (%)	TN (%)	$\delta^{13}C$ (‰)	C/N
MRI-S1	Bank of a channel parallel to Macquarie River, northern MM	River mud	1.36		-26.2	
MRI-S2		Surface soil close to coring site	2.00	0.09	-25.4	22
LOLA-S1	Loudens Lagoon, northern MM	Surface soil from dry land in lagoon centre	2.07	0.15	-23.3	14
LOLA-S2		Soil near reed beds	3.93	0.22	-24.4	18
LOLA-S3		Soil at coring site	2.25		-25.7	
2LOLA-S1		Surface sediment	3.91	0.36	-26.4	11
MMB3-S1	Bora channel east of the lagoon which has remained inudated for a long time, northern MM	Surface sediment	5.50	0.49	-27.2	13
LSW-S1	Longstowe Station, northern MM	Coring site mud	1.61		-25.9	
LSW-S2		Soils from swamp bank under a red gum tree	8.55	0.31	-23.1	28
LSW-S3		Surface sediment	5.18	0.27	-24.8	19
MC-C6	Monkeygar Creek, southern MM	Surface sediment	5.36	0.33	-23.4	16
CT-S1	East side of Monkeygar Creek, end of Campsite Trail, southern MM	Surface sediment	1.80	0.22	-23.6	8
SL-C1	South Lagoon, southern MM	Surface sediment	2.85	0.24	-23.7	12

Samples vary in their TOC and TN depending on the input of organics to the sediments.Generally, high TN values were observed in samples from colonial waterbird breeding sites where bird guano had an impact on soil chemistry such as the total nitrogen content (Wait et al., 2005).

Despite the variation in the TOC and TN values, the $\delta^{13}C$ values are slightly different between samples from different sites. These values are close to the values from previous lacustrine sediments concluded by Meyers and Ishiwatari (1993), ranging from -23 to -29 ‰ although slightly more positive than the measured range of modern plants (-27.0 to -31.5 ‰) from the MM. In watercourses or lagoons with greater input of OM from algae, the $\delta^{13}C$ values tended to be more positive; whereas in sampling sites where there was greater input of higher plants, the $\delta^{13}C$ values tended to be more negative.

The C/N values of these surface sediment samples vary from 8 to 28 depending on the locations. As in these samples, TOC values are all greater than 1 %, the C/N values can be reliable indicators of OM source (Meyers, 2003). Samples collected from near the centre of the lagoon (2LOLA-S1, CT-S1, SL-C1) show C/N values lower than those closer

to the shore (LOLA-S1, LOLA-S2, LSW-S3 and MC-C6) or on floodplains (LSW-S2 and MRI-S2). Talbot and Johannessen (1992) found that C/N ratios decrease with increasing distance from shore in Lake Victoria, East Africa and inferred that it was due to the decrease in primary productivity. This might also explain the results of Macquarie Marshes.

Meyers (1994; 2003) described the $\delta^{13}C$ and C/N values of major sources of plant OM from lake sediments and suggested they discriminate the major sources of OM in lake sediments. Accordingly, the MM data (Figure 3.13) are located between those of lacustrine algae and C_3 land plants, indicating both lacustrine algae (such as *Chara australis*) and C_3 vascular land plants (such as *Phragmites australis*) are the main organic sources for these surface sediment samples.

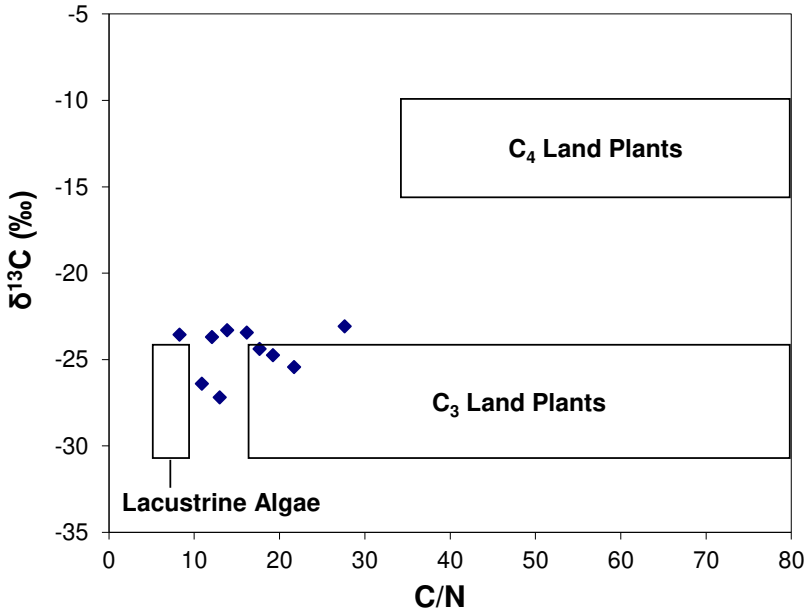

Figure 3.13. Generalised $\delta^{13}C$ and C/N values of major sources of organic matter (fields from Meyers, 2003), with the data from modern surface sediments from the Macquarie Marshes.

The trace-element data of the surface sediment samples (Table 3.6) from the XRF showed that Ba and Zr were present in high contents (100-500 ppm), followed by Sr, Rb, Zn, Ce, La, Cu, Y, Pb, Co, Ga, Nb, Th and Sn in decreasing order (from ~ 100 to ~ 10 ppm). As, U, W, Ta, Hg and Sb were found in very low levels. A significant decrease in elements whose abundances are strongly affected by weathering (e.g. Ba, Sr, Rb, U) was found among LOLA-S2 and LOLA-S3. Table 3.7 (Page 60) shows the correlation matrix of the trace elements with other proxies discussed previously in this chapter. Data are highlighted for those showing significant correlation (R^2>0.9 or <-0.9). Most of the elements, except Ce, Y, Nb and As, are correlated to certain particle sizes. Ce, La and Hg showed negative correlation to TOC while Zr showed negative correlation to TN. Only Zr, Sr, Co, Sn and W showed some correlation with the $\delta^{13}C$ values.

Table 3.6
The XRF trace-elements of the surface sediments (in ppm).

Sample ID	Ba	Zr	Sr	Rb	Zn	Ce	La	Cu	Y	Pb
MRI-S1	334	308	85	80	59	51	35	26	27	16
MRI-S2	370	369	91	86	67	85	49	31	31	18
LOLA-S1	577	405	84	56	38	51	35	24	24	13
LOLA-S2	315	377	87	69	53	48	35	35	27	16
LOLA-S3	259	347	68	53	35	35	19	23	20	11
2LOLA-S1	390	234	107	93	74	72	35	41	31	20
LSW-S1										
LSW-S2	329	211	104	81	72	29	31	33	25	16
LSW-S3	396	263	99	97	87	< 2.0	39	40	30	20
MC-C6										
CT-S1	432	236	110	102	92	58	34	38	31	21
SL-C1	338	383	87	74	57	37	26	29	27	16

Sample ID	Co	Ga	Nb	Th	Sn	As	U	W	Ta	Hg	Sb
MRI-S1	11	14	13	10	8	3	2.0	2.4	4.1	0.7	< 3
MRI-S2	18	16	15	12	7	4	2.1	1.9	0.9	< 1.0	< 3
LOLA-S1	43	9	11	8	6	7	1.8	3.1	1.2	< 1.0	< 3
LOLA-S2	22	13	12	9	7	3	1.5	2.6	< 1.0	< 0.4	< 3
LOLA-S3	< 3	9	9	7	9	2	1.2	2.6	< 1.0	< 0.3	< 3
2LOLA-S1	18	18	14	12	8	4	2.7	1.8	< 1.0	< 1.0	< 3
LSW-S1											
LSW-S2	< 7	15	12	10	7	2	2.3	0.7	2.6	0.4	< 3
LSW-S3	24	19	15	12	6	4	3.5	0.4	< 1.0	0.5	< 3
MC-C6											
CT-S1	< 8	19	16	13	7	4	3.0	0.7	1.4	0.6	< 3
SL-C1	< 3	13	12	10	5	3	1.6	2.2	2.9	< 0.4	< 3

Table 3.7
The correlation matrix of trace elements with other proxies in the surface sediment samples.

	Water Content (%)	Sand (%)	Silt (%)	Clay (%)	TOC (%)	TN (%)	$\delta^{13}C$ (‰)	Quartz	Musco-vite	Illite 1	Kaolin, BISH1 2	Ortho-clase 1	Biotite	Albite	Gyp-sum	Labra-dorite	Chlorite	Anke-rite
Ba	-.931	-.119	.892	-.561	-.496	-.157	.332	-.594	.870	-.404	.573	.861	.556	.723	.018	.723	-.536	-.536
Zr	.564	-.941	-.641	.933	-.735	-.927	-.994	.917	-.676	-.800	-.927	.303	-.935	.511	-.978	.511	-.702	-.702
Sr	-.879	.683	.920	-.995	.345	.654	.935	-.998	.938	.439	.996	.165	.994	-.063	.777	-.063	.301	.301
Rb	-.963	-.019	.933	-.641	-.406	-.058	.424	-.672	.915	-.311	.652	.806	.636	.651	.118	.651	-.449	-.449
Zn	-.998	.315	1.000	-.860	-.079	.278	.702	-.880	.997	.023	.867	.562	.857	.360	.442	.360	-.126	-.126
Ce	-.412	-.779	.322	.177	-.961	-.803	-.422	.137	.277	-.928	-.163	.971	-.183	1.000	-.685	1.000	-.973	-.973
La	.057	-.981	-.153	.613	-.980	-.988	-.794	.580	-.199	-.995	-.601	.751	-.618	.881	-.945	.881	-.969	-.969
Cu	-.954	.529	.978	-.956	.158	.496	.850	-.967	.987	.258	.960	.352	.954	.131	.641	.131	.111	.111
Y	-.858	-.282	.805	-.416	-.633	-.319	.171	-.453	.776	-.551	.429	.933	.410	.828	-.148	.828	-.669	-.669
Co	.661	-.893	-.730	.970	-.647	-.874	-1.000	.959	-.761	-.721	-.966	.184	-.971	.402	-.946	.402	-.610	-.610
Pb	-.940	-.094	.903	-.581	-.474	-.133	.355	-.614	.881	-.382	.593	.848	.576	.706	.043	.706	-.515	-.515
Ga	-.990	.109	.971	-.734	-.286	.070	.537	-.761	.959	-.187	.743	.723	.729	.548	.244	.548	-.331	-.331
Nb	-.753	-.447	.687	-.249	-.760	-.482	-.006	-.288	.652	-.690	.262	.982	.242	.914	-.321	.914	-.790	-.790
Th	-.956	-.044	.923	-.622	-.429	-.083	.402	-.653	.904	-.335	.633	.820	.616	.669	.093	.669	-.471	-.471
Sn	.784	-.798	-.840	.998	-.501	-.774	-.982	.994	-.865	-.586	-.997	.006	-.998	.232	-.873	.232	-.459	-.459
As	-.521	-.695	.437	.054	-.920	-.723	-.306	.013	.394	-.875	-.040	.993	-.060	.994	-.590	.994	-.938	-.938
U	-.999	.218	.992	-.804	-.179	.180	.627	-.828	.984	-.077	.813	.643	.800	.452	.350	.452	-.225	-.225
W	.754	-.825	-.814	.993	-.541	-.802	-.990	.988	-.840	-.623	-.992	.052	-.994	.277	-.895	.277	-.500	-.500
Ta	.967	-.489	-.987	.941	-.111	-.455	-.824	.954	-.994	-.212	-.946	-.396	-.939	-.178	-.604	-.178	-.064	-.064
Hg	.140	-.994	-.234	.676	-.959	-.997	-.842	.646	-.280	-.983	-.666	.693	-.681	.839	-.969	.839	-.945	-.945

*green high shaded areas indicate significant correlation (R^2>0.9 or <-0.9)

3.2.2.2.3 Sediment cores

As shown in Figure 3.14, the TOC and TN curves of core MMB3 exhibited similar trends with depth, increasing 20-fold from a depth around 95 cm to the surface. The bulk $\delta^{13}C$ values vary from -26.4 ‰ to -28.1 ‰, falling within the range of values found in *Chara australis* (-26.6 ‰) and *Phragmites australis* (-27.4 to -28.7 ‰), indicating the dominance of C_3 plants (Hesse et al., 2004). The C/N ratios range from 7.7 to 15.8, also falling within the range of values found in aquatic plants and emergent plants (*Chara australis* 11, *Phragmites australis* 30). These results indicate that algae and emergent plants including *Chara australis* and *Phragmites australis* were the main, and constant organic input to the sediments. The shift of $\delta^{13}C$ values to lower values may indicate the input of aquatic plants in wet years, while the shift to higher values may indicate more input of higher plants in dry years. In general, C/N ratios slightly increase from the deeper part of the core to the surface sediments, indicating the shift of organic contribution from aquatic plants in the past to higher plants in past 50-60 years. Core MMB3 was the only one of the four cores studied here that has $\delta^{15}N$ data. The $\delta^{15}N$ values along the core varied from 2.0 ‰ to 4.8 ‰ and are much lower values than those found (13.3 ‰) in ornithogenic sediments elsewhere (Liu et al., 2006a) and, which relate to trophic enrichment of ^{15}N in OM as they pass up the food chain to the consumer that excretes the nitrogen. Two small peaks of $\delta^{15}N$ at depths of 73 cm (~ 1840 AD) and 54 cm (~ 1942 AD) may relate to the input of waterbird guano. However, these data need to be further explored with the assistance of other information.

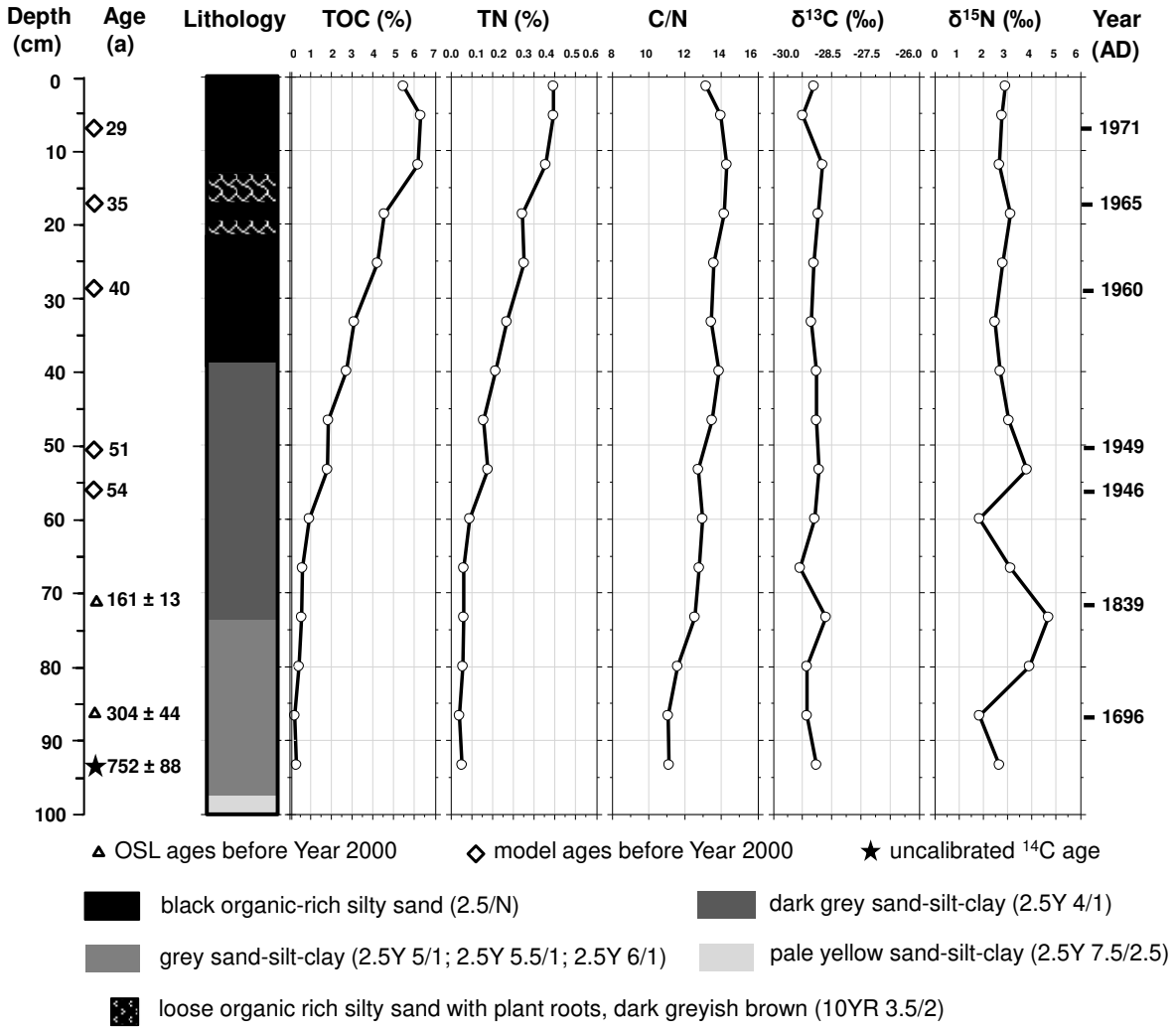

Figure 3.14. Chronology, lithology, TOC, TN, C/N, $\delta^{13}C$ and $\delta^{15}N$ of core MMB3.

The major-element data from core MMB3 (Figure 3.15) were limited to five samples. Generally from around 310 years ago onwards (~1700 AD), SiO_2, CaO and MnO decrease while Al_2O_3, Fe_2O_3, K_2O, MgO, Na_2O, SO_3 and P_2O_5 increase. The consistently low Ti/Al ratio (0.03) throughout the core profile indicated that the sediments at this site originated from a deeply weathered source area. Close inspection of the trace-element data of core MMB3 (Figure 3.16 on Page 65 and Figure 3.17 on Page 66) indicates fluctuations for many of the elements about 60 years ago (at the depth of ~ 50 to 56 cm). The pattern of changes in the trace-element data (Figure 3.16 on Page 65 and Figure 3.17 on Page 66)

match the mineralogical data (Section 3.2.1.2) and reinforce the explanation that the change of water flow after the construction of Burrendong Dam caused a change in the sediments carried and deposited in the Marshes. The trace-element data for core sediments (and surface sediments) give no indication of waterbird colonial events.

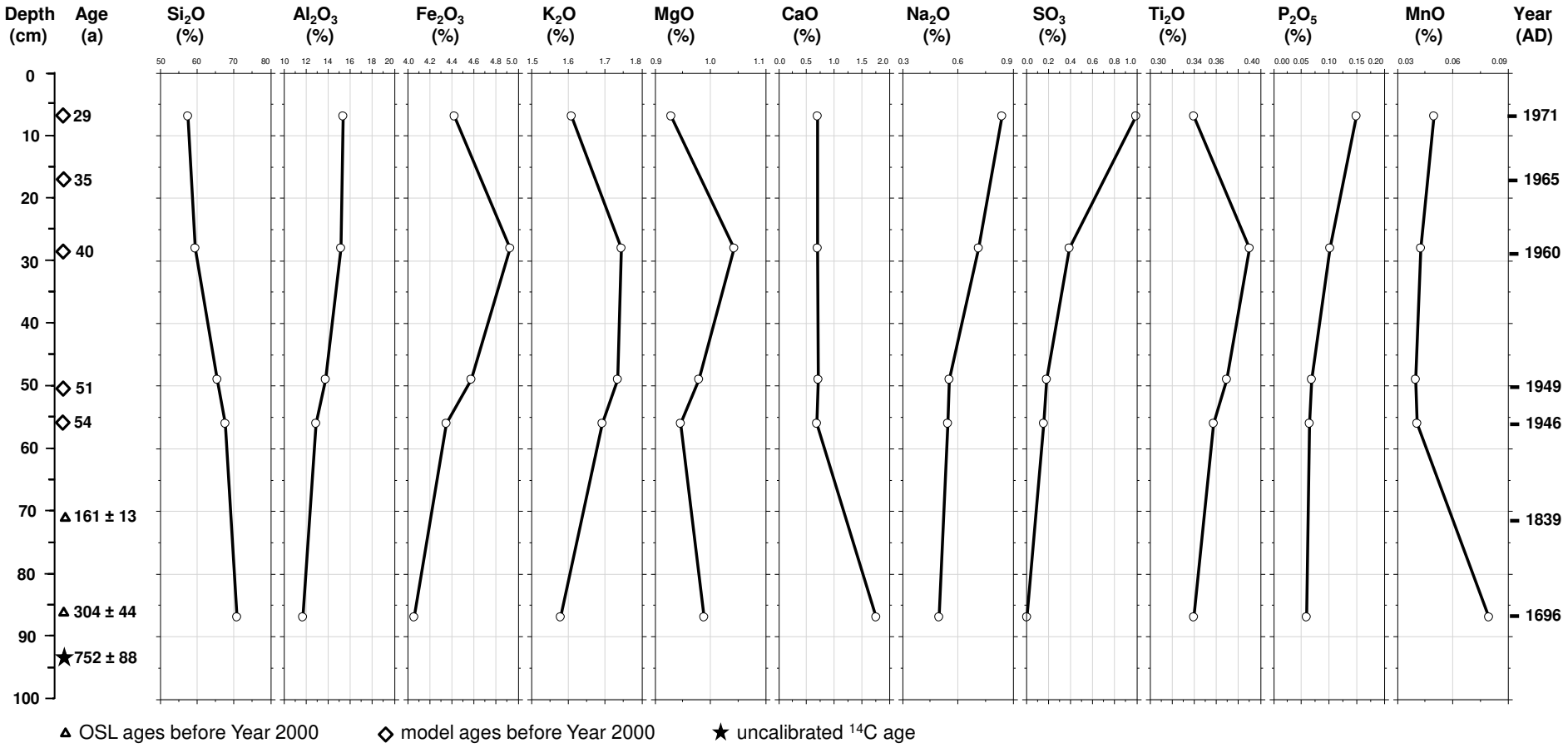

Figure 3.15. Major-element data for whole-sediment from core MMB3.

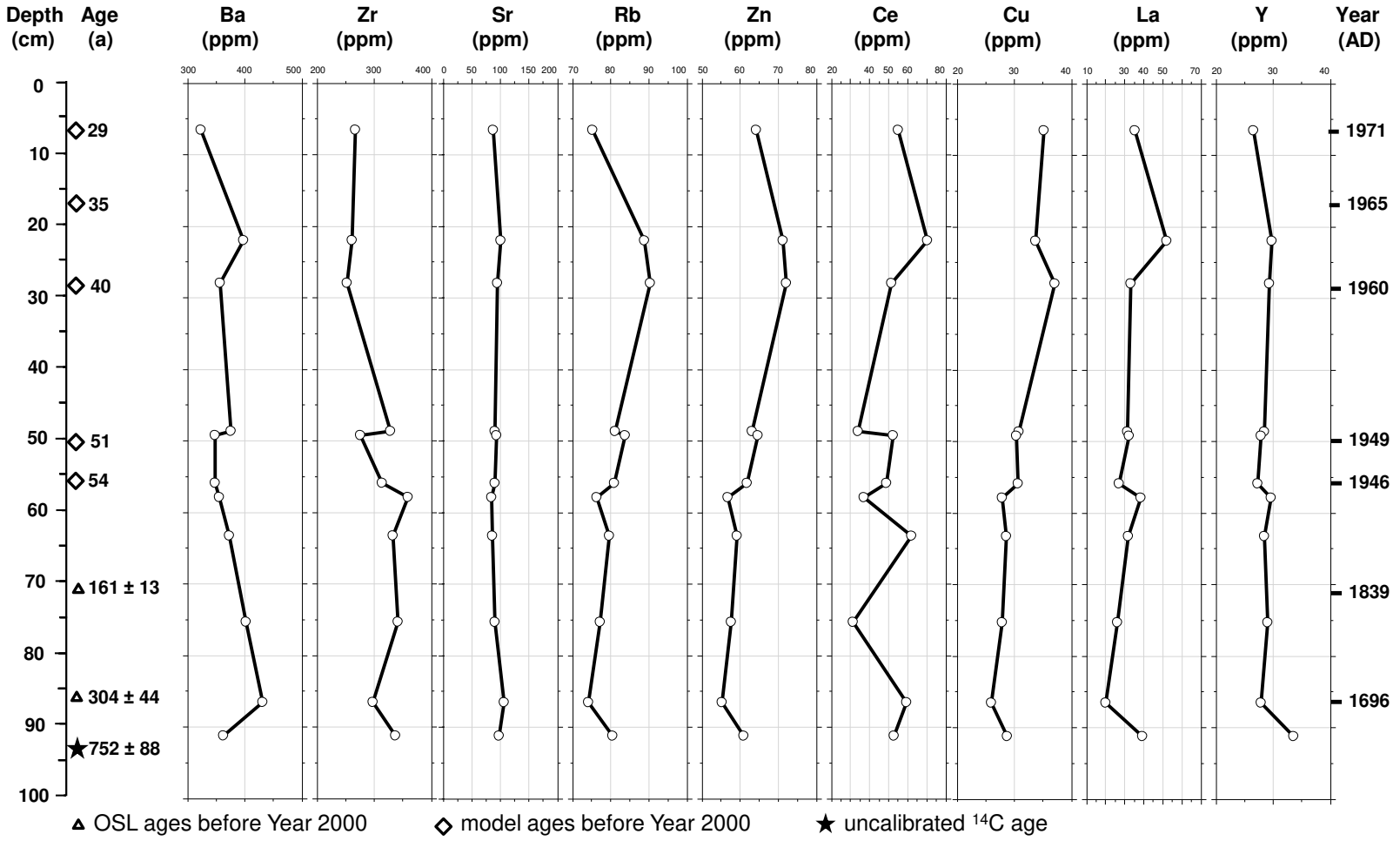

Figure 3.16. Trace-element data for whole-sediment from core MMB3.

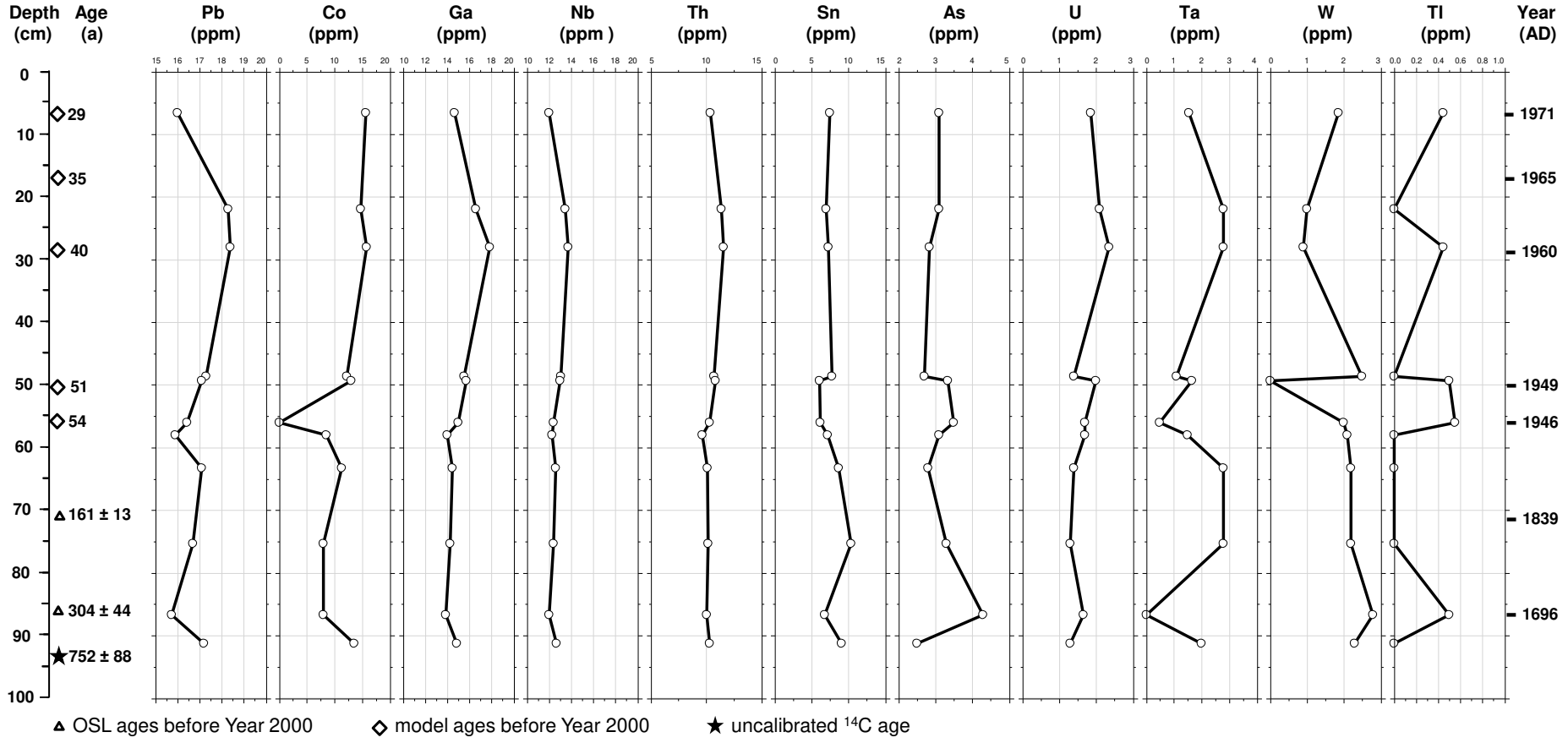

Figure 3.17. Trace-element data for whole-sediment from core MMB3.

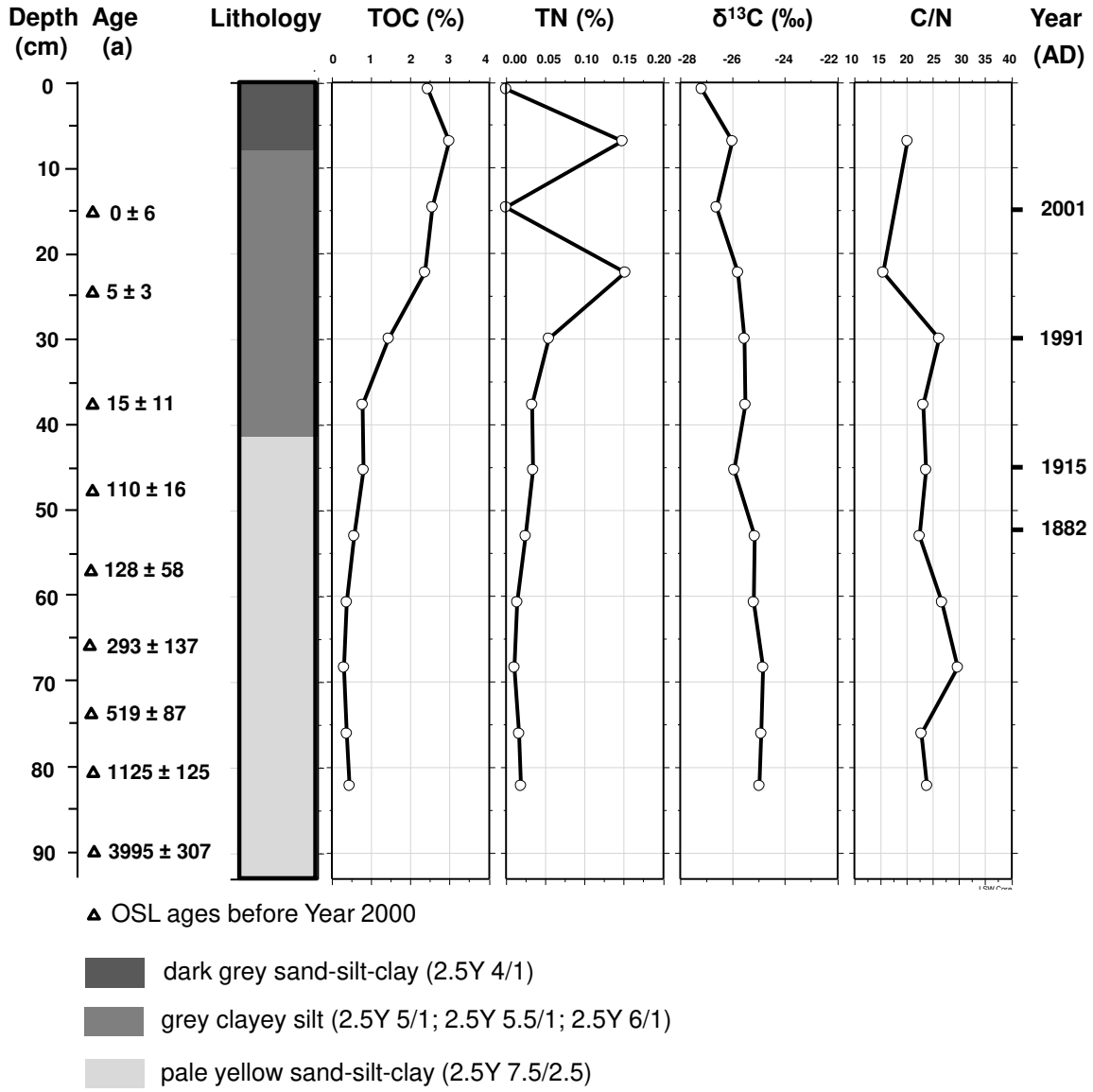

Figure 3.18. Chronology, lithology, TOC, TN, C/N and $\delta^{13}C$ of core LSW.

The TOC values of core LSW are generally 40-50 % lower than those from core MMB3, although the trend is similar showing an increase from 0.3-0.4 % at the deeper part to 2.5-3 % close to the surface (Figure 3.18). The TN curve increases gradually from 0.01 % at the base of the core to 0.05 % at 30 cm depth, with a further increase to 0.15 % at ~22 cm. The bulk $\delta^{13}C$ values are more positive than those of MMB3 but are still within the range of C_3 plants, probably due to more aquatic organic input. This is very likely because the LSW site is a swampy while MMB3 is in a water channel. The $\delta^{13}C$ values

fluctuate between -24.8 ‰ and -25.2 ‰ between 82 cm to 52 cm, then progressively change to more negative values between -25.5 ‰ and -27.2 ‰. The C/N curve showed two significant changes at depths of 70 cm (~ 415 years old) and the depth of 30 cm (~ 17 years old) and remains relatively constant from 53 cm to 30 cm (about 130 to 17 years old).

The TOC and TN values of core LOLA (Figure 3.19) increase steadily from the deeper part of the core to the surface. This is a much older sedimentary sequence than those cored from other sites, and with a major break in sedimentation at ~ 123 cm. The TOC values fluctuate slightly at around 105-60 cm (~ 2,300 to 1,000 years old), overlapping one of the TN peaks. The $\delta^{13}C$ values fluctuate between -24.4 ‰ and -26.2 ‰ from 208 cm to 108 cm, shift to -17.0 ‰ at 98 cm, and fluctuate between -23.7 ‰ and -25.1 ‰ from 78 cm to the surface. Except for the less negative value at 98 cm indicative of C_4 plants, the other $\delta^{13}C$ values are within the range for C_3 plants (e.g. Hesse et al., 2004). A significant change of vegetation type and organic input may have occurred around 2,000 years ago.

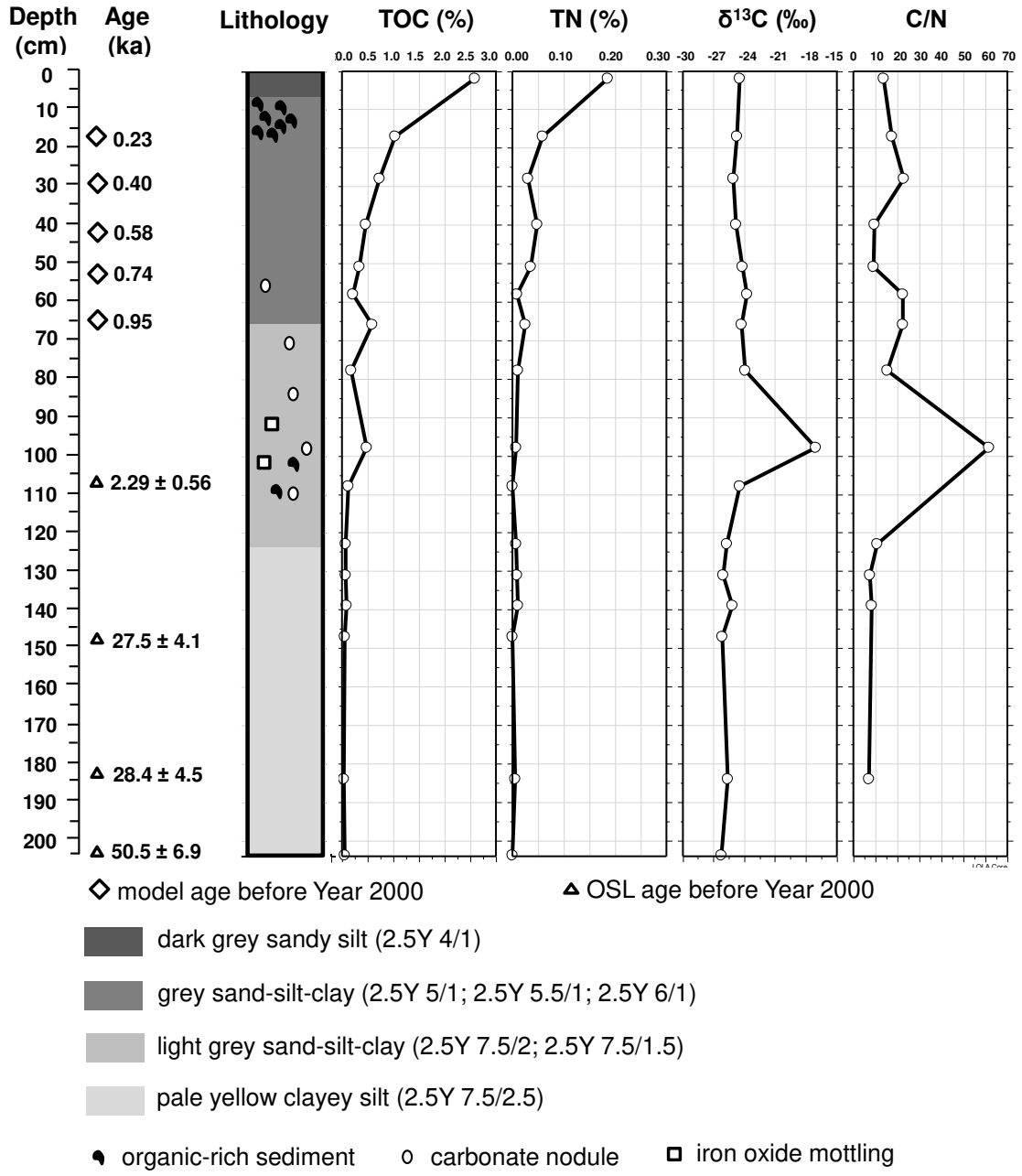

Figure 3.19. Chronology, lithology, TOC, TN, C/N and $\delta^{13}C$ of core LOLA.

The TOC values of core 2LOLA (Figure 3.20) gradually increase from 0.02 % at the base to 0.89 % at 52 cm, then increase further to 2 % at 40 cm and remain relatively steady from 40 cm to 15 cm. TOC is high (8.79 %) in the surface sediment. The TN curve shows a similar trend. The $\delta^{13}C$ values decrease within the range of C_3 plants, from -23.5 ‰ at the base to -27.2 ‰ at the surface, consistent with a shift from more aquatic plants to

higher terrestrial plants. The C/N curve fluctuated along the core and the values are close to those of core MMB3.

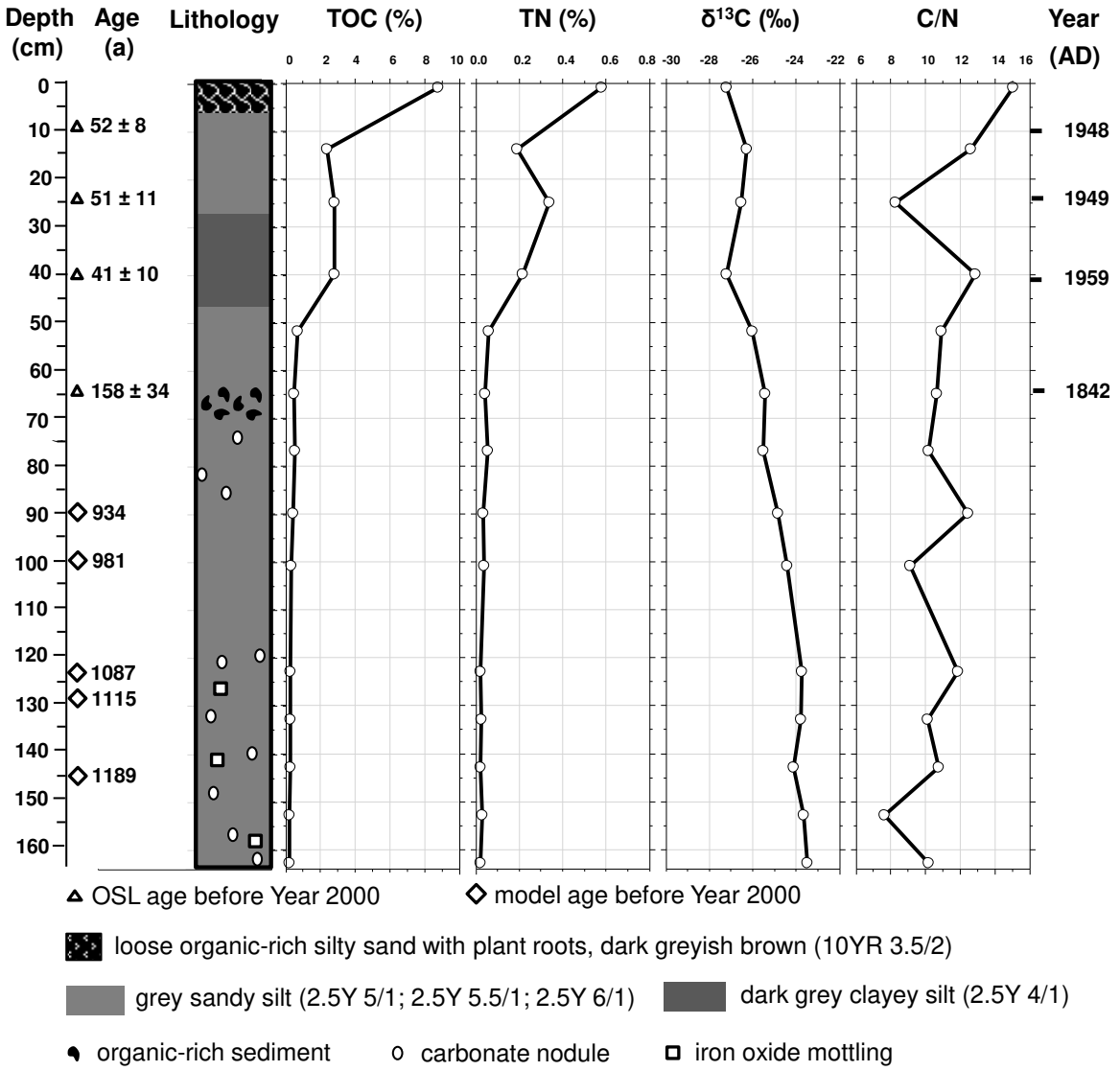

Figure 3.20. Chronology, lithology, TOC, TN, C/N and $\delta^{13}C$ of core 2LOLA.

3.2.3 Discussion and conclusions

As the Macquarie Marshes are a complex wetland ecosystem with diverse biota and variable climate, none of the physical or geochemical proxies alone can explain the changes/trends in the marshes' environment. In this section, data from several proxies will

be assembled for analysis and interpreted, within limits, to represent and reconstruct some aspects of environmental change.

3.2.3.1 Modern biota

The analysis of the TOC, TN, $\delta^{13}C$ and C/N values from modern plants seems promising for the identification of OM sources in the MM sediments. In particular, the $\delta^{13}C$ and C/N values are distinguishable between different species of terrestrial/aquatic plants and algae. Bird guano samples were not collected for analysis in this study. However in a previous study of sediments in the Macquarie Marshes, Cull (2007) also found that OM and phosphorus were poorly preserved and would not be a reliable technique to verify breeding habits. A study of the ornithogenic sediments from Antarctica also found that the $\delta^{13}C$ values are close to those in fresh lake sediments and are not influenced by penguin guano and thus cannot be used as evidence for the influence of guano on the sediments (Liu et al., 2006a). The OM preserved in the Macquarie Marshes sediments is probably more indicative of the surrounding vegetation than of waterbird guano.

3.2.3.2 Spatial variation (surface sediments of the northern and southern MM)

The lithology, sedimentology, mineralogy and elemental analysis data show that the surface sediments from both the northern and southern MM originate from the same source – silty fluvial sediments transported not far from the upper main stream. The average flow velocity on the lower Macquarie River is 0.25 m s^{-1} at high flow conditions and 0.054 m s^{-1} at low flow conditions (Yonge and Hesse, 2009), both of which are relatively low compared to most fluvial systems (Yonge and Hesse, 2009 and references

therein). As reflected by a Hjülstrom (1935) diagram, only clay, silt and a small fraction of fine sand will be transported in suspension at such flow velocities. These particular size fractions in most of the samples are mainly composed of plant roots/debris, seeds/oospores and a few fragments of clay/silt that are probably formed as a result of wetting and drying cycles (Yonge and Hesse, 2009). In this study, the major and trace elements (e.g. P, S) were also not capable of indicating past bird nesting as their concentrations were not only affected by the material source, but also by other factors such as the dilution, particle-size effects and degree of preservation (Liu et al., 2006a; Cull, 2007).

However, the water content, TOC, TN, $\delta^{13}C$ and C/N values show greater variation among sites. Generally, the $\delta^{13}C$ values of surface sediment samples from the southern marshes (MC, SL sites) are higher than those from the northern marshes, reflecting different vegetation types. As is observed in the field, the southern marshes are drier than the northern marshes; river red gum is the main vegetation type in the south while river red gum (*Eucalyptus* sp.) and reed beds (*Phragmites australis*) dominate in the north. The combination of the $\delta^{13}C$ and C/N values has been successful in distinguishing various sources of OM contributed by land/aquatic plants at each sampling site. Kingsford (2000) concluded that the major sources of organic matter in Australian floodplain wetlands include materials carried by water flow, such as accumulated eucalypt leaf litter, aquatic macrophytes from the last filling, and/or terrestrial plants that colonise dry wetlands. From the above discussion, we can infer that in the Macquarie Marshes the main source of OM preserved in the sediments is from the accumulation of terrestrial/aquatic plants from the surrounding environment rather than due to transportation by water flow. This will be further explored using molecular-level organic markers in Chapter 5.

3.2.3.3 Temporal variation (Core analysis from northern marshes)

The four cores from the northern marshes studied here represent different environmental settings, sedimentation and importantly, a variety of time scales.

Core MMB3 is close to the main channel (Bora Channel), but is the most northerly (i.e. downstream) of the four cores. Sedimentation at this site depends on floods and thus is more sensitive to the variation of the flow within the Marshes. This core covers a time span of the last ~750 years, with good chronological coherence. The preservation of pebbles in this core likely indicate a major flood around 300 years ago . Sedimentation rates reflect the 'Dry (1895-1946 AD)-Wet (1947-1978 AD)-Dry (1979 AD onwards)' climate pattern reported by Hogendyk (2007). In addition, the construction of Burrendong Dam (1946-1967 AD) is recorded in the sediments by the variation of particle size, mineral composition and thus elemental composition and organic proxies.

Core LSW is closest to the main channel (Bora Channel) and south of core MMB3. This site receives more sediment during dry years when the flow rate is slower. Therefore it provides higher resolution on the dry years, in particular the past 30 years. It also records the flood around 300 years ago with increase of sand fractions. Despite the poor preservation of OM, the variation of the $\delta^{13}C$ and C/N values reveals the change of dominant vegetation from aquatic plants/algae to more terrestrial plants around 120 years ago (upon European arrival).

Core LOLA and 2LOLA are in the southwest of the northern marshes and far from the main channel (Bora Channel). Despite their location close to the Bypass Channel which was constructed in 1972 AD, sediments in both cores seem to be rarely impacted. It is likely that the sediments delivered by this small tributary and deposited at these sites are much less than transported by heavy floods in the Marshes. Therefore the sediments

deposited in these two sites are older compared to those from the MMB3 and LSW sites. The LOLA site is adjacent to an elevated area; therefore it receives less sediment than the 2LOLA site. It functions as a lateral pondage receiving water only after other areas within the marshes have been inundated.

Core LOLA spans the longest record among the four cores dated, covering the last ~50 ka. It covers the important intervals like the Last Glacial Maximum (LGM), the mid-Holocene when the Marshes were established, the big dry period in 2-1.5 ka and the most recent flood around 0.3 ka. The OSL dating results (Chapter 4 for detail) show a large hiatus between 27.5 ka at 149 cm depth and ~ 2.3 ka at 108 cm depth, covering the time when the Macquarie Marshes were formed in the mid-Holocene (Herron et al., 2002). The older sediments are very distinctive with pale yellow colour and low abundance of TOC and TN. The (local) formation time of the Macquarie Marshes may occur at the layer where the sediment colour changed from pale yellow to grey. The sedimentation rate is relatively low in this sampling site compared to the other three sites (further discussed in Chapter 4, Section 4.5.3.5.3). One explanation for this, at least for the upper part (less than 1,000 years old), is that the LOLA site was a lagoon system with low sedimentation. It is also likely that the dry period (at ~ 2 ka) led to sediment deflection, at this site, prior to establishment of marsh sedimentation. The bulk organic proxy $\delta^{13}C$ and C/N values showed significant peaks at ~ 2.1 ka likely due to the dry period demonstrated by the presence of carbonate nodules and iron oxides in the core. A GIS-based vegetation map at the LGM showed that this area was covered by shrub woodland (Ray and Adams, 2001), which accords with the $\delta^{13}C$ and C/N values at the deeper part of the core. The shift of the $\delta^{13}C$ values in the upper 80 cm may be due to a change of vegetation or relative proportions of plant species. However, the formation of marshes at 8-6 ka did not

significantly impact the bulk C and N proxies as only a small peak was observed in the $\delta^{13}C$ value. At this stage, it is hard to explain the fluctuation of particle size fractions and the C/N curve in the upper part of the core (< 2.1 ka) and these will be further explored with organic markers in Chapter 5.

Core 2LOLA appears similar to cores MMB3 and LSW at its shallower depths and is more like core LOLA at deeper levels. Although the OSL dating did not provide high-resolution ages for the upper 40 cm and base 50 cm (depth of 90 cm to 160 cm), this sampling site received more sediment in these two depositional periods. It records more information of the dry period in ~ 2-1.5 ka with abundance of carbonate and iron oxides as well as significant changes in mineralogy. The flood around ~ 300 years is also recorded in this core. Like core MMB3, it also reveals the 'Dry-Wet-Dry' climate pattern in the past ~ 110 years.

The aggregate of the four cores provides a broader chronological record of the Macquarie Marshes from ~50 ka years ago to the present, spanning the pre-formation, formation and deterioration of the Macquarie Marshes. The environmental changes in this area revealed by the multi-proxies will be further discussed in Chapter 5 with the organic biomarkers.

In summary, the physical and geochemical proxies studied in this chapter offer a general view of how this ecosystem has responded to environmental changes and how such processes have been recorded in the sediments. The contribution of waterbird guano to OM in the sediments is far less than those from vegetation/algae. Further detailed information is needed to reconstruct the palaeoenvironmental changes and this will be further explored in the organic geochemistry chapter (Chapter 5).

CHAPTER 4 OSL DATING

Establishing a reliable chronology has always been a key element in Quaternary research. Establishing the timing of geological changes, together with other parameters and records such as biomarkers and climate proxies, will assist in tracing and reconstructing the environmental history. This is particularly useful when the historical record is sparse or insufficient (Gale, 2009).

4.1 Choice of dating techniques for MM samples

The significant milestone in development of dating methods is the discovery of the decay of radioactive elements during and immediately after the Second World War and the first radiocarbon dating laboratory established at the University of Chicago in 1948., which formed a basis for dating (Walker, 2005). Since then, dating methodology and technology have undergone dramatic development In his book, Walker (2005) reviewed the development of dating techniques with a focus on the 1950s onwards: During the 1950s and 1960s, other radiometric methods were developed with the technological progress and the increasing understandings of the nuclides and their decay process. In the 1960s and 1970s the amino acid geochronology technique was developed with advances in molecular biology. The technological innovations in the last two decades of the twentieth century led to a further expansion in the range of dating techniques and significant improvements in analytical precision. The development of accelerator mass spectrometry (AMS) not only revolutionised radiocarbon dating but also the technique of cosmogenic nuclide dating.

The various dating techniques applicable to the study of Quaternary were divided into two groups (Walker, 2005): numerical dating methods and relative dating methods.

The numerical dating methods, "mainly involve radiometric dating methods, such as radiocarbon dating, long-lived and short-lived radioactive isotope dating and cosmogenic exposure dating". Relative dating methods "determine the age by grouping sedimentary horizons, fossils, artefacts, etc., and ranking them in terms of relative order of age". Some of these methods are based on the principles of stratigraphy where relative age can be determined by the superposition of stratigraphic units in a geological sequence; others use the degree of time-dependent degradation or chemical alteration on rock surfaces, in soils or in fossils, to establish the relative order of age (Walker, 2005). The dating techniques that are most commonly used in Quaternary studies were summarised and listed in Figure 4.1 (Walker, 2005).

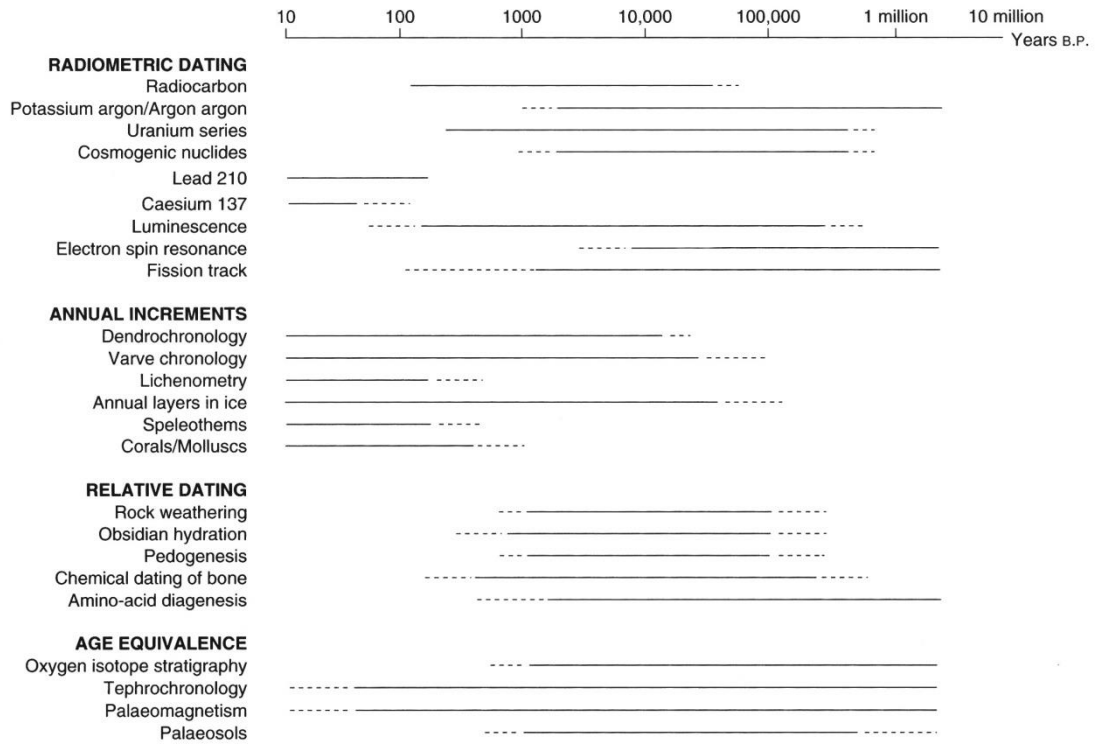

Figure 4.1. Quaternary dating techniques (Walker, 2005).

This thesis focus on the Late Quaternary timescale especially the last 2,000 years. Among the radiometric dating methods listed in Figure 4.1, radiocarbon, Lead-210 (^{210}Pb), Caesium-137 (^{137}Cs) and luminescence dating are appropriate to the timescale of interest. Radiocarbon dating can date material from 100a BP to about 50,000a BP with the use of shells, wood, charcoal and bones (e.g. Hormes et al., 2009; Hua, 2009). Some studies conduct radiocarbon dating methods on whole sediments and basically date the bulk organic materials (e.g. Watanabe et al., 2007; Long et al., 2011). As most of these samples have more than one organic contributor (including reworked material), the errors in dating bulk organic material may be significant (Brock et al., 2010). Radiocarbon dating can also be applied to specific organic fractions or compounds (e.g. Smittenberg et al., 2002; Ohkouchi and Eglinton, 2008). In such case, radiocarbon ages from organic biomarkers may be particularly useful. However, because these compounds exist in sediments in trace amounts (10-1000 ng/g), their extractions from a 2-cm thick slice of cored sediment may be insufficient for radiocarbon dating. In addition, bioturbation or penetration of plant roots in these wetland ecosystems may lead to disturbance of the sediment sequence and the downward movement of younger sediments thus causing errors in dating.

Measurement of ^{210}Pb in conjunction with fallout ^{137}Cs is the most common approach to determining a sediment chronology spanning the 'modern' period (last 100 years) (e.g. Madsen et al., 2005; Gale, 2009). The traditional radiocarbon, ^{210}Pb and ^{137}Cs dating methods are not able to fully date the period from 100 to 250 years which spans the period of European settlement in Australia and potential accompanying changes in landscape function and sediment erosion.

Luminescence methods appear to be the most suitable dating technique for the MM samples, because it may be used from ~50a BP to about 300,000a BP (Lian & Roberts,

2006). Given the ubiquity and abundance of quartz in sedimentary environments, the optically stimulated luminescence (OSL) dating technique has the potential to bridge the gap between other dating methods and provide chronological continuity. Recent advances in instrumentation and analysis methods have enabled the OSL dating technique to date fluvial and alluvial material with less than 10 years (e.g. Ballarini et al., 2003; Madsen et al., 2005; Page et al., 2007; Rustomji and Pietsch, 2007; Pietsch, 2009). The OSL signal of the grains is highly dependent on their bleaching and thermal history before burial, which is related to the environment of transportation and deposition. As such, the luminescence characteristics of the grains also provide information about sediment transport and depositional history. Moreover, OSL dating materials (quartz grains) are readily extractable from most sediment.

This thesis mainly uses the OSL dating. One ^{14}C date for bulk organic matter for sediment at 95 cm depth in core MMB3 was analysed by the ANTARES facility at the Australian Nuclear Science and Technology Organisation (ANSTO) (Fink et al. 2004). The age is an uncalibrated radiocarbon age rounded according to Stuiver and Polach (1977). It is used as independent age control for the OSL ages. The concentrations of ^{137}Cs were obtained from high-resolution gamma spectrometry at the CSIRO Land and Water Radionuclide Laboratory at Black Mountain, Canberra (Olley et al., 1996). It assists independent age control of the OSL ages that are less than 100 year old.

4.2 Introduction to the OSL dating technique

4.2.1 Theory of OSL dating

Optically stimulated luminescence (OSL) dating is a radiation-exposure dating technique, by which a chronology is obtained through the measurement of the cumulative energy of nuclear radiation absorbed by the minerals of interest, such as quartz and feldspars (Huntley et al., 1985; Aitken, 1998). The technique is based on the fact that natural minerals have structural impurities or defects which can absorb and store ionizing energy from radiation emitted from their surrounding environment (Aitken, 1985). These ionizing energies generate free charges that are subsequently trapped and accumulated within the crystal defects. Once a mineral is exposed to sufficient light (e.g. sunlight), or is heated to a high temperature (e.g. ~500 ºC), some or all of these trapped charges (or stored energies) will be released, which is accompanied by light emission, so-called luminescence. For sediments, exposure to daylight is the process that resets ("bleaches" or "zeroes") the luminescence clock. After burial, the minerals are hidden from light and subjected to environmental radiation again. The longer the material is buried, the more charges are trapped and, thus, more luminescence signal will be released once it is stimulated (Figure 4.2). By measuring the energy stored in the mineral, together with the radiation received per year, the time elapsed since the daylight exposure can be determined.

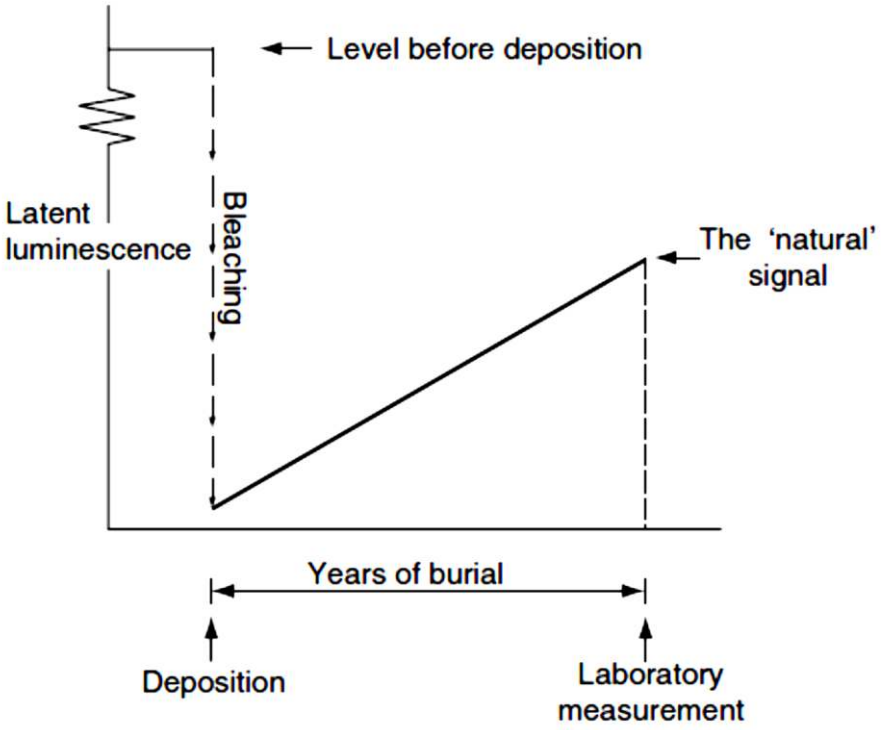

Figure 4.2. Simplified schematic diagram of the process of luminescence dating(Feathers, 2008). (Latent luminescence refers to the accumulation of trapped charge, while 'bleaching' can be from exposure to either light or heat.)

An optical age can be derived from:

$$Age(a) = \frac{D_e(Gy)}{\dot{D}(Gy \cdot a^{-1})}$$

where D_e is the equivalent dose (in Grays) which is the laboratory dose of radiation that produces the same intensity of OSL as did the environmental radiation dose; $\dot{D}$ is the dose rate either measured directly or calculated from knowledge of the natural radioactivity (Aitken, 1985; 1998).

4.2.2 OSL dating materials

The most widely used minerals in OSL dating are quartz and feldspar, both of which are the most common occurring minerals in the natural sedimentary environment (e.g. Aitken and Smith, 1988; Murray and Roberts, 1998; Duller, 2003). Quartz and feldspars differ in their chemical composition and structure (Götze et al., 2001). As is shown in Figure 4.3, quartz is composed of Si and O atoms with a tetrahedral structure. The two basic types of defect within quartz are intrinsic defects related to structural imperfections such as missing oxygen or silicon atoms and extrinsic defects related to impurities such as the replacement of Si atoms with Al (Götze et al., 2001; Bøtter-Jensen et al., 2003). In comparison, feldspars are alumina-silicate minerals composed of AlO_4 and SiO_4 tetrahedral units, with the oxygen atoms being shared between adjacent tetrahedral (Götze et al., 2001; Bøtter-Jensen et al., 2003). Elements such as K, Na and Ca can substitute for Si or Al, and therefore affect the luminescence emission (Bøtter-Jensen et al., 2003).

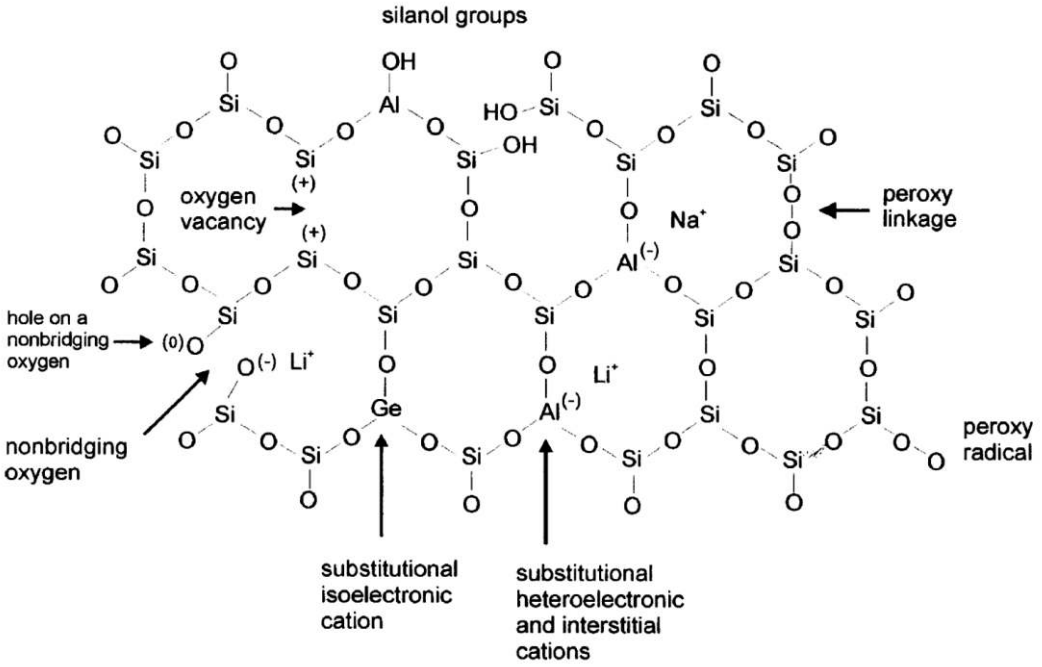

Figure 4.3. Structure of quartz and common defects.(from Götze et al., 2001)

Although the first OSL measurements were made using quartz (Huntley et al., 1985), in the 1990s feldspar studies became more common because the stimulation can be achieved using infrared (IR) light (Hütt et al., 1988), which is relatively cheap. Compared to the quartz OSL signal, the luminescence emitted from feldspar is usually much more intense and saturates at a much larger radiation dose (Aitken, 1998), making it preferable for dating both very young and very old samples. However, when dating feldspar, anomalous fading—refers to the loss of electrons from traps that are expected to be thermally stable at ambient temperature over geological time, to other defects and centres in the crystal lattice—usually causes age underestimation (Wintle, 1973; Aitken, 1985), while dating quartz appears not to have the same difficulty. In the last decade, quartz OSL dating has been widely used (Lian and Roberts, 2006), mainly due to the introduction of halogen lamp stimulation sources and then later blue light emitting diode sources (Bøtter-Jensen et al., 2003), and the development of the single-aliquot regenerative-dose (SAR) protocol (Murray and Wintle, 2000).

4.2.3 Methods for determining equivalent dose

Two methods have been widely used to determine the equivalent dose using quartz OSL: single-aliquot and single-grain. In the single-aliquot method, many quartz grains (from tens to hundreds of grains) are mounted on 10 mm-diameter stainless-steel discs and measured simultaneously. In the single-grain method, individual quartz grains are measured separately.

4.2.3.1 Single-aliquot method

The SAR dose procedure is one of the most widely used approaches to determine the equivalent dose (Murray and Wintle, 2000; 2003). For the MM study, the aliquots were measured using a SAR procedure as listed in Table 4.1. Each aliquot was firstly preheated to a temperature T (usually from 160 to 300 °C) for 10 s (Step 2) to remove any unstable signals, before measuring the 'natural' OSL signal (L_n) at 125 °C (Step 3) to avoid re-trapping of charge at the 110 °C thermal luminescence peak and to increase the rate of OSL signal decay (Murray and Wintle, 2000). After that, a small test dose was given (Step 4), and the sample was then preheated to a lower temperature (Step 5) before the test dose signal (T_n) was measured (Step 6) to monitor the sensitivity of the natural signal. Then a 'hot' bleaching (an OSL measurement at a temperature higher than the preheat temperature) was conducted to minimise recuperation (the effect of thermal charge transfer from shallow, light-insensitive traps to deeper light-sensitive traps (Aitken and Smith, 1988)) for the next steps for young samples. Such cycles were then repeated by applying different laboratory doses (usually 5-6 points) to a constant dose-response curve

(Step 7). A sensitivity-corrected dose-response curve is usually constructed by giving the smallest dose first, and then giving increasing doses up to some larger value that is greater than the expected natural dose (Wintle and Murray, 2006). Then a measurement is obtained when no dose is given (Step 8) and then one of the dose points is repeated (Step 9). An IR depletion test was conducted to check the purity of quartz, or contamination of feldspar grains, by repeating another recycling point but incorporating an IR bleaching before OSL measurement (Step 10). The natural dose of the sample can be determined by interpolating the sensitivity-corrected natural signal (L_n/T_n) onto the dose response curve (L_i/T_i).

Table 4.1
Generalised quartz SAR protocol (Murray and Wintle, 2000; 2003).

Step	Treatment	Observed
1	Give dose[a], D_i	
2	Preheat[b] (160-300 ºC for 10s)	
3	Optically stimulate[c] for 40s at 125 ºC	L_i[d]
4	Give test dose, D_T	
5	Cut-heat[b] (160-300 ºC)	
6	Optically stimulate[c] for 40s at 125 ºC	T_i[d]
6*	Optically stimulate[c] for 40s at > preheat	
7	Repeat Step 1 to 6(6*) for 5-6 increasing regeneration dose points	
8	Repeat Step 1 to 6(6*) for zero dose point as recuperation test	
9	Repeat Step 1 to 6(6*) at the lowest regeneration dose point as recycling test	
10	Repeat Step 1 to 6(6*) at the lowest regeneration dose point as IR depletion test	

[a] For the natural sample, i=0 and D_0 is the natural dose
[b] Aliquot cooled to <60 ºC after heating. In Step 5, the TL signal from the test dose can be observed, but it is not applied in routine applications.
[c] The stimulation time is dependent on the stimulation light intensity and wavelength (e.g. 40 s for blue light diodes, 100-125 s for lamp-based green light sources).
[d] L_i and T_i are derived from the stimulation curve, typically the first 1-10 s of initial OSL signal, minus a background estimated from the last part of the stimulation curve.
6* Only applied to 'young' (<50 yr old) surface sediment samples.

As shown in Table 4.1 (Page 87), there are three different thermal treatments in the SAR protocol, including preheat for the regenerative doses and cut-heat for the test doses. The main purpose of the preheat for the regenerative doses is to remove charge from thermally unstable but optically sensitive traps that are empty for natural samples but are filled during laboratory irradiations, and to transfer charge from the thermally unstable traps to the deep OSL traps (Wintle and Murray, 1999). The cut-heat for test dose is usually set at a temperature high enough to remove any unstable signals that may interfere with the OSL measurement, but kept low and short enough to minimise any additional heat-induced sensitivity changes. To determine the most appropriate preheat temperature, a preheat plateau test is usually conducted. This test involves measuring the D_e values using different preheat temperatures ranges from 160 to 300 °C with 20 °C intervals before measurement of the natural signal (L_n) or regeneration dose response (L_x). The best preheat temperature lies within a preheat temperature range that produces consistent D_e values, the so-called preheat plateau (Murray and Wintle, 2000). Due to the limitation of dating materials in the samples in this study, the preheat plateau tests were conducted on naturally bleached and laboratory dosed quartz samples that were used for dose recovery tests (further discussed in Section 4.6.1.3.5).

The reliability of the SAR protocol can be tested by a number of internal checks during the measurement cycles in the SAR sequence. These internal checks include:

(i) A recycling ratio test, where two regenerative-dose points of equal dose value are measured and compared. The repeated dose is usually chosen to be identical to the first (given after measurement of the natural signal) since the sensitivity change is usually found to be progressive and thus the first and last measurements will give the widest

spread in sensitivity change. If the ratios of these two sensitivity-corrected dose points are within ±10 % of unity, the test doses are considered adequately accounted for by the sensitivity changes (Murray and Wintle, 2000).

(ii) A recuperation test, where the signal at zero dose-point is measured and expressed as a proportion of the natural signal. More detailed information concerning recuperation is in Appendix A1.2. Murray and Wintle (2000) suggest if this value exceeds 5 %, recuperation is considered to have occurred as a result of the previous irradiation, optical stimulation or preheating.

Apart from the thermal treatment, the effective choice of test dose size is another controversial issue. Earlier applications of the SAR protocol suggested that the test dose should be kept small with respect to the natural dose to avoid recuperation effects (Murray and Roberts, 1998). However, for very young and/or dim samples, it has been found it is better to use a larger test dose to increase the strength of the test dose signal (Murray and Wintle, 2000).

Finally, after the above experimental conditions were determined, the validity of the SAR protocol can be tested using a dose recovery test, which involves giving a known dose to bleached aliquots and then measuring these aliquots as 'natural' samples using the SAR protocol (Murray and Roberts, 1998). Although an unsuccessful dose recovery may indicate that the measured D_e values are unreliable, a success in dose recovery does not necessarily guarantee a reliable estimation of the natural dose.

4.2.3.2 Single-grain method

The SAR protocol has been applied not only to the single-aliquot but quite robust results have also been found using single grain measurements (e.g. Murray and Wintle, 2000;

Jacobs et al., 2006b; Wintle and Murray, 2006; Rhodes et al., 2010). The steps are similar except they are applied to individual single grains instead of single aliquots. The ages obtained for the Macquarie Marshes sediments in this thesis mainly rely on the single-grain method. The reasons for this are discussed in the following section.

4.2.4 Application of the OSL technique to date young sediments

In the earlier work, Aitken and Smith (1988) pointed out that recuperation might be the limiting factor in dating young material. In the 1990s during the focus on feldspars, there were some successful applications to date modern or young feldspars (e.g. Ollerhead et al., 1994; Wolfe and Ollerhead, 1995). Dating very young (<500 years old) OSL quartz samples has only become popular since the late 1990s (e.g. Olley et al., 1998; Ballarini et al., 2003; Madsen et al., 2005; Ballarini et al., 2007; Page et al., 2007; Rustomji and Pietsch, 2007). These studies provide new insights for environmental settings and fill a gap in the timescale where other traditional geochronological dating techniques are limited. Analysis has been undertaken on both single-aliquot and single-grain scales from a great variety of environmental settings. These young samples include alluvial and fluvial sediments mixed with partially-bleached grains and fully bleached grains, well-bleached aeolian inland deposits, and coastal dune and marine deposits also composed of fully bleached wind-blown sediment grains (e.g. Murray and Clemmensen, 2001; Ballarini et al., 2003; Madsen et al., 2005; Ballarini et al., 2007; Page et al., 2007; Rustomji and Pietsch, 2007; Hu et al., 2010). Madsen and Murray (2009) reviewed and summarised studies on coastal and marine deposits which received sufficient light exposure before burial and found encouraging young ages. Despite some successful applications in single aliquots with very high precision and good agreement with known age (e.g. Ballarini et al., 2003;

Hu et al., 2010), most of the studies are based on the single-grain analysis (e.g. Ballarini et al., 2007; Page et al., 2007; Rustomji and Pietsch, 2007). The main advantage of single grains for OSL dating is that heterogeneous bleaching within a sample may be recognised through dose-distribution analysis. Comparatively, single aliquots will mask the variability caused by incomplete bleaching which is usually the case for alluvial and fluvial sediments.

Pietsch (2009) reviewed recent work in dating young materials and indicated three challenges with the OSL technique. Firstly, young samples usually give low radiation doses which require carefully choice of dating material and an analysis procedure to achieve detectable luminescence signals and to avoid inherent risk of age overestimation. Secondly, the raw data given by young samples require a more appropriate method to calculate the statistically representative luminescence value. Thirdly, among Australian samples, there are very few truly 'known age' samples in the 0-500 year age rage to compare with OSL dating. In particular alluvial and fluvial sediments have proved more difficult to date than aeolian sediments because the former are much less likely to be adequately bleached by exposure to sunlight prior to burial (Olley et al., 1998). As summarised by Rittenour (2008), partial bleaching (zeroing) of the luminescence signal prior to deposition in fluvial environments is due to a number of reasons, including attenuation of light through the water column (enhanced by increased suspended sediment concentrations), water depth, the mode of sediment transport (suspension, saltation or bedload) and transport distance. However, steady development has been seen in instrumentation to reduce the sample size to individual grains (Bøtter-Jensen et al., 2000) and modified analytical protocols introduced to improve the grains' sensitivity and eliminate contamination (e.g. isolating the well-bleached fast component of the quartz

OSL signal using a curve-fitting procedure) (Murray and Wintle, 2000; Olley et al., 2004; Cunningham and Wallinga, 2009). Previous research has also highlighted the importance of applying rigorous statistical data analysis and age models to obtain the most representative dose value (Roberts et al., 2000). All of these efforts are made to distinguish the true D_e for different age groups for age calculation and to improve the reliability and precision of OSL dating results.

In the review by Madsen and Murray (2009), they noted that a time-dependent dose rate is also a problem specific to dating young sediments. Alternations of sedimentary environments such as changing water content, sediment matrix or sample depth will results in a change in dose rate with time and therefore lead to an overestimate/underestimate of the real age.

In the review by Rhodes (2011), the author pointed out that although dating in fluvial contexts can be problematic, owing to low quartz sensitivity and incomplete zeroing issues; dense sampling strategies and appropriate use of the single-grain OSL can still provide solutions for dating fluvial sediments.

Most of the published work on young materials is based on quartz-rich sediments (e.g. Olley et al., 1997; Ballarini et al., 2003; Madsen et al., 2005; Ballarini et al., 2007; Page et al., 2007; Rustomji and Pietsch, 2007), which are abundant, sandy and subjected to multiple erosion, transport and burial cycles in most dryland environments (e.g. Bateman et al., 2007b). In the Australian sedimentary environment, quartz has been repeatedly buried and re-exposed during its transportation to a generally flat landscape (e.g. Pietsch et al., 2008; Pietsch, 2009). This natural recycling process is believed to have increased the luminescence sensitivity of quartz, making quartz a robust dosimeter for dating young samples (Bateman et al., 2007b). Modification of the analytical approaches

such as using thinner optical filters (Ballarini et al., 2007) in order to detect low doses is usually unnecessary. Australian quartz grains are known to be generally suitable for the SAR protocols (Pietsch, 2009). For these reasons, in this thesis, single-grain quartz was chosen for dating.

4.3 Sample preparation

The modified sample preparation procedure extracts pure coarse-grain fractions of quartz for D_e determination. To estimate the dose in mineral grains, the sample must be extracted without exposure to light to avoid any bleaching of the luminescence signal. In the laboratory, the samples were handled in filtered dim red or orange light. Any outer bulk sediment material that may have been exposed to daylight was removed, dried overnight at 100 ºC in a muffle oven and milled into a fine powder for dose rate determinations.

For samples from core MMB3, standard procedures described in Aitken (1998) and Bøtter-Jensen et al. (2003) were followed. Samples were treated with HCl to remove carbonates and with H_2O_2 to remove OM. Various grain size fractions (<90 µm, 90-125 µm, 125-180 µm, 180-212 µm, >212 µm) were extracted by sieving. Sand-sized quartz grains were then concentrated by heavy-liquid separation using sodium polytungstate (SPT) at 2.70 g/cm^3 to remove heavy minerals and at 2.62 g/cm^3 to remove feldspars. The separates were then etched in 40 % HF to remove any residual feldspar and the outer ~10 µm layer of the grains that was irradiated by alpha particles. Clean and dry samples were sieved a second time before being loaded to measurement discs to remove powder produced by etching.

Of the five samples from core MMB3, except the bottom layer (64-66 cm), very little quartz could be extracted from the bulk material of the four upper layers. For example, for

the uppermost sample (4-6 cm), the quartz extracted was only enough to make up 4 discs for the single aliquots (diameter 0.5 µm) analysis using the 90-125 µm fraction and 5 discs for the single grain analysis using the 125-180 µm fraction. Most of the quartz extracted after the chemical reaction procedures was lost during heavy liquid separation using 2.62 g/cm^3 SPT, because most of the quartz grains floated with the "feldspar" layer. Particle-size distribution results (Figure 3.7 in Chapter 3) from the duplicate core of MMB3 showed that the upper sediment layers sampled for OSL dating were very silty and had less than 30 % sand content. Except for MMB3-04 (48-51 cm) which only contained 11 % sand, the others should have provided more quartz than MMB3-04 even though their sand content were less than 30 %. XRD analysis was conducted in bulk sediments from core MMB3 to identify the minerals present and to determine their relative abundance. Figure 4.4 shows an example of the XRD graph for MMB3-04 to indicate the purity of the quartz separate. Accordingly, the loss of quartz must have occurred during the preparation procedures. As the materials are fine, clay-rich sediments, the minerals tended to clump together. HCl and H_2O_2 reactions before wet-sieving might not be able to break them down so that the reaction to remove the coating of each individual grain might not be complete. This might explain why some "quartz" floated on the 2.62 g/cm^3 SPT. The XRD results again prove that it is more practical to choose quartz rather than feldspar for dating the sediments from the Macquarie Marshes.

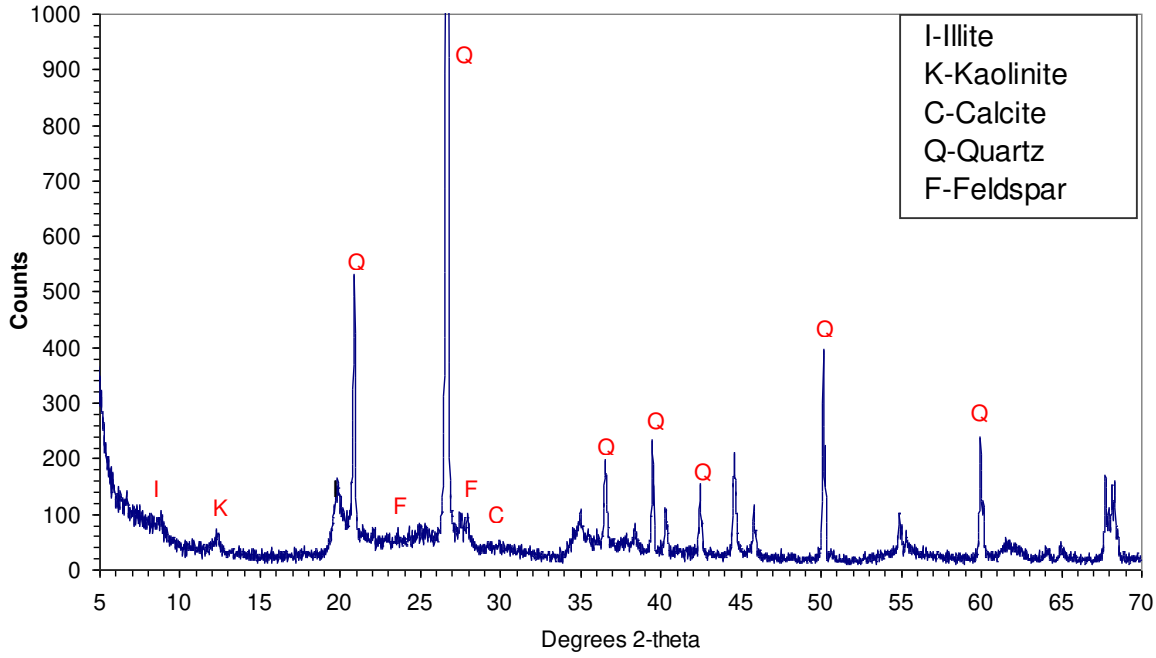

Figure 4.4. The X-ray diffractogram of prepared sample MMB3-4 (48-51 cm) showing the minerals present.

Accordingly, a modified procedure based on standard procedures and experience from core MMB3 samples (Table 4.2) was used for the other samples. It is worthwhile to choose OSL samples based on the particle-size distribution results so as to ensure the extraction of more quartz for dating. The preparation of samples from the other cores showed the extraction efficiency did improve so that sufficient quartz grains were recorded to produce statistically representative data for D_e evaluation.

Table 4.2
OSL Sample preparation procedures.

Step	Action	Aims
1	Wet-sieving	• To separate different size fractions (<90 µm, 90-125 µm, 125-180 µm, 180-212 µm, >212 µm) • To wash out the water-soluble coating of organic-rich grains
2	HCl reaction	To remove carbonates
3	H_2O_2 reaction	To remove organic matter
4	HF etching	• To remove residual feldspar • To etch the outer ~10 µm layer of the grains
5	SPT separation	To remove heavy minerals
6	Second sieving	To remove interference powder produced by etching

4.4 OSL instrumentation

Samples were analysed using Risø TL/OSL readers in the OSL laboratory at the University of Wollongong. Single-aliquot analysis and dose recovery tests were made using a Risø 5 which is used primarily for measurement of linearly modulated (LM) OSL. The majority of the single-grain analyses were made with a Risø 3 which is an automated Risø TL/OSL DA-15 reader equipped with blue LEDs and a single-grain laser system attachment that allows OSL stimulation of individual grains. Both readers are equipped with a $^{90}Sr/^{90}Y$ beta irradiator source for laboratory irradiation and have been cross calibrated for consistency. Both readers are controlled with "Mini-Sys" programs.

The light source is a blue LED for single aliquots and a green laser for single grains. Only 90 % of the maximum stimulation power was used. For single aliquots, the stimulation time was 40 seconds with a data collection interval of 0.16 seconds; for single grains, the stimulation time was 2 seconds with a data collection interval of 0.02 seconds.

Single aliquots were prepared on 10 mm-diameter stainless-steel discs. The discs were covered by masks with 0.5 mm diameter holes individually and sprayed using silicone oil (Silkospray). Therefore a uniform and consistent number of grains (~50-80 grains of size 125-180 µm) can adhere to the sprayed surface of the discs for analysis. The reason a hole of 0.5 mm diameter was chosen is the smaller aliquot usually consists of fewer grains and thus can increase in the probability of selecting only well bleached grains from a mixed sample (Olley et al., 1999).

Single-grain discs were prepared on 10 mm-diameter stainless-steel discs with 100 holes arranged in a regular 10×10 grid. Each hole has a diameter of 300 µm and depth of 300 µm (Figure 4.5). Grains of 180-212 µm size can be placed in each hole by brushing grains over the surface of the discs. The reason for choosing 180-212 µm size is that this fraction has been shown to be better bleached than the finer fractions and yields a more representative dose in young fluvial sediments (Olley et al., 1998). For those samples that did not have enough quartz sized 180-212 µm, the 125-180 µm fraction was used although visual inspection under a microscope was used to pick out extra grains from the hole by needle so that each hole contained only a single grain.

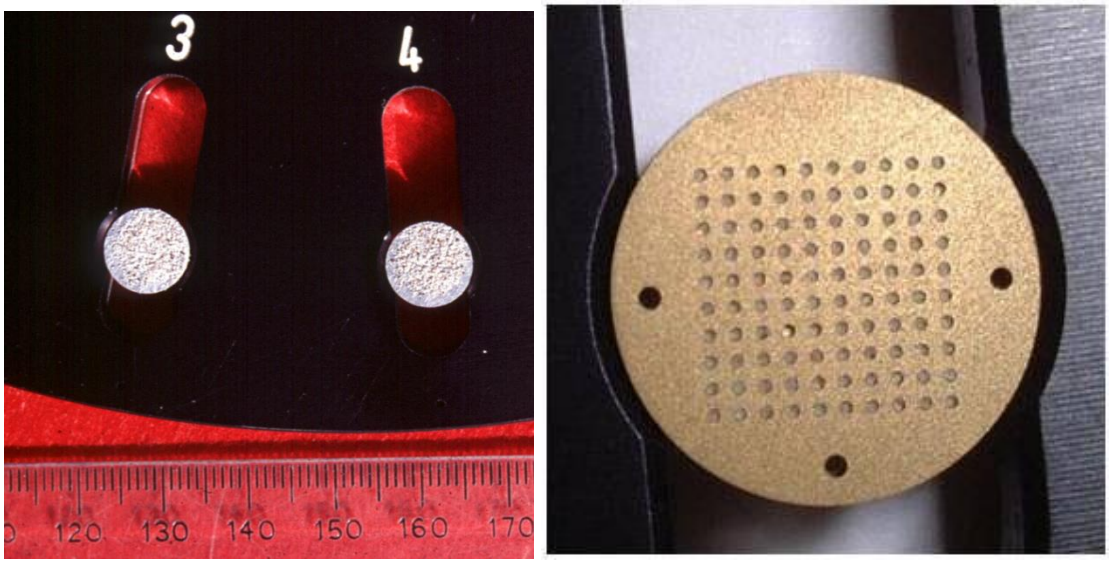

Figure 4.5. The single-aliquot (left) and single-grain (right) discs.(photo source from webpage http://cas.uow.edu.au/laboratories/index.html)

4.5 Environmental dosimetry

4.5.1 Natural radioactivity

Once mineral grains are buried, exposure to environmental radiation causes the redistribution and accumulation of trapped electrons in the impurities of their crystal lattice. These naturally-occurring ionising radiations come in four forms, namely alpha, beta, gamma and cosmic radiation. Alpha particles are heavy energetic particles but have a short range (a few micrometres); beta particles have a range of about 2 mm; gamma rays can penetrate up to about 30 cm through sediments; and cosmic radiation is highly penetrating (Aitken, 1998). Cosmic rays are derived from outer space, while the other three radiation sources are derived from the radioactive decay of radionuclides — mainly potassium (^{40}K), uranium (^{238}U and ^{235}U, and their daughter products) and thorium (^{232}Th and its daughter nuclides). The environmental dose a sample receives from these different forms can be divided into internal dose and external dose. The internal dose comes from

within the sedimentary grains themselves as a result of alpha and beta radiation; while the external dose come from alpha, beta and gamma radiation in the bulk sediment matrix surrounding the grain and also from cosmic rays.

Because the internal radioactivity of quartz is usually very low and insignificant, in this study, the calculation of total environmental dose rates mainly focuses on the external dose rate arising from the surrounding sedimentary matrix and cosmic rays.

4.5.2 Dose rate determination

The dose rate can be determined in the field or in the laboratory. Field measurements can be performed by portable *in-situ* gamma spectrometry (IGRS), as described by Lian and Scott (2007). When field measurements are not possible or inappropriate, the dose rates can still be calculated by determination of radionuclide concentrations measured in the laboratory. Radionuclide concentrations from representative sediment subsamples are usually determined either by direct measurement of U, Th and K (e. g., neutron activation (NAA), atomic absorption spectrometry (AAS) and inductively coupled plasma mass spectrometry (ICP-MS) measurements), or emission counting methods that measure the alpha and beta particles and gamma ray emissions within the sample over a certain time period (e.g., thick source alpha counting (TSAC), Risø GM-25-5 beta counting and high resolution gamma spectrometry (HRGS).

In this study, the HRGS, XRF, alpha and beta counting were used for determining radionuclide concentrations. Cosmic ray dose rates were calculated following the standard procedure as described in Prescott and Hutton (1994). The water content and organic content were also taken into account in calculating the dose rates. Detailed information is

presented in Appendix A1.1. The results of dose rate and other parameters (water content and total organic carbon) are presented in Table 4.3.

Table 4.3
Dose rates and other parameters.

Sediment Sample ID	Core Depth (cm)	Water Content (%)	TOC (%)	Gamma Dose Rate (Gy/ka)	Beta Dose Rate (Gy/ka)	Cosmic-Ray Dose Rate (Gy/ka)	Total Dose Rate (Gy/ka)
MMB3-1	5-8	155.85	6.34	0.406±0.029	0.719±0.048	0.143±0.014	1.267±0.101
MMB3-2	16-19	68.00	4.80	0.550±0.043	0.823±0.066	0.146±0.015	1.518±0.130
MMB3-3	27-29	55.50	4.25	0.490±0.034	0.947±0.065	0.151±0.015	1.586±0.120
MMB3-4	48-51	47.03	1.88	0.593±0.043	1.039±0.077	0.145±0.014	1.776±0.138
MMB3-5	55-57	41.69	1.83	0.706±0.053	0.951±0.071	0.147±0.015	1.804±0.140
MMB3-6	69-72	38.50	0.70	0.672±0.042	0.914±0.065	0.142±0.014	1.729±0.121
MMB3-7	85-88	31.64	0.29	0.755±0.054	0.980±0.070	0.144±0.014	1.880±0.136
LSW1	14-16	31.21	2.60	0.636±0.054	0.953±0.075	0.189±0.019	1.778±0.139
LSW2	24-26	29.15	2.10	0.540±0.038	1.070±0.080	0.180±0.018	1.790±0.128
LSW3	36-38	26.00	0.80	0.594±0.049	1.147±0.088	0.172±0.017	1.913±0.146
LSW4	47-49	22.91	0.70	0.755±0.065	0.974±0.071	0.167±0.017	1.895±0.143
LSW5	56-58	20.50	0.48	0.771±0.061	0.897±0.059	0.161±0.016	1.830±0.127
LSW6	65-67	19.11	0.40	0.884±0.072	0.836±0.059	0.162±0.016	1.881±0.136
LSW7	73-75	21.00	0.40	0.760±0.064	0.981±0.072	0.157±0.016	1.898±0.142
LSW8	80-82	23.91	0.48	0.740±0.062	0.981±0.085	0.151±0.015	1.872±0.153
LSW9	89-91	27.50	0.65	0.574±0.040	0.940±0.071	0.145±0.015	1.659±0.120
LOLA-1	17-20	12.00	1.68	0.877±0.068	1.227±0.083	0.185±0.018	2.289±0.155
LOLA-2	28-31	13.50	0.85	0.738±0.061	1.283±0.083	0.180±0.018	2.220±0.148
LOLA-3	40-42	12.50	0.65	0.768±0.064	1.419±0.093	0.180±0.018	2.368±0.161
LOLA-4	51-53	12.00	0.42	0.844±0.065	1.283±0.088	0.176±0.018	2.303±0.157
LOLA-5	63-69	12.31	0.60	0.852±0.060	1.017±0.075	0.173±0.018	2.043±0.139
LOLA-6	104-111	18.28	0.13	0.891±0.021	1.188±0.051	0.155±0.015	2.234±0.083
LOLA-7	146-151	15.87	0.06	1.051±0.024	1.283±0.055	0.151±0.015	2.485±0.090
LOLA-8	181-187	19.40	0.05	0.959±0.021	1.414±0.062	0.139±0.014	2.512±0.097
LOLA-9	202-207	17.15	0.06	0.990±0.024	1.415±0.061	0.139±0.014	2.544±0.097
2LOLA-1	8-12	28.90	4.20	0.675±0.046	1.187±0.079	0.200±0.020	2.062±0.139
2LOLA-2	23-27	33.85	2.95	0.741±0.054	1.084±0.075	0.173±0.017	1.998±0.144
2LOLA-3	39-43	28.30	2.35	0.813±0.046	1.082±0.077	0.165±0.017	2.060±0.136
2LOLA-4	63-67	22.50	0.45	0.830±0.063	1.194±0.088	0.157±0.016	2.182±0.158
2LOLA-5	88-92	22.50	0.50	0.878±0.070	1.191±0.091	0.152±0.015	2.220±0.168
2LOLA-6	128-131	21.00	0.25	0.843±0.064	1.205±0.087	0.147±0.015	2.195±0.158
2LOLA-7	144-147	18.50	0.22	0.832±0.064	1.259±0.108	0.148±0.015	2.239±0.177

4.6 Equivalent dose determination

Choosing the best instrumental conditions for single-grain D_e analysis is essential in OSL age determination. To ensure accurate and representative results, the analysis of the OSL signal and the proper calculations and interpretations of D_e data are also very important. The following sections will further discuss these issues.

In this thesis, all samples were measured using the SAR procedure (Table 4.2, Page 96) with a slight modification made with the thermal treatments. Unless specified, the cut-heat mentioned here was actually a preheat held for 5 seconds before T_n/T_x measurements. The purpose was to avoid possible insufficient thermal treatment of the quartz due to poor contact between the sample discs and the heater. Several tests have been established to ensure the reliability of the D_e obtained. The performance of the SAR protocol for our samples wae tested using a preheat plateau test, recycling ratio and recuperation. The same SAR protocol is also used in dose recovery test and sample analysis, except for the 'young' surface sediment samples (<50 yr old) for which an extra Step 6^* was added to reduce recuperation (Murray and Wintle, 2003). For most of the samples that have sufficient dating material, we ran the SAR protocol in 3-5 samples with regeneration dose based on estimated dose and modified the regeneration dose according to the preliminary results for the rest of the samples. In the light of the bright quartz, we chose to apply a small test dose as suggested by Murray and Roberts (1998) to avoid recuperation effects.

4.6.1 Equivalent dose determination using single aliquots

In this thesis, the single aliquot methods were conducted on the dose recovery tests in order to determine the best thermal conditions for analysing samples from different

sampling sites. It is also applied to one of the core samples (core MMB3) to compare with data obtained from single-grain methods.

4.6.1.1 OSL decay curves

It has been demonstrated that the OSL signal from quartz is typically made up of more than one exponentially decaying component (Bailey et al., 1997; Jain et al., 2003), namely the 'fast' (sometimes divided into 'ultra-fast', 'fast'), 'medium' and 'slow' (sometimes divided into 'slow 1', 'slow 2', 'slow 3', 'slow 4'). These components are named according to their relative decay rates during continuous-wave (CW) OSL stimulation. These components have different thermal stabilities, degrees of sensitisation, recuperation levels and dose-response curve shapes (Jain et al., 2003; Singarayer and Bailey, 2003). In particular, the fast and medium components will exhibit differences in bleaching rate with stimulation wavelength (Singarayer and Bailey, 2004). Therefore the OSL signal can vary greatly between samples with different components and even samples with the same components but different proportions. Ideally, the OSL signal used for D_e estimation in the SAR protocol is the fast component (Wintle and Murray, 2006). Therefore, the dominance of the fast component in the OSL signal is desired when using this approach.

CW-OSL measurements, where the power of the stimulating light source is kept constant, usually result in a sum of exponentially decaying components (Jain et al., 2003; Singarayer and Bailey, 2003). A typical OSL decay curve from samples MMB3-3 and MMB3-5 obtained using continuous wave (CW) OSL stimulation is shown in Figure 4.6. A sharp decay was observed in the first 1 s of stimulation, indicating that these samples are dominated by the fast component.

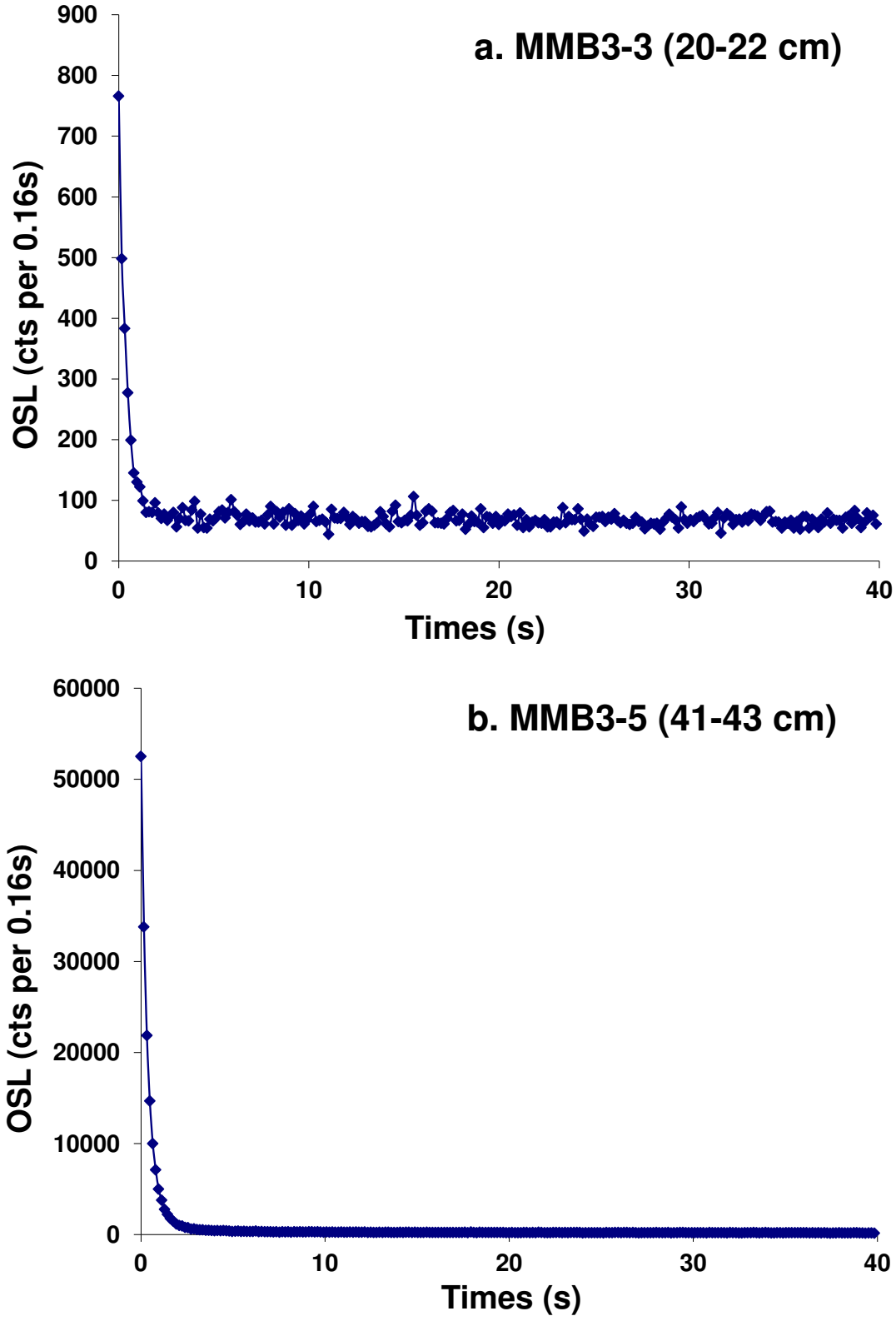

Figure 4.6. Decade curves of two single-aliquot samples from core MMB3.

To further confirm that the OSL from our samples is dominated by the fast component, a linear modulation (LM) OSL stimulation was conducted on several samples (MMB3-05, LSW-CC), in which the OSL was recorded by linearly ramping the stimulation power of the blue LEDs from zero to its full power. Single aliquots containing ~50-80 grains were given a beta dose of 50 Gy and preheated for 10 s to 260 °C. The LM-OSL signal was measured at 125 °C for 3600 s by linearly ramping the power of the blue LEDs from zero to 90 %. Figure 4.7 provides examples of LM-OSL curves for samples MMB3-05 and LSW-CC, both of which have three repeats. It shows the dominance of fast components. The shine-down curves here were in agreement with those found in Australian quartz by Jain et al. (2003). Although the general trend of the curves was the same among aliquots from the same sample, the intensity of the OSL signal varied as much as 5 fold. These might have been caused by the inhomogeneous characteristic among the quartz grains. Here the shine-down curve of LM-OSL reassures the suitability of the SAR protocol for the Macquarie Marshes samples.

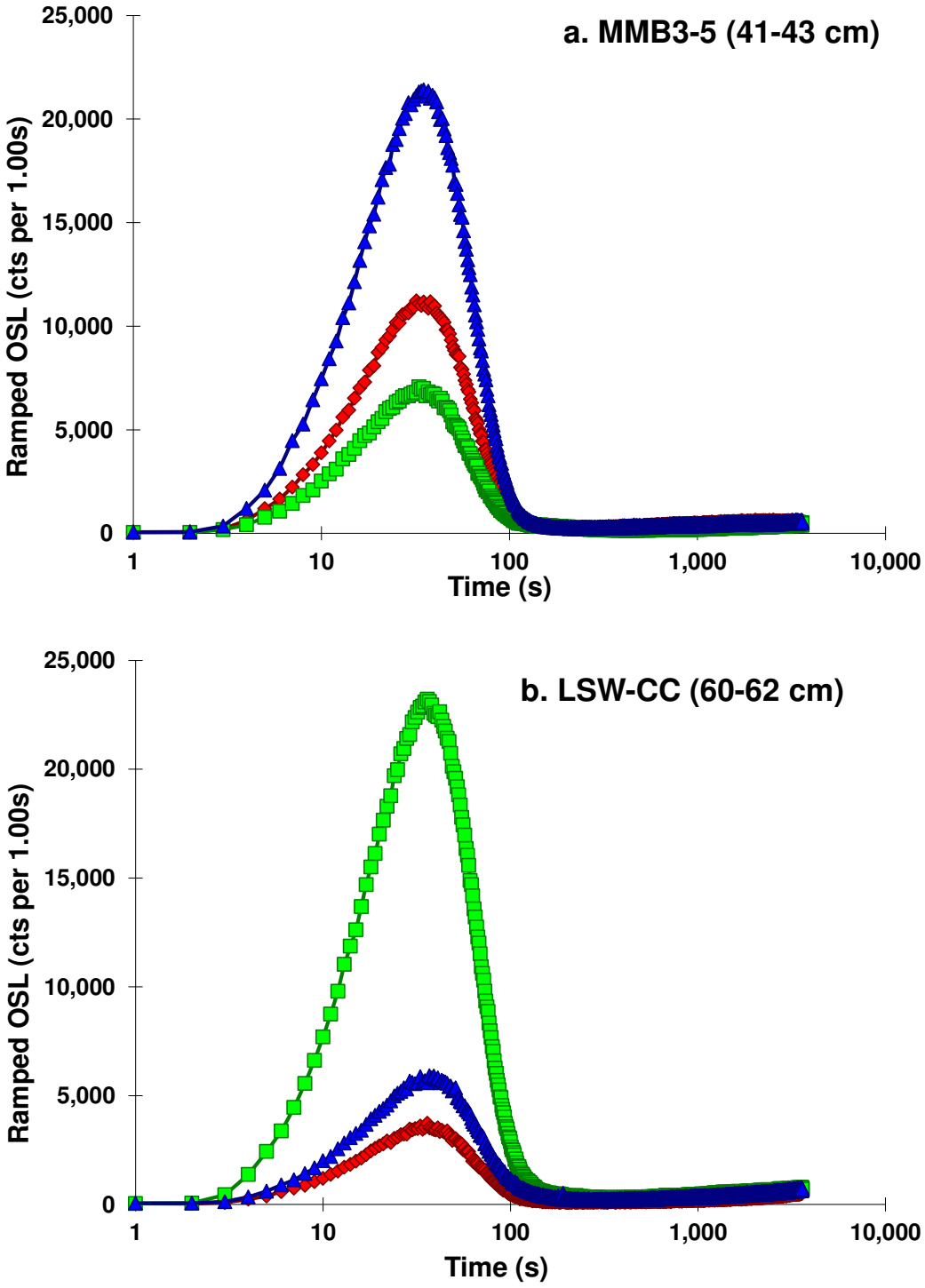

Figure 4.7. LM-OSL shine-down curves of two samples from cores (a) MMB3 and (b) LSW. (The triplicates of each sample are presented by markers with different colours.)

4.6.1.2 Dose response curve

In the SAR protocol, the natural dose of the sample is determined by interpolating the natural signal onto the dose response curve, which is a constitution of several regeneration dose points. The natural signal and regeneration signals are all corrected by dividing their OSL response signals (L_n or L_x) to a test dose response signal (T_n or T_x). These signals are net OSL signals obtained by summing the initial portion (0.1s) of the decaying OSL signal and subtracting a mean 'late-light' background signal (final 0.2s). In addition, the same background signal was also used to derive the subsequent net test-dose response. Relatively small test doses were carefully chosen for each sample in the SAR protocol in particular for the young samples, to minimise the risk of significant recuperation and dose constitution through the analysed cycle (Pietsch, 2009). In this study, standard background subtraction was used to sample only the initial fast signal and remove any signal contributed by slower OSL components or instrument noise that might interfere with the D_e calculation (Murray and Wintle, 2000).

Typical dose response curves (DRCs) from samples MMB3-3 and MMB3-5 are shown in Figure 4.8 (Page 108). For relatively young samples (D_e less than 5 Gy), the DRCs were fitted using a linear fit (Figure 4.8 a) described as:

$$I = I_0 + k \cdot D$$

Where I is the sensitivity-corrected luminescence intensity (a.u.), I_0 represents the initial offset of the signal from the 0 Gy dose-point, D is the regeneration laboratory dose and k the additional linear term that accounts for continued growth at high doses.

The samples that are relatively old (D_e more than 5 Gy) were fitted using a saturating-exponential-plus-linear function (Figure 4.8 b) described as:

$$I = I_0 + I_{\max}(1 - e^{-D/D_0}) + k \cdot D$$

Where I is the sensitivity-corrected luminescence intensity (a.u.), I_0 represents the initial offset of the signal from the 0 Gy dose-point, I_{max} represents the intensity of the luminescence signal at saturation and D is the regeneration laboratory dose, with D_0 being a constant defining the onset of signal saturation and k the additional linear term that accounts for continued growth at high doses.

All of the D_e and DRCs were analysed using the "Analyst" software. All of the parameters described above were set as the analyst condition. Instrument reproducibility tests have not been measured in this study, but an instrument uncertainty of 2 % has been adopted for each OSL measurement, according to the previous finding by Jacobs et al. (2006a).

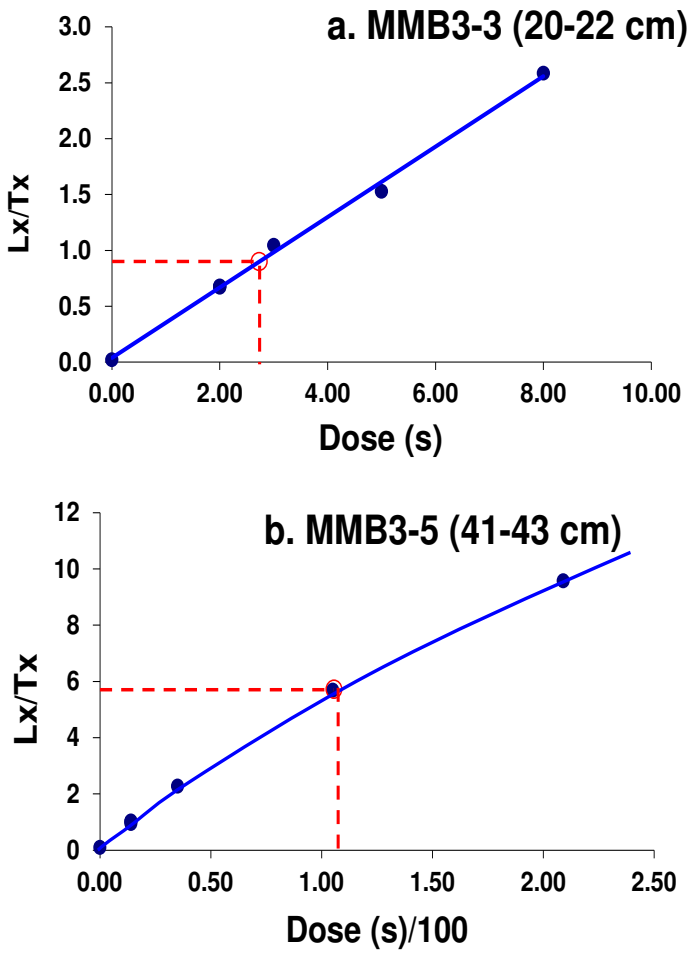

Figure 4.8. Regeneration dose curves of two single-aliquot samples from core MMB3.

4.6.1.3 SAR performance of single aliquots

In order to observe the thermal transfer and optimise the SAR performance, dose recovery tests were conducted on sunlight bleached samples from each of the cores. The reason for choosing sunlight bleaching instead of laboratory stimulated bleaching (e.g. using blue LEDs) is that bleaching under daylight conditions would be more representative of the conditions experienced by the quartz grains in nature. The samples selected based on the abundance of quartz extracted, were bleached in natural sunlight for 2-5 days and kept in the dark overnight before analysis.

Though sample MMB3-05 had the most quartz, only 9 discs of aliquots (0.5 mm in diameter) were prepared from the material extracted. The dose recovery tests for core MMB3 were conducted on three groups of empirical preheat (PH) and cut-heat (CH) combinations. For the other two cores (LSW and LOLA), various combinations of preheat (10 seconds) and cut-heat (5 seconds) ranging from 180-280 °C and 140-200 °C were tested. Experiments using cut-heat with various preheat temperatures were also conducted on the core LSW.

The procedures for the dose recovery tests were built on the conventional SAR protocol for analysing true D_e values, except that at the beginning of the test on the first step, the sun-bleached and traps-emptied aliquots were given a certain dose to represent the natural dose. In this study, most of the dose recovery tests were conducted on a given dose of 50 Gy. A lower given dose of 5 Gy, which would be more representative of those young samples, was also utilised for the aliquots of quartz from the core LOLA for comparison.

Samples were examined in the following steps: IR depletion, sensitivity changes, recuperation and recycling ratio. Results of the dose recovery tests were assessed by the recovery ratio (the dose recovered divided by the dose given). They are presented as a function of preheat and cut-heat temperatures to allow assessment of thermal transfer. The most suitable preheat and cut-heat temperatures which did not lead to significant thermal transfer and with recovery ratios closest to 1.00 were then chosen for each set of core samples.

4.6.1.3.1 IR depletion tests

As described in Section 4.2.2, the different characteristics of quartz and feldspar cause different behaviours in OSL dating. Therefore it is important to work with a single mineral (e.g. quartz or feldspar). In this thesis, the focus is on dating the quartz and therefore contamination by feldspar should be minimised. Though most of the feldspars had been removed during the sample preparation procedures, IR depletion tests proposed by Duller (2003) have been conducted to confirm no feldspar contamination. These tests were done by adding one further measurement at the end of the SAR measurement sequence. These involved adding another repeated dose measurement except that, prior to preheating, the aliquots/grains were exposed to an IR laser diode (or IR LEDs) at just above room temperature (50 °C under computer control) for 100 seconds. If there were feldspar contamination, the depletion of feldspar after IR exposure would lead to a reduction of the measurement signal from the previous measurement of the same regeneration dose. Reductions of more than 10 % of unity would be considered to indicate significant feldspar contamination (Duller, 2003).

For core MMB3 samples (Figure 4.9 a), the three preheat and cut-heat combinations all give consistent IR recycling ratios close to 1. The values for LSW and core LOLA samples (Figure 4.9 b, c and d) are mostly acceptable, falling within ±10 % of unity. For samples given a cut-heat for 0 seconds, except those of 150 °C, the other two thermal combination results are relatively consistent, giving IR depletion ratios close to 1. Results show that IR recycling ratios are more consistent with different thermal treatments and closer to 1 when given high regeneration doses, indicating that the modified sample preparation procedure had been successful in extracting pure quartz and the presence of feldspar contamination is not a contributing factor in this study.

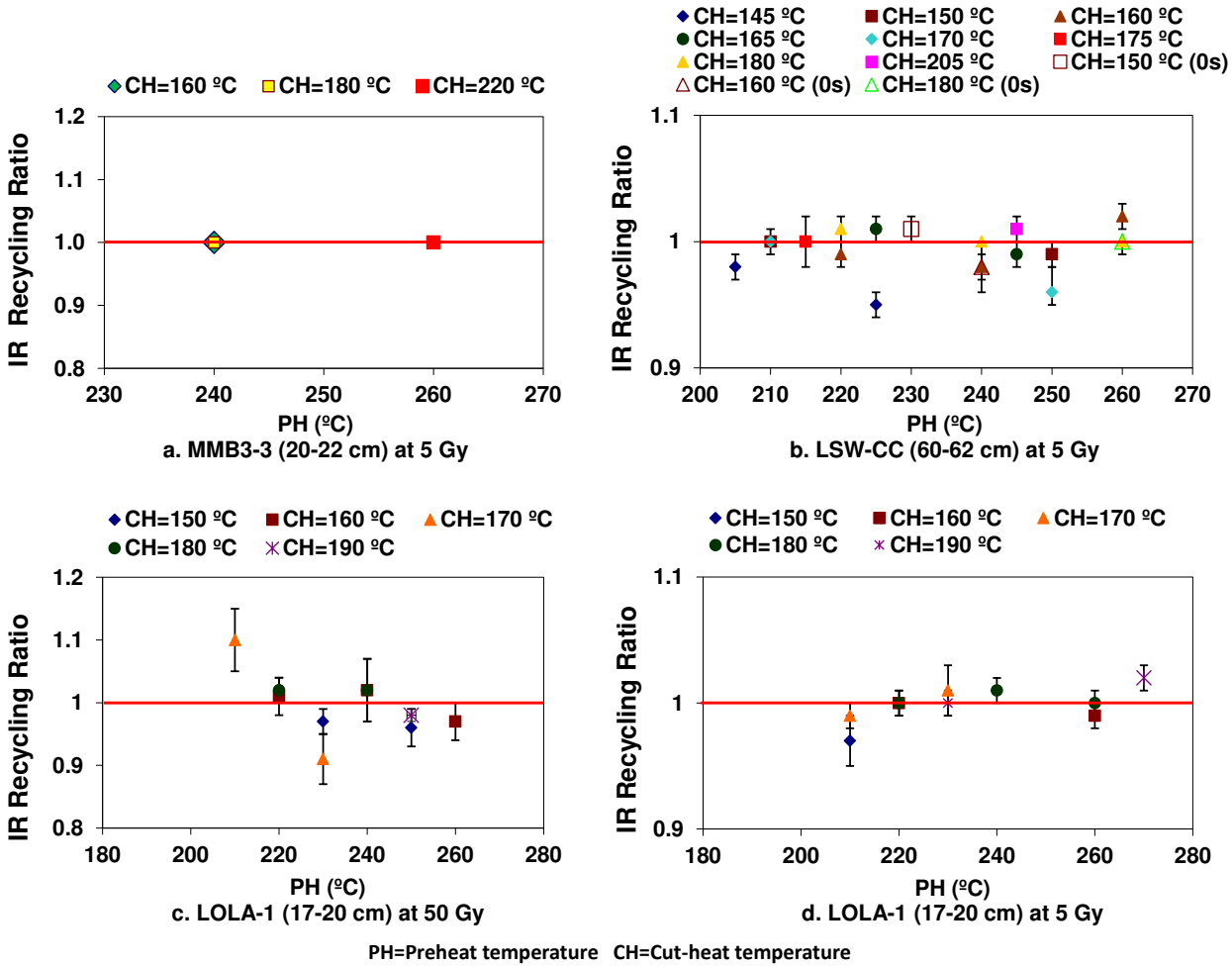

Figure 4.9. IR depletion recycling ratios for cores MMB3, LSW and LOLA.

4.6.1.3.2 Sensitivity changes

The sensitivity changes that occur through the SAR measurement cycles can be investigated by observing changes in the test dose response (T_x). By using a broad range of preheat temperatures, the degree of sensitivity change can be observed (Murray and Wintle, 2000). This can be seen when T_x/T_n is plotted as a function of measurement cycle during the construction of a dose response curve using different doses. The T_x/T_n curve will appear to be linear when ideally no sensitivity changes occur.

For sample MMB3-5, despite different combinations of preheat and cut-heat temperature applied, the T_x/T_n curves show similar trends (Figure 4.10). The curves increase with increasing regeneration dose during the previous five cycles and are relatively stable during the last three cycles. The degree of increase becomes higher at lower preheat and cut-heat temperatures. Of the three preheat and cut-heat combinations, the one with a preheat of 240 °C and a cut-heat of 180 °C shows a relatively consistent trend among three discs of the same preheat and cut-heat conditions.

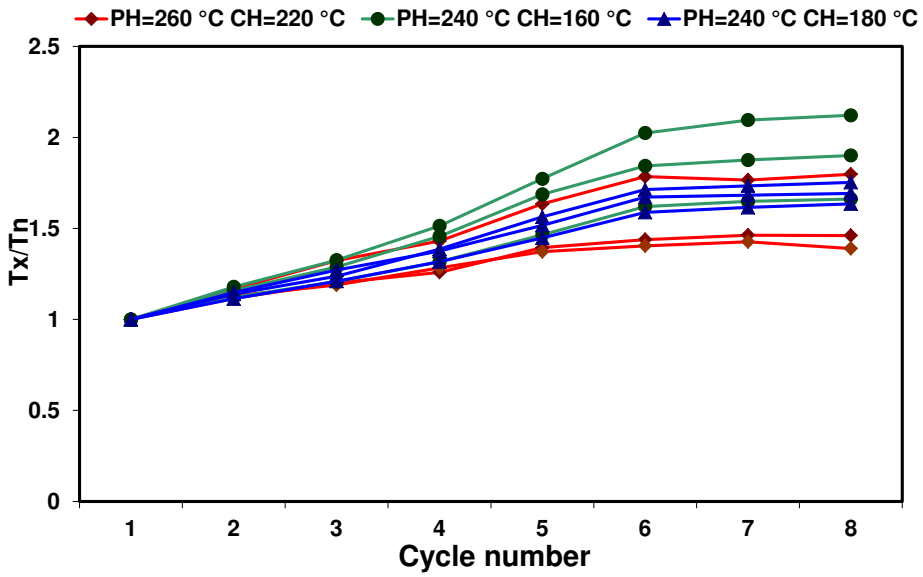

Figure 4.10. Changes of test dose responses for sample MMB3-5.

The T_x/T_n curves of the 14 groups of preheat and cut-heat combinations for core LSW show similar increasing trend as those of sample MMB3-5 (Figure 4.11). Of all the combinations, the three sets (Figure 4.11 b, f, g) with preheat of 220, 250 and 280 °C show more consistency among different aliquots tested. For the discs that received a cut-heat for 0 seconds (Figure 4.11 h), the T_x/T_n curves all behave the same as those with a 5-second 'cut-heat'.

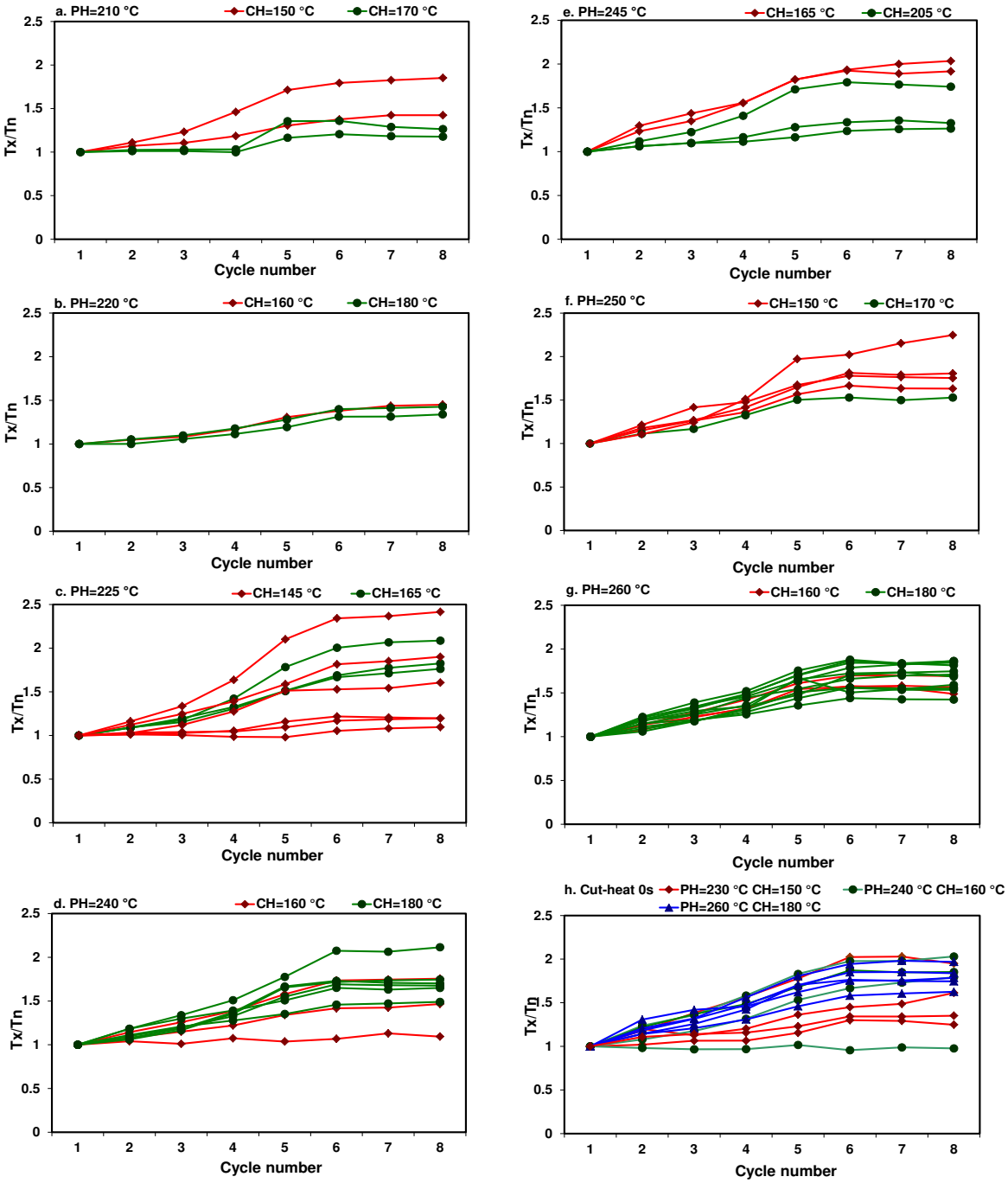

Figure 4.11. Changes of test dose responses for sample LSW-CC.

In order to check how the T_x/T_n curves respond to different given doses, dose recovery tests were conducted both with high and low given beta irradiation doses. The high given dose was proximately 50 Gy as the two cores described above, while the low given dose was 10 times lower (~5 Gy). Most of the curves (Figure 4.12 a) show an

increasing trend with the increase of regenerated doses when given a high dose, which are consistent to those of the other two cores. The sensitivity can increase (up to 40 %) over eight cycles. The T_x/T_n curves become flatter at low given doses (Figure 4.12 b), indicating there is less change in sensitivity. For these samples with lower given dose, the regenerated doses were relatively low, therefore the change in sensitivities was less significant.

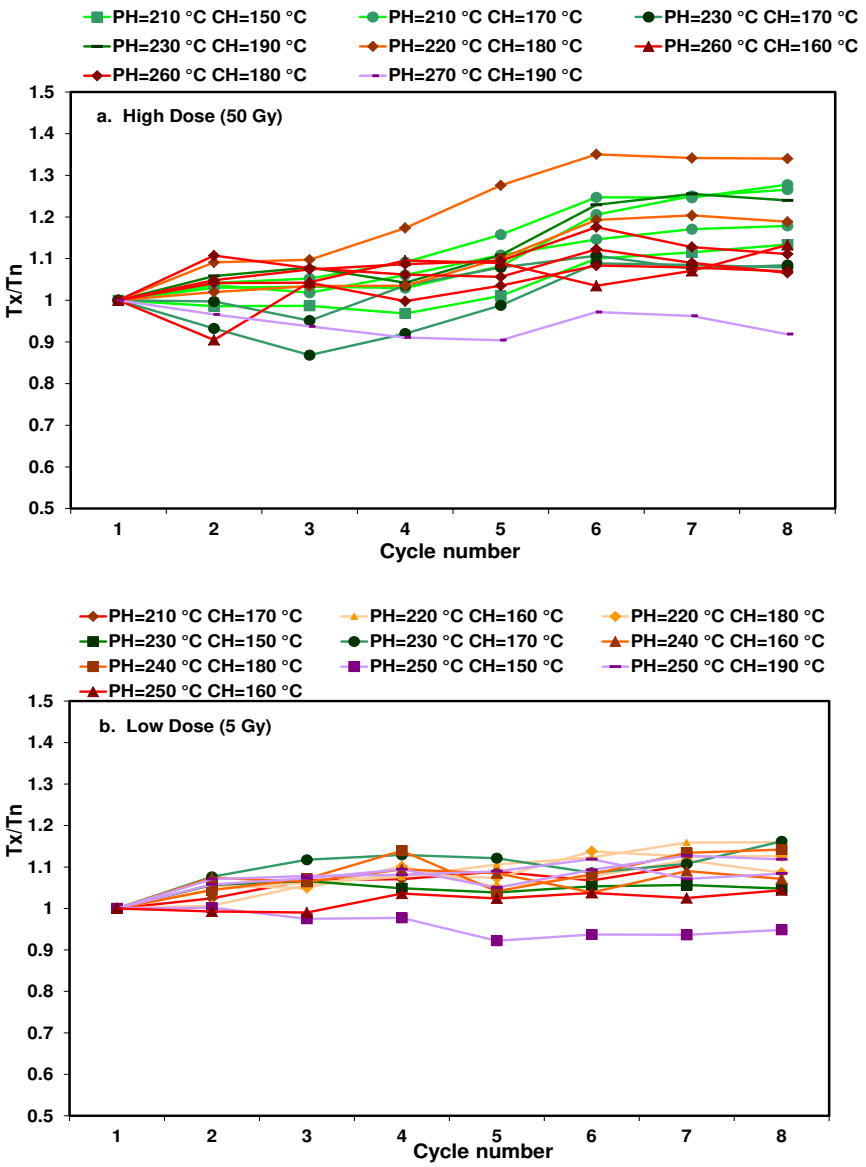

Figure 4.12. Changes of test dose responses for sample LOLA-1.

In the study of Armitage et al. (2000), the T_x/T_n curves show a similarly increasing trend at temperatures higher than 220 °C, but tend to decrease during the regeneration cycles at temperatures ranging from 160 to 220 °C. In this study, the T_x/T_n curves of MM samples are mostly independent of preheat and cut-heat temperatures.

For most of the samples, the most significant T_x/T_n changes occur during cycles 2 to 6, after which little or no change is noted. Cycles 2 to 5 are the procedures where regeneration doses were given and tested in increasing order; while cycles 6 to 8 are the procedures where zero dose and repeated regeneration dose were given. These results suggest that the higher the regenerated dose, the more likely quartz tended to change in T_x/T_n. It has been found that Australian quartz is transported and buried repeatedly (Pietsch, 2009). It is expected that this natural cycling has the same sensitivity effect as that observed to operate in the laboratory, where the cycling of quartz through various irradiating, heating and bleaching treatments increases its luminescence sensitivity. It is probable that the laboratory-induced sensitivity changes for the MM samples were caused by not only thermal treatment but also by repeated irradiation.

4.6.1.3.3 Recuperation

Recuperation is caused by thermal transfer of charges from shallow, light-insensitive traps to deeper light-sensitive traps (Aitken and Smith, 1988). Murray and Wintle (2000) suggested two potential sources for recuperation: (i) thermal transfer from optically-insensitive traps which are partly but incompletely drained by the preheat; (ii) thermal transfer of photon-transferred charge, during the test dose OSL measurement, into thermally-shallow but light-insensitive traps that are not emptied by the cut-heat.

In this study, the recuperations (Figure 4.13) for most of the tested samples are less than 5 %. These values are similar to those observed by Murray and Wintle (2000) within sediment samples and higher than for the heated samples. There are no systematic changes in the recuperation for these samples with different preheat temperatures, at least within the range 200 to 280 °C. Under the same thermal conditions (Figure 4.13 a, b and c), recuperation values of samples given a higher dose are more consistent; for those given lower doses (Figure 4.13 d), the recuperation values are more scattered and are relatively higher. Because the recuperation is calculated by the sensitivity-corrected dose at zero-dose point (L_x/T_x) divided by the sensitivity-corrected natural dose (L_n/T_n), it is expected that a lower recuperation is obtained for a higher L_n/T_n value, and, hence, the lower the D_e, the greater the recuperation.

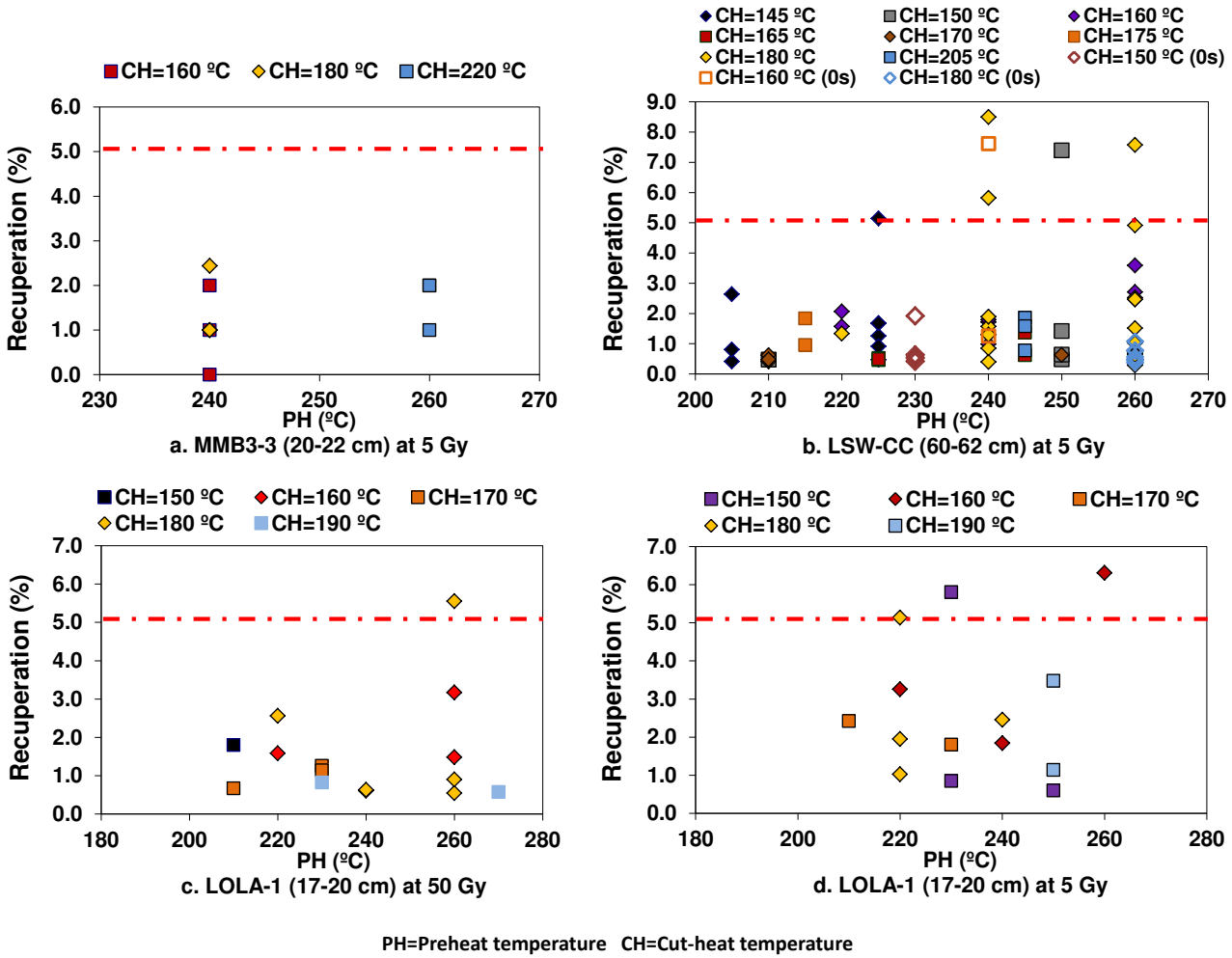

Figure 4.13. Recuperation test results for cores MMB3, LSW and LOLA.

4.6.1.3.4 Recycling ratio

The recycling ratio test involves repeating a dose point within the SAR measurement cycle. It tests for the reliability of sensitivity correction. The recycling ratios of aliquots from the MMB3, LSW and LOLA core samples are shown in Figure 4.14 as a function of preheat temperatures.

For core MMB3 samples, the recycling ratios of different thermal treatment combinations exhibit no temperature dependence.

LSW samples with a 'cut-heat' of 5 seconds are more scattered but all fall within 10 % of unity except for the combination of preheat 245 °C and cut-heat 165 °C.

Core LOLA samples also show recycling ratios that are less dependent on preheat temperatures but more dependent on given doses. Recycling ratios are more consistent to 1 at higher given doses. With the low given dose, relatively low thermal treatments (preheat of 220-260 °C and cut-heat of 160-180 °C) should be used in order to achieve acceptable recycling ratios.

In conclusion, the recycling results demonstrate that the sensitivity correction of the SAR protocol works well for the MM samples.

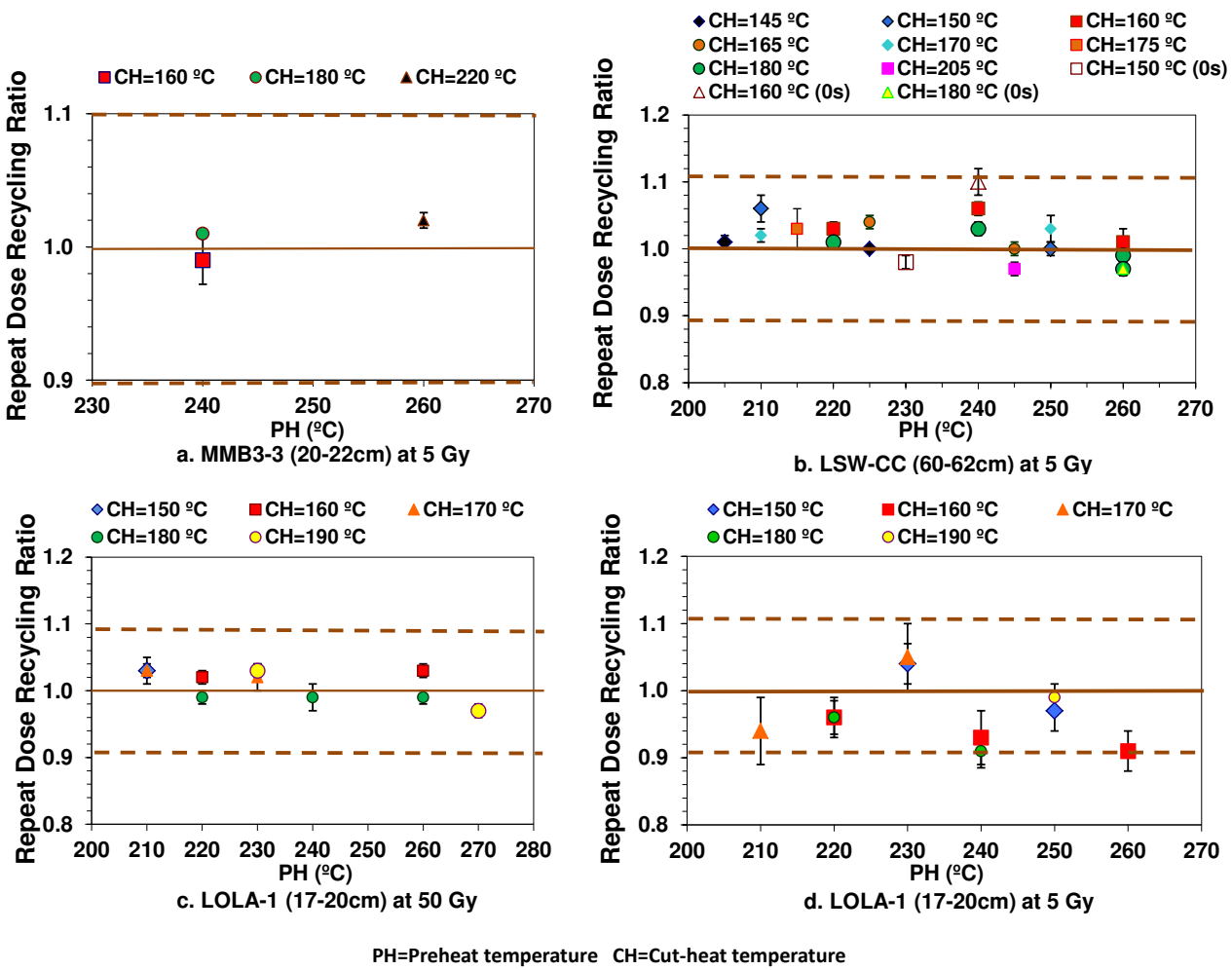

Figure 4.14. Recycling ratio test results for cores MMB3, LSW and LOLA.

4.6.1.3.5 Dose recovery test results

Dose recovery tests were conducted using different preheat temperatures. The ratios of the recovered dose to the given dose versus preheat temperature are plotted in Figure 4.15 (Page 123).

The three preheat and cut-heat combinations of sample MMB3 (Figure 4.15 a) all give a recovery ratio lower than 1, suggesting that underestimation of the true D_e values in the samples may be possible using these conditions. The combination of preheat 240 °C and cut-heat 160 °C appears to give a more satisfactory recovered ratio of 0.92 ± 0.18, and, hence, was chosen as the setup parameter for the MMB3 sample natural dose analysis.

Weighted recovered ratios of each preheat and cut-heat combinations of the LSW samples are plotted in Figure 4.15 b. It suggests that combinations of preheat within 220-260 °C and cut-heat within 145-175 °C are the most suitable combination for giving dose recovery close to 1 (within ±5 % error). Taking the sensitivity change (described above) into consideration, a combination of preheat 260 °C and cut-heat 180 °C was chosen for the LSW samples.

For core LOLA, except for one sample with high preheat (270 °C) and cut-heat (190 °C) combination, the other samples (Figure 4.15 c, d) are able to recover the given dose despite the different thermal treatments used. Both sets of samples with preheat of 220 °C and cut-heat of 160 or 180 °C show good recovery ratios close to 1 (within ±5 % error). In this case, it is safe to apply the same thermal treatment to samples with both high and low D_e. The standard error of the 180°C cut-heat is relatively lower, thus is chosen with the combination of 220 °C preheat as the thermal treatment conditions for the core LOLA sample D_e analysis.

Because the 2LOLA2 core was collected close to core LOLA, a separate dose recovery test was not performed. However, a single grain dose recovery test for 2LOLA2 core was conducted at 220 °C preheat and 180 °C cut-heat (same as core LOLA) (further discussed in the next section).

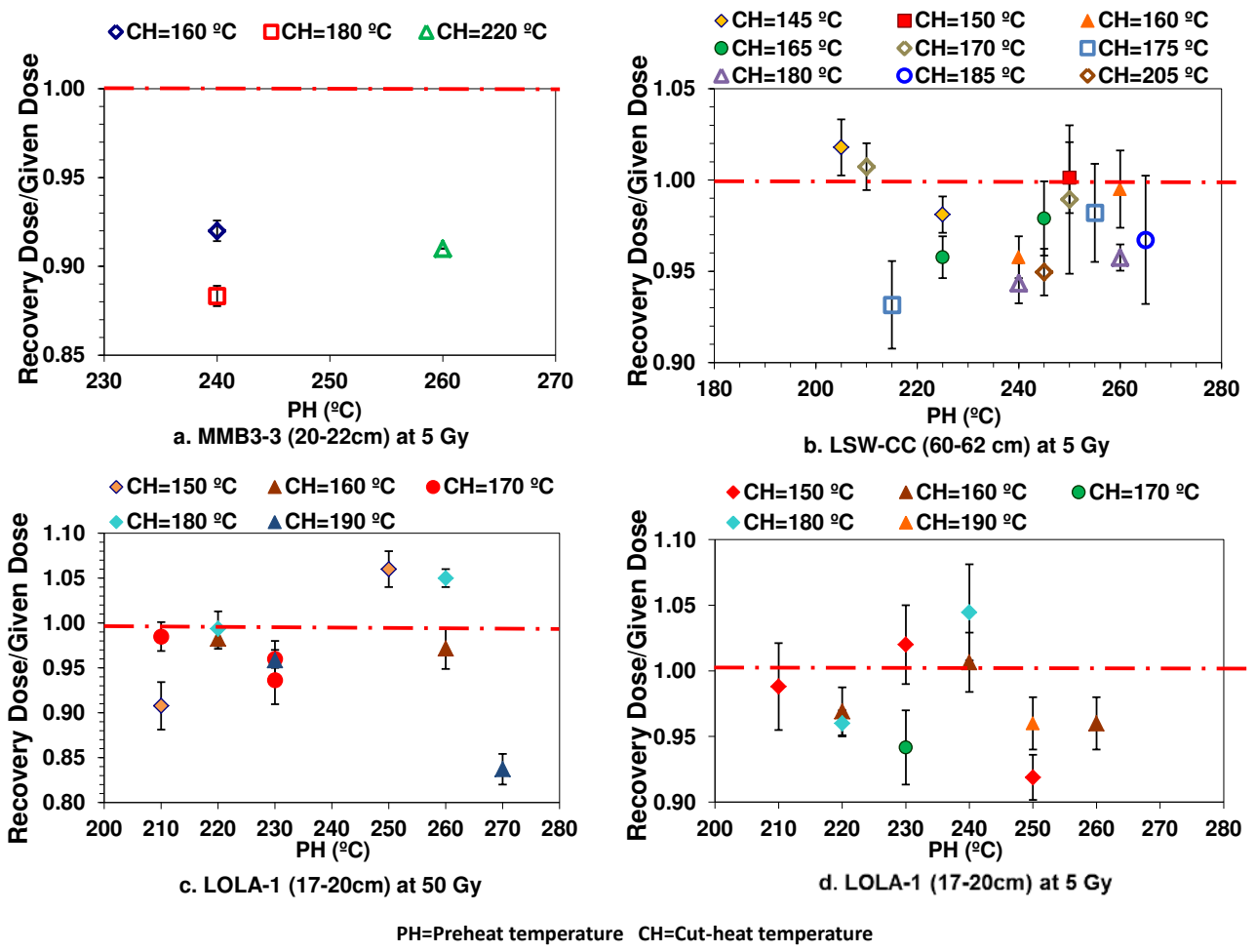

Figure 4.15. The D_e recovery results for cores MMB3, LSW and LOLA.

4.6.1.4 Selected thermal conditions for equivalent dose determination

From the above discussion, conventional single-aliquot OSL dating method -- the SAR protocol reported in the literature is applicable to the samples in this study. Thermal transfers are unlikely to be problematic with preheat temperatures ranging from 200 to 280 °C, which are high enough to overcome the 110 °C thermal peak and lower than the 325 °C optical luminescence peak. Possible sensitivity changes can be corrected by the internal checks of the SAR protocol. However modifications have been made to the SAR procedure including the following:

1) There is no significant variation in dose recovery results between cut-heat and 5 seconds preheat under the same preheat condition. In order to reach the desired temperature before recording the test dose signal, a 'cut-heat' which is actually a preheat for 5 seconds is chosen.

2) IR depletion tests were added to the conventional SAR protocol to confirm no feldspar contamination. Results again showed that the modified sample preparation procedure had been successful in extracting pure quartz and there is no significant feldspar contamination in this study.

3) Various responses to thermal treatments are observed within the same sample and among samples from different sites (Table 4.4). Therefore it is essential to perform dose recovery tests ideally to each sample of interest, or at least to each suite of related samples.

Table 4.4
Selected thermal conditions for analysing samples from the various MM sites.

Site	PH* (°C)	CH** (°C)	Recuperation (%)	Recycling Tests		Recovery of D_e	
				Ratio (%)	Error	Ratio (%)	Error
MMB3	240	160	1.33	0.99	0.02	0.92	0.01
LSW	260	180	1.95	1.01	0.02	0.95	0.03
LOLA (High Dose)	220	180	2.56	0.99	0.01	0.99	0.02
LOLA (Low Dose)	220	180	2.70	0.96	0.03	0.96	0.01
2LOLA	220	180	-	-	-		

* PH= Preheat temperature ** CH=Cut-heat temperature

4.6.2 Equivalent dose determination using single grains

4.6.2.1 OSL decay curves

A typical OSL decay curve from sample MMB3-07 obtained using continuous-wave (CW) OSL stimulation is shown in Figure 4.16. A sharp decay was observed in the first 0.5 s of stimulation, further confirming that our samples are dominated by the fast component.

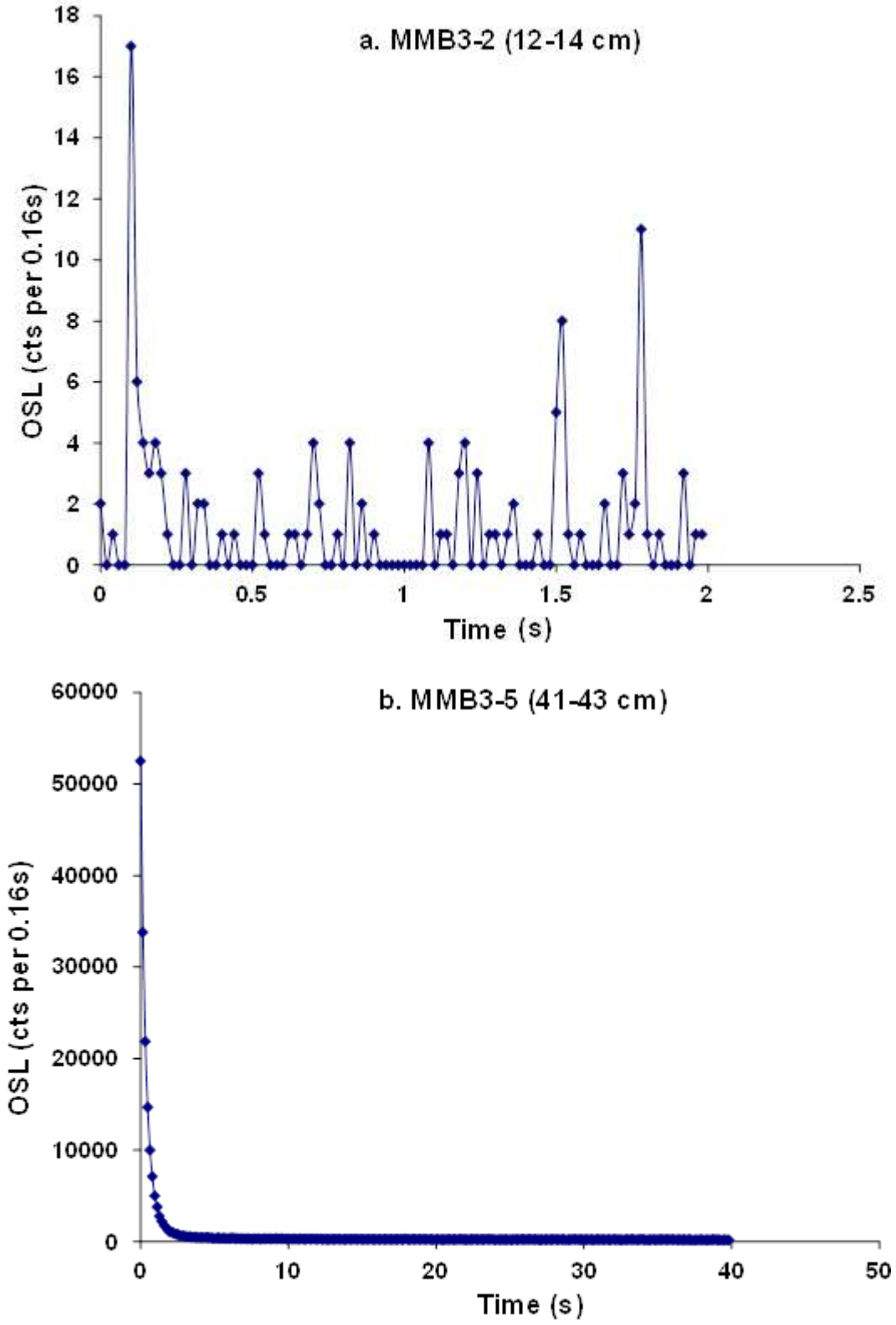

Figure 4.16. Decade curves for two single-grain samples from core MMB3.

4.6.2.2 Dose response curves

Typical dose response curves (DRCs) from samples MMB3-04 and MMB3-07 are shown in Figure 4.17. In this study, for relatively young samples (D_e less than 5 Gy), the DRCs were fitted using a linear fit (Figure 4.17 a); while the samples that are relatively old (D_e more than 5 Gy) were fitted using a saturating-exponential-plus-linear function (Figure 4.17 b).

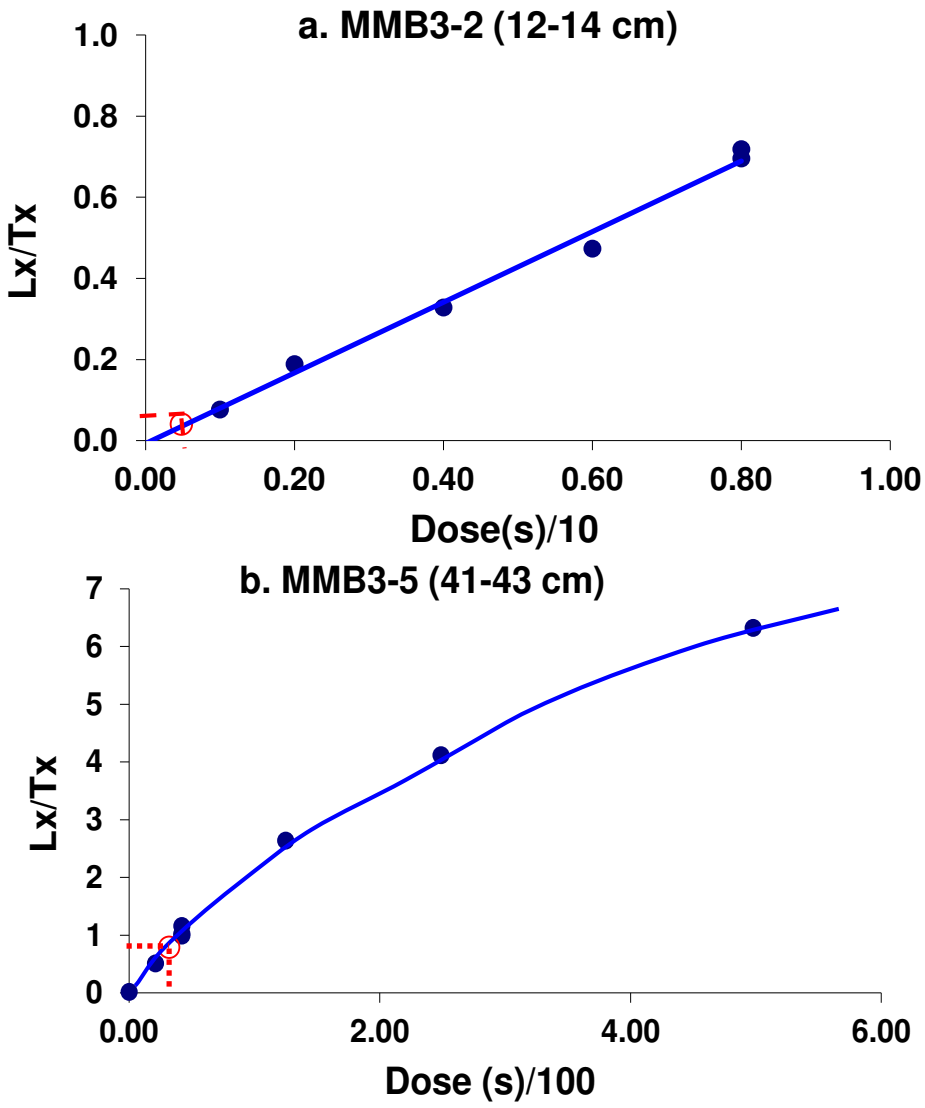

Figure 4.17. Regeneration dose curves for two single-grain samples from core MMB3.

4.6.2.3 SAR performance of single grains

4.6.2.3.1 Dose recovery for LSW samples

In order to test if the thermal treatment conditions obtained using single aliquots (discussed in the previous section) are applicable to single grains, a dose recovery test was first conducted on 5 single-grain discs (500 grains in total) made up of core LSW materials. The modified SAR protocol was applied with a 10 seconds preheat of260 °C and 5 seconds preheat of 180 °C for test dose. Each of the sun-bleached quartz grains was given a beta dose of 348 seconds (~ 40 Gy). Altogether 500 single-grain data were collected and analysed under seven selection criteria (Appendix A1.2).

The dose recovery results for single-grain data analysed with the seven selection criteria are listed in Table 4.5. On the first selection procedure, about 39 % (194 out of 500) of grains were rejected due to low signal intensity probably caused by the incomplete stimulation they received. Only half of the remaining grains survived the recycling ratio tests. A majority of 84 % of grains passed the IR depletion ratio check. About 68 grains were rejected as they failed in either one of the selection criteria from criteria 4 to 7. About 39 out of the 68 grains were rejected because their recuperations were greater than 5 %. Among the 60 grains left after the seven selection criteria above, only 34 have errors within 10 % of unity. The ratio of recovery dose and given dose for these 34 grains was calculated and plotted in Figure 4.18; 66 % (22 out of 34) gave good recovery (ratio of recovery dose and given dose fall within the range of 0.90 and 1.10). Generally, the thermal treatment conditions tested by single aliquots are applicable to the single grains. Quartz grains that undergo significant sensitivity change during the thermal treatment in the SAR procedure will be noted by the internal checks and thus those data will be rejected or corrected when interpreting the true D_e value.

Table 4.5
Single-grain dose recovery tests data selection results for LSW-CC (60-62 cm).

	Start	Criterion 1	Criterion 2	Criterion 3	Criteria 4-7	End
Grains Failed		194	153	25	68	
Grains remaining	**500**	306	153	128	60	**60**

Criterion 1-Signal intensity check (reject Tn<3XBG)
Criterion 2-Sensitivity correction-recycling ratios
Criterion 3-IR depletion ratio check
Criterion 4-Saturation and Monte Carlo fit check
Criterion 5- T_x/T_n curve
Criterion 6-Decade curve
Criterion 7-Recuperation (<5 %)

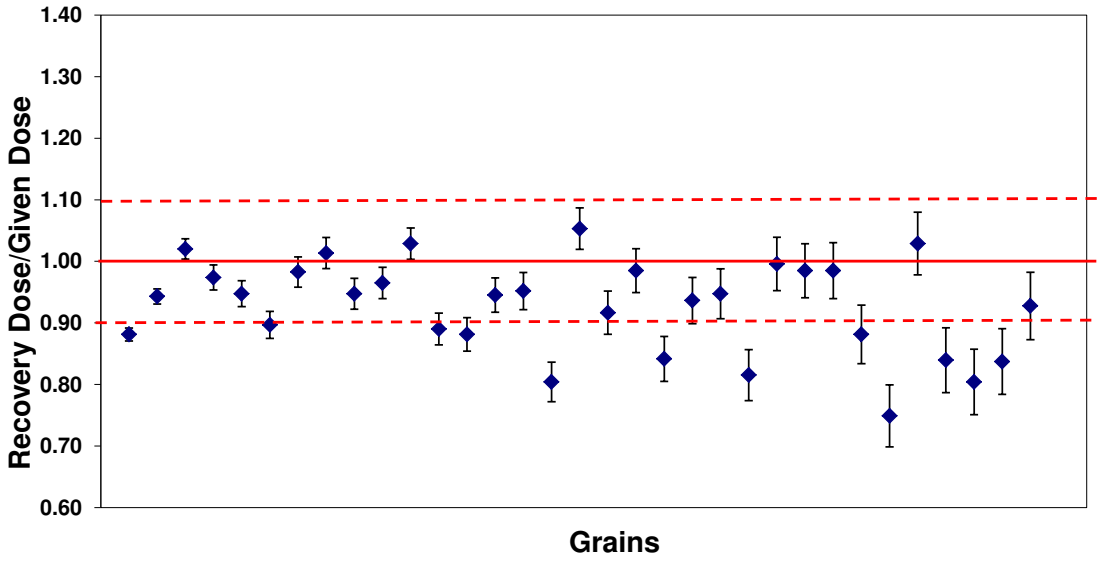

Figure 4.18. D_e recovery results for single-grain dose recovery test for core LSW (LSW-CC, 60-62 cm).

4.6.2.3.2 Dose recovery for LOLA samples

For core LOLA, LOLA-1 (17-20 cm) which has the most abundant material was chosen. Dose recovery tests on 5 combinations of preheat (220 to 260 °C) and cut-heat (160 to 180 °C) temperatures were conducted (Table 4.6). Each combination of temperatures was tested on 2 discs consisting of ~ 200 single grains. Procedures and selection criteria for data analysis were the same as for the core LSW (discussed above) except the variation of preheat and cut-heat temperatures. Generally, results from the 5 combinations were very

similar with respect to the number of grains accepted and their recovery. The set with lowest temperatures (preheat 220 °C and cut-heat 160 °C) was not very satisfactory because it yielded lower recovery and the number of grains accepted was also proportionately lower than the others. Among all, the set with preheat 220 °C and cut-heat 180 °C seemed to be more applicable for its higher acceptance of grains, higher recovery with remaining lower errors and overdispersion values. This set of parameters also matched those tested by the single-aliquot dose recovery test and again proved the thermal treatment conditions tested for single aliquots are adoptable for the single-grain analysis.

Table 4.6
Single-grain dose recovery tests results for LOLA-1 (17-20 cm) on 5 combinations of preheat (PH) and cut-heat (CH) temperatures.

PH	CH	Grains Analysed	Grains Accepted	% of Grains Accepted	Given dose (Gy)	Recovery dose (Gy)	Recovery (%)	Overdispersion (%)
260	180	179	65	36.3	40.5	40.0 ± 0.6	99 ± 1	9.56 ± 1.08
260	160	175	76	43.4	40.5	40.3 ± 0.5	100 ± 1	10.23 ± 1.02
220	160	179	54	30.2	40.5	39.2 ± 0.4	97 ± 1	5.75 ± 0.94
220	180	184	75	40.8	40.5	40.0 ± 0.3	99 ± 1	5.30 ± 0.78
240	180	172	59	34.3	40.5	40.6 ± 0.4	100 ± 1	4.68 ± 1.17

4.6.2.3.3 Dose recovery for 2LOLA2 samples

The parameters (preheat 220 °C and cut-heat 180 °C) of the core LOLA was applied to the 2LOLA2 core as they were collected near to each other in Loudens Lagoon. However, the sample of core 2LOLA2 chosen for the single grain dose recovery test was from the upper surface layer of the core (2LOLA2-1, depth 8-12cm). As shown in Table 4.7, the acceptance of grains and recovery were lower than those for core LOLA but the overdispersion value appeared to be higher. The reason for this needs to be further investigated. From the previous tests, applying medium preheat and cut-heat temperatures

did not cause significant alteration in dose recovery test. Therefore it is safe to proceed with this set of parameters for samples from the 2LOLA2 core.

Table 4.7
Single-grain dose recovery tests results for 2LOLA2-1 (8-12 cm).

PH	CH	Grains Analysed	Grains Accepted	% of Grains Accepted	Given dose (Gy)	Recovery dose (Gy)	Recovery (%)	Overdispersion (%)
220	180	300	110	36.7	40.5	38.8 ± 0.4	96 ± 1	9.71 ± 0.86

4.6.3 Selection criteria applied to D_e value determinations

Several criteria have been suggested and widely used for the analysis of single-grain D_e data (Olley et al., 2004; Jacobs et al., 2006a; Delong and Arnold, 2007; Arnold et al., 2008). They usually make reference to grain sensitivity, dose-signal repeatability, IR response and the precision of the final D_e. In this study, seven selection criteria (Appendix A.1.2) were used for single grain D_e determinations, according to those criteria that are most accepted, as well as based on the results of dose recovery tests. The aliquots and grains were rejected if they failed any of the selection criteria. Only those that passed all selection criteria were accepted for further analysis. These criteria were based on the following checks in sequence. The raw data were copied and pasted into a spreadsheet designed for checking signal intensity, recycling ratio, IR depletion ration and recuperation. The saturation check, T_x/T_n curve check and decay curve check were visually inspected under "Analyst" software window.

4.7 D_e analysis and age determination

Developments in OSL instrumentation and measurement protocols allow the acquisition of numerous D_e values from aliquots and single grains. These data can be used not only for statistical analysis and calculation, but also for investigating the types of pre-depositional, depositional and post-depositional processes that might have occurred and affected the buried sediment sample.

Despite proceeding from the same material, after selecting for appropriate grain size and applying same measurement conditions, the D_e values obtained from the same sample usually vary to some extent. In some cases, these variations can be large, depending on the sample. Experimental sources such as counting statistics and systematic instrumental uncertainty (arising from non-uniform measurement conditions applied to individual grains or aliquots), can cause the scatter of D_e values. However they were corrected by instrumental uncertainty of 2 % as reported by other studies (Jacobs et al., 2006a). At this stage, only the natural factors that caused the scatter of D_e values were considered. These natural factors can be concluded as following:

1) Partial bleaching – also termed "incomplete" or "non-uniform" bleaching in some references, is commonly found in many depositional environments (Olley et al., 1998; 1999 and 2004) due to surface coatings (e.g. water or organic matter) on grains and/or poor exposure to sunlight during sediment transport. This results in grains being deposited with a heterogeneous distribution of residual trapped charge and a correspondingly wide range of measured D_e (Olley et al., 2004). In all environments, grains may be transported at night and receive no light exposure and theoretically ~50 % of deposition occurs in the dark. However the last transport event is not necessarily the most important, as the grains may have been exposed to sufficient light in the previous transport cycles (Rhodes, 2011).

Apart from the environmental factors, sample characteristics are also important for successful OSL bleaching. Rhodes (2011) summarised that samples containing grains recently eroded from bedrock, typically have low OSL sensitivity and are relatively difficult to bleach. In contrast, quartz that has experienced multiple cycles of reworking over the recent geological past (e.g. desert dune sands, or significant heating by wildfires or in hearths) usually has high OSL sensitivity and is more easily bleached to a low residual level. In our study, sample characteristics are not a significant issue as most of the grains appear to be bright and sensitive in their OSL signals (Sections 4.6.1.1 and 4.6.2.1).

2) Post-depositional mixing – is the mixing of the deposit through physical disturbance (Richard et al., 1998; Bateman et al., 2007a; David et al., 2007). One of the most common disturbances is bioturbation, which refers to the post-depositional translocation, either vertically or laterally of sediments and soils either through mixing or exhumation by flora and fauna (Balek, 2002). In theory, sediments at or just below the surface are more likely to undergo maximum mixing and disturbance as this is where animal and plant activity is most intense and soil overturn rates are high (Heimsath et al., 2002). This process usually leads to intrusion of younger grains into older deposits or *vice versa*, and the grains affected might exhibit various palaeodoses (D_e) within one sample. Vegetation, in particular trees, usually disturbs sediment both though the growth and decay of root systems and via tree throws (Heimsath et al., 2002). Whereas the latter is clearly surficial, tree root growth can extend to great depths in areas with deep water tables. In such case, bioturbation is most intensive within a metre or so of the surface (Bateman et al., 2007b). Unlike partial-bleaching, bioturbated samples will display D_e values both higher and lower than the true burial dose (Bateman et al., 2007a). Arnold and Roberts (2009) concluded sediment mixing has the potential to affect the appearance of D_e

distribution in various ways including: symmetrically increasing the overall spread of D_e values, or increasing either positive skewness (where the dominant intrusion is by younger grains) or negative skewness (where the intrusive grains are mostly older), creating discrete dose populations (including zero-age grains) and multi-modal D_e distributions.

3) Microdosimetry – is caused by beta-dose heterogeneity among individual buried grains (Murray and Roberts, 1997; Olley et al., 1997) and occurs when beta particles from ^{40}K of the high radioactivity minerals (termed as hotspot) fluctuate. For example, if potassium feldspar grains, which have an internal K concentration of ~14 %, are dispersed in low abundance among quartz grains in sediments with an average bulk K content of 0.1-4 %, the D_e distributions are likely to be positively skewed (Arnold et al., 2008). Unlike bioturbation and partial bleaching which are highly dependent on the depositional environment, beta heterogeneity is an intrinsic aspect of exposure and affects all single grain distributions to a certain extent (Mayya et al., 2006).

4) Intrinsic grain-to-grain variability – is caused by variation of luminescence behaviour and differing responses to fixed SAR conditions (Jacobs et al., 2003).

4.7.1 Graphic display of D_e distribution

The use of single-aliquot and single-grain dating procedures will yield multiple values of D_e for each sample. When displayed graphically, these values can provide information on the reliability of individual measurements. Moreover they provide insight into whether the distribution of D_e values is normal or skewed, thus allowing consideration of the potential causes of D_e variations. Olley et al. (1999) propose that the shapes of dose distributions and their degree of asymmetry can be used to infer the degree of partial bleaching contamination in samples and thus may be useful in selecting appropriate age models.

There are two extensively used methods of displaying the D_e data – histograms and radial plots (Olley et al., 1998; 1999; Bøtter-Jensen et al., 2003). Histogram plots are a straightforward form of data presentation for dose estimates that have similar relative errors (precisions) (Olley et al., 1999). To construct a histogram, the individual D_e values must be sorted and entered into bins of finite D_e width. The bin width will affect the resolution of the shape of the distribution. In order to gain better resolution, a smaller bin width should be chosen. Histograms for a normal distribution will approximate a Gaussian distribution. However aliquots or single grains typically vary greatly in their OSL intensities, and the precisions of their dose estimates differ substantially. As histogram plots take no account of difference in precision associated with individual dose estimates, the inclusion of relatively imprecise values may seriously distort a histogram plot and results in incorrect inferences being drawn about the true pattern of the dose distribution (Olley et al., 1999). Despite this disadvantage, histograms are still widely used as a general-purpose graph as they are nearer to the raw data, easier to use and more convincing (Galbraith, 2010). For a better interpretation of the D_e values, histograms have been improved by adding scatter plots of standard error (Galbraith, 2010) or ranking D_e value with standard errors (Demuro, 2009).

A more appropriate and informative method proposed by Galbraith (1988) is conventionally known as the "radial plot". Unlike the histograms, in a radial plot each D_e value is plotted as an individual point on the graph. The x-axis expresses the measurement of the precision as well as the relative error (expressed as a percentage). The more precisely the D_e value is, the further it plots to the right on the diagram. The y-axis is usually the values of D_e expressed in logarithmic terms which are calculated by subtracting a reference value from each of the log doses and then dividing each of the

differences by the associated standard error (Galbraith et al., 1999; Olley et al., 1999). The choice of reference value is arbitrary, but the mean value of D_e is the value usually chosen. Altering the reference value causes the data points to rotate about the origin (Bøtter-Jensen et al., 2003). Another useful feature of the radial plot is that it naturally sorts the data. If the individual estimates are consistent with a common dose, about 95 % of the points should fall within a band ±2 units vertically around some radial line (Galbraith, 1988). If the data arise from two distinct populations, then the points should mostly lie within two such radial bands. If there is a minimum dose, the data should almost all lie within or above the radial band corresponding to that dose.

Here D_e values are displayed using both improved histogram format and the radial plot format. The histograms with ranked D_e values shown in this study were drawn using the Microsoftware Excel program, each individual D_e value was shown as a bold dot with its error bars. For samples with positive D_e values, the radial plots were drawn using the Radial Plot v1.3 software developed by Jon Olley and programmed by Michael Reed. For samples with negative D_e values, the radial plots were drawn using the RadialPlotter v2.1 software developed by Pieter Vermeesch (2009). The ±2σ bands in blue were drawn using the D_e value calculated by the Central Age Model and those in red were drawn using the D_e values calculated by the Minimum Age Model (detail in the following sections).

4.7.2 Introduction to age models

With the use of one of the formats discussed above, the distribution pattern of the D_e values can be obtained. However, for the age calculation, only one single D_e value is used. It is necessary to calculate the D_e value that is most representative of the dose – the one that has accrued since the event of interest using the appropriate age model. The age

models are statistical methods developed to isolate grains representative of the true burial dose. If the palaeodose shows a normal distribution, the representative dose could be the central parameter such as the average or the median of this distribution. In the case of a non-normal distribution, the selection of representative dose requires firstly decoupling the mixing dose populations and thus becomes more complicated. This study focuses on the central age model and the minimum age model, which have been shown to provide the most accurate optical age estimates for all of the known-age samples (Arnold et al., 2007). They are more applicable to the Macquarie Marshes samples, since partial bleaching is the dominant cause of D_e scatter in these fluvial samples (further discussed in the following sections).

4.7.2.1 Central age model (CAM)

The "central age model (CAM)" was developed by Galbraith et al. (1999) to obtain the best estimate of D_e. This model is based on the assumption that the logarithms of the true D_e values are drawn from a normal distribution with a mean μ and standard deviation (usually termed 'overdispersion (OD)') σ. These parameters are determined from the measured data set according to the equations developed by Galbraith et al. (1999). The over-dispersion parameter (usually reported as a percentage) is obtained from applying the CAM and has been used extensively as an indicator of spread in dose distributions. High σ values (e.g. >10 %) may indicate grain mixing or incomplete zeroing (Rhodes, 2011). OD represents the fraction of the observed spread in D_e which is not accounted for by the spread of the data as expected from the size of the errors on the individual D_e estimates (Bailey and Arnold, 2006). Thomsen et al. (2012) reviewed the previously published single-grain OD values and found most samples have an OD larger than 15 % despite

uncertainty (counting statistics and instrument reproducibility) were considered. Because such significant over-dispersion are also found in laboratory dose recovery experiments where all extrinsic sources of variability have been eliminated, the authors pointed out the significant over-dispersion in natural well-bleached samples is caused by intrinsic (Thomsen et al., 2012). In this study, CAM is used as an informative comparison to the other age models and also an estimate of the overdispersion value.

4.7.2.2 Minimum age model (MAM)

The "minimum age model (MAM)" has been described and tested in simulations by Galbraith and Laslett (1993) and Galbraith et al. (1999). This model is based on the assumption that the logarithms of the true D_e values are drawn from a truncated normal distribution including 3 to 4 parameters: the lower truncation point (the minimum age) is denoted by γ; the unknown proportion of fully bleached grains is denoted by p; the rest of the population that has ages in excess of γ is approximated by a truncated normal distribution, with mean μ and deviation σ. If the log D_e distribution is not truncated, then μ and σ would correspond to its mean and standard deviation. In cases where the 4-parameter model (usually termed "MAM4") does not fit, a more robust estimate of γ may be obtained using a 3-parameter model (usually termed "MAM3") in which $\gamma=\mu$. The MAM4 will converge to the CAM when γ is small and p is close to zero. In various geomorphic settings, the application of the MAM provides the most accurate estimate of the burial dose while the weighted mean D_e (as obtained using the 'central age model') gives rise to burial age overestimates of up to a factor of 10 (Olley et al., 2004). However, the minimum age model does not always provide a reliable age estimate due to inferred cause of variations in D_e values (e.g. Galbraith et al., 1999). For example, applying the

MAM for samples that have undergone post-depositional disturbance will result in the intrusion of grains from younger strata (Galbraith et al. 1999). The authors also pointed out in the case of grains that experienced unusually low beta dose rates, the minimum log palaeodose γ does not relate to the most fully bleached grains.

4.7.2.3 Finite mixture age model (FMM)

In nature, various bleaching and burial process occur with a discrete D_e component, and in this case the "finite mixture age model (FMM)" can offer a useful alternative for D_e determination (Galbraith and Green, 1990; Galbraith and Laslett, 1993). This model was first proposed by Galbraith and Green (1990) and originally designed for fission track dating (Galbraith and Laslett, 1993). The model has been used in OSL studies of mixed sediments (Roberts et al., 2000; Jacobs et al., 2006a; Bateman et al., 2007a; David et al., 2007; Jacobs et al., 2008). This model estimates the number of discrete dose populations in a mixture, their corresponding palaeodoses and their relative proportion among the age groups. It has been shown that this age model should only be applied to single-grain scale of analysis (David et al., 2007; Arnold and Roberts, 2009), because multi-grain aliquots may consist of grains drawn from more than one dose population resulting in spurious dose populations.

The FMM is based on the assumption that the overdispersions for each dose population are the same, which may not always be the case for natural samples (e.g. Arnold and Roberts, 2009). These heterogeneously bleached fluvial sediments are composed of grains with log D_e values that are not normally distributed and/or that consist of multiple or discrete dose components with significant different oversdispersion values; and thus not suitable for applying the FMM.

The FMM was not applied to the samples studied here as most of them were suitable for applying the MAM because partial-bleaching was the dominant influence on the D_e values. However, further studies can be done with the application of the FMM to determine the relative abundance of the D_e value groups, in particular for those that contain a broad range of D_e values.

The above age models all use the natural logs of individual D_e estimates. In the case of very young and modern samples which contain negative, zero or close to zero D_e values, the log-transformed D_e datasets can pose problems. Arnold et al. (2009) revised the original version of the central and minimum age models so that they can be applied to un-logged D_e estimates and their associated absolute standard errors. These un-logged versions of the central and minimum age models have been shown to be capable of producing accurate burial dose estimates for modern-age and very young (<350 yr) fluvial samples that contain (i) more than 20 % of well-bleached grains in their D_e distributions, or (ii) smaller sub-populations of well-bleached grains for which the D_e values are known with high precision (Arnold et al., 2009).

In practice, no single age model is appropriate for all situations. Bailey and Arnold (2006) evaluated a selection of the various statistical approaches and showed that significantly different estimates of the D_e values can be obtained by applying the different methods. They proposed a decision-support criterion to help with choosing the most appropriate model for D_e determination. Fuchs and Owen (2008) cautioned to be careful when using these methods. They pointed out that the underlying problem is that the uncertainty regarding the causes of a broad distribution of D_e values is more complex than the bleaching history, since it may also be due to effects such as microdosimetry and

luminescence characteristics. Thus, the application of the statistical models requires knowledge of the potential variability present in well-bleached samples.

In this study, the 'central age model' was only applied to a few samples which were less dispersed in their D_e values with low overdispersion values (<20 %). For the rest of the samples, the most mathematically rigorous of the age models – the 'minimum age model' was applied to obtain representative D_e values for most of the fluvial samples. Only for the upper surface sediment samples which contain negative, zero or close to zero D_e values, was the un-logged version of the original age model used. The rest of the samples were still calculated by the original (log-transformed) version of the central and minimum age models, since these age models are better suited to the statistical properties of typical single-grain and multi-grain single-aliquot D_e datasets for most routine dating applications (Arnold et al., 2009). Thomsen et al. (2012) emphasised that analysis of single grain dose distributions requires knowledge of the dispersion of the well-bleached part of the dose distribution, which can be estimated by measurement of a suitable analogue, e.g. a well-bleached sample. Herein, the OD values from the dose recovery test (on well-bleached samples with known laboratory dose) for each core were used as a guide for applying the age models.

As the D_e distribution of either single grain or aliquot is highly dependent on the environmental settings, the sedimentology was considered when interpreting the data. Accordingly, the environmental setting of the sampling sites were reviewed before interpreting the D_e values and estimated the ages of the cores.

4.7.3 D_e distributions and age determination for core MMB3

Core MMB3 was collected in Bora channel where marsh vegetation was growing nearby at the time of sampling. The water was relatively shallow, with a depth of about 5-10 cm. At this fluvial sampling site, we would expect OSL quartz samples with a mix of partially and fully-bleached quartz grains.

4.7.3.1 D_e distributions of single aliquots

Due to the limitation of material used for single aliquot analysis, 24 aliquots from each of the deeper parts of the core (MMB3-5 and MMB3-7) were analysed while only 12 aliquots from MMB3-4 were analysed.

The shape of the dose distributions can be used to assess the likelihood that the aliquots consist only of grains that were well-bleached at the time of deposition (Olley et al., 1999). Figure 4.19 shows the histograms with ranked D_e values (on the left) and the radial plots (on the right) for the three samples. The spread of D_e values is large, ranging 8-10 times from the smallest values to the largest ones within the same sample. However, the ratio of maximum and minimum doses in these samples is much lower than other fluvial samples (100-400 times) found by Olley et al. (1998). The three samples show asymmetric distributions to some extent and a "tail" at higher D_e values in their histograms. The D_e distributions from samples taken progressively deeper down the core (from MMB3-4 to MMB3-7), have the leading edge of each distribution as well as the "tail" values moved systematically to larger dose values. Comparatively, MMB3-4 and MMB3-5 are more asymmetric with longer tails while MMB3-7 is more symmetric with a shorter tail. These asymmetric distributions are similar to those found by Olley al. (1998, 1999) among various young fluvial sediments, in which cases they suggested the lowest D_e values might

be more representative of the true burial dose while the high D_e values of poorly bleached grains might yield overestimated results. In the radial plots, despite the limited number of available data, the precision for almost all the samples (except one sample from MMB3-7) are relatively high. The deeper the sample (i.e. older) is, the more precise the D_e values are. Of all the radial plots, very few D_e values fall within the $\pm 2\sigma$ band with central age model value and these data cannot be simply grouped into two populations by plotting an additional $\pm 2\sigma$ band with minimum age model value.

Considering these data were obtained by applying the same instrumental conditions to the same sample and selected by the seven criteria discussed in Appendix A1.2, and the heterogeneous characteristic and behaviour among the grains would not have caused such a great variation of D_e values, the asymmetric distribution and variation of D_e values are more likely to be caused by the "contamination" of partially-bleached grains in the fully-bleached grains.

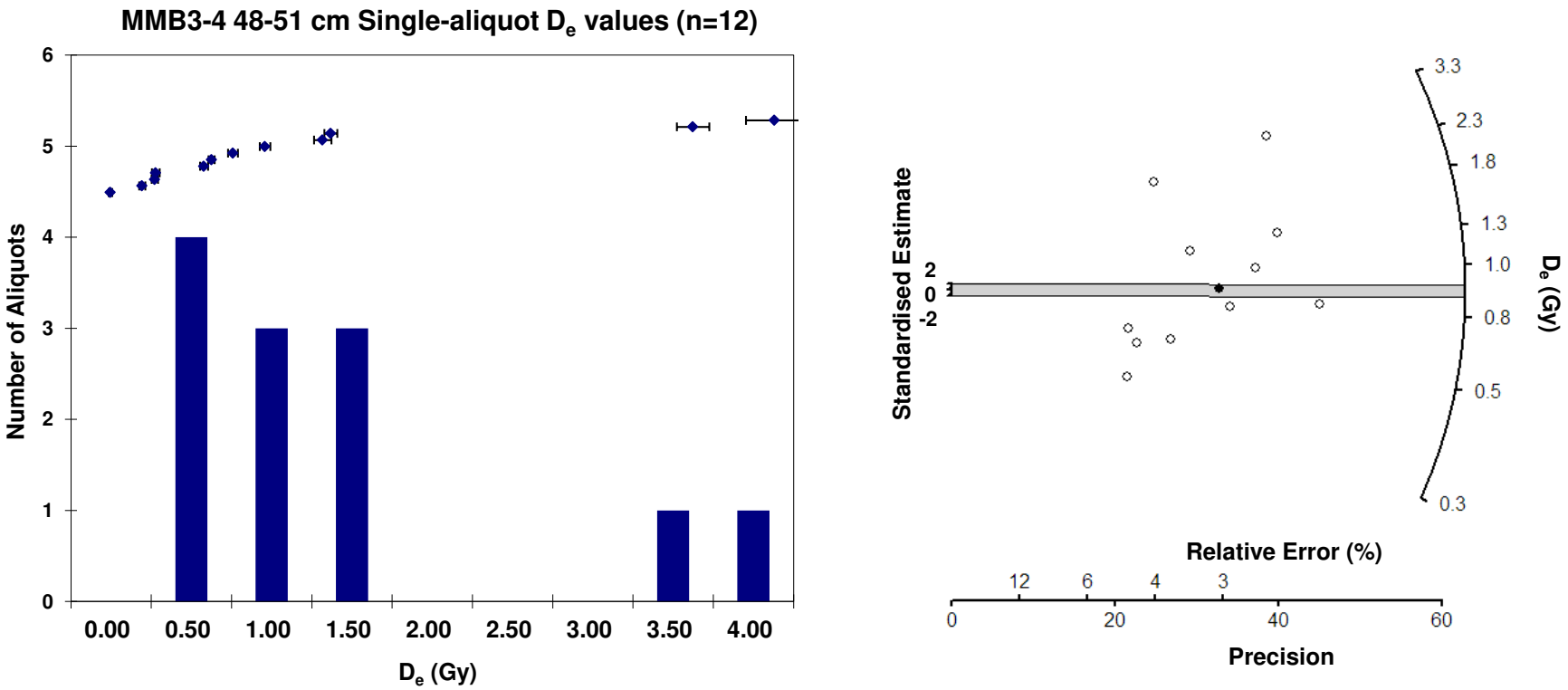

Figure 4.19. Histograms with ranked D_e values (left) and radial plot (right) of single-aliquot data from core MMB3.

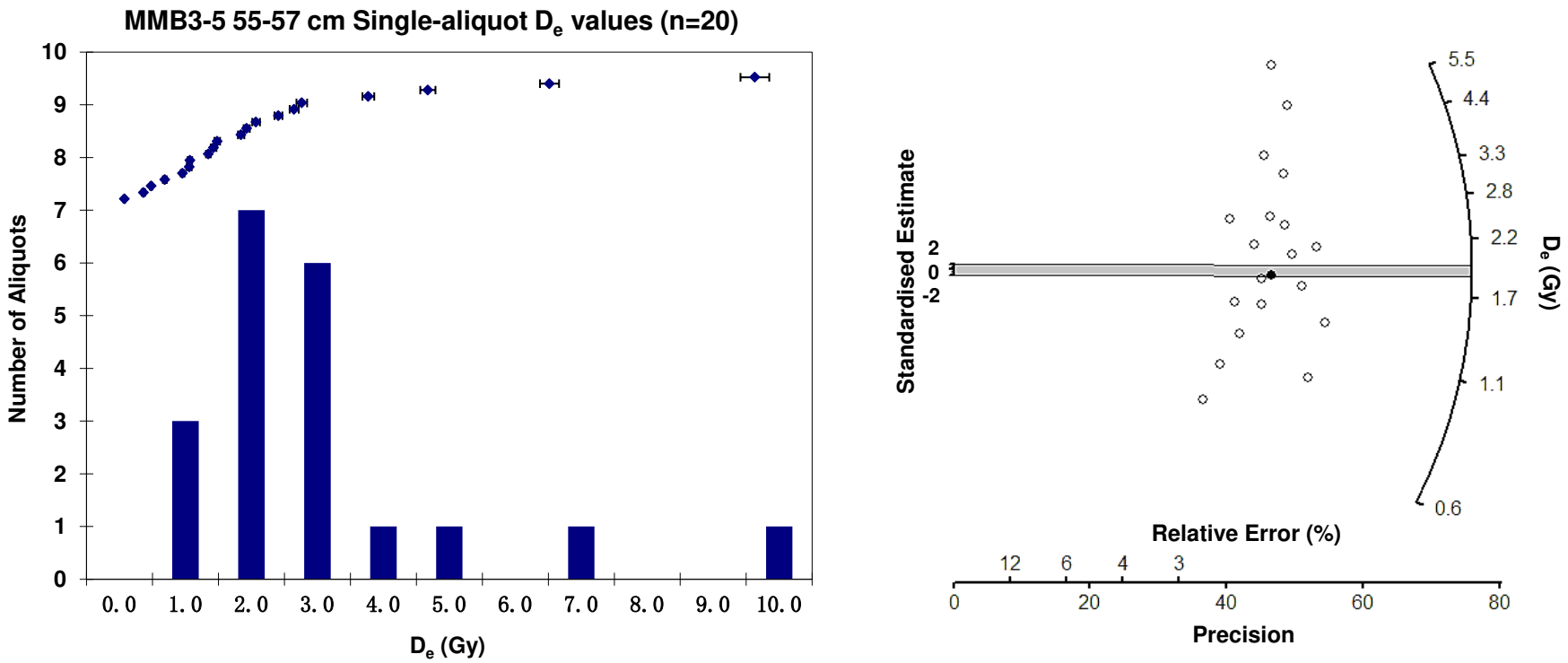

Figure 4.19 (continued). Histograms with ranked D_e values (left) and radial plot (right) of single-aliquot data from core MMB3.

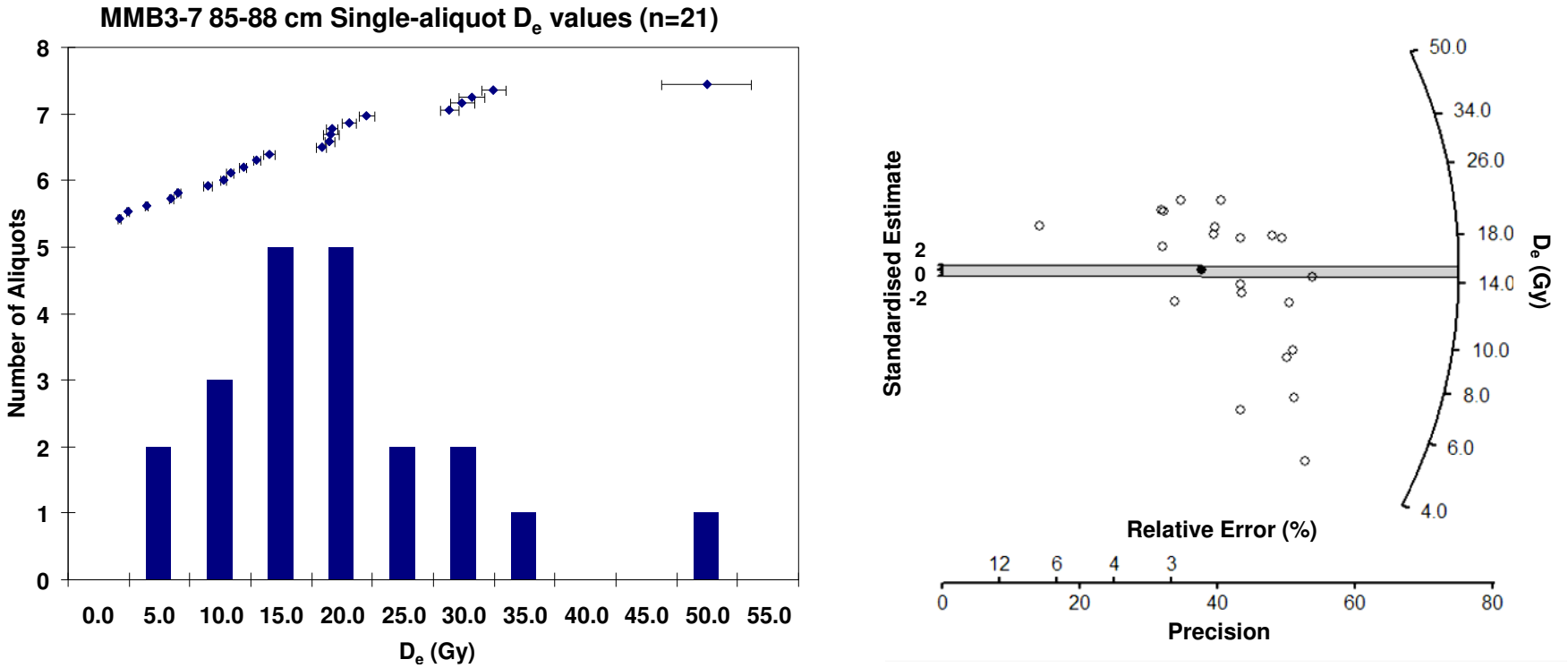

Figure 4.19 (continued). Histograms with ranked D_e values (left) and radial plot (right) of single-aliquot data from core MMB3.

4.7.3.2 D_e distributions of single grains

Given the possible insufficient bleaching problem shown in the single aliquot results shown above, single grain measurements were conducted in order to identify fully bleached grains. Selected D_e values (survivors of the seven selection criteria) of single grains for the seven core sections of MMB3 are plotted in both histograms with ranked D_e and radial plots in Figure 4.20. For comparison, D_e distributions of single grains for dose recovery test (Section 4.3.5) are shown in Figure 4.21 (Page 155).

Of the seven core sections, only sample MMB3-1 contains negative D_e values, which is statistically reasonable for weak OSL signals. This could also indicate possibly sensitisation during the initial (and uncorrected) natural OSL measurement in the SAR protocol (Bateman et al., 2007a).

+

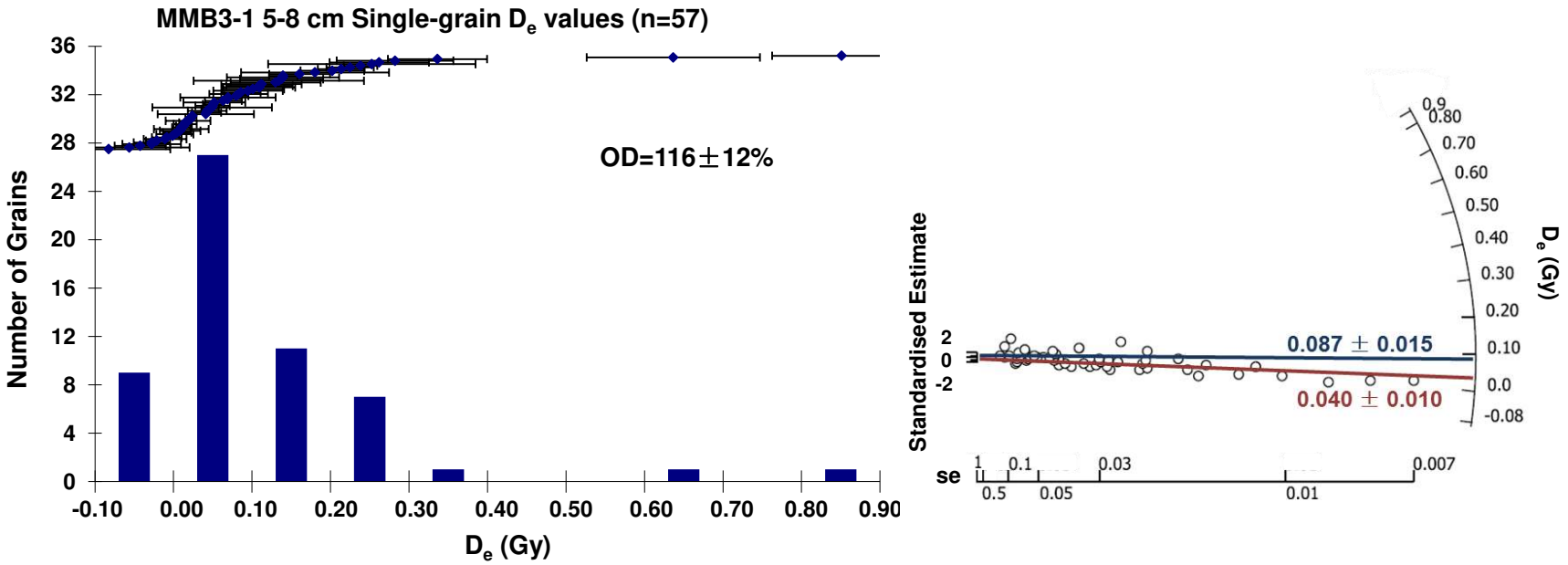

Figure 4.20 Histograms with ranked D_e values and radial plot of single-grain data from core MMB3. (left graph: histogram; right graph: radial plot, blue line and number indicate D_e calculated by central age model, red line and number indicate D_e calculated by minimum age model)

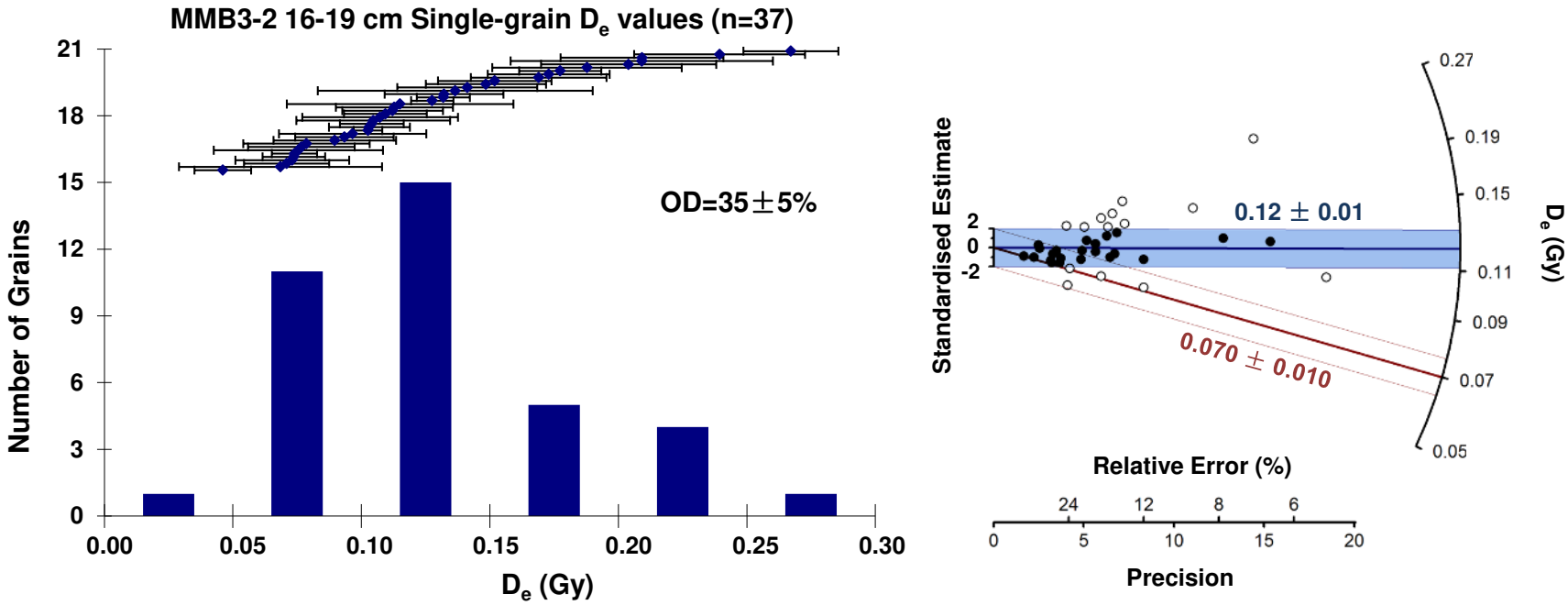

Figure 4.20 (continued). Histograms with ranked D_e values (left) and radial plot (right) of single-grain data from core MMB3.

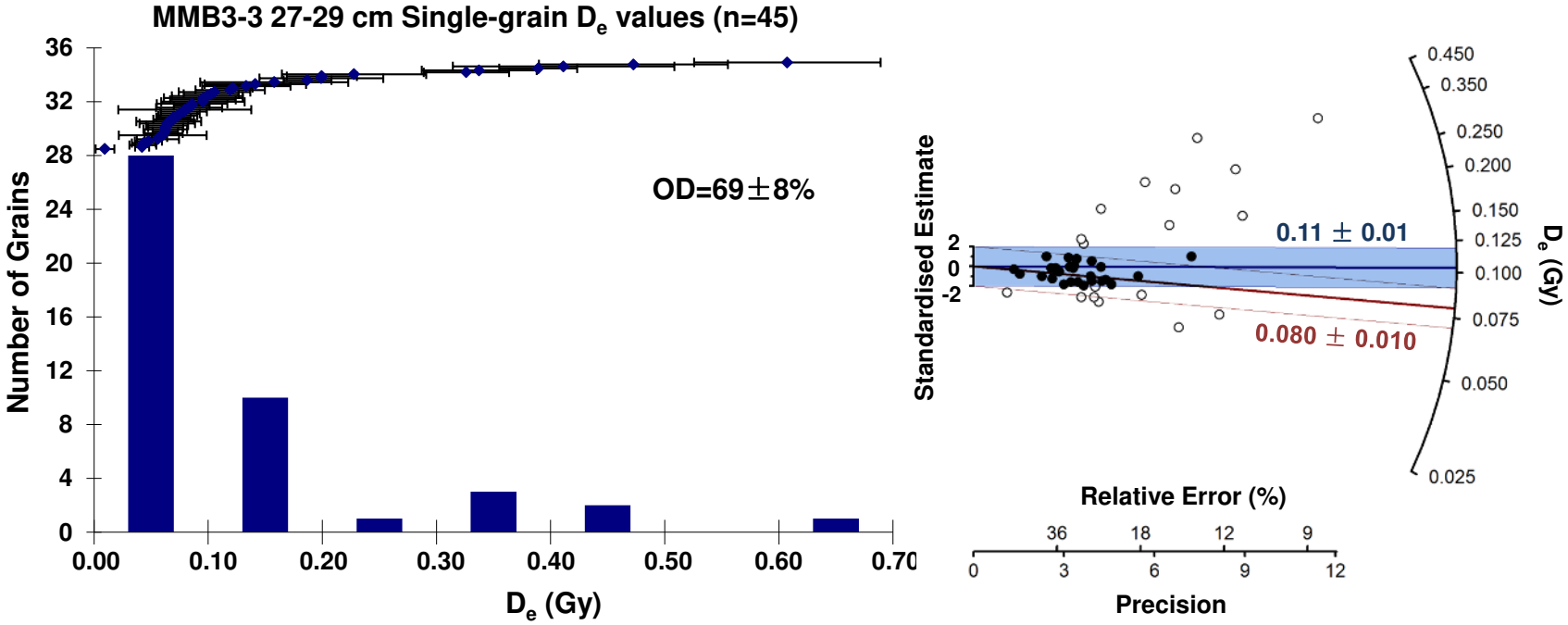

Figure 4.20 (continued). Histograms with ranked D_e values (left) and radial plot (right) of single-grain data from core MMB3.

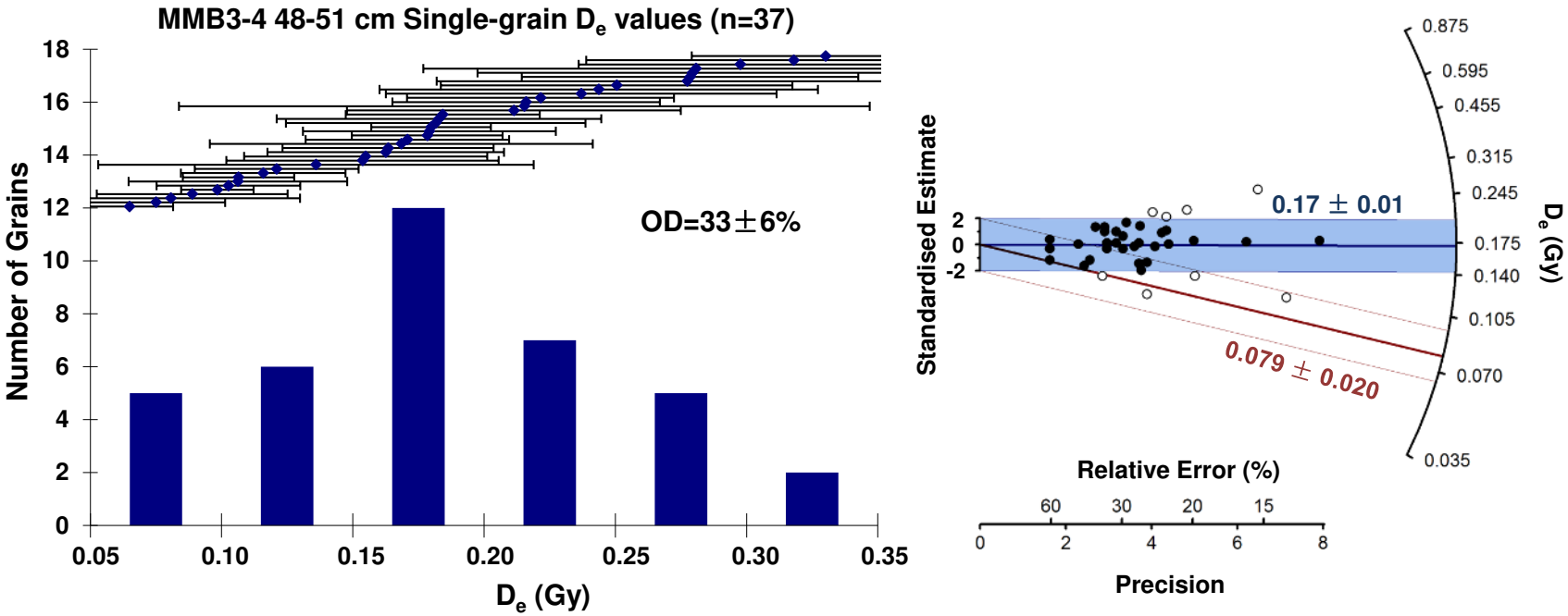

Figure 4.20 (continued). Histograms with ranked D_e values (left) and radial plot (right) of single-grain data from core MMB3.

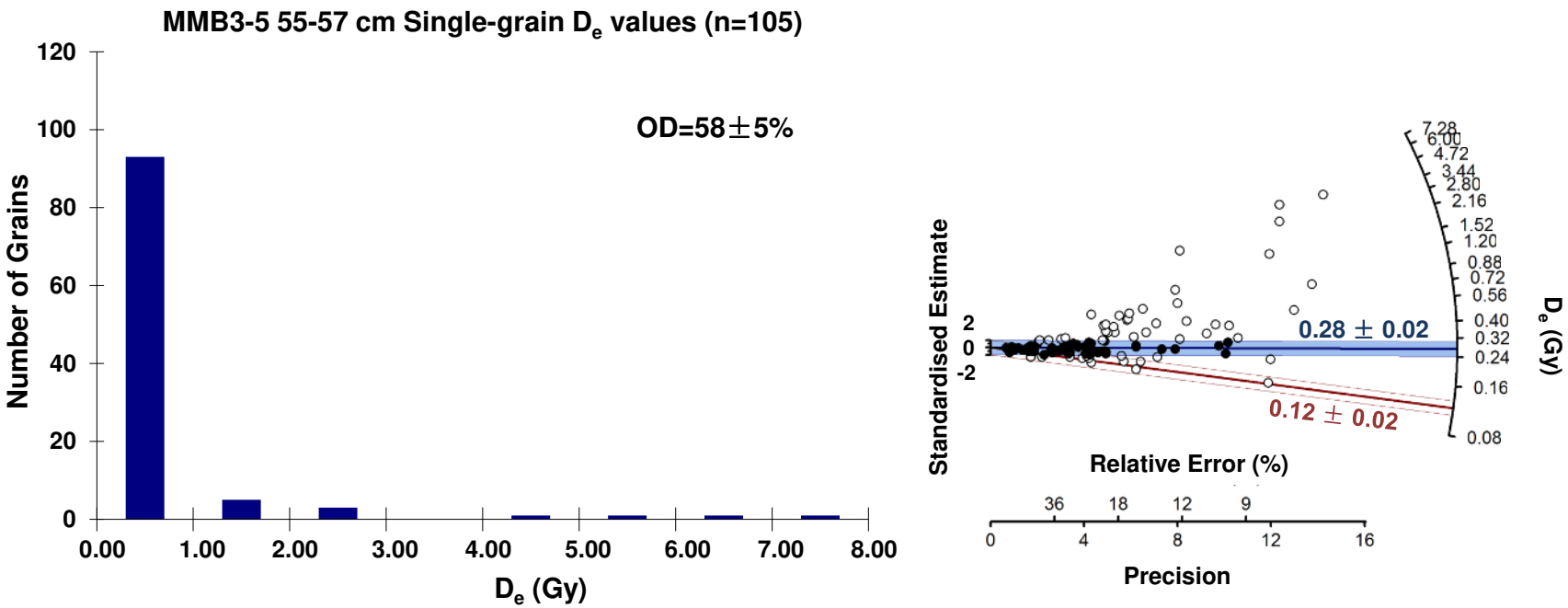

Figure 4.20 (continued). Histograms with ranked D_e values (left) and radial plot (right) of single-grain data from core MMB3.

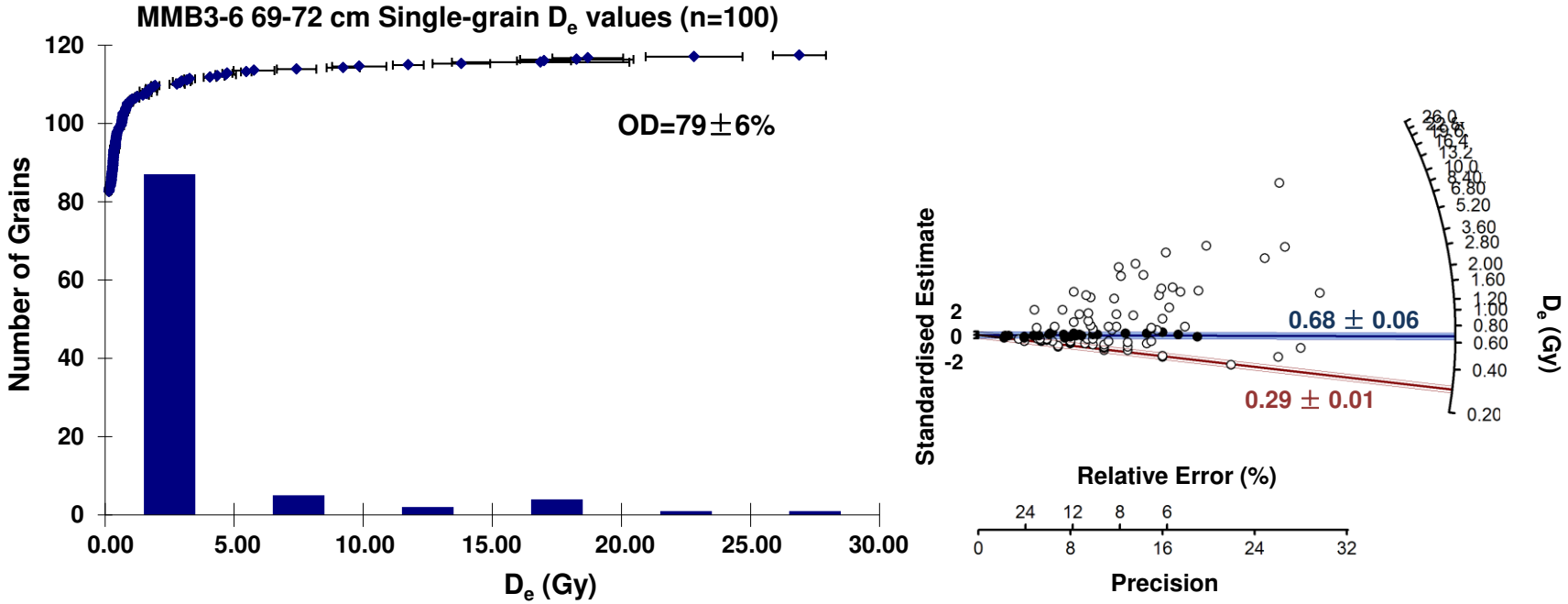

Figure 4.20 (continued). Histograms with ranked D_e values (left) and radial plot (right) of single-grain data from core MMB3.

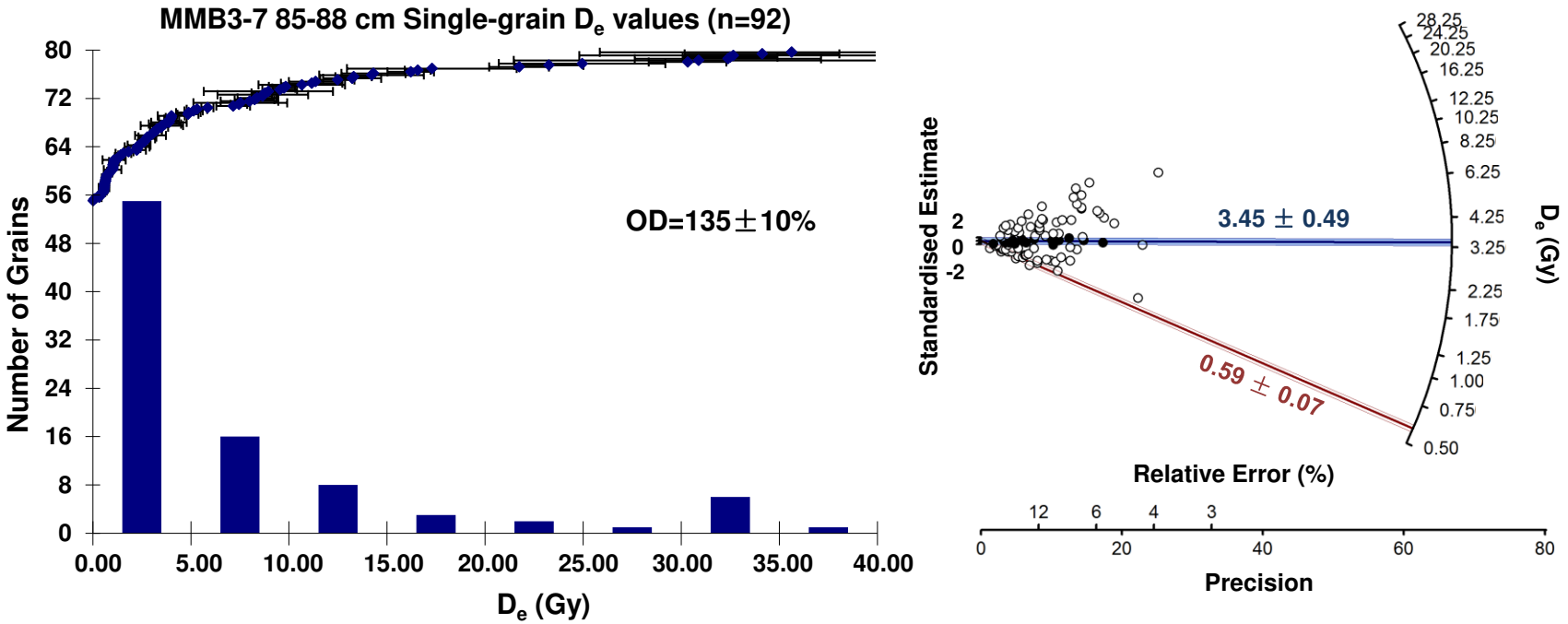

Figure 4.20 (continued). Histograms with ranked D_e values (left) and radial plot (right) of single-grain data from core MMB3.

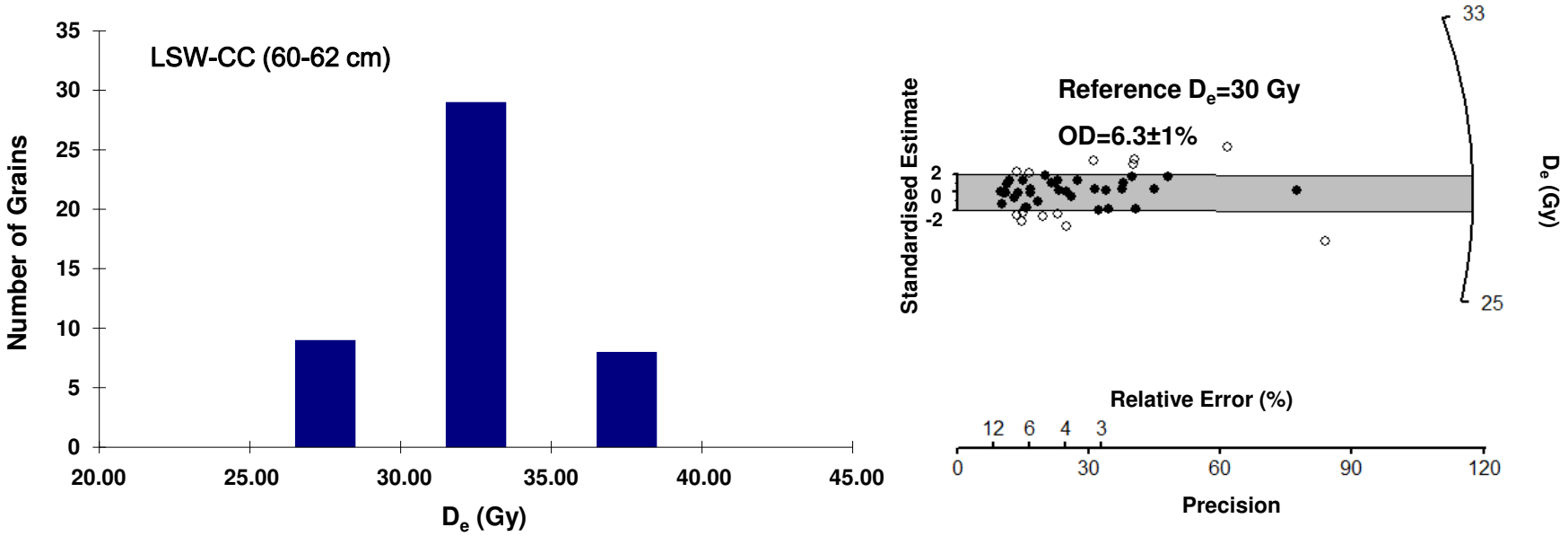

Figure 4.21. Histograms with ranked D_e values (left) and radial plot (right) of single-grain data from dose recovery test (LSW-CC).

The MMB3-3, MMB3-5, MMB3-6 and MMB3-7 data generally show more positive skewness in the histograms and the range between the minimum and maximum values range from 60 to 800 times. They reveal typical fluvial samples similar to those found by Olley et al. (1998); skewed dose distributions with a minority of high dose estimates forming an extended high value tail. It is likely that grains of these samples were carried by a flood upstream of Bora Channel and deposited at the sampling site. The coverage of water and vegetation, and insufficient exposure time to the Sun led to heterogeneous bleaching of the grains, thus causing the great variation of D_e values. A recent study by Rhodes (2011) found that deep water attenuates the UV end of the spectrum, reducing the bleaching rates of the grains, and the same can be affected by vegetation coverage. It is also likely that the higher proportion of partially-bleached grains in these samples may indicate they were deposited in deep water with good vegetation coverage in the surrounding area. As suggested by Olley et al. (1999), the asymmetrical distribution can reveal the increasing proportion of unbleached grains. The higher proportions of partially-bleached grains among these samples also indicate the flow rate was comparatively fast at the time period represented by these sections. Comparatively, MMB3-1, MMB3-2 and MMB3-4 show relatively more symmetrical distribution in their histograms with D_e values ranging 5-10 times between the minimum and maximum values. They may reveal either a contribution of aeolian grains deposited in the dry years or fluvial grains with higher proportion of fully-bleached grains (Olley et al., 1999). The contribution of aeolian sand is very unlikely in particular in MMB3-1 and MMB3-2 samples because the sampling site close to Bora channel has been inundated for a relatively long time (Kingsford and Auld, 2003). The addition of a high proportion of fully-bleached fluvial sand is more likely to

happen during the relatively dry years when the flow rate was relatively slow and the grains were carried from upstream and more fully bleached before burial.

The uppermost sediment samples (MMB3-1 to MMB3-4) generally show two distinctive groups on their individual radial plots. The deeper core sections (MMB3-5 to MMB3-7) show a large spread of data in their radial plots. The spread of D_e values indicates grains from these core sections may be a mixture of grains from different sources, or they may have undergone complicated processes before and after their burial. In this case, no single explanation – such as partial bleaching, is sufficient to explain the observed spread of D_e values. The grains may have originated as fluvial sediments, experienced partial-bleaching before burial, affected by bioturbation at a certain time period, but they remained undisturbed until recent excavation. Such broad distribution of the D_e is very unlikely to have been caused by microdosimetry (Murray and Roberts, 1997; Mayya et al., 2006), because too little time has elapsed since deposition to expose these grains to sufficiently high dose rates (Arnold et al., 2009). Further investigation is needed to understand the influence of microdosimetry at this sampling site. Considering this sampling site was in a fluvial setting, partial bleaching would still be the main cause of D_e scatter.

Similar to the single-aliquot data, all these single-grain D_e data, again, generally tend to increase with the increase of core depth. Zero-doses D_e grains are not found among samples from the deeper core sections, indicating they have not been in recent contact with the ground surface (Bateman et al., 2007a). These observations further confirm that, compared to partial-bleaching, bioturbation and reworking of sediments in recent years are not the main cause of the variation of D_e values.

Due to the limitation of dating material, the 180-212 μm grain-size was used for three sections (MMB3-2, MMB3-6 and MMB3-7). For all the others, the 125-180 μm grain-size fractions was used. It is worth mentioning that although a larger grain-size was used when dating these samples, the spread of D_e values caused by the contamination of partial-bleached grains still existed and the proportions of these contaminants were too large to be neglected. The notion that coarser fractions may be better bleached than the finer fractions (Olley et al., 1998; Hu et al., 2010) is obviously not the case in core MMB3 sections. This again proves that partial-bleaching effects are profound in these environmental settings.

As is shown in the ranked histogram and radial plot of the single-aliquot data, the relative standard error tends to increase with the increase of D_e value within a given sample. However, this is not always the case for single-grain data. In particular, for the near-surface sediment sample, the relative standard error of D_e values displays a great variation. This finding is similar to those found by Porat et al. (1996) and Greenbaum et al. (2000) and is thought to be attributed to inadequate sunlight exposure of the grains prior to burial (Thorndycraft et al., 2008).

4.7.3.3 Age models

Initially, the D_e values of all the samples were calculated by the 'Central Age Model (CAM)'. MMB3-1 was calculated by un-logged CAM (UCAM) as it contains negative numbers. The data for MMB3-2, MMB3-3 and MMB3-4, which contain low D_e values close to zero, were also calculated by UCAM for comparison. As shown in Table 4.8 (Page 160), CAM gives over-dispersion values from 35 % to 135 % for all the samples, which are all greater than the recommended value (20 %) to apply this age model. This, again, indicates that partial bleaching should be the main consideration when choosing the

appropriate age model for interpreting D_e distribution of these samples. A previous study by Bateman et al. (2007b) proposed high OD values together with zero dose values may be particularly useful in highlighting samples currently undergoing bioturbation and also in identifying older samples which were once bioturbated. They found within a modern bioturbation core profile, the OD values declined from the surface modern soil to the underlying sand unit. Such a trend of declining OD was not found in the core MMB3 profile and the OD values exhibit random distribution along the core. This again proves in this sampling site, the bioturbation effect on the dose distribution is relatively minor compared to the partial-bleaching effect. We can also see from Table 4.8 that the D_e values of UCAM and CAM are very similar in samples MMB3-2 and MMB3-3, but the overdispersion values calculated by UCAM are greater than CAM. However, in sample MMB3-3, the D_e value calculated by UCAM is larger than that for CAM while the overdispersion values are similar.

Table 4.8
The D_e values of core MMB3 calculated by different age models.

	Sample ID	Depth (cm)	Grain size (μm)	Total Dose Rate (Gy/ka)	UCAM			CAM			UMAM4		MAM	
					De (Gy)	Age (a)	Overdispersion (%)	De (Gy)	Age (a)	Overdispersion (%)	De (Gy)	Age (a)	De (Gy)	Age (a)
SG	MMB3-1	5-8	125-180	1.27 ± 0.10	0.087 ± 0.015	67 ± 13	116 ± 12	-	-	-	**0.04 ± 0.01**	**31 ± 8**	-	-
	MMB3-2	16-19	180-212	1.52 ± 0.13	0.13 ± 0.02	81 ± 12	80 ± 8	0.12 ± 0.01	78 ± 9	35 ± 5	**0.07 ± 0.01**	**45 ± 8**	-	-
	MMB3-3	27-29	125-180	1.59 ± 0.12	0.12 ± 0.02	75 ± 11	66 ± 4	0.11 ± 0.01	65 ± 9	69 ± 8	**0.08 ± 0.01**	**49 ± 7**	-	-
	MMB3-4	48-51	125-180	1.78 ± 0.14	0.18 ± 0.02	97 ± 11	57 ± 6	0.17 ± 0.01	96 ± 10	33 ± 6	**0.08 ± 0.02**	**44 ± 12**	-	-
	MMB3-5	55-57	125-180	1.80 ± 0.14	-	-	-	0.28 ± 0.02	150 ± 66	58 ± 5	**0.12 ± 0.02**	**65 ± 10**	-	-
	MMB3-6	69-72	180-212	1.73 ± 0.12	-	-	-	0.68 ± 0.06	385 ± 43	79 ± 6	**0.29 ± 0.01**	**165 ± 13**	-	-
	MMB3-7	85-88	180-212	1.88 ± 0.14	-	-	-	3.5 ± 0.5	1805 ± 289	135 ± 10	**0.58 ± 0.07**	**306 ± 43**	-	-
SA	MMB3-4	48-51	90-125	1.78 ± 0.14	-	-	-	0.89 ± 0.20	503 ± 122	79 ± 16	-	-	0.22 ± 0.03	124 ± 20
	MMB3-5	55-57	125-180	1.80 ± 0.14	-	-	-	1.90 ± 0.31	1053 ± 1889	74 ± 11	-	-	0.49 ± 0.04	273 ± 31
	MMB3-7	85-88	180-212	1.88 ± 0.14	-	-	-	15 ± 2	7988 ± 1247	64 ± 10	-	-	4.15 ± 0.35	2209 ± 248

* Values in bold are the most representative dose and age
** SG: Single-grain
SA: Single-aliquot

Considering the fluvial setting of this sampling site and the partial bleaching characteristic of the D_e values discussed in the previous section, we applied the minimum age model (MAM) to calculate the true D_e values. Given the negative values in MMB3-1 and near-zero values among the other samples, the un-logged MAM (UMAM) version proposed by Arnold et al. (2009) was applied as it has proven to offer the most suitable means of deriving accurate burial dose estimates for very young and modern-age samples. We applied 4-parameter MAM (MAM4) for core MMB3 as it has been suggested that both the MAM3 and MAM4 D_e estimates are stable when the number of samples exceed 20 (Galbraith et al., 1999). All of the samples return the most representative D_e values (best fit for the age model, maximum likelihood) with the input OD value less than 10 %. Results (Table 4.8, Page 160) calculated by UMAM4 show good chronological sequence with increasing D_e values down the core. The D_e values of MMB3-2, MMB3-3 and MMB3-4 calculated by UMAM are very close to each other disregarding their absolute errors. The grains from these three samples may have been deposited over a short time interval. The D_e values calculated by UMAM will be further examined by independent age control in the following section.

4.7.3.4 Comparison between single-aliquot and single-grain data

A study of coastal dune sediments by Ballarini et al. (2007) compared D_e obtained from single-grain analysis to those obtained by means of similar single-aliquot methods. They found the results were comparable although the D_e determined through the single-aliquot methods was more precise. However, this is not the case for the Macquarie Marshes samples. For core MMB3 samples, the D_e values of the aliquot results are 2-5 times higher than the single-grain results for the same sample, despite applying the same age model to

single-grain and single-aliquot data sets (Table 4.8, Page 160). Compared to well-bleached coastal dune grains, the Macquarie Marshes sediments are more likely to have a heterogeneous bleaching of the grains transported by a fluvial environment. Each aliquot may include grains that were insufficiently bleached before burial. The intrusion of such grains leads to an overestimation of the true D_e. Although small aliquots (ID 0.5 mm) consists of a small amount of grains, the averaging effect is still large. Single-grain analysis enables the separation of those grains that were well bleached prior to deposition from those that were partially bleached. We can thus exclude the insufficiently bleached grains from the age calculation. The D_e distribution between the single-aliquot and single-grain data from the same sample (MMB3-4, MMB3-5 and MMB3-7) shows large differences in both histogram and radial plots. These findings are similar to those by Arnold et al. (2007) indicating that individual samples do not necessarily display the same types of dose distribution at both the single-grain and single-aliquot scale of analysis.

Olley et al. (1999) pointed out that aliquots with the lowest dose will yield the true burial dose only if the high-dose (unbleached) grains constitute <7 % of the grain population. In our study, as revealed by the histogram of the single-grain data, grains with high D_e constitute a relatively high proportion (>7 %) of the grain population in such heterogeneous samples. Thus, single-aliquot data would not yield ages close to reliable ages as single grains do. We would need to choose single grains to calculate more appropriate ages.

Olley et al. (1999) demonstrated that single-grain dating of fluvial material is possible and practicable using standard Risø optical dating equipment, and suggested using the lowest dose population (5 %) to estimate the burial dose, this being the best available means of obtaining reliable luminescence ages for heterogeneously bleached fluvial

sediments. Accordingly we chose single grain instead of single aliquots for dating the other core sections.

4.7.3.5 Age calculation and independent age control

The doses calculated by UMAM and dose rates presented in Section 4.5.2 are used to calculate the age for each individual sample. The OSL ages for core MMB3 (measured in 2007 AD) generally exhibit good stratigraphic coherence with increasing ages down the core (Table 4.9 and Figure 4.22).

Table 4.9
The OSL and ^{14}C ages of core MMB3.

Depth (cm)	OSL Ages (a)	^{14}C Age (a)	Ages before Year 2000 (a)
7	32 ± 8		25 ± 8
17	46 ± 8		39 ± 8
28	50 ± 7		43 ± 7
49	44 ± 12		37 ± 12
56	66 ± 10		59 ± 10
71	168 ± 13		161 ± 13
87	311 ± 44		304 ± 44
93		752 ± 88	802 ± 88

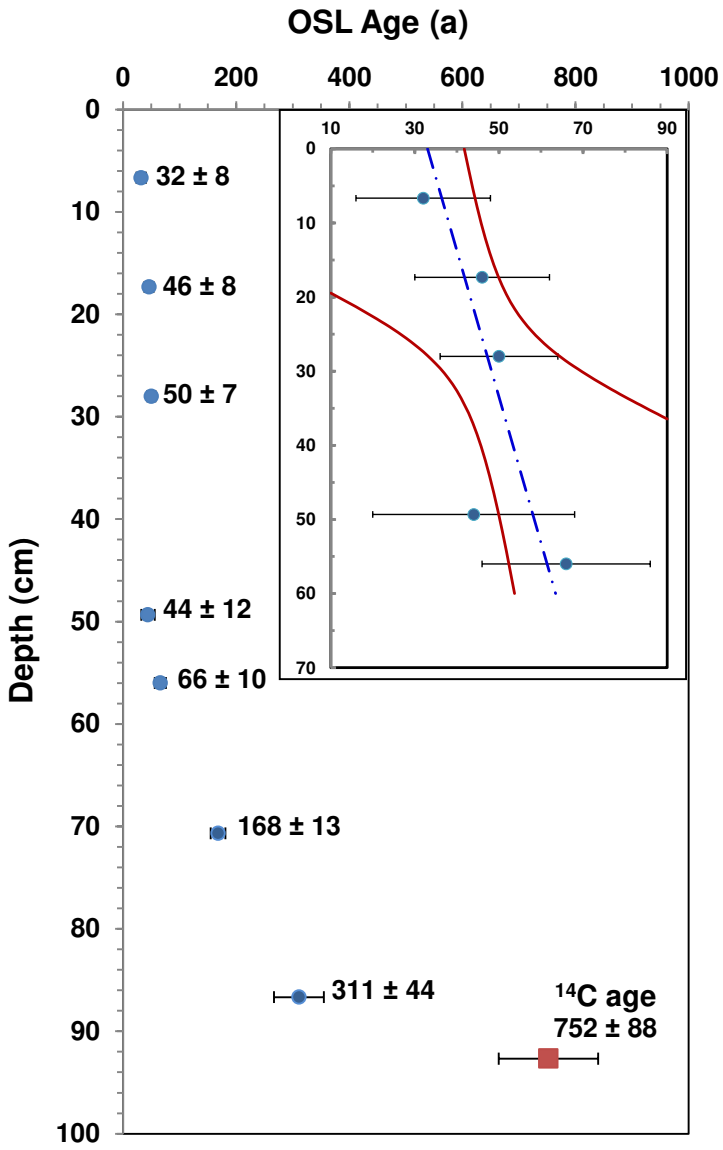

Figure 4.22. Chronology of core MMB3. (●: OSL single grain age before Year 2007; ■ : ^{14}C dating age; graph insert: the linear regression of the ages between depths of 7 to 56 cm; blue dashed line: the linear regression line; red curves: the error envelope)

Though special attention has been paid in order to acquire all the appropriate parameters for age determinations in OSL dating, additional information is still necessary to test the results for those unknown age samples. The ^{14}C dating result (on bulk organic matter) of one sample (92-94 cm deep) from a duplicate core, gives an uncalibrated age of 752±88

years BP. The HRGS results (Table 4.10) show that the concentrations of ^{137}Cs in the surface sediment sample (0-5 cm in depth) are relatively high, indicating the input of atmospheric nuclear testing products in the late 1950s and mid-1960s. Although sample MMB3_HRGS02 shows a small amount of ^{137}Cs, taking into account the standard error, the absolute concentration is negligible compared to the surface sediment sample (0-5 cm in depth). The HRGS results suggest that the surface sediment sample (0-5 cm in depth) must be younger than 50 years old, the middle layer (56-61 cm in depth) may be close to 50 years old and the bottom layer (87-89 cm depth) should be older than 50 years. The fact that the concentrations of ^{137}Cs are decreasing from the top layer to the bottom layer also suggests that extensive bioturbation and reworking of sediments is very unlikely to occur in this sampling site and the chronology should be stratigraphically coherent. Using UMAM for core MMB3, samples above 50 cm depth are calculated less than 50 years, while the other samples all fall within the age range of 50-310 years old. The ages calculated would not match the independent age control if calculated by CAM. It is also shown in Table 4.8 (Page 160) that the ages would be greatly over-estimated if the single-aliquot data were used. Therefore, the ages determined by single-grain OSL and calculated by the minimum age model are appropriate at this sampling site.

Table 4.10
High resolution gamma spectrometry results of core MMB3 samples.

Sample ID	Depth (cm)	^{137}Cs (Bq/kg)
MMB3_HRGS01	0-5	1.73 ± 0.18
MMB3_HRGS02	56-61	0.37 ± 0.15
MMB3_HRGS03	87-89	0.08 ± 0.14

Based on the results in Figure 4.22 (Page 164), the sedimentation rates fluctuated. From the depth of 56 to 7 cm (~ 1940 to 1975 AD), the sedimentation rate was high (about

1.45 cm/a) reflecting likely 'wet' years when the floods brought in more sediments that were deposited in the Marshes. From the depth of 7 to 0 cm (~ 1975 AD onwards) and the depth of 87 cm to 56 cm (~ 1840 to 1940 AD), the sedimentation rates were ~1/10 lower (0.11 to 0.22 cm/a) reflecting 'dry' years. The results of the upper layers (less than 71 cm in depth) fit in the historical record of Macquarie Marshes dated back to 1895 AD (Hogendyk, 2007). It is recorded that from 1895 to 1946 AD, the Macquarie Marshes were experiencing a 'dry phase' and then a 'wet phase' lasting for three decades from 1947 to 1978 AD before another 'dry phase' from 1978 onwards. Since Bora channel is a major channel in the Macquarie Marshes, the sedimentation rate recorded in this fluvial system will reflect the climate change in this area. It is observed that the sediment rate increases from 0.14 cm/a in 'dry phase' (~ 1840 to 1940 AD) to 1.45 cm/a in 'wet phase' (~ 1940 to 1975 AD) and decreases again to 0.22 cm/a in the second 'dry phase' (~ 1975 AD onwards). This recorded history and sedimentation rate calculation again support the accuracy of the OSL data.

Assuming that the sediments were deposited sequentially without erosional hiatus, the ages of the other part of the core (used for core interpretations in Chapter 3 and 5), were obtained directly by interpolation between the two OSL ages bracketing the part of interest. For the section from 56 to 7 cm, a linear regression (see blue dashed line in the insert graph of Figure 4.22) was obtained by the software Isoplot (Version 4.15), which is a geochronological toolkit designed by Kenneth R. Ludwig from the Berkeley Geochronology Centre. The best least square fit line (blue dash line in inserted graph of Figure 4.22) with 2σ confidence (two red curves in inserted graph of Figure 4.22) was obtained considering the ages, their 1σ error and their relevant depth. Thus, an equation

was generated from this line. The ages of the sediments in this section were then obtained by projecting the depth onto the trend line according to the following equation:

$$\text{Age (a)} = (\text{depth (cm)} + 65) / 1.97$$

The ages calculated based on the sedimentation rates are referred as "model age" in the other chapters. The ages used for core interpretations are listed in Table 4.11.

Table 4.11
The ages and respective calendar years of core MMB3.

Depth (cm)	OSL Age before Year 2000 (a)	Model Age before Year 2000 (a)	Year (AD)
0			2007
7		29	1971
17		35	1965
28		40	1960
49		51	1949
56		54	1946
71	161 ± 13		1839
87	304 ± 44		1696

4.7.4 D_e distributions and age determination for core LSW

Core LSW was collected from a swampy site, where river red gum (*Eucalyptus* sp.) and cumbungi (*Typha* sp.) were growing by the watercourse. The water was as shallow as the location of core MMB3 with depth of about 10-20 cm, which favoured the growth of cumbungi (*Typha* sp.). The growth of the plant might cause disturbance of the sediments (in particular for those from the upper surface). However, partial-bleaching may still be the main influence on the dose distributions.

4.7.4.1 D_e distributions of single grains

The histograms and radial plots for each core sections are presented in Figure 4.23. According to the similarity in the overall shapes, they can be divided into two groups. The near-surface sediment samples (LSW-1 and LSW-2) and the deepest sample (LSW-9) showed relatively symmetrical D_e distributions and centralised data points in their radial plots. The ratio of the minimum and maximum D_e values range from 3-6 times. These samples may be deposited in dry years when the flow rate is slower and water was shallower. The remaining samples (in particularly LSW-4 to LSW-8) showed significant levels of scatter, positive skewness in the histograms and the ratio of the minimum and maximum values ranged hundreds of times. However, the most abundant D_e populations of these samples have low values. In addition, they displayed multi-model distributions in higher D_e values indicating the scatter of D_e values might not simply relate to partial bleaching. Considering the coring site was close to where cumbungi (*Typha* sp.) was growing, these near-surface unconsolidated silt deposits may have been highly prone to bioturbation. Such findings were similar to those found by Bateman et al. (2007a) that mixing and exhumation associated with bioturbation increase the degree of inter-grain scatter and leads to a heterogeneous D_e distribution non-normally distributed around a sample mean.

Negative dose grains were observed in the uppermost sediments (LSW-1 to LSW-3), whilst zero/close-to-zero dose grains were also found down to 81cm (LSW-8). It is worth noting that some high D_e values (20-30 Gy) were found in middle-profile samples (from LSW-4 to LSW-8) but not in the deepest layer (LSW-9 90 cm in depth). It is most likely that these minority high D_e groups are partially-bleached grains deposited at the time when when the water was deeper and the dense coverage of vegetation prevented their efficient

exposure to the sunlight. The highest D_e values increased from 20 Gy at 48-57 cm to 30 Gy at 66-74 cm. One possible explanation for such variation is that they had experienced different exposure to sunlight: the 20 Gy grains were perhaps deposited in a less energetic fluvial environment (lower flow rate) and were more fully bleached than the 30 Gy grains. The fact that sample LSW-9 (90 cm in depth) does not contain zero/close-to-zero D_e and high D_e (20-30 Gy) as do the upper layers indicates that this layer was not significantly bioturbated.

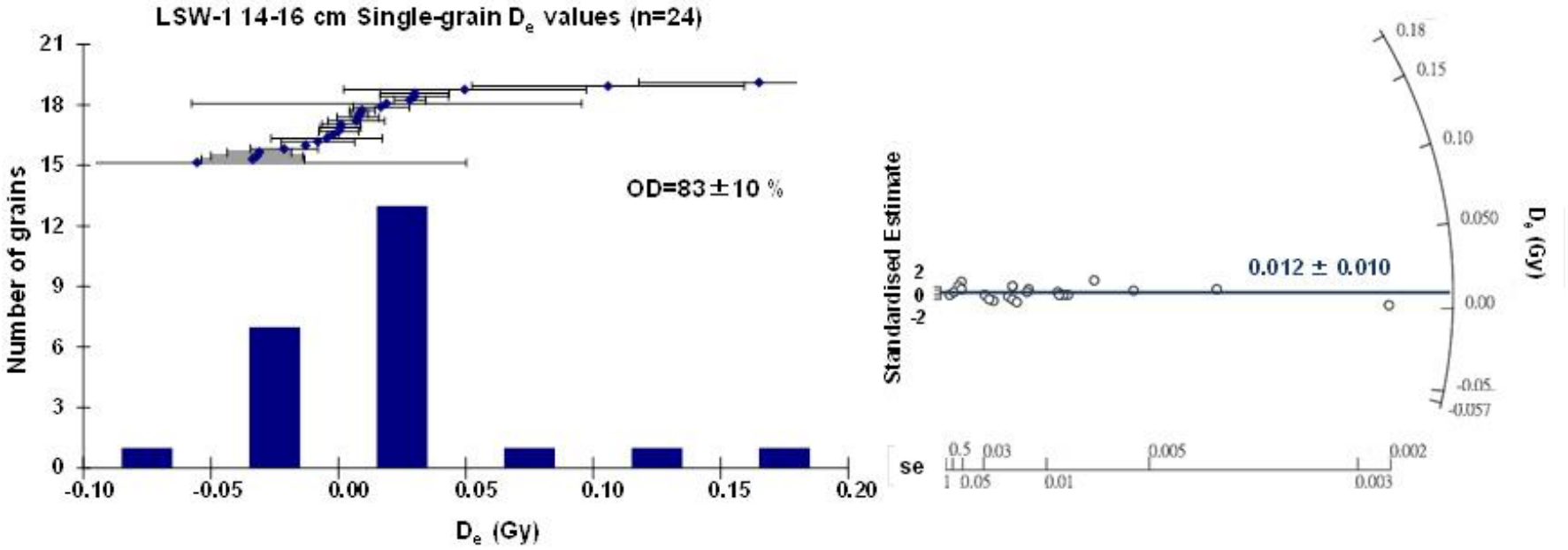

Figure 4.23. Histograms with ranked D_e values and radial plot of single-grain data from core LSW. (left graph: histogram; right graph: radial plot, blue line and number indicate D_e calculated by central age model, red line and number indicate D_e calculated by minimum age model)

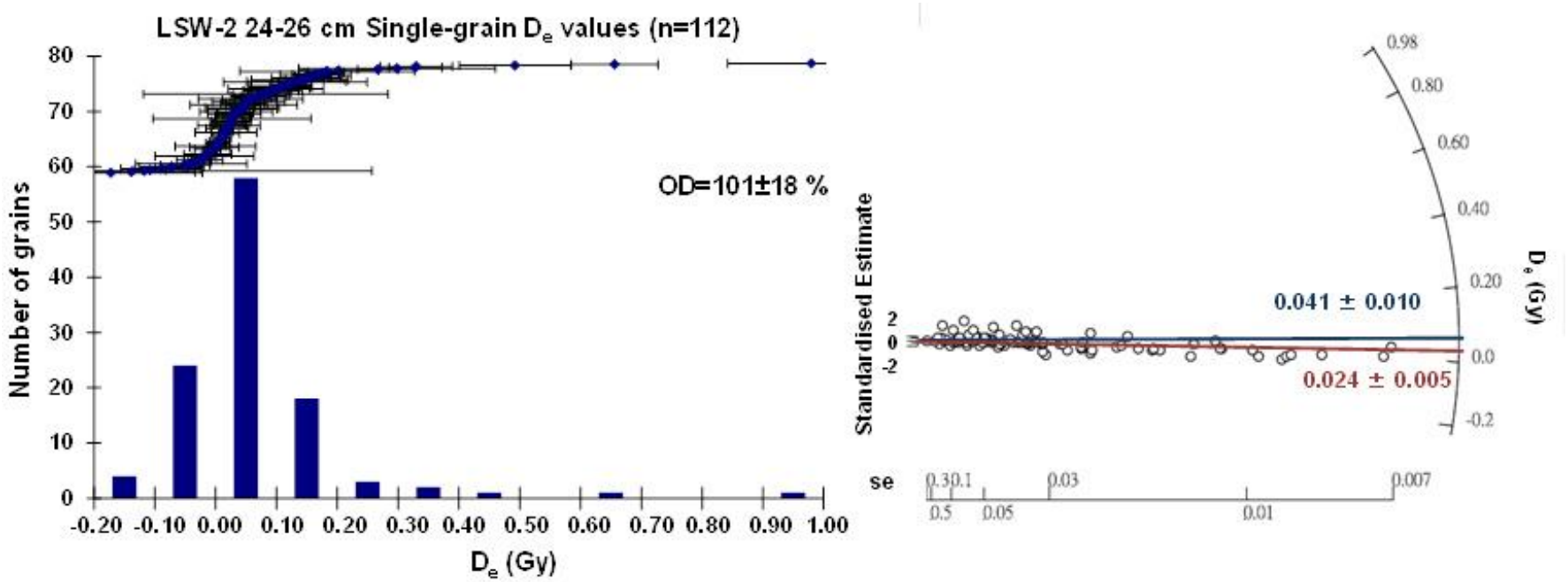

Figure 4.23 (continued). Histograms with ranked D_e values (left) and radial plot (right) of single-grain data from core LSW.

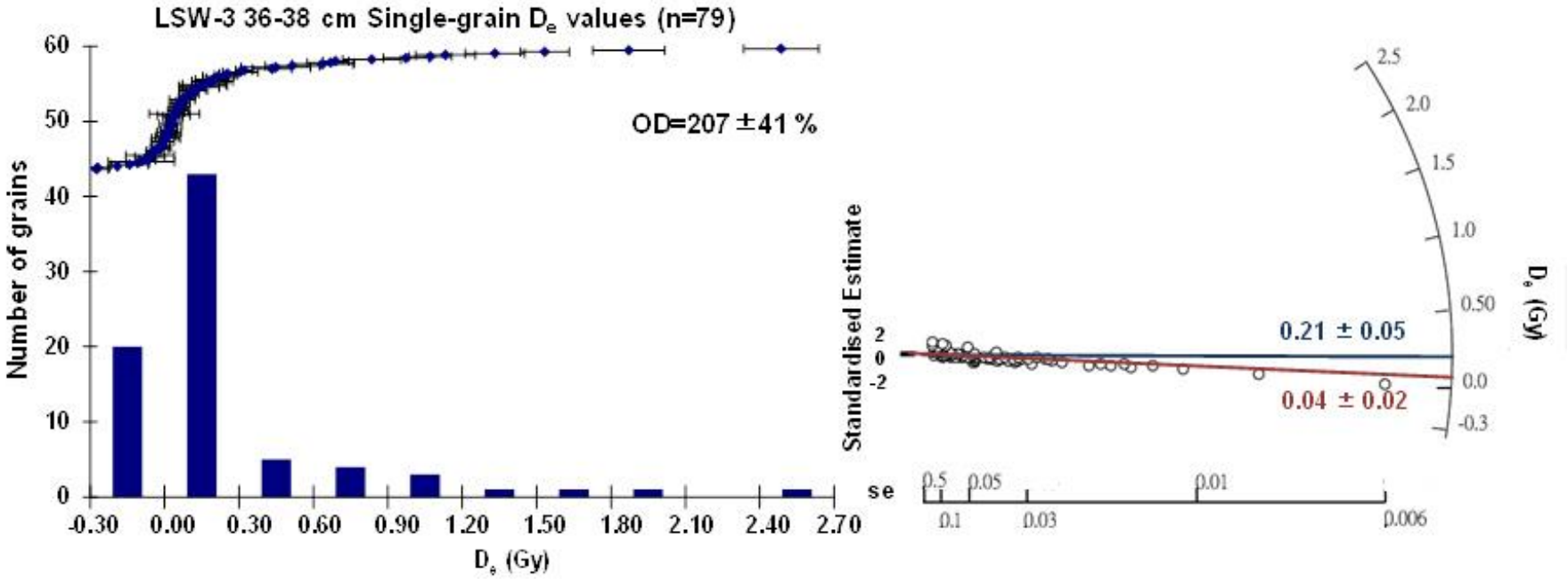

Figure 4.23 (continued). Histograms with ranked D_e values (left) and radial plot (right) of single-grain data from core LSW.

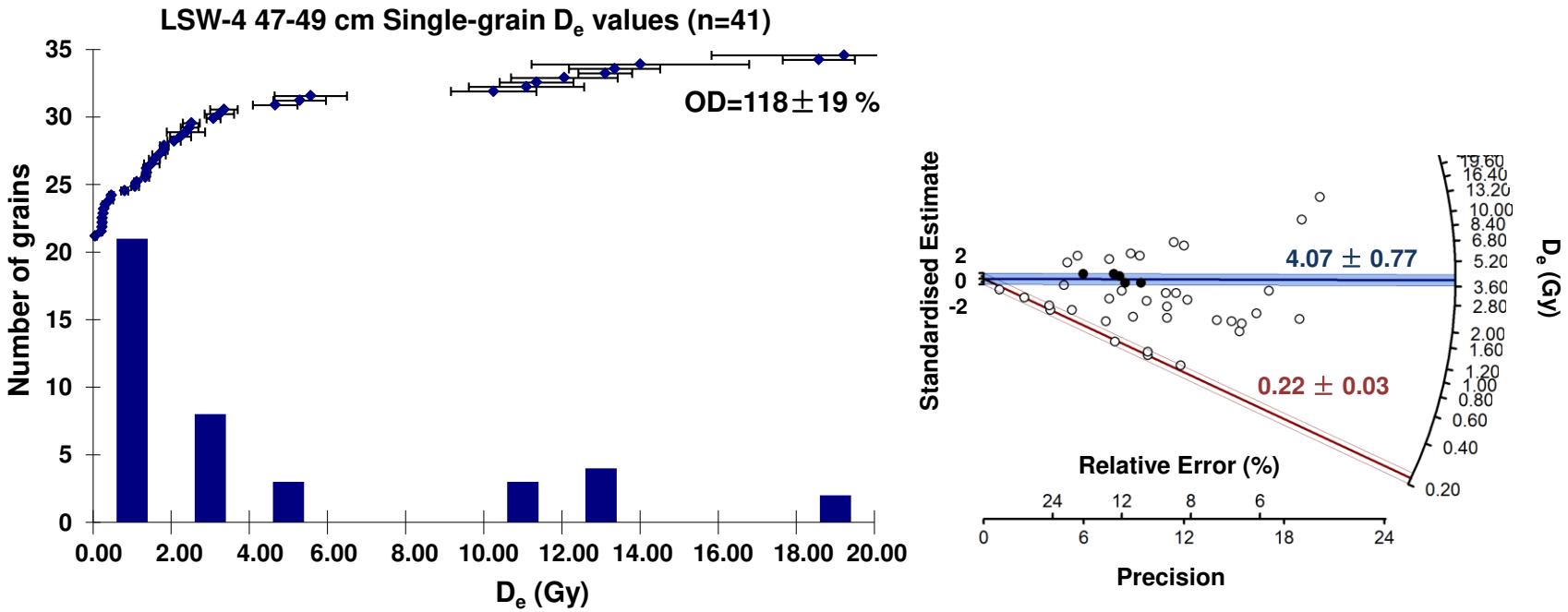

Figure 4.23 (continued). Histograms with ranked D_e values (left) and radial plot (right) of single-grain data from core LSW.

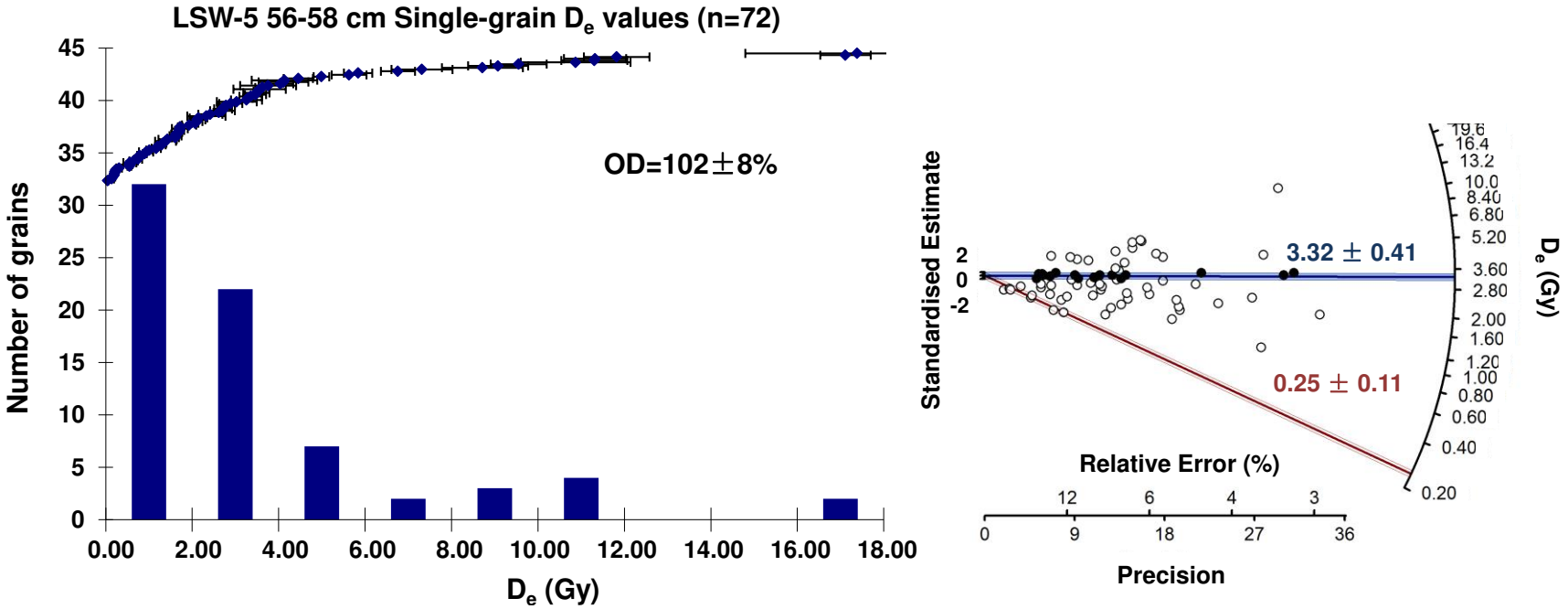

Figure 4.23 (continued). Histograms with ranked D_e values (left) and radial plot (right) of single-grain data from core LSW.

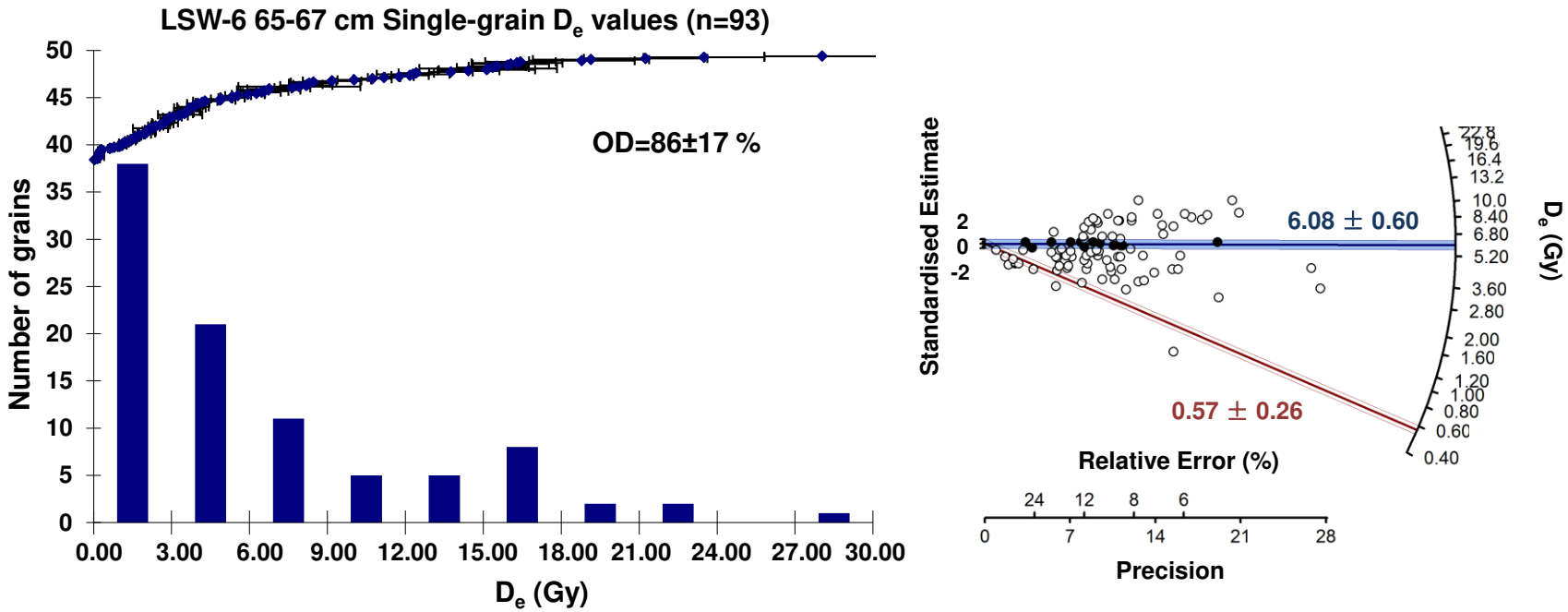

Figure 4.23 (continued). Histograms with ranked D_e values (left) and radial plot (right) of single-grain data from core LSW.

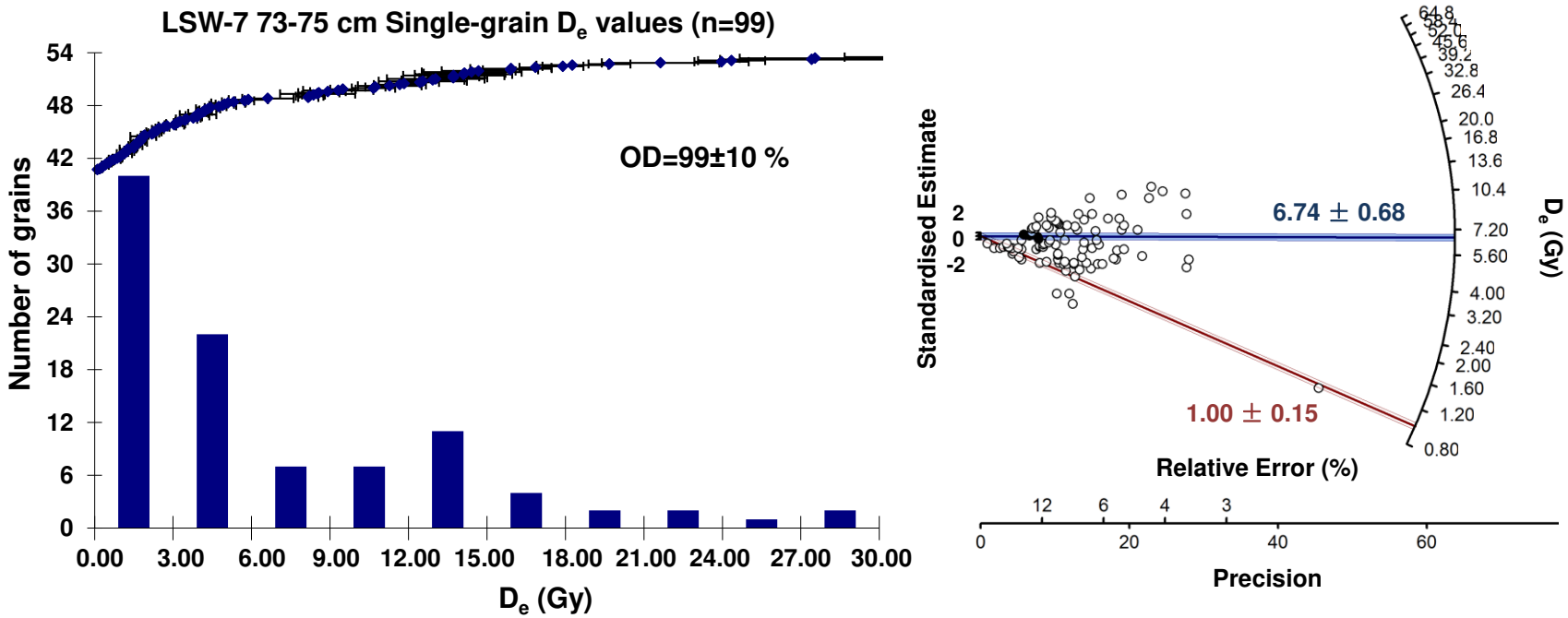

Figure 4.23 (continued). Histograms with ranked D_e values (left) and radial plot (right) of single-grain data from core LSW.

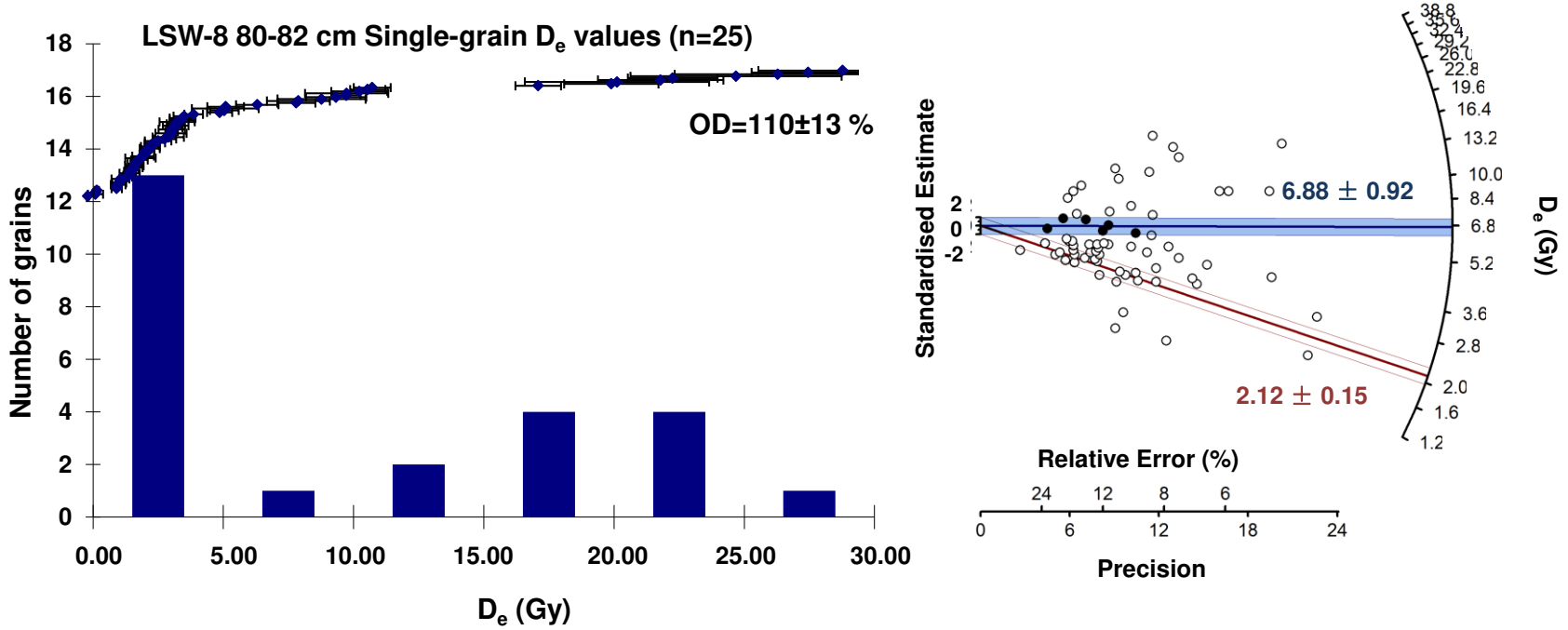

Figure 4.23 (continued). Histograms with ranked D_e values (left) and radial plot (right) of single-grain data from core LSW.

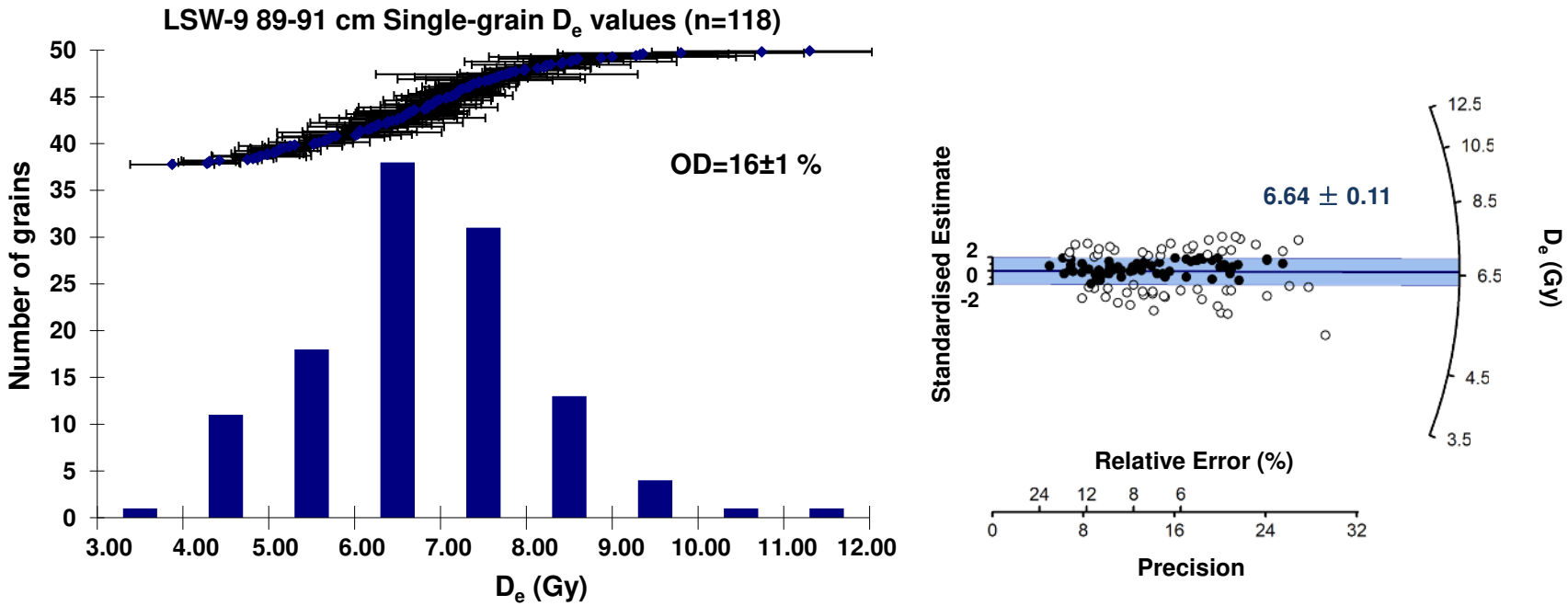

Figure 4.23 (continued). Histograms with ranked D_e values (left) and radial plot (right) of single-grain data from core LSW.

4.7.4.2 Age models

At the LSW sampling site, most of the grains originated from fluvial sediment that experienced partial-bleaching to various extents. Being close to where the plants grew actively, bioturbation cannot be diminished. The complexities of such depositional and post-depositional environment make it harder to interpret the D_e value and relevant ages in core LSW compared to core MMB3. Herein, various age models were applied, and then the most appropriate D_e value was chosen by calculating their relevant age and assessing with independent age control.

As shown in Table 4.12 (Page 181), all the samples were calculated with the central age model to obtain a general idea of over-dispersion for each of the samples, The UCAM was applied for all the samples as the upper surface sediment samples contained negative D_e values and almost all samples (except LSW-9) contained zero/close-to-zero D_e values. Except the near-surface sediment samples (LSW-1 to LSW-3), the other samples were also calculated by CAM for comparison. Only for sample LSW-9, were the D_e value calculated by UCAM and CAM similar within the error range. For the other samples (LSW-4 to LSW-8), D_e values calculated by UCAM were about 2 times higher than those calculated by CAM, while the OD values were similar. The OD value for LSW-9 is higher (16 %) than that for the dose recovery test (5.6 %), but less than the recommended value (20 %) (Arnold et al., 2009). Therefore it is appropriate to apply the CAM for sample LSW-9. Compared to core MMB3, the OD values of core LSW sections (except LSW-9, 89-91 cm depth) are relatively high and irregular through the core. The pattern found by Bateman et al. (2007b), namely that OD values decline from the surface modern soil to the

underlying sand unit, was not found in core LSW. Thus the variation of D_e values cannot simply be attributed to bioturbation.

Table 4.12
The D_e values and age of core LSW calculated by different age models.

Sample ID	Depth (cm)	Grain Size (μm)	Total Dose Rate (Gy/ka)	UCAM			CAM			UMAM	
				De (Gy)	Age (a)	Overdispersion (%)	De (Gy)	Age (a)	Overdispersion (%)	De (Gy)	Age (a)
LSW-1	14-16	180-212	0.64 ± 0.05	0.012 ± 0.010	7 ± 6	83 ± 10				**0.012 ± 0.010**	**7 ± 6**
LSW-2	24-26	180-212	0.54 ± 0.04	0.041 ± 0.010	23 ± 6	101 ± 18				**0.024 ± 0.005**	**13 ± 3**
LSW-3	36-38	180-212	0.60 ± 0.05	0.21 ± 0.05	109 ± 28	207 ± 41				**0.044 ± 0.020**	**23 ± 11**
LSW-4	47-49	180-212	0.76 ± 0.07	4.07 ± 0.77	2146 ± 437	118 ± 19	1.89 ± 0.42	995 ± 233	140 ± 16	**0.22 ± 0.03**	**118 ± 16**
LSW-5	56-58	180-212	0.77 ± 0.06	3.32 ± 0.41	1816 ± 257	102 ± 11	1.98 ± 0.27	1079 ± 168	116 ± 10	**0.25 ± 0.11**	**136 ± 58**
LSW-6	65-67	180-212	0.88 ± 0.07	6.08 ± 0.60	3231 ± 401	86 ± 17	3.46 ± 0.46	1839 ± 280	126 ± 9	**0.57 ± 0.26**	**301 ± 137**
LSW-7	73-75	180-212	0.76 ± 0.06	6.74 ± 0.68	3552 ± 450	99 ± 10	3.82 ± 0.47	2011 ± 291	121 ± 9	**1.00 ± 0.15**	**527 ± 87**
LSW-8	80-82	180-212	0.74 ± 0.06	6.88 ± 0.92	3762 ± 579	110 ± 13	4.41 ± 0.52	2353 ± 340	96 ± 8	**2.12 ± 0.15**	**1133 ± 125**
LSW-9	89-91	180-212	0.57 ± 0.04	**6.64 ± 0.11**	4003 ± 307	**16 ± 1**	6.62 ± 0.12	3992 ± 308	18 ± 1		

*numbers in bold are the values chosen for age calculations.

Table 4.13
The D_e values calculated by UMAM with different OD (σ) values (Unit Gy).

Sample ID	σ=0.05	σ=0.1	σ=0.15	σ=0.2	σ=0.25	σ=0.5	σ=0.8
LSW-1	**0.012 ± 0.010**	0.015 ± 0.025	-	-	-	-	-
LSW-2	**0.024 ± 0.005**	0.042 ± 0.010	0.047 ± 0.010	0.047 ± 0.020	0.048 ± 0.025	-	-
LSW-3	-	-	**0.044 ± 0.020**	0.056 ± 0.025	0.069 ± 0.030	0.15 ± 0.07	-
LSW-4	**0.22 ± 0.03**	0.24 ± 0.04	0.25 ± 0.06	0.26 ± 0.08	0.28 ± 0.09	0.80 ± 0.17	1.13 ± 0.20
LSW-5	0.16 ± 0.06	0.18 ± 0.05	0.20 ± 0.08	**0.25 ± 0.11**	0.32 ± 0.12	0.76 ± 0.18	1.29 ± 0.20
LSW-6	0.23 ± 0.03	0.22 ± 0.05	0.23 ± 0.07	0.24 ± 0.09	0.26 ± 0.12	**0.57 ± 0.26**	1.26 ± 0.26
LSW-7	-	-	0.30 ± 0.09	0.34 ± 0.11	0.44 ± 0.14	**1.00 ± 0.15**	1.00 ± 0.26
LSW-8	-	-	-	-	-	**2.12 ± 0.15**	2.52 ± 0.15

* Values in bold are the most representative dose and age

Various over-dispersion values were applied to UMAM to estimate the D_e values for samples from LSW-1 to LSW-8 (Table 4.13, Page 182). Considering the OD values in the dose recovery test and in sample LSW-9, the age models were run a number of times with input OD values of 5 %, 10 %, 15 %, 20 %, 50 % and 80 % until the best fit for the model was obtained. Table 4.13 summarises the D_e values estimated by UMAM with various input D values, and the data in bold show the best fit for the age model and with maximum likelihood. Not all the input OD values produce a result. For example, LSW-1 can be only run with input OD values of 5 % and 10 % while LSW-8 can be run only with high input OD values of 50 % and 80 %. As shown in Table 4.13, when the input OD values were less than/equal to 25 %, the calculated D_e values for LSW-1, LSW-4 and LSW-6 were independent of the input OD values -- the increase of input OD values only affects their error; when the input OD values exceed 25 %, LSW-4 and LSW-6 showed increasing D_e values with an increase of OD values. Comparatively, LSW-7 and LSW-8 showed independent D_e values with an increase of input OD values when OD values exceed 50 %.

Unlike core MMB3 samples, if the same input over-dispersion was applied to the model, the D_e values for core LSW did not follow stratigraphic order. This perhaps indicates that core LSW samples experienced more complicated depositional and post-depositional processes which affected the D_e variations and the over-dispersion for each sample differed from the others. In reality, the true over-dispersion for each sample is unknown. However by fitting the UMAM with various estimated OD values, the most representative D_e values can be extracted. As shown in Table 4.12 (Page 181), the calculated D_e values in bold showed relatively good chronological order. The D_e values for LSW-1 to LSW-5 were calculated by UMAM using relatively small input OD values (<25 %), while those for LSW-6 to LSW-8 used relatively high input OD values (50 %). If

a lower input OD value was used for LSW-6 and LSW-7, the UMAM would return a relatively low D_e value which is not the best fit for the age model. It is most likely these layers were disturbed at the time when the marshes were growing and the animals (i.e. worms and snails) in the marshes were active so that the grains were transported and mixed upward and downward. Therefore the bioturbation influences were more profound at those time periods.

The analysis of D_e distribution makes it possible to exclude samples that are not suitable for age determination by the CAM, and the MAM should be used. Thus for sample LSW-9, the D_e values calculated by the UCAM are identical to the CAM results within error. As discussed above and in the previous section, most of the core LSW samples (LSW-1 to LSW-8, and particularly LSW-3 to LSW-8) had undergone complicated processes (mainly partial bleaching and the mixing and exhumation of grains) that brought together grains with very different palaeodoses in the same layer. The true burial ages cannot simply be derived from CAM as it will average out the lower and higher age groups. Only one sample (LSW-1) shows similar D_e values for UMAM and UCAM. For the rest of the samples (LSW-2 to LSW-8), the D_e values calculated by UMAM are lower than those by UCAM. However, the application of UCAM with various input OD values were able to distinguish the most representative D_e values for each core sample, even when both partial-bleaching and bioturbation had affected the variation of D_e values to certain extents. This suggests that compared to partial-bleaching, the bioturbation effect was relatively minor. It has been discussed (Arnold and Roberts, 2009) that field identification of sediment mixing is commonly difficult because the absence of depositional bedding is not necessarily indicative of sediment mixing, whilst the presence of sedimentary structure does not necessarily preclude post-depositional disturbance. The

sedimentology and micro-fossil analysis in the previous chapter cannot provide adequate evidence for bioturbation, in this case.

4.7.4.3 Age calculation and independent age control

The doses calculated in the previous section and dose rates presented in Section 4.5.2 are used to calculate the age for each individual sample. The OSL ages for core LSW generally exhibit good stratigraphic coherence with increasing ages in progression down the core (Figure 4.24 and Table 4.14).

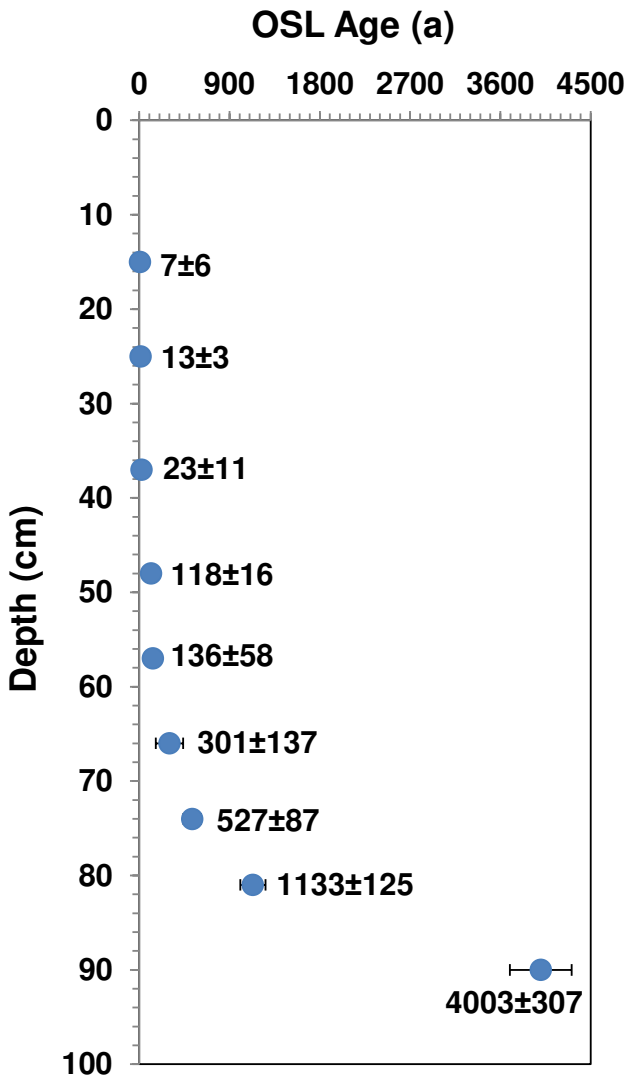

Figure 4.24. Chronology of core LSW determined by OSL techniques. (●: OSL single-grain age before Year 2008)

Table 4.14
The OSL ages of core LSW.

Depth (cm)	OSL Ages (a)	Ages before Year 2000 (a)
15	7 ± 6	-1 ± 6
25	13 ± 3	5 ± 3
37	23 ± 11	15 ± 11
48	118 ± 16	110 ± 16
57	136 ± 58	128 ± 58
66	301 ± 137	293 ± 137
74	527 ± 87	519 ± 87
81	1133 ± 125	1125 ± 125
90	4003 ± 307	3995 ± 307

There are no chronological data from other dating techniques (e.g. ^{14}C dating) for core LSW. However, the HRGS results can provide some information (Table 4.15) and show that the concentrations of ^{137}Cs in the upper surface sediment sample (23-28 cm depth) are relatively high, indicating the input of atmospheric nuclear testing in the late 1950s and mid-1960s. The LSW-6_Dose sample shows negligible ^{137}Cs concentration results compared to an overlying sediment sample. These HRGS results suggest that the younger sediment sample (23-28 in depth) must be less than 50 years old; the lower layer (more than 65 cm in depth) should be older than 50 years.

Table 4.15
High resolution gamma spectrometry results of core LSW samples.

Sample ID	Depth (cm)	^{137}Cs (Bq/kg)
LSW-2_Dose	23-28	2.22±0.18
LSW-6_Dose	65-68	0.18±0.21

The chronological profile of core LSW (Figure 4.24, Page 186)) displays a similar trend to core MMB3 and the sedimentation rates also fluctuated significantly. The deposition rate is less than 0.01 cm/a deeper in the sample profile (90 cm depth) and gradually increase upwards in the core. The near-surface layers (less than 40 cm depth, ~ 1985 AD onwards) shows rapid deposition (1.2 to 2.1 cm/a) and are comparatively younger than those in core MMB3 (~ 1960 to 1970 AD in the upper 40 cm). The 'dry (1895-1946 AD)-wet (1947-1978 AD)-dry (1978 AD onwards)' pattern found in core MMB3 was not found in core LSW, indicating the depositional rate of this sampling site did not follow the general cycle of the Macquarie Marshes. Despite the drought since the late 1970s, this sampling site has remained wet and has been receiving significant sediment. This is mainly because the LSW site is located close to the main watercourse.

Assuming that the sediments were deposited sequentially without erosive hiatus, the ages of other parts of the core (used for core interpretations in Chapter 3 and 5), were obtained directly by interpolation between OSL ages bracketing the section of interest. The ages calculated based on the sedimentation rates are referred as "model age" in the other chapters. The ages used for core interpretations are listed in Table 4.16.

Table 4.16
The ages and respective calendar years of core LSW.

Depth (cm)	OSL Age before Year 2000 (a)	Model Age before Year 2000 (a)	Year (AD)
0			2008
15	-1 ± 6		2001
25	5 ± 3		1995
30		9	1991
37	15 ± 11		1985
45		84	1915
48	110 ± 16		1890
52		118	1882
57	128 ± 58		1872
66	293 ± 137		1707
74	519 ± 87		1481
81	1125 ± 125		875
90	3995 ± 307		

4.7.5 D_e distributions and age determination for core LOLA

Core LOLA was collected from Loudens Lagoon, which had been dry since the 1990s and was flooded early in 2008. At the time of sampling (November 2008), the site was again dry. Patches of reed beds (*Phragmites australis*) and dead river red gum (*Eucalyptus* sp.) trees were observed at this site, indicating that it had changed from river red gum (*Eucalyptus* sp.) / cumbungi (*Typha* sp.) woodland landscape (as for the site of core LSW) to common reed beds (*Phragmites australis*) landscape. When we revisited this sampling site after one year (November 2009), the reeds (*Phragmites australis*) were dead and the surface was completely dry. As for the LSW site, most of the deposits in this less dynamic lagoonal system originate from fluvial sediments which in most cases would not be expected to be excessively bleached. Bioturbation of upper surface sediments was also expected to affect some of the OSL data.

4.7.5.1 D_e distributions of single grains

The D_e distribution characteristics of the nine samples from core LOLA (Figure 4.25, Page 192) reveal that these sediments were subjected to a diverse array of bleaching conditions prior to deposition and post-deposition histories.

The lowest D_e values increase from -1.41 Gy in the upper sample (LOLA-1 17-20 cm depth) to 48.58 Gy in the deepest sample (LOLA-9 202-207 cm depth). This pattern is not evident in the highest D_e values, however the highest D_e values generally range from 4.75 Gy in the upper part (LOLA-3 40-42 cm depth) to 448.8 Gy in the deepest sample (LOLA-9 202-207 cm depth). Two upper sediment samples (LOLA-1 and LOLA-2) show relatively centralised D_e values in their radial plots while the D_e values of the other samples spread out to different extent in radial plots (LOLA-3 to LOLA-9).

Two upper sediment samples (LOLA-1 and LOLA-2) contain higher D_e values than the highest D_e values in LOLA-3, probably due to different partial-bleaching scenarios. These two samples represent typical partial bleaching of fluvial samples with positive skewness and a long tail of high D_e value in the histograms. There is also some 'contamination' — grains with a negative dose and close-to-zero dose appearing in these samples. They may be related to reeds (*Phragmites australis*) at this site or are surface sediment samples that fell into desiccation cracks during dry years. The LOLA-3 and LOLA-4 samples show a more symmetrical D_e distribution in their histograms and relatively centralised points in their radial plots, indicating a relatively drier deposition environment where grains were better bleached before burial. An abrupt increase of the high D_e values is observed in the LOLA-5 sample, possibly indicating a significant age transition near the depth of 63-69 cm. This is supported by the presence of an indurated layer at about 60 cm noted during

the coring operations. Lithology and sedimentology (Chapter 3) also indicate a change in this section. The LOLA-5 and LOLA-6 samples also show partial-bleaching D_e distribution pattern with a long tail in their histograms but large dispersions of D_e values in the radial plots. Samples from LOLA-7 to LOLA-9 again show less asymmetry in their histograms with a shorter tail and less spread in their radial plots. It is likely that these older deposits have undergone considerably longer transport and more numerous deposition cycles prior to final deposition (allowing for greater bleaching) than modern and recently deposited sediments in the same depositional system (*cf* data by Jain et al., 2004). The results are also similar to those found by Murray et al. (1995) and Rittenour (2008) where the levels of non-bleached signal contributes a large proportion of the measured D_e in young samples and is reduced in older samples that have higher burial doses.

In general, the histograms and radial plots reveal two depositional environments (wet and dry) in this less dynamic lagoon environment. During the wet years when the flow rate was relatively high, the grains were deposited rapidly and therefore might not necessary be fully bleached before their burial. The reed (*Phragmites australis*) canopy and the coverage of water and organic matter may have also reflected the light thereby reducing the grains' exposure to sunlight. Therefore grains that were deposited in wet years would display a partial-bleaching pattern in their histograms and a large spread in the radial plots. Comparatively, grains deposited in dry years show less asymmetry in their histograms and more cluster in their radial plots.

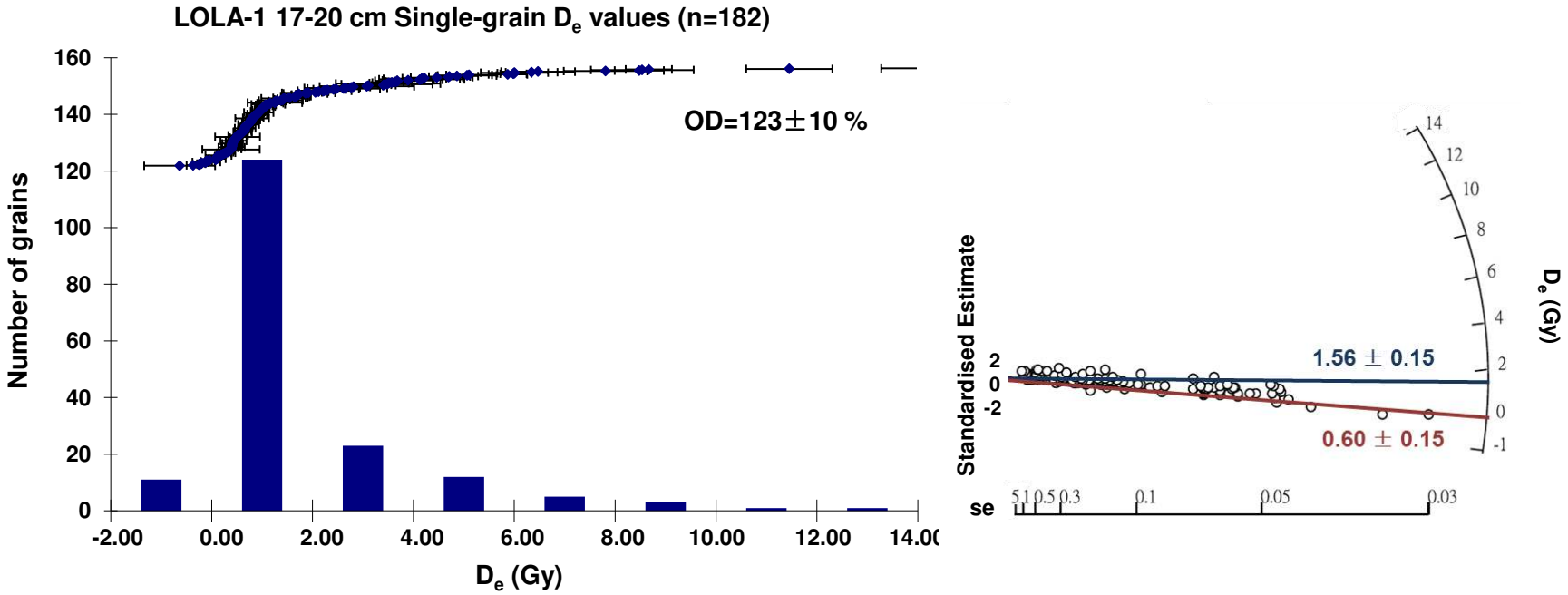

Figure 4.25. Histograms with ranked D_e values and radial plot of single-grain data from core LOLA. (left graph: histogram; right graph: radial plot, blue line and number indicate D_e calculated by central age model, red line and number indicate D_e calculated by minimum age model)

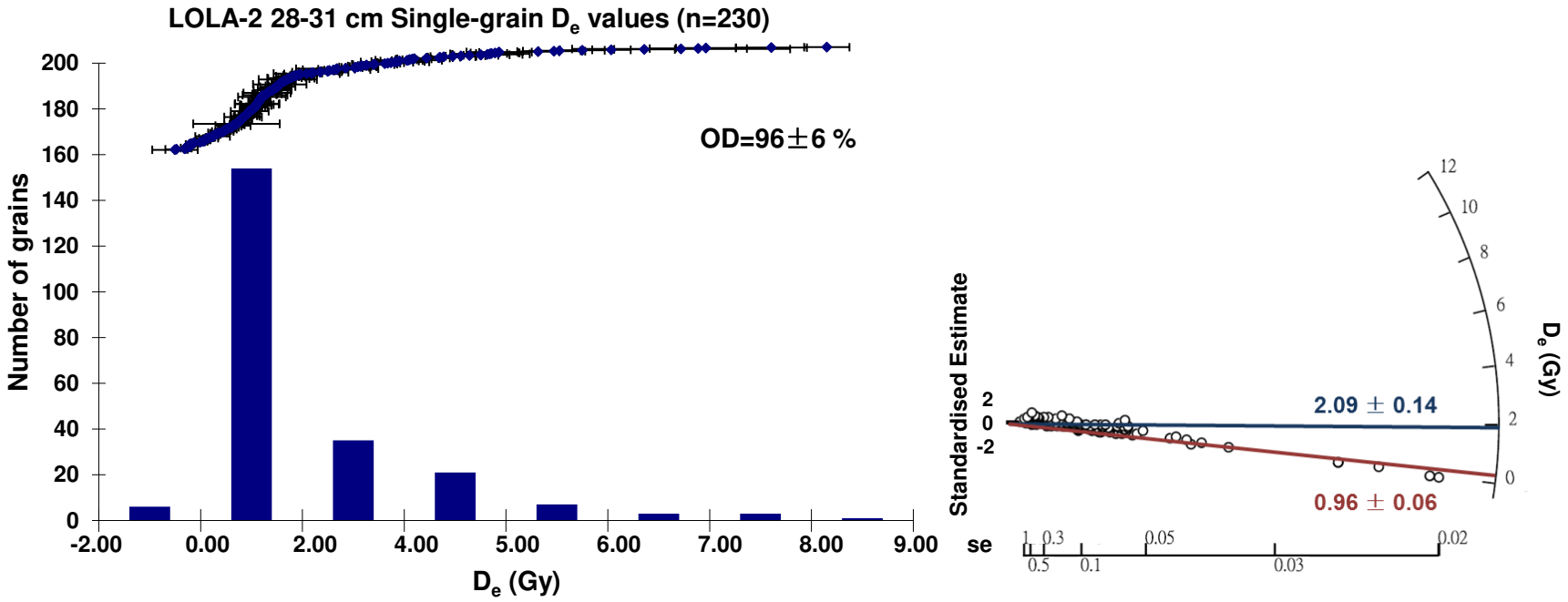

Figure 4.25 (continued). Histograms with ranked D_e values (left) and radial plot (right) of single-grain data from core LOLA.

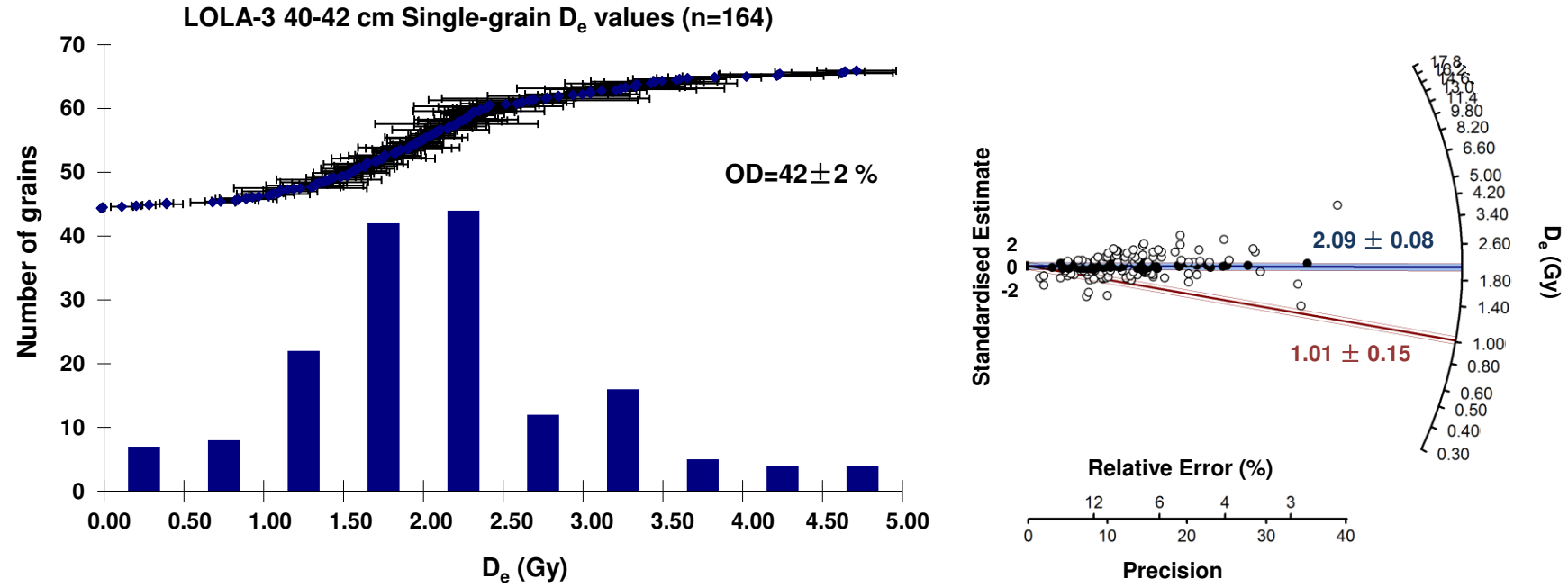

Figure 4.25 (continued). Histograms with ranked D_e values (left) and radial plot (right) of single-grain data from core LOLA.

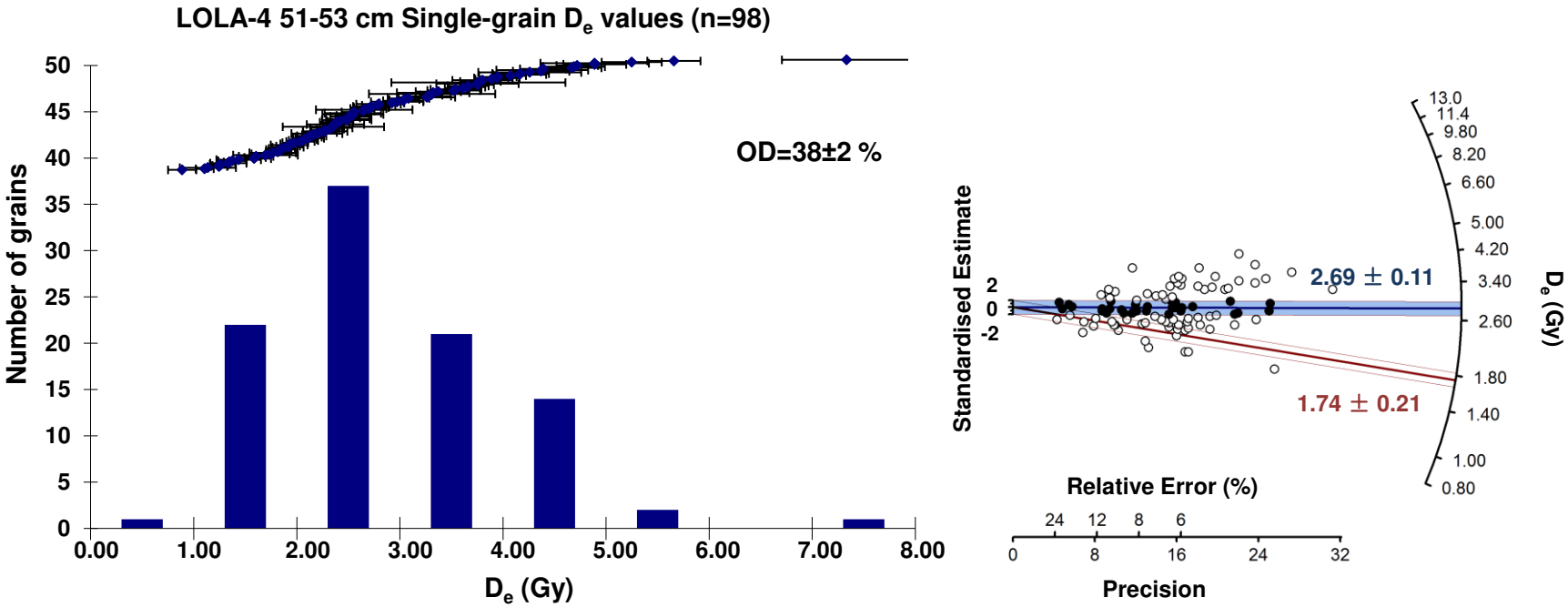

Figure 4.25 (continued). Histograms with ranked D_e values (left) and radial plot (right) of single-grain data from core LOLA.

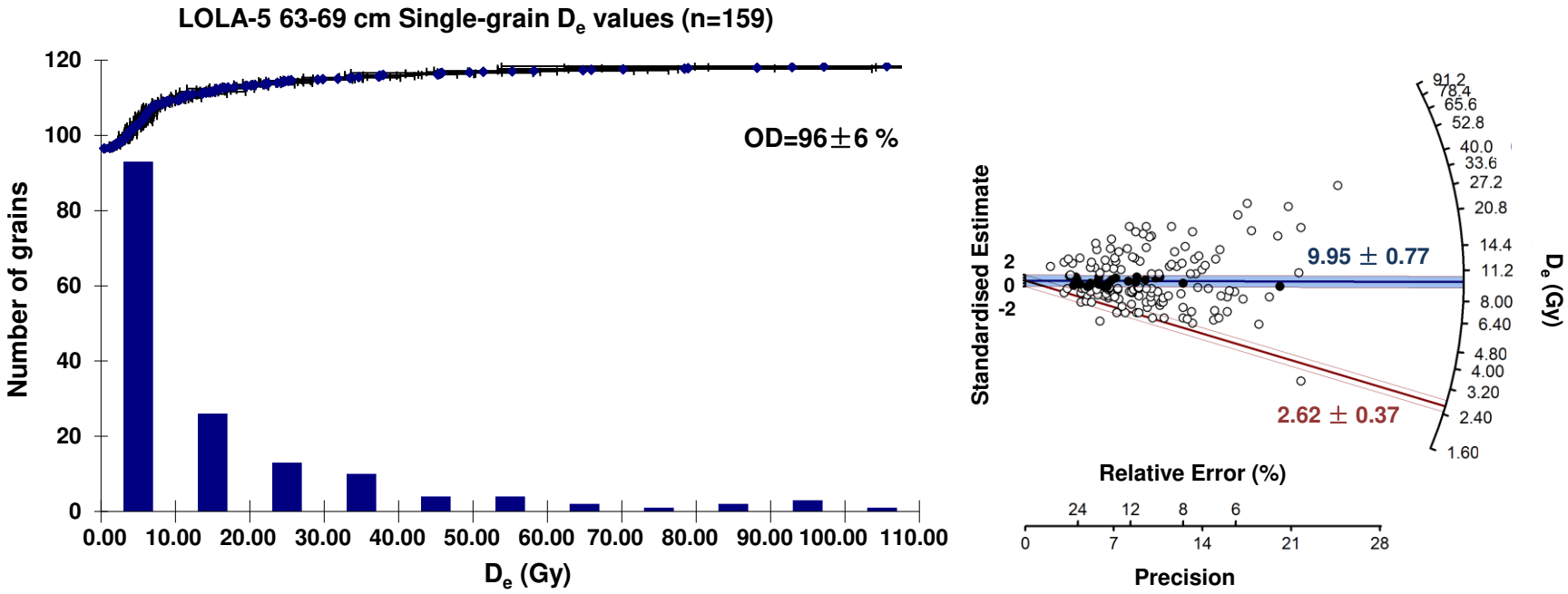

Figure 4.25 (continued). Histograms with ranked D_e values (left) and radial plot (right) of single-grain data from core LOLA.

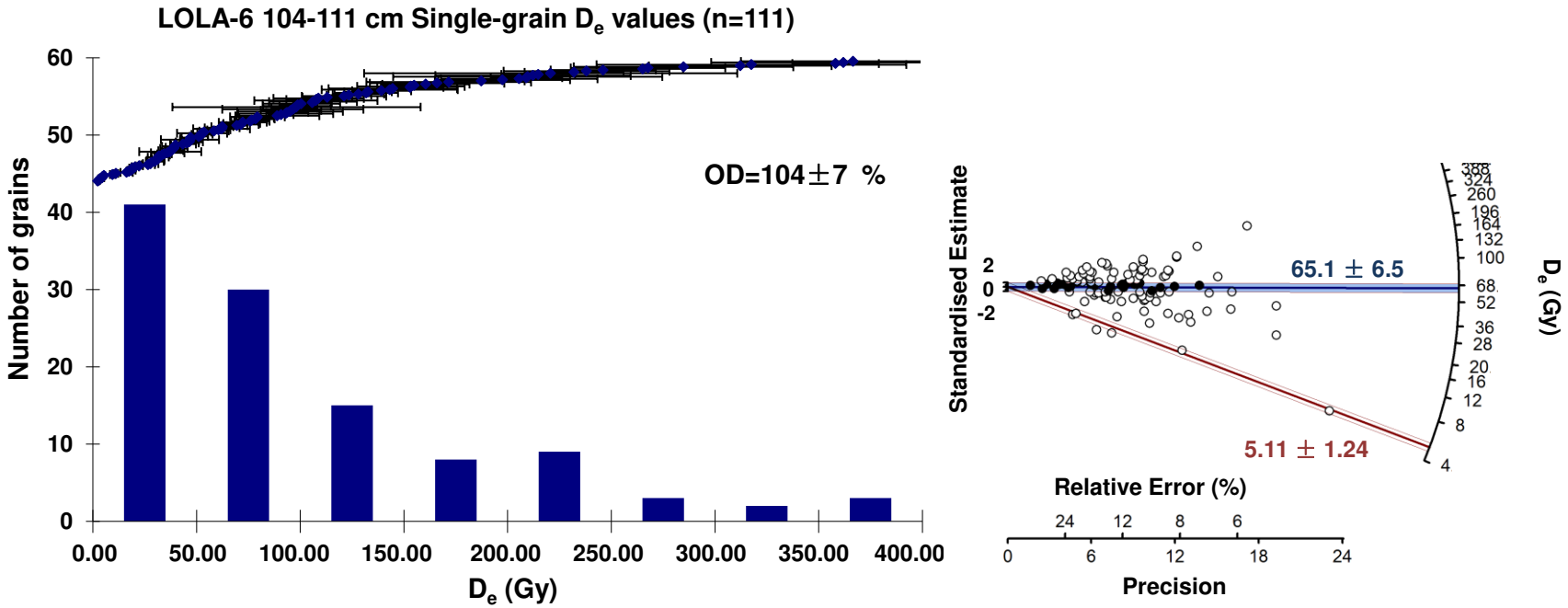

Figure 4.25 (continued). Histograms with ranked D_e values (left) and radial plot (right) of single-grain data from core LOLA.

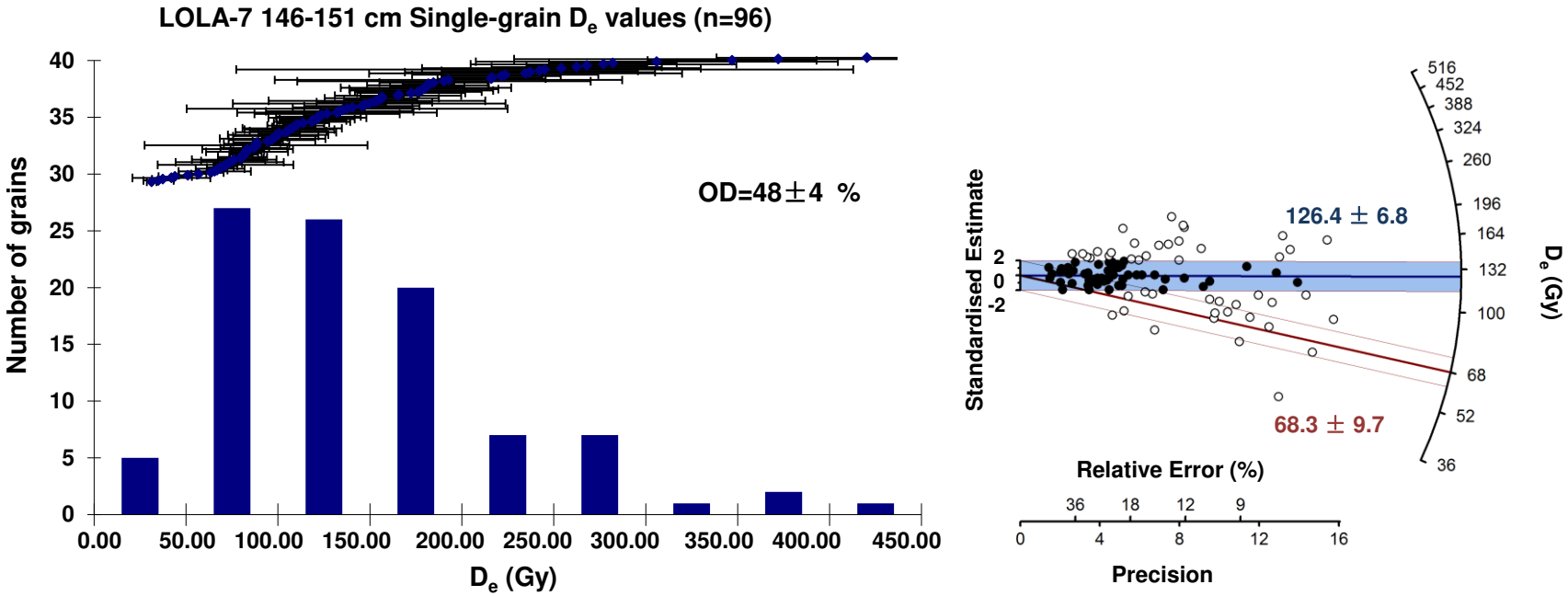

Figure 4.25 (continued). Histograms with ranked D_e values (left) and radial plot (right) of single-grain data from core LOLA.

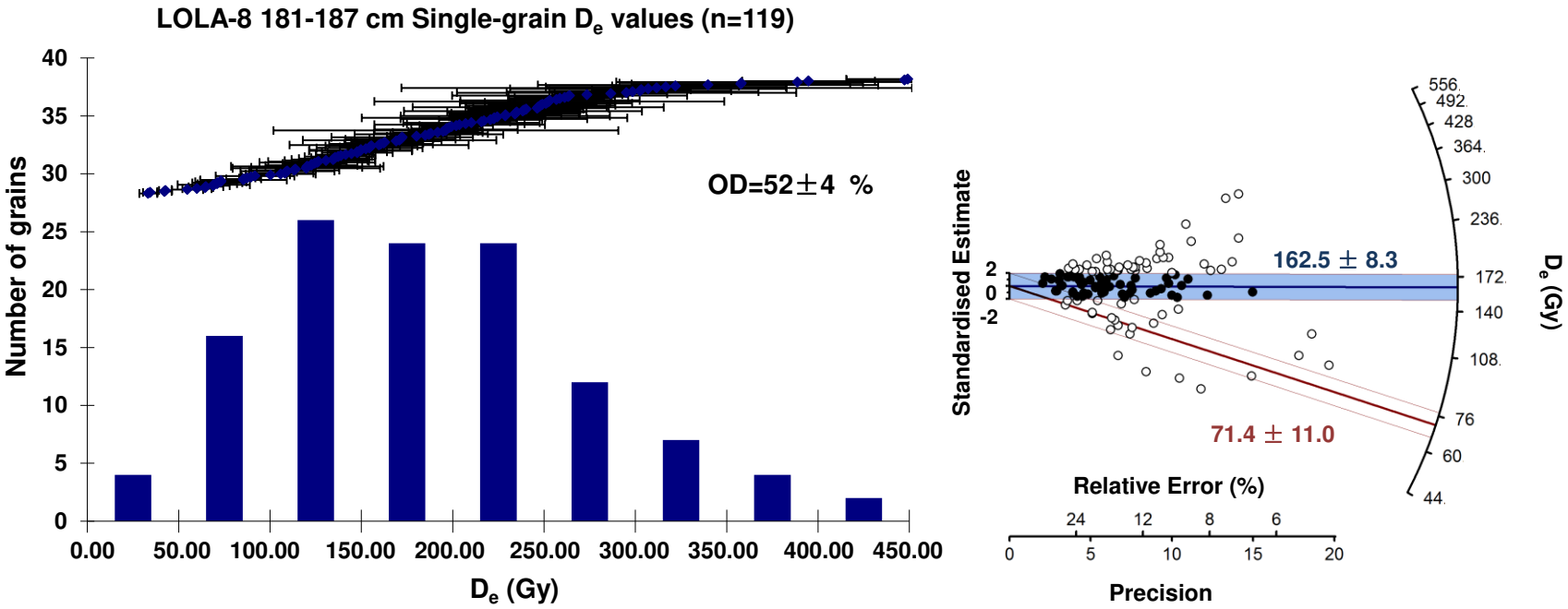

Figure 4.25 (continued). Histograms with ranked D_e values (left) and radial plot (right) of single-grain data from core LOLA.

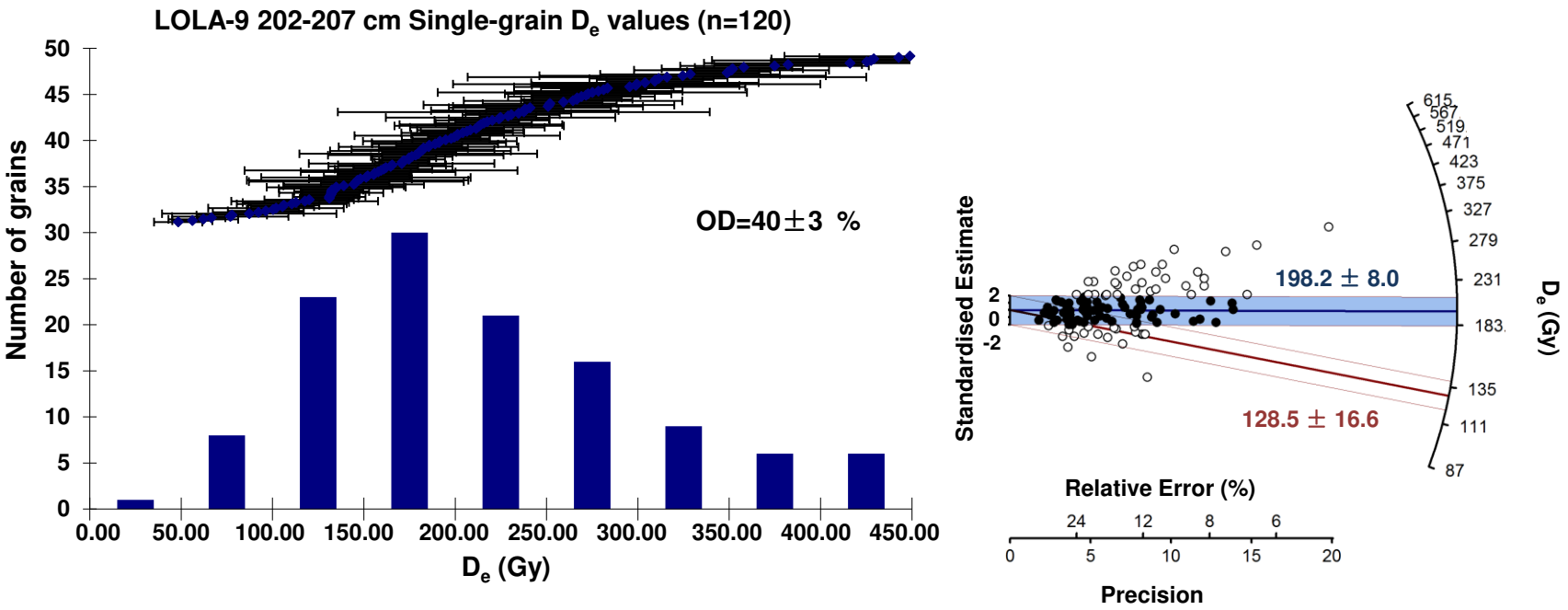

Figure 4.25 (continued). Histograms with ranked D_e values (left) and radial plot (right) of single-grain data from core LOLA.

Table 4.17
The D_e values and age of core LOLA calculated by different age models.

Sample ID	Depth (cm)	Grain Size (μm)	Total Dose Rate (Gy/ka)	CAM			UCAM			MAM		UMAM	
				De (Gy)	Age (ka)	Overdispersion (%)	De (Gy)	Age (ka)	Overdispersion (%)	De (Gy)	Age (ka)	De (Gy)	Age (ka)
LOLA-1	17-20	180-212	0.88 ± 0.07				1.59 ± 0.15	0.68 ± 0.08	123 ± 10			**0.60 ± 0.15**	**0.26 ±0.07**
LOLA-2	28-31	180-212	0.74 ± 0.06				2.09 ± 0.14	0.94 ± 0.09	96 ± 6			**0.96 ± 0.06**	**0.43 ± 0.04**
LOLA-3	40-42	180-212	0.77 ± 0.06				2.09 ± 0.08	0.87 ± 0.07	42 ± 2	**1.01 ± 0.15**	**0.42 ± 0.07**	0.56 ± 0.08	0.23 ± 0.04
LOLA-4	51-53	180-212	0.84 ± 0.07	2.69 ± 0.11	1.15 ± 0.09	38 ± 3	2.86 ± 0.12	1.22 ± 0.10	38 ± 2	**1.74 ± 0.21**	**0.75 ± 0.10**	1.26 ± 0.10	0.54 ± 0.06
LOLA-5	63-69	180-212	0.85 ± 0.06	9.95 ± 0.77	4.80 ± 0.50	96 ± 6				**2.62 ± 0.37**	**1.26 ± 0.20**		
LOLA-6	104-111	180-212	0.89 ± 0.02	65.1 ± 6.5	28.7 ± 3.1	104 ± 7				**5.11 ± 1.24**	**2.25 ± 0.55**		
LOLA-7	146-151	180-212	1.05 ± 0.02	126.4 ± 6.8	50.2 ± 3.4	48 ± 4				**68.3 ± 9.7**	**27.1 ± 4.0**		
LOLA-8	181-187	180-212	0.96 ± 0.02	162.5 ± 8.3	63.9 ± 4.3	52 ± 4				**71.4 ± 11.0**	**28.1 ± 4.5**		
LOLA-9	202-207	180-212	0.99 ± 0.02	198.2 ± 8.0	76.9 ± 4.5	40 ± 3				**128.5 ± 16.6**	**49.9 ± 6.8**		

* Values in bold are the most representative dose and age.

4.7.5.2 Age models

In the previous two sections, the application of MAM has been successful to determine the ages of two cores (core MMB3 and core LSW). For core LOLA, MAM was also applied to extract the D_e values while CAM was used to estimate the overdispersion.

The un-logged CAM was applied to LOLA-1 to LOLA-4 as they contained negative D_e or close-to-zero D_e values. The CAM was applied to LOLA-4 to LOLA-9. As shown in Table 4.17 (Page 201), the D_e values are generally in good chronological order (except LOLA-2 and LOLA-3 overlap within their error ranges). For LOLA-4 which was calculated by both UCAM and CAM, the D_e values are similar within their error range and the OD values are the same. All of the OD values are higher than the recommended OD value (20 %) to apply CAM/UCAM model while in the dose recovery test (Section 4.3.5), the same quartz from this sampling site found OD values less than 10 %. It is very unlikely these high OD values are caused by heterogeneity of beta microdosimetry. There are two reasons for this inference: 1) the OD values are higher than those (23 %) found by Murray and Roberts (1997) among well bleached single-grain quartz that experienced heterogeneous microdosimetry in their burial environment; 2) the variation of D_e values (discussed in the previous section) are greater than those (46 % to 18 % relative standard deviation) found by Mayya et al. (2006) among well bleached single-grain quartz that also experienced microscopic heterogeneity of potassium distribution. Therefore the possible explanation for elevated OD values and dispersion of D_e values is partial bleaching. The OD values of the two upper sediment samples (LOLA-1 and LOLA-2) and two mid-depth samples (LOLA-5 and LOLA-6) are relatively high (90-125 %); while the OD values of the remaining samples (LOLA-3 to LOLA-4, LOLA-7 to LOLA-9) are very similar and

small (about 40-50 %). Apart from partial-bleaching, the high OD values of the two upper sediment samples may have been caused by bioturbation and those for the middle layer samples may have been caused by mixing of 'young' and 'old' sediments in the transition layers.

The OD values estimated by the dose recovery test and by CAM among the samples were used as guides to apply the MAM. For samples LOLA-1 to LOLA-4 which contain negative D_e and/or close-to-zero D_e, the un-logged MAM was applied. Only LOLA-1, LOLA-2 and LOLA-4 yielded a reasonable chronological order. The D_e values of LOLA-3 calculated by UMAM was even lower than the uppermost sediment sample (LOLA-1), which is likely due to contamination by younger material. It seems that the application of UMAM in core LOLA was not as successful as for core LSW to distinguish the bioturbated samples and partial-bleaching samples. However, applying the log model (MAM), those low D_e values contribute less than those of the un-logged model. For sample LOLA-3, the D_e values calculated by the MAM returned 1.01 Gy which excludes the contaminated younger D_e values (0.56 Gy) calculated by the UMAM. Similarly, the D_e values of sample LOLA-4 calculated by the MAM yielded 1.74 Gy while those by the UMAM gave 1.26 Gy from the likely contaminated grains. The D_e values calculated by MAM for LOLA-3 and LOLA-4 were in coherent order with the two upper sediment samples. And the D_e value calculated by MAM for LOLA-3 (1.01 Gy) was very close to the D_e value calculated by UMAM for LOLA-2 (0.96 Gy), again (as found in CAM results) indicating these two layers are not distinguishable within the resolution of the OSL single-grain dating technique. Therefore, the D_e values by MAM were chosen instead of UMAM for the age calculation of LOLA-3 and LOLA-4 samples (discussed in a later section). For LOLA-5 and deeper samples, the MAM was applied to extract the most

representative D_e values. Results (Table 4.17, Page 201) show the D_e values by UMAM and MAM are in stratigraphic order.

In summary, the UMAM was applied to the upper sediment samples (LOLA-1 and LOLA-2) while the MAM was applied to the remaining samples (LOLA-3 to LOLA-9). This is reasonable as suggested by Bailey and Arnold (2006) that the optimum choice of statistical methods may be different for each sample and is dependent on the dominant mechanisms affecting D_e scatter (e.g. partial bleaching, post-depositional mixing or dose-rate heterogeneity).

4.7.5.3 Age calculation and independent age control

The doses calculated by the MAM/UMAM in the previous section and dose rates presented in Section 4.5.2 are used to calculate the age for each individual sample. The OSL ages for core LOLA generally exhibit good stratigraphic coherence with increasing ages in progression down the core (Figure 4.26).

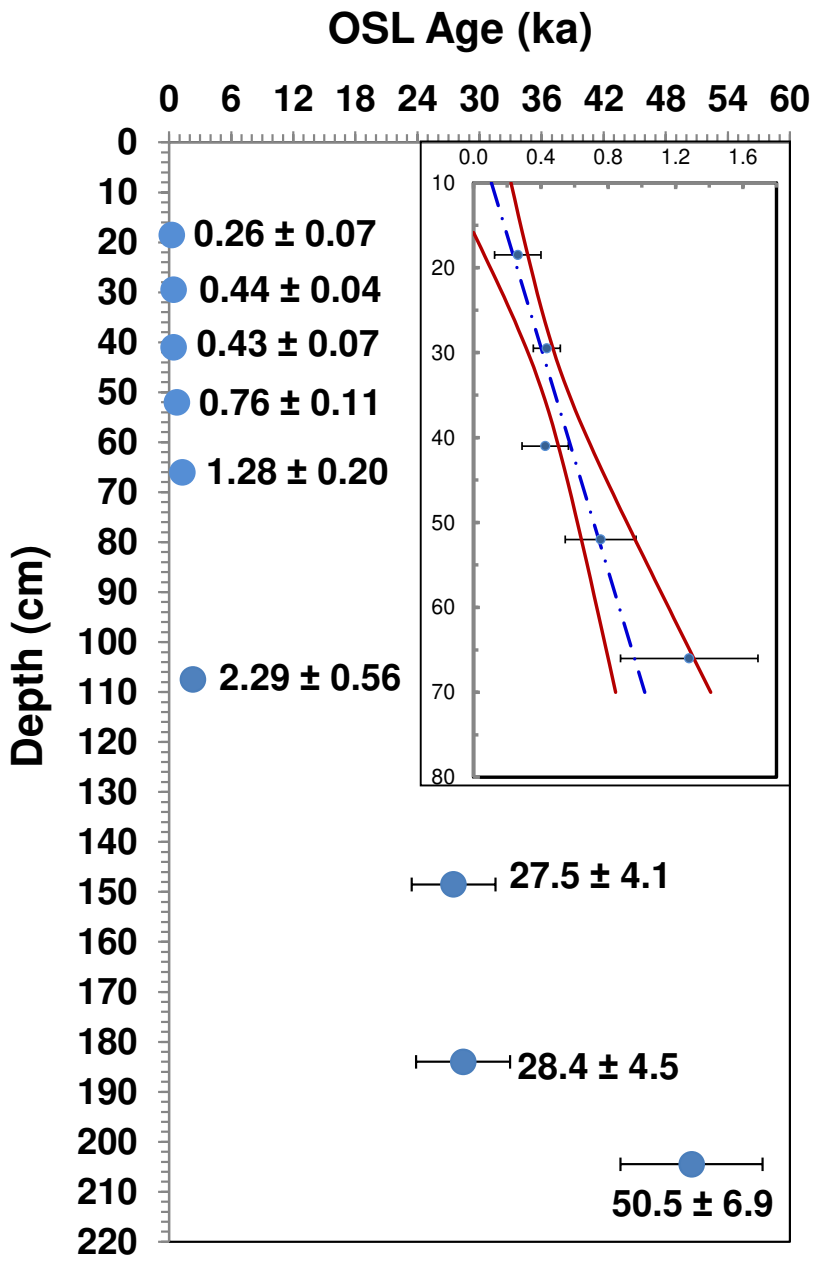

Figure 4.26. Chronology of core LOLA determined by OSL techniques. (●: OSL single-grain age; graph insert: the linear regression of the ages at depths of 66 to 19 cm; blue dashed line: the linear regression line; red curves: the error envelope)

The independent age control for core LOLA is only limited to the HRGS results (Table 4.18) of the deeper layers. The concentrations of ^{137}Cs in these deeper samples fluctuate and are very irregular along the core. Most of the samples show low ^{137}Cs concentrations. Although LOLA-DR-02 shows the highest ^{137}Cs results, it is negligible when comparing

the absolute value (taking into account its standard error) to those from MMB3 and LSW core samples. It seems that samples of the deeper layers should be older than 50 years, as is clear from the OSL dating results.

Table 4.18
High-resolution gamma spectrometry results for core LOLA samples.

Sample ID	Depth (cm)	^{137}Cs (Bq/kg)
LOLA-DR-04	105-111	0.11±0.15
LOLA-DR-03	145-151	-0.08±0.24
LOLA-DR-02	181-186	0.48±0.22
LOLA-DR-01	201-207	0.14±0.19

The OSL ages of core LOLA are much older compared to the previously described two cores (MMB3 and LSW). The Loudens Lagoon system is less dynamic than the fluvial systems and thus the deposition rate is much slower. The younger sedimentation of the past few hundreds of years has not been identified (unless it is compressed in the upper 15 cm). It is likely that, in this exposed site, the sediments have been deflated, particularly during dry periods. The ages of LOLA-2 (28-31 cm depth) and LOLA-3 (40-42 cm depth); LOLA-7 (146-151 cm depth) and LOLA-8 (181-187 cm depth) are not distinguishable within the resolution of the OSL single-grain dating technique. Generally, the sedimentation rates calculated are less than 0.01 cm/a among the older layers (from the core base to 108 cm, except the layers between 149 cm and 184 cm where the ages are identical). The rate fluctuates from 0.03 cm/a to 0.07 cm/a in the younger sediments (< 2.29 ka around the depth of 108 cm).

For the section from 66 to 19 cm, a linear regression (see blue dashed line in the insert graph of Figure 4.26) was obtained by the software Isoplot (Version 4.15). The best least-squares fit line with 2σ confidence (two red curves in insert graph of Figure 4.26) was obtained considering the ages, their 1σ error and their relevant depth. Thus, an equation was generated from this line. The ages of the sediments in this section were then obtained by projecting the depth onto the trend line according to the following equation:

$$\text{Age (a)} = (\text{depth (cm)} - 3) / 66$$

Except for the age hiatus (149 to 108 cm) and the upper layer (66 to 19 cm), the ages of the other parts of the core (used for core interpretations in Chapter 3 and 5) were obtained by interpolation between the two ages bracketing the section of interest.

The ages calculated based on the sedimentation rates are referred as “model age” in the other chapters. The ages used for core interpretations are listed in Table 4.19.

Table 4.19
The OSL and model ages of core LOLA.

Depth (cm)	OSL Age (ka)	Model Age (ka)
0		
19		0.23
30		0.40
41		0.58
52		0.74
58		0.83
66		0.95
78		1.33
98		1.97
108	2.29 ± 0.56	
149	27.5 ± 4.1	
184	28.4 ± 4.5	
205	50.5 ± 6.9	

4.7.6 D_e distributions and age determination for core 2LOLA

Core 2LOLA was collected near a moist reedbed (*Phragmites australis*) within the west of Loudens Lagoon, which was dry at the time of sampling (November 2009). Compared to the LOLA sampling site, this site was less impacted by the drought since the 1990s. Despite being close to the LOLA site, 2LOLA was more elevated and the environmental setting for deposition of sediments would not necessarily be the same.

4.7.6.1 D_e distributions of single grains

As shown in Figure 4.27 (Page 210), the patterns of the D_e histograms and radial plots for core 2LOLA were similar to the three cores discussed in the previous sections. Partial bleaching is very common among most of the samples (2LOLA-3 to 2LOLA-7), which

display a long tail in the histogram and a spread of D_e values in the radial plot. The two near-surface sediment samples (2LOLA-1 and 2LOLA-2) show a small peak of negative D_e values, probably sourced from the contamination of 'young' grains by bioturbation although the extent of impact cannot be accessed. The points in the radial plots of these two near-surface sediment samples tend to be more centralised than the other samples.

The minimum and maximum D_e values both increase downwards in core 2LOLA, indicating that the sediments are well-preserved and generally in chronological order and that the disturbance in the upper sediment samples is relatively minor. The ratio of the minimum and maximum D_e values is less than a hundred times in these two upper sediment samples and rises to hundreds of times among the other samples.

The D_e distributions of the core 2LOLA samples are typical of fluvial sediments which contain various proportions of partially bleached grains and fully bleached grains (e.g. Ballarini et al., 2003). Compared to the previous three cores, the sediment input of core 2LOLA seems to be more consistent as illustrated by their histograms and radial plots. Therefore, the choice of age model and age interpretation for core 2LOLA should be less complicated.

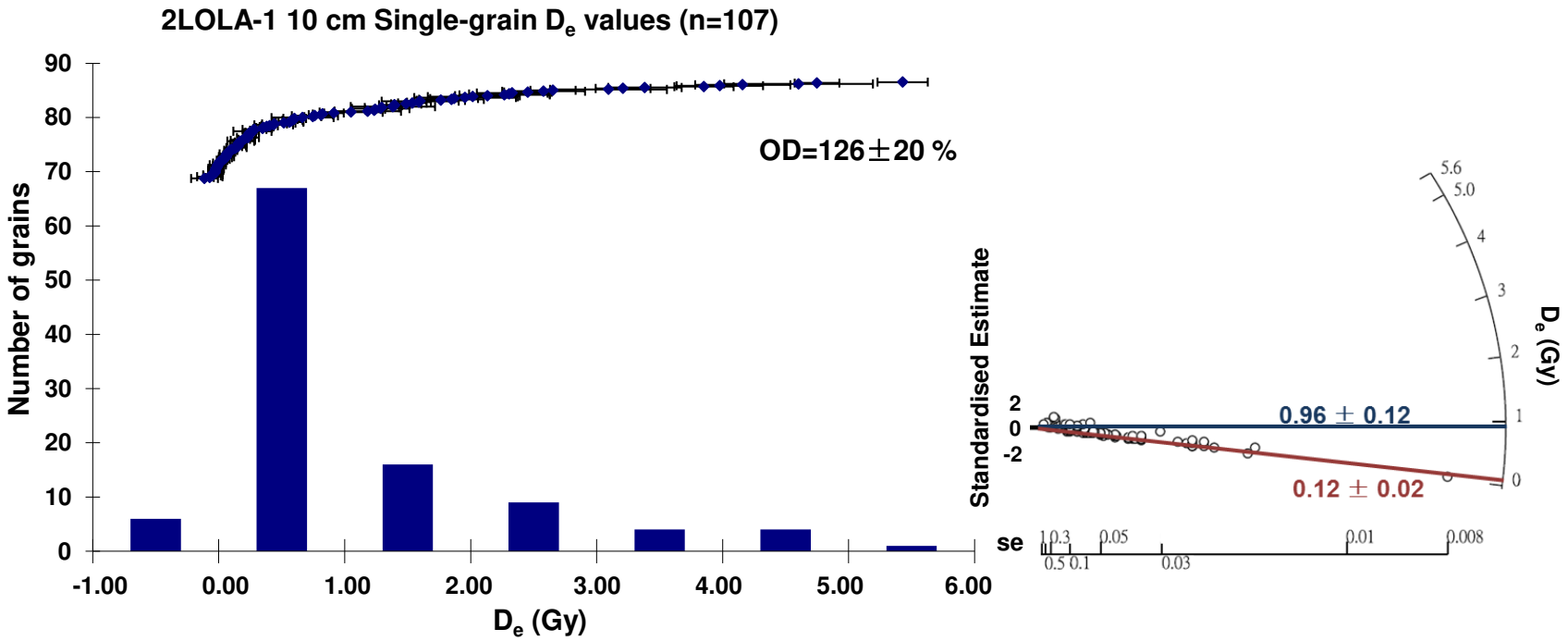

Figure 4.27. Histograms with ranked D_e values and radial plots of single-grain data from core 2LOLA2. (left graph: histogram; right graph: radial plot, blue line and number indicate D_e calculated by central age model, red line and number indicate D_e calculated by minimum age model)

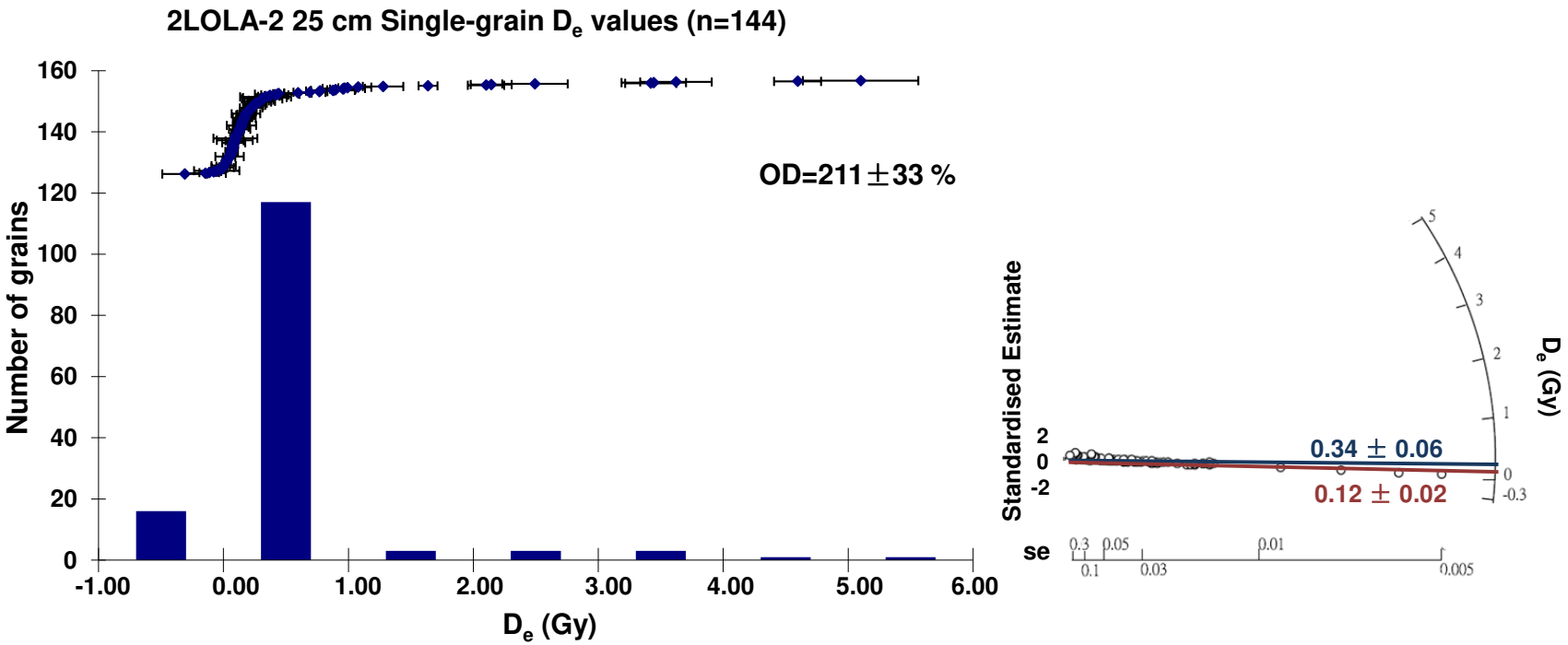

Figure 4.27 (continued). Histograms with ranked D_e values (left) and radial plot (right) of single-grain data from 2LOLA2 core.

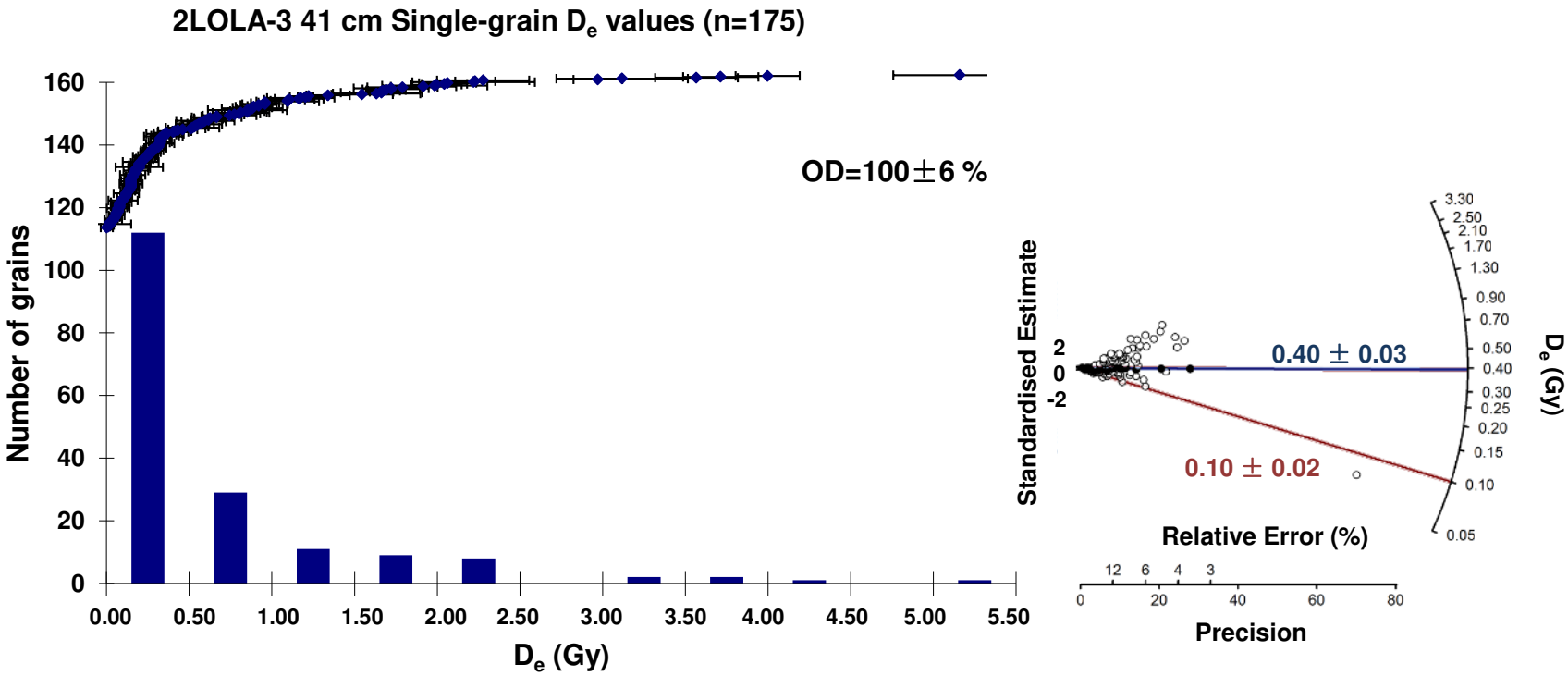

Figure 4.27 (continued). Histograms with ranked D_e values (left) and radial plot (right) of single-grain data from 2LOLA2 core.

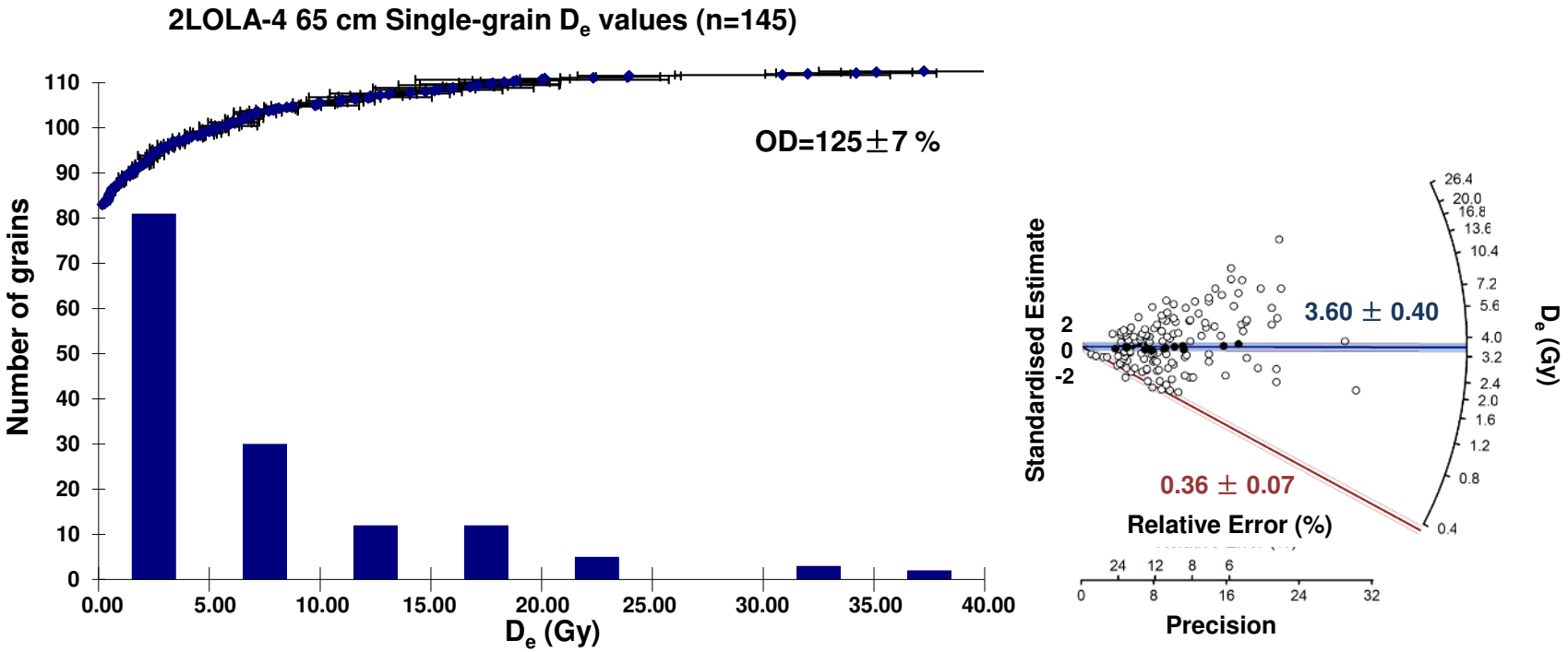

Figure 4.27 (continued). Histograms with ranked D_e values (left) and radial plot (right) of single-grain data from 2LOLA2 core.

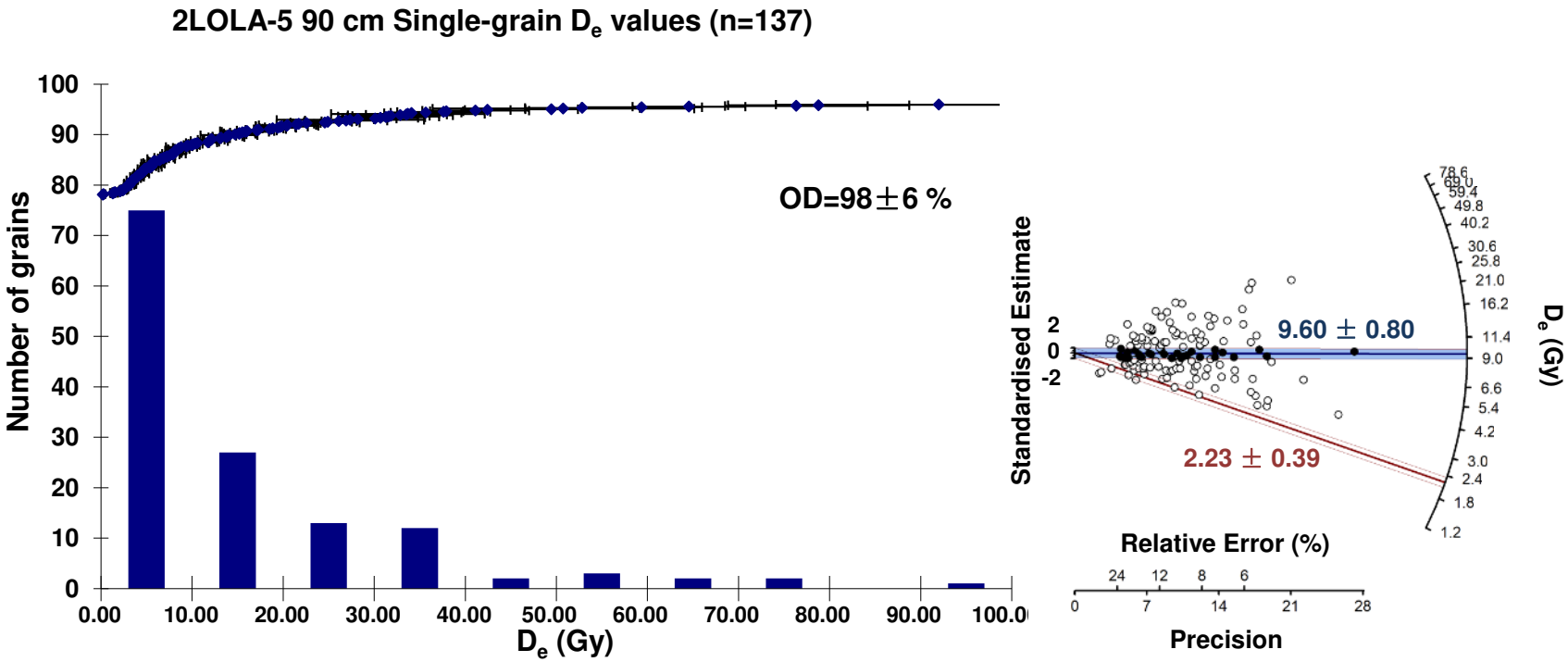

Figure 4.27 (continued). Histograms with ranked D_e values (left) and radial plot (right) of single-grain data from 2LOLA2 core.

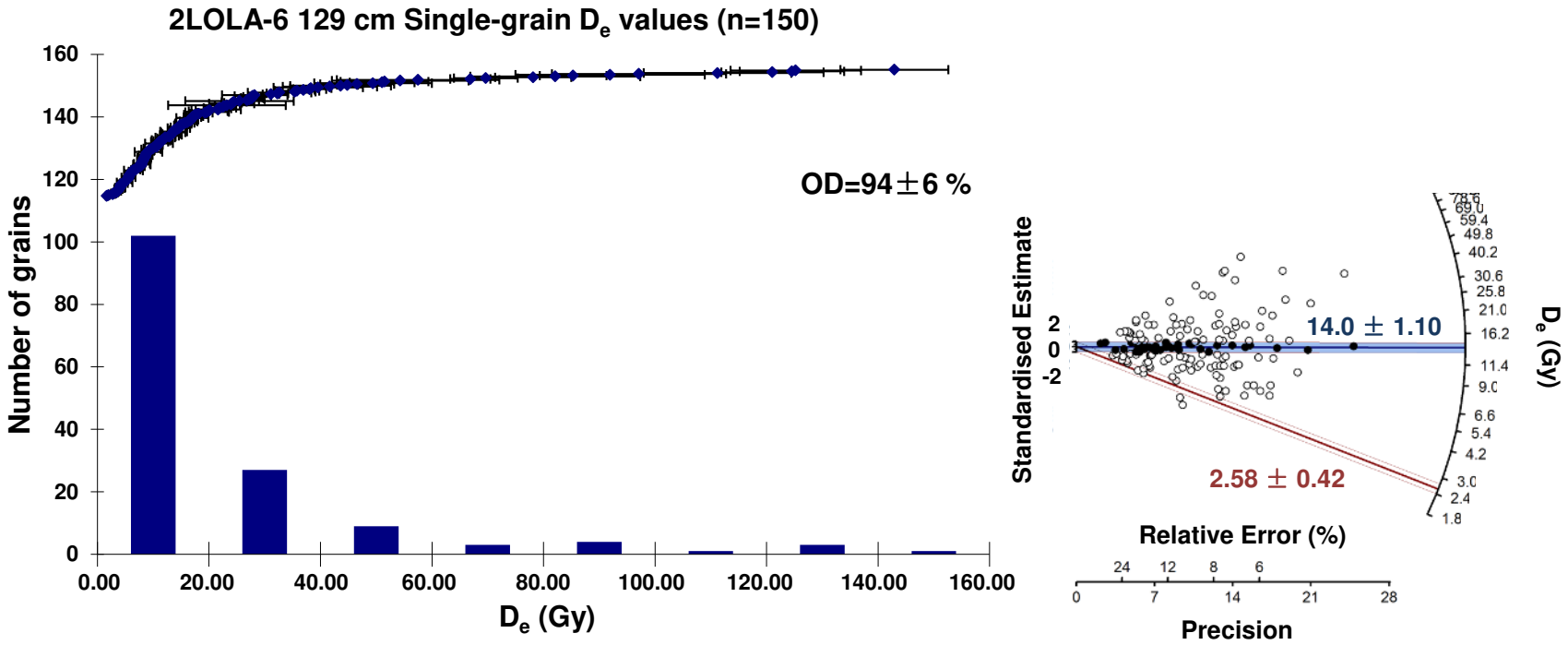

Figure 4.27 (continued). Histograms with ranked D_e values (left) and radial plot (right) of single-grain data from 2LOLA2 core.

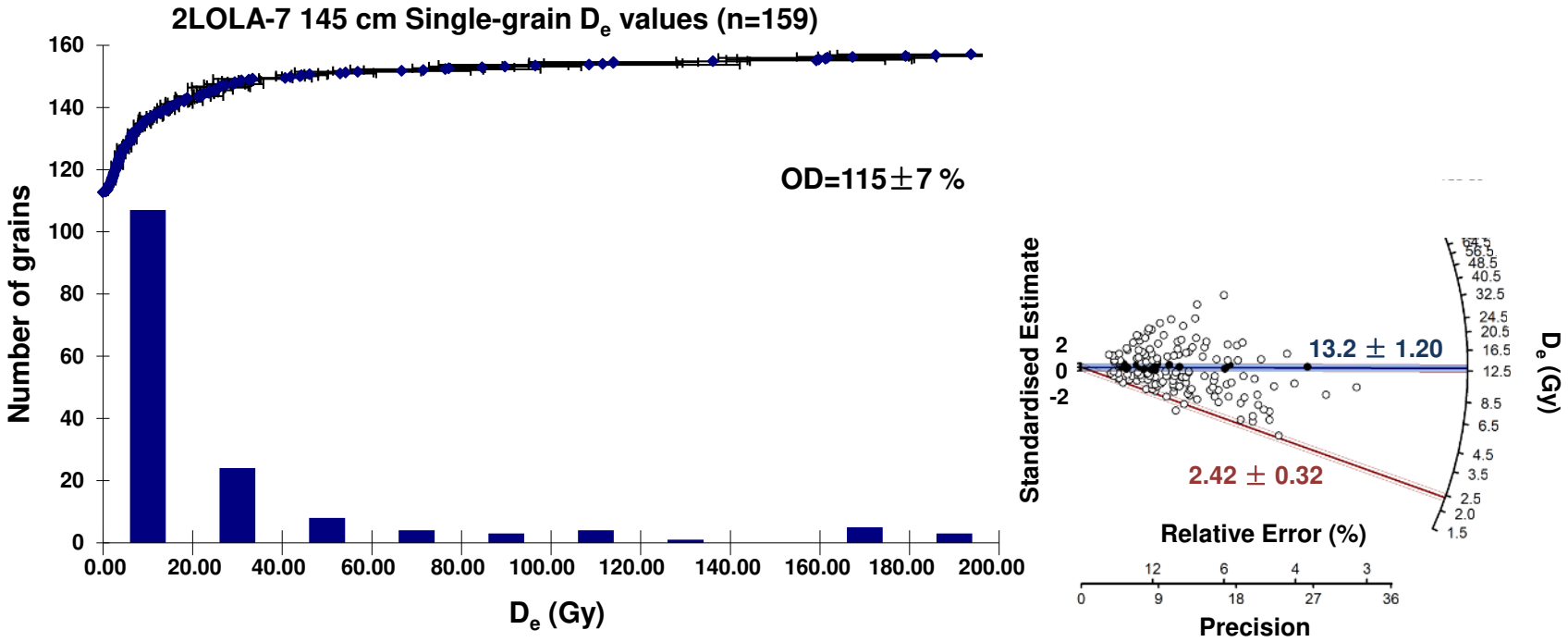

Figure 4.27 (continued). Histograms with ranked D_e values (left) and radial plot (right) of single-grain data from 2LOLA2 core.

4.7.6.2 Age models

As with the previous cores, samples of core 2LOLA were collected from fluvial sediments where partial-bleaching had clearly occurred. In light of this, the lowest D_e values extracted by the MAM (Table 4.20), were selected for use in age calculation. The CAM/UCAM was also applied before the MAM/UMAM to estimate the OD values.

The un-logged CAM was applied to 2LOLA-1 and 2LOLA-2 as they contained negative D_e values while the CAM was applied to the rest of the samples. The D_e values calculated by CAM/UCAM do not follow stratigraphic order along the core and the D_e values of 2LOLA-2 and 2LOLA-3; and 2LOLA-6 and 2LOLA-7 are very similar. All of the OD values are more than 100 % even in the two upper sediment samples which show less dispersion in their histograms and radial plots. When applying the UCAM, the OD values were calculated by dividing maximum likelihood values of the sigma by the mu. For the two near-surface sediment samples, the mu parameters which are the D_e values, were relatively low and thus increased the OD values. In fact, the true overdispersions for these two samples remain unknown.

Although the dose recovery test (Section 4.6.2.3.3) of core 2LOLA samples yielded an OD value less than 10 %, the UMAM was still run a number of times with various input OD values until the best fit/maximum likelihood was obtained for 2LOLA-1 and 2LOLA-2. The input OD values were 10 % for 2LOLA-1 and 20 % for 2LOLA-2. This again proves that the OD values calculated by the UCAM for these two samples were not representative. For the rest of the samples, the MAM was applied.

Table 4.20
The D_e values and age of core 2LOLA calculated by different age models.

Sample ID	Depth (cm)	Grain Size (μm)	Total Dose Rate (Gy/ka)	CAM			UCAM			MAM		UMAM	
				De (Gy)	Age (ka)	Overdispersion (%)	De (Gy)	Age (ka)	Overdispersion (%)	De (Gy)	Age (ka)	De (Gy)	Age (ka)
2LOLA-1	17-20	180-212	2.06 ± 0.14				0.92 ± 0.12	0.44 ± 0.06	126 ± 20			**0.12 ± 0.02**	**0.060 ± 0.008**
2LOLA-2	28-31	180-212	2.00 ± 0.14				0.34 ± 0.06	0.17 ± 0.03	211 ± 33			**0.12 ± 0.02**	**0.059 ± 0.011**
2LOLA-3	40-42	180-212	2.06 ± 0.14	0.40 ± 0.03	0.19 ± 0.02	100 ± 6				**0.10 ± 0.02**	**0.049 ± 0.010**		
2LOLA-4	51-53	180-212	2.18 ± 0.16	3.60 ± 0.40	1.63 ± 0.22	125 ± 7				**0.36 ± 0.07**	**0.17 ± 0.03**		
2LOLA-5	63-69	180-212	2.22 ± 0.17	9.60 ± 0.80	4.42 ± 0.49	98 ± 6				**2.23 ± 0.39**	**1.01 ± 0.19**		
2LOLA-6	104-111	180-212	2.20 ± 0.16	14.0 ± 1.10	6.29 ± 0.68	94 ± 6				**2.58 ± 0.42**	**1.18 ± 0.21**		
2LOLA-7	146-151	180-212	2.24 ± 0.18	13.2 ± 1.20	5.81 ± 0.71	115 ± 7				**2.42 ± 0.32**	**1.08 ± 0.17**		

* Values in bold are the most representative dose and age

4.7.6.3 Age calculation

The doses calculated by the MAM/UMAM in the previous section and dose rates presented in Section 4.5.2 are used to calculate the age for each individual sample. The OSL ages for core 2LOLA generally exhibit reasonable stratigraphic coherence with increasing ages in progression down the core (Figure 4.28 and Table 4.21).

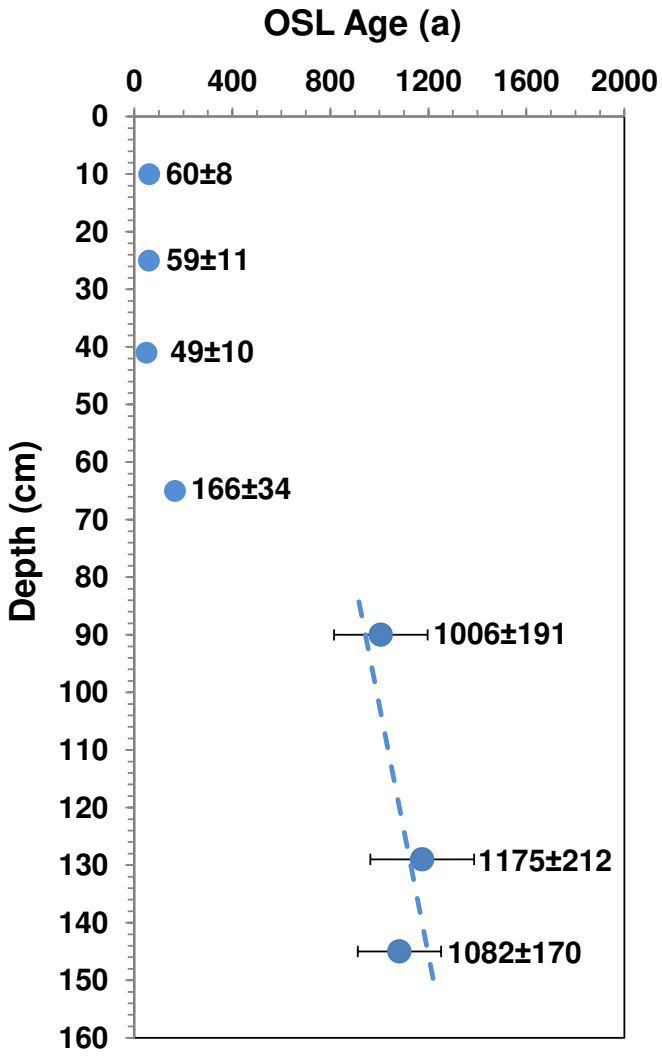

Figure 4.28. Chronology of core 2LOLA determined by OSL techniques. (●: OSL single-grain age before Year 2008; blue dashed line: the linear regression of the ages at depths of 145 to 90 cm)

Table 4.21
The OSL ages of core 2LOLA.

Depth (cm)	OSL Ages (a)	Ages before Year 2000 (a)
10	60 ± 8	52 ± 8
25	59 ± 11	51 ± 11
41	49 ± 10	41 ± 10
65	166 ± 34	158 ± 34
90	1006 ± 191	998 ± 191
129	1175 ± 212	1167 ± 212
145	1082 ± 170	1074 ± 170

Like the previous three cores, the chronological profile of core 2LOLA depicts fluctuating sedimentation rates. The ages for core 2LOLA are comparable to core MMB3 and core LSW but younger than its neighbouring core LOLA. Unlike core LOLA, the 2LOLA core site was not completely desiccated so that the potential deterioration of the surface sediments was not as profound. The OSL ages of core 2LOLA can be divided into three sections: from 145 cm to 90 cm represents sediments greater than 1,000 years old; followed by a compressed/deflated/lost section from 90 cm to 65 cm; and with the upper 65 cm representing sediments younger than ~158 years old (before Year 2000). The 'dry (1895-1946 AD)-wet (1947-1978 AD)-dry (1978 AD onwards)' pattern found in core MMB3 is likely present in the upper 65 cm of core 2LOLA.

There are no independent dating controls, including HRGS, ^{137}Cs results, to assist in assessing the OSL ages for core 2LOLA.

For the lower section between 145 cm to 90 cm, a linear regression (blue dashed line in Figure 4.28) was obtained to calculate the sedimentation rate. The ages for this section were calculated using the following equation:

$$\text{Age (a)} = (\text{depth (cm)} + 113.6) / 0.2$$

The ages calculated based on the sedimentation rates are referred to as "model ages" in the other chapters. The ages used for core interpretations are listed in Table 4.22.

Table 4.22
The OSL and model ages of core 2LOLA.

Depth (cm)	OSL Age before Year 2000 (a)	Model Age before Year 2000 (a)	Year (AD)
0			2008
10	52 ± 8		1948
25	51 ± 11		1949
41	41 ± 10		1959
65	158 ± 34		1842
90		934	
100		981	
123		1087	
129		1115	
145		1189	

4.8 Summary

4.8.1 OSL methodology

Conventional OSL dating methodology including sample preparation and SAR protocols are applicable to sediment samples from the Macquarie Marshes. Thermal transfers are unlikely to be problematic with preheat temperatures ranging from 200 to 280 °C, which are high enough to overcome the 110 °C thermal peak and lower than the 325 °C optical luminescence peak. Possible sensitivity changes can be corrected by the internal checks of the SAR protocol. However modifications have been made including the following:

1. Sample preparation procedure

It has been shown that initial particle-size distribution analysis is very important before selecting the core samples for OSL dating, especially when dating silty fluvial

samples like these. Sections with a high content of sand should be chosen for OSL dating. It is also practical to wet sieve the samples before conducting chemical reactions when dealing with fine silt samples so as to concentrate the quartz by removing its silty coating.

2. SAR analysis procedure

1) There is no significant variation in dose recovery results between cut-heat of 0 seconds and 5 seconds under the same preheat condition. In order to ensure reaching the desired temperature before recording the test dose signal, a "cut-heat" which is actually a preheat for 5 seconds was chosen.

2) IR depletion tests were added to the conventional SAR protocol to test for no feldspar contamination. Results again showed that a modified sample preparation procedure had been successful in extracting pure quartz and that there is no significant feldspar contamination for the samples used in this study.

3) Various responses to thermal treatments are observed within the same sample and among samples from different sites (Table 4.4, Page 125). Therefore it is essential to perform dose recovery tests ideally to each sample of interest, or at least each suite of similar samples.

4.8.2 OSL dating results

The OSL dating results reveal that the samples have been subjected to a diverse array of bleaching conditions and post-depositional process. Water attenuates the blue end of the spectrum (the most efficient bleaching wave-lengths) and the relatively high levels of organic compounds also attenuate the daylight spectrum (Madsen et al., 2005). Thus, quartz is more unlikely to be well zeroed before burial in particular in young sediments. In fluvial systems like the MM, offsets of several hundred to a few thousand years are

common (Murray and Olley, 2002). When plotting the D_e values as histograms, the well-bleached samples are characterised by narrow and almost symmetrical normal distributions, whereas poorly bleached samples have a broad distribution and are skewed towards the smaller D_e values. For "modern"/ "young" sediment, the degree of bleaching is the most pronounced of all the samples analysed. Although coarser sand grains (125-180 μm or 180-212 μm) were chosen for OSL dating, the partial bleaching effect seems to be inevitable. Individual samples did not display the same types of dose distribution at both the single-aliquot and single-grain scale of analysis, which again proves that the quartz grains were not homogeneous and were not excessively bleached. Intrusion of younger grains by bioturbation (in particularly with the growth of plants) was also observed in some surface/near surface sediment samples. However, such influence on the D_e distributions was negligible compared to the partial-bleaching.

Multiple age distributions were common but the internal consistency of age estimates was high. For the Macquarie Marshes samples in this study, issues of partial bleaching and bioturbation seem to be manageable with appropriate calculation by the most suitable age model. For almost all samples with incomplete bleaching, a minimum age model (MAM/UMAM) was used, in which the distribution of D_e values was approximated by a truncated logged-/un-logged normal distribution with the truncation point giving the best estimate of the true burial dose. Generally, these age models yield OSL ages that are stratigraphically consistent and consistent with independent age control.

The ages obtained from the four cores, by the OSL dating technique alone, range from 7 ± 6 years old to 50.5 ± 6.9 ka, a range not attainable by other dating techniques. Three short (<100 cm) cores, including cores MMB3, LSW and 2LOLA, are dated younger than ~1,000 years. One long (220 cm) core (LOLA) shows that 'young'

sediments (< 2 ka) were deposited on palaeo-sediments (20-50 ka) which predate formation of the marshes. The oldest section at 210 m depth has been dated at ~ 50 ka. The deposition rates calculated by the OSL ages vary from site to site and are generally rapid during the last 100 years or so. The 'dry (1895-1946 AD)-wet (1947-1978 AD)-dry (1978 AD onwards)' pattern reported in the literature has also been found in core MMB3 and core 2LOLA. It has been discussed in Chapter 3 and will be further discussed in Chapter 5 with the organic proxies.

Despite the complexity required to obtain the OSL data and in calculating ages, the OSL dating technique has worked well for the Macquarie Marshes sediments.

CHAPTER 5 ORGANIC GEOCHEMISTRY

In Chapter 3, the total organic carbon content (TOC), its stable isotope $\delta^{13}C$, total nitrogen (TN) and carbon/nitrogen (C/N) values revealed that algae and C_3 higher plants are the main organic matter (OM) sources for the surface sediments in the Macquarie Marshes. In the sediment cores, these proxies also indicate the changes of vegetation from dominantly aquatic plants to land plants. This chapter will further test these findings by analysing specific organic molecular markers, which will provide further information on the organic matter sources and assess their contribution at the level of individual compounds. A pilot study to investigate the colonial waterbird breeding events in Macquarie Marshes (Cull, 2007) using phosphorus, nitrogen and total organic matter content of sediments was not particularly successful. Accordingly, this chapter will utilise specific organic compounds to investigate changes in the wetland ecosystem, including the variation of dominant vegetation and the possible cause of the decline of colonial waterbirds. Some anthropogenic organic pollutants will also be analysed and discussed to assess if there is/was any contamination in this Nature Reserve wetland.

5.1 Introduction to organic geochemical proxies for palaeoenvironmental reconstruction

Organic matter (OM) consists of a complex mixture of lipids, carbohydrates, proteins and other organic compounds (Meyers, 2003; Choudhary et al., 2009). Although lipids are only a small proportion of total OM (less than 5 %) (Tissot and Welte, 1984), they are important constituents of the OM, because lipids contain the basic skeletal structure and functional group details of the original source (Venkatesan, 1988b). Compared to the use

of bulk OM, lipids can better distinguish the heterogeneous sources of OM from a molecular level (Meyers and Ishiwatari, 1993; Fisher et al., 2003; Brodie et al., 2011). Biological lipids (commonly referred to as 'biomarkers'), synthesised by living organisms, have distinctive chemical structures and can be used for assigning sources to particular groups of organisms (e.g. terrestrial plants, bacteria, microalgae, etc.) (Peters et al., 2005 and reference therein).

Biomarkers extracted from recent or ancient marine, lacustrine and bog/peat sediments have been widely used to reconstruct past environmental conditions, including determining the nature of the main or specific vegetation inputs to sedimentary OM, assessing vegetation modification triggered by climate and/or natural environmental changes or anthropogenic activities (e.g. agricultural practices) (e.g. Cranwell et al., 1987; Meyers and Ishiwatari, 1993; Logan and Eglinton, 1994; Van Aarssen et al., 2000; Meyers, 2003; Otto and Simpson, 2005; Hautevelle et al., 2006; Feakins et al., 2007; Zheng et al., 2007; McKirdy et al., 2010; Seki et al., 2010; Trendel et al., 2010; Huguet et al., 2012; Lopes Dos Santos et al., 2012).

Among the biomarkers studied, *n*-alkanes, widely found in marine and lacustrine sediments, have been extensively used for palaeovegetation changes and their associated palaeoclimate because they are more resistant to microbial degradation (e.g. Logan and Eglinton, 1994; Van Aarssen et al., 2000; Meyers, 2003; Otto and Simpson, 2005; Hautevelle et al., 2006; Seki et al., 2010). Apart from the lipids, some organic compounds are also of geological importance as they can be used as markers/proxies to indicate environmental change in the past (e.g. fire, pollution, etc.) (Killops and Massoud, 1992; Mortimer, 2000; Shivaramaiah et al., 2002; Simoneit, 2002). For example, Killops and Massoud (1992) found pyrolytic originated benzo[e]pyrene, benzo[g,h,i]perylene and

coronene in ancient sediments as evidence of Jurassic vegetation fires. The persistent organic pollutants DDT and DDE were used to trace the usage of pesticides in cotton-farming regions in New South Wales, Australia, in the 1950s (Shivaramaiah et al., 2002).

Wetlands comprise only about 5–8 % of the terrestrial land surface (Mitsch and Gosselink, 2007), but they are globally important carbon sinks because 20–30 % of the Earth's soil pool of 2500 Pg of carbon is stored in wetlands (Roulet, 2000; Bridgham et al., 2006). Many of the world's wetlands are thought to be highly sensitive to climate change (Erwin, 2009), so it is important to know the sources of OM in wetland ecosystem sediments and the factors controlling their distributions in order to understand global biogeochemical cycles. As with lacustrine sediments, wetland sediments have a heterogeneous array of organic materials derived from aquatic (autochthonous OM, e.g. phytoplankton, macrophytes) and/or terrestrial origin from the surrounding areas (allochthonous OM, e.g. trees, shrubs, grasses, animals) (Meyers and Ishiwatari, 1993; Meyers, 2003). When Australian floodplain wetlands receive water from rivers, the flow carries organic matter; other accumulated organic matter within the wetland may consist of *Eucalyptus* spp. leaf litter, aquatic macrophytes from the last filling, or terrestrial plants that colonise wetlands when they dry (Kingsford, 2000 and references therein). In floodplain wetlands, the fluctuation in the hydrological cycle additionally controls the chemistry and biology of the water column and a variety of sedimentary processes, which are distinctively recorded in the composition of the sedimentary OM (da Silva et al., 2008). Thus organic geochemical studies of wetland sediments may be used to recognise the source of organic materials and their depositional conditions.

Compared with marine and lacustrine sediments, organic geochemical studies on wetland sediments are limited and mainly focus on coastal marshes (e.g. Zheng et al.,

2007; Seki et al., 2010; Lin et al., 2013). Therefore the study of inland freshwater wetlands, in particular from semi-arid/arid floodplain wetlands like the Macquarie Marshes (MM) becomes increasingly important to understand the composition, origin and transport of OM of dynamic and complex ecosystems which depend on flood/dry cycles.

As a first step in the study of OM biomarkers, a preliminary study was performed to analyse the biomarkers of modern plants and surface sediments collected adjacent to the core sites, in order to help assign the organic sources. These provided a database used to distinguish specific biomarkers, and to identify the sources of organic matter in the sediments. The study of the surface sediments assisted in the evaluation of how the organic compounds and their proxies can indicate the sources of OM and their relative contribution. Then the most appropriate molecular markers and proxies were used to reconstruct the past climate and ecosystem histories using the sediment cores.

Several organic compounds were targeted in order to answer questions about vegetation change, birds and pollutants. These include:

- Compounds that indicate vegetation input to the organic matter pool, ideally unique to particular plant species;
- Compounds that indicate the existence of waterbirds, e.g. unique biomarkers of their guano;
- Compounds that indicate environmental events/changes, e.g. climate (temperature, rainfall, humidity, etc.), fire, flood, drought, land clearance, etc.; and,
- Compounds that indicate pollutants from anthropogenic activities that may or may not affect the well-being of wetlands.

The selected organic-compound classes are *n*-alkanes, *n*-alkanols, *n*-alkanoic acids, sterols, α-phellandrene, polycyclic aromatic hydrocarbons (PAHs) and organochlorine pesticides (OCPs). A summary of the application of these organic compounds for sediments in MM is given in Table 5.1 and they will be further discussed in the following paragraphs.

Table 5.1
Selected organic compounds and their applications to the sediments of the Macquarie Marshes.

Compounds	Source	Applications
n-alkanes	Naturally occurring	Indicate the OM sources from algae, aquatic macrophytes, and land plants and thus reveal the relevant environment conditions (flood/drought).
n-alkanols	Naturally occurring	Indicate the OM sources from algae, aquatic macrophytes, and land plants and thus reveal the relevant environment conditions (flood/drought).
n-alkanoic acids	Naturally occurring	Indicate the OM sources from algae, aquatic macrophytes, and land plants and thus reveal the relevant environment conditions (flood/drought).
sterols	Naturally occurring /Anthropogenic	Indicate the OM sources from algae, aquatic macrophytes, and land plants and thus reveal the relevant environment conditions (flood/drought); coprostanol is a faecal biomarker for birds, higher animals and humans.
α-phellandrene	Naturally occurring	Contribution from *Eucalyptus* spp.
polycyclic aromatic hydrocarbons (PAHs)	Naturally occurring /Anthropogenic	Pyrogenic PAHs (e.g. retene, perylene and high molecular weight PAHs) can be used as indicators of fires (either naturally occurring, commonly during droughts, or by anthropogenic combustion in land clearance campaigns); Some PAHs (e.g. retene and perylene) are formed naturally by the biogenic precursors and can indicate the relevant plant species.
organochlorine pesticides (OCPs)	Anthropogenic	Contribution from agricultural usage of pesticides and herbicides.

5.1.1 *n*-alkanes

Normal alkanes, indicated by the prefix *n*- (for normal), are straight-chain saturated hydrocarbons, which normally constitute a very small fraction of the total OM in both biota and sediments (Meyers, 1993). However, they are a group of compounds that are less susceptible to microbial degradation compared to other types of organic biomarkers and are generally used as robust indicators to trace the origins of OM in the sediments (e.g. Volkman et al., 1980; Meyers and Ishiwatari, 1993; Ficken et al. 2000). For example, the two principal sources of biotic hydrocarbons found in lake sediments have distinctively different suites of hydrocarbons; these characteristic molecules can serve as proxies for estimating the sources of OM (Meyers, 2003) – whether OM is derived from algae, bacteria and vascular plants that live around or within the lake, or only from the vascular plants that live around it. Meyers (2003), in a review paper, concluded that the abundance of C_{17} *n*-alkane reflects the input of algae and photosynthetic bacteria, the abundance of C_{21}, C_{23} or C_{25} *n*-alkanes reflects the input of non-emergent (submerged and floating) macrophytes, and the abundance of C_{27}, C_{29} and C_{31} *n*-alkanes, typical of waxy coatings, reflects the input of vascular plants living on land or along the edges of lakes. Emergent aquatic plants have *n*-alkane distributions midway between non-emergent and terrestrial plants. The author also suggested that the absolute amounts of biomarker hydrocarbons should be interpreted cautiously as they might be exaggerated by the diagenetic loss of the non-hydrocarbon components and which is particularly relevant for sediments with organic inputs mainly from land-plants.

Table 5.2
Some *n*-alkane proxies and their application in palaeoenvironmental reconstructions.

Proxies	Applications	References
Carbon preference index $CPI_{\text{alk}} = \frac{1}{2}\left(\frac{C_{25}+C_{27}+C_{29}+C_{31}+C_{33}}{C_{24}+C_{26}+C_{28}+C_{30}+C_{32}} + \frac{C_{25}+C_{27}+C_{29}+C_{31}+C_{33}}{C_{26}+C_{28}+C_{30}+C_{32}+C_{34}}\right)$	Indicator of OM sources: high values (>5) are probably due to contribution of vascular plants; low values (~1) can probably be attributed to greater input from microorganisms	Kennicutt et al., 1987; Rieley et al., 1991a
Odd-even predominance $OEP = \frac{C_i + 6C_{i+2} + C_{i+4}}{4C_{i+1} + 4C_{i+3}}$	Indicator of contribution of OM from vascular plants (higher plants synthesise hydrocarbons with a strong odd-over-even predominance by a factor of 10 or more)	Scalan and Smith, 1970; Bianchi and Canuel, 2011
Terrigenous/aquatic ratio $TAR = \frac{C_{27}+C_{29}+C_{31}}{C_{15}+C_{17}+C_{19}}$	Indicator of possible changes in the terrigenous/aquatic mixtures of hydrocarbons in core sediments; the presence of high TAR values can probably be attributed to higher contributions of terrigenous lipids	Bourbonniere and Meyers, 1996; Jeng and Huh, 2006
Average chain length $ACL = \frac{25(C_{25})+27(C_{27})+29(C_{29})+31(C_{31})+33(C_{33})}{C_{25}+C_{27}+C_{29}+C_{31}+C_{23}}$	Indicator of variation in plant species; in some cases used to assess petrogenic and biogenic hydrocarbons (input of petrogenic hydrocarbons can result in lower ACL values and wider ACL range)	Cranwell, 1973a; Jeng, 2006
$P_{aq} = \frac{C_{23}+C_{25}}{C_{23}+C_{25}+C_{29}+C_{31}}$	Indicator of macrophyte and terrestrial plant inputs: values range from 0.01 to 0.23 for terrestrial plants and from 0.48 to 0.94 for submerged and floating species of macrophytes	Ficken et al., 2000
$P_{wax} = \frac{C_{27}+C_{29}+C_{31}}{C_{23}+C_{25}+C_{27}+C_{29}+C_{31}}$	Indicator of the relative proportions of waxy hydrocarbons derived from emergent macrophytes and terrestrial plants to total hydrocarbons	Zheng et al., 2007

Therefore, the relative amounts of hydrocarbon biomarkers have been widely used as palaeoenvironmental proxies. Table 5.2 (Page 232) summarises the most commonly used *n*-alkane proxies (indices and their formulae) and their applications in palaeoenvironmental reconstructions. These proxies integrate the potential sources from a great variety of samples and are more straightforward and easy to compare among different samples. Carbon preference index (CPI) values summarise the relative proportion of even- and odd-numbered *n*-alkane carbon molecules of biological and geological samples (Kennicutt et al., 1987; Rieley et al., 1991a). Biomarkers of different biological origin have different CPI values: *n*-alkanes from the waxes of higher plants have a strong odd/even predominance with high CPI values (>5) whereas *n*-alkanes from bacteria and algae show a weak odd/even predominance with low CPI values (~1) (Cranwell et al., 1987). Odd-even predominance (OEP) values were originally proposed to be used in the form of a plot versus the carbon chain length to characterise the series of normal alkanes separated from crude oils, ancient rocks, and modern sediments (Scalan and Smith, 1970). OEP can be used as an indicator of the contribution of OM from vascular plants, as higher plants synthesise hydrocarbons with a strong odd-over-even predominance by a factor of 10 or more (Bianchi and Canuel, 2011 and references therein). In this thesis, OEP was calculated based on the C_{25} to C_{31} *n*-alkanes. The *n*-alkane average chain length (ACL) is the weight-averaged number of carbon atoms of the higher plants C_{25}-C_{33} *n*-alkanes (Cranwell, 1973a; Jeng, 2006). Lipid analysis of aquatic plants reveals that non-emergent (submerged and floating-leaved) species display enhanced abundances of mid-chain length C_{23} and C_{25} *n*-alkanes; while emergent aquatic plants and terrestrial plants display typically long-chain length homologues (>C_{29}) (Ficken et al., 2000). Therefore, a proxy P_{aq} was proposed to reflect the non-emergent aquatic macrophyte input to lake sediments

relative to that from emergent aquatic and terrestrial plants (Ficken et al., 2000): for modern plants, P_{aq} averages 0.09 for terrestrial, 0.25 for emergent and 0.69 for submerged/floating species. As applied to sediment extracts, a given value will reflect a particular mixture of inputs from two or more of these sources (Ficken et al., 2000). Another proxy, P_{wax}, was used as indicator of the relative proportions of waxy hydrocarbons derived from emergent macrophytes and terrestrial plants to total hydrocarbons (Zheng et al., 2007). Based on the difference of molecular distributions in various plants, some proxies/ratios can be used to indicate the relative proportion of algae and bacteria/higher plants (C_{17}/C_{31}), emergent aquatic plants and terrestrial plants/C_3 grass (C_{27}/C_{31} or $(C_{27}+C_{29})/2C_{31}$) (Seki et al., 2010). For example, high C_{27}/C_{31} values indicate a higher contribution from tree-leaf derived waxes than grasses and aquatic plants; while low values indicate wetland emergent vegetation dominated by C_3 grasses (Seki et al., 2010).

The proxy ratios were suggested can be diagenetically insensitive because they are based on the relative abundance of chemically similar compounds within a limited molecular weight range (Hedges and Prahl, 1993). Compared with the approach using more sophisticated geochemical techniques like isotopic analysis, the proxy ratio method is still a rapid screening tool (Jeng, 2006).

The use of ternary diagrams of the high molecular *n*-alkanes is another straightforward way to indicate organic sources. They are usually plotted to show the relative composition of the three most abundant *n*-alkanes (nC_{27}, nC_{29} and nC_{31}, in some cases nC_{29}, nC_{31} and nC_{33}) in plants and soils/sediments and to estimate the contribution of plant biomass to soils/sediments (Schwark et al., 2002; Wiesenberg et al., 2004). For

example, elevated nC$_{31}$ is attributed to grass input whereas nC$_{27}$ or nC$_{29}$ predominance is related to tree-leaf origin (Cranwell, 1973b; Schwark et al., 2002).

5.1.2 *n*-alkanols

The lipid n-alkanols have not been as widely applied in palaeolimnological reconstructions as either *n*-alkanes or *n*-alkanoic acids, although *n*-alkanols contain equally useful information about the source of OM in sedimentary records. Contributions from algae and photosynthetic bacteria can be identified via the large proportion of C$_{16}$-C$_{22}$ *n*-alkanols (Robinson et al., 1984; Volkman et al., 1999); submerged and floating macrophytes have a predominance of C$_{22}$ and/or C$_{24}$ *n*-alkanols (Ficken et al., 1998); vascular land plants and emergent macrophytes contain large proportions of C$_{22}$-C$_{30}$ *n*-alkanols (Eglinton and Hamilton, 1967; Cranwell, 1984; Rieley et al., 1991b). For example, the study by Trendel et al. (2010) found C$_{26}$ *n*-alkanols dominating in all grasslands (more especially in pastures), while C$_{28}$ *n*-alkanols dominate in beech forests (typical for North Hemisphere) and C$_{24}$ *n*-alkanols dominate in oak forests (typical for North Hemisphere). Castañeda et al. (2011) found C$_{28}$ – C$_{32}$ *n*-alkanols present in lake sediments as biomarkers for terrestrial higher plants.

CPI values of *n*-alkanols (CPI$_{OH}$) summarise the relative proportions of even- and odd-numbered carbon molecules (Bray and Evans, 1961; Kvenvolden, 1970) and is calculated by the following equation:

$$CPI_{OH} = \frac{1}{2}\left(\frac{\left(C_{20}+C_{22}+C_{24}+C_{26}\right)+\left(C_{22}+C_{24}+C_{26}+C_{28}\right)}{C_{21}+C_{23}+C_{25}+C_{27}} \right)$$

In undegraded lipid material, even-numbered chains dominate the composition of *n*-alkanols while odd-numbered chains dominate *n*-alkane composition (Tissot and Welte, 1984; Meyers and Ishiwatari, 1993). It has been found that low CPI_{OH} values (<18.9) are indicative of root-derived lipids from vascular plants (Huang et al., 2011). In this thesis, due to the low concentrations of odd *n*-alkanols in sediments from deeper parts of the core profiles, CPI_{OH} values are only calculated and discussed among the modern biota and surface sediment samples. The ratios of short-chain and long-chain *n*-alkanols show the predominant *n*-alkanols, thus indicating the organic source (Duan and Ma, 2001): the lower ratios indicate the input of higher plants, such as herbaceous plants; whereas the higher ratios indicate the input of microbes (Rieley et al., 1991a).

5.1.3 *n*-alkanoic acids

The fatty acids are typically of C_{12} and C_{36} chain length and in animals they are predominantly saturated (referred to as 'alkanoic acids'), whereas in plants more unsaturated (referred to as 'alkenoic acids') and polyunsaturated acids are present. Fatty acids are more sensitive to degradation and modification than most types of lipid biomarkers (Volkman et al., 1980). This thesis only focuses on the saturated fatty *n*-alkanoic acids. Similar to *n*-alkanes and *n*-alkanols, the different molecular weights of *n*-alkanoic acids can be indicative of a variety of types of plants: large proportions of C_{16} and C_{18} *n*-alkanoic acids usually originate from algae and photosynthetic bacteria (Robinson et al., 1984; Volkman et al., 1999); while C_{24}-C_{30} *n*-alkanoic acids are usually derived from vascular land plants and emergent macrophytes (Cranwell, 1974; Wiesenberg and Schwark, 2006). Apart from the *n*-alknoic acids, the unsaturated (e.g. $C_{16:1}$, $C_{18:1}$) and branch-chain iso/anteiso (C_{14}, C_{15}) alkanoic acids, usually detected in

relatively low abundance, are indicative of bacterial origin (Matsuda and Koyama, 1977; Perry et al., 1979; Volkman et al., 1980; Cranwell, 1984).

The CPI value of *n*-alkanoic acids (CPI_{FA}) summarises the relative proportions of even and odd-numbered carbon molecules (Bray and Evans, 1961; Kvenvolden, 1970), and is calculated by the following equation:

$$CPI_{FA} = \frac{1}{2}\left(\frac{\left(C_{22} + C_{24} + C_{26} + C_{28} + C_{30}\right) + \left(C_{24} + C_{26} + C_{28} + C_{30} + C_{32}\right)}{C_{23} + C_{25} + C_{27} + C_{29} + C_{31}} \right)$$

Similar to *n*-alkanols, even-numbered chains dominate the composition of *n*-alkanoic acids in undegraded lipid material (Tissot and Welte, 1984; Meyers and Ishiwatari, 1993). Due to the low concentration of odd *n*-alkanoic acids in modern biota and sediments from the deeper part of the MM core profiles, CPI_{FA} values can only be calculated and discussed among the near-surface sediment samples. The ratios of short-chain and long-chain *n*-alkanoic acids show the predominant *n*-alkanoic acids and thus indicate the organic source.

The relative composition of the three most abundant *n*-alkanoic acids (nC_{22}, nC_{24} and nC_{26}) in plants and soils/sediments can be plotted in a ternary diagram to estimate the contribution of plant biomass to soils/sediments (Wiesenberg et al., 2004). For example, elevated nC_{22} (>40 %) is characteristic of C_3 plants whereas nC_{24} is related to C_4 plants (Wiesenberg et al., 2004).

5.1.4 Sterols

Sterols are crystalline compounds and contain an alcohol group. They occur free or as esters of the higher fatty acids, and are isolated from the unsaponifiable portion of oils and fats; therefore they are considered to be more stable than fatty acids in sediments (Volkman et al., 2008). The sterols are numbered as shown in Figure 5.1 (Lipidlibrary, http://lipidlibrary.aocs.org/Lipids/plant_st/index.htm), with structures of 1,2-cyclopentenophenanthrene skeleton. According to the Lipidlibrary (http://lipidlibrary.aocs.org/Lipids/plant_st/index.htm), the prefix α and β before the number of the carbon atom is used to denote the function group below (α) or above (β) the plane of the nucleus; the prefix 'nor' preceded by the number of the carbon atom indicatea methylene group is missing from the side-chain; the prefix 'nor' preceded by a small capital letter indicate a ring has been contracted; the prefix 'nor' preceded by the number designating that methyl group in some cases indicate the loss of an angular methyl group.

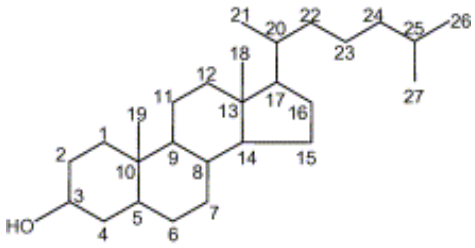

Figure 5.1. Structure of 4-desmethylsterol with carbon numbers. (Source from http://lipidlibrary.aocs.org/Lipids/plant_st/index.htm)

Sterols are widely distributed among animals and plants in the form of oils or fats. Sterols are essential membrane components with various biophysical functions and are found in all eukaryotic organisms (e.g.Volkman, 2003). In microalgae, they usually possess C_{27}-C_{30} skeletons, with differences in alkylation at C_{24} and double bonds in the

nucleus (most common in C number 5, marked as Δ^5) and side chain (most common in C number 22, 24(28), marked as Δ^{22}, Δ^{24}, $\Delta^{24(28)}$).

In sediments, the structural diversity of sterols and their derivatives provide important information about the origin of the OM. Table 5.3 summarises some common sterols used in palaeoenvironmental reconstructions. Generally C_{29} sterols are among the major sterols in higher plants and microorganisms such as cyanobacteria and Chlorophyceae. Consequently, the variation of C_{29} sterols may reflect changes in both productivity and terrigenous supply (da Silva et al., 2008). C_{27} and C_{28} sterols usually reflect algal contribution to the sediment (Volkman, 2003; da Silva et al., 2008). Biota can also contribute C_{27} - C_{29} sterols to the sediment by their excretions and can usually be distinguished by the abundance of coprostanol which is unique to higher animals including human beings. In an open environment, the OM source may not be constrained to just one source. In most of the cases, the sterol profile may indicate several sources as there may be more than one source of OM in an open environment, and they may alternate due to environmental changes. Therefore proxies calculated by the ratio of particular compounds can be further examined to assist in source identification. For example, the ratio of coprostanol/(coprostanol+cholestanol) is used to indicate significant sewage pollution (Grimalt et al., 1990).

Table 5.3
Sterol proxies and their application in palaeoenvironmental reconstructions.

Proxies	Applications	Reference
Cholesterol	Principal sterol synthesised by animals, small quantities synthesised by other eukaryotes (e.g. plants and fungi); completely absent among prokaryotes (including bacteria)	Volkman, 2003
Coprostanol	Formed from the biohydrogenation of cholesterol in the gut of most higher animals and birds; biomarker for the presence of human faecal matter in the environment	Leeming et al., 1996; Bull et al., 2003; Tindale et al., 2009
Cholest-5,22-dien-3β-ol, 24-methylcholesta-5,22E-dien-3β-ol	Diatom sterol	Volkman, 2003
C_{29} sterols	Commonly associated with higher plants; also abundant in cyanobacteria and Chlorophyceae	Volkman, 2003; Sonibare and Sojinu, 2009
$\frac{\text{Coprotanol}}{\text{Total Sterols}}$	< 0.01-0.02 may indicate the formation of coprostanol in anaerobic sediment in pristine environments without faecal pollution	Leeming et al., 1996
$\frac{\text{Coprostanol}}{\text{Coprostanol + Cholestanol}}$	≥0.7 indicate significant sewage pollution	Grimalt et al., 1990

5.1.5 Other organic markers

5.1.5.1 α-phellandrene

α-phellandrene (Figure 5.2) is the isomer of β-phellandrene, both of which are cyclic monoterpenes, insoluble in water but miscible with ether. α-phellandrene is named after *Eucalyptus phellandra* (*Eucalyptus radiata*) (Merck, 1996) and is also a constituent of the essential oil of *Eucalyptus dives* (Jacobs and Pickard, 1981). In this thesis α-phellandrene was found in some of the surface sediments where *Eucalyptus* spp. grew (discussed in Section 5.4.5.1) and used as a specific biomarker for studying the vegetation changes in the core profiles.

Figure 5.2. Structures of α-phellandrene and β-phellandrene (Merck, 1996).

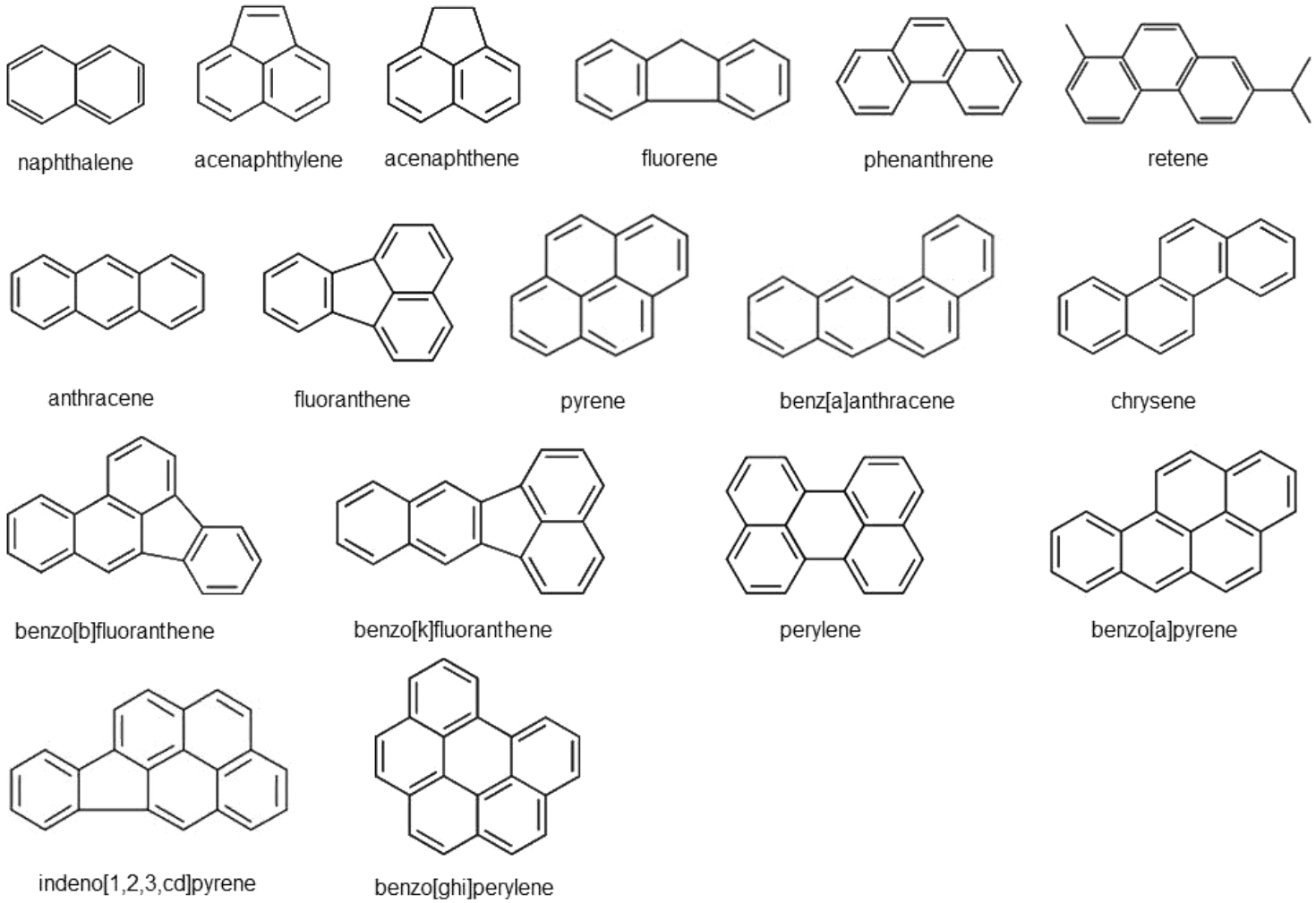

Figure 5.3. Structures of 18 polycyclic aromatic hydrocarbons (PAHs) (source from Wikipedia).

5.1.5.2 Polycyclic aromatic hydrocarbons (PAHs)

Polycyclic aromatic hydrocarbons (PAHs) are a variety of compounds consisting of fused aromatic rings (Figure 5.3, Page 242). PAHs do not occur naturally in organisms, but are the products of OM alteration and are created by one of three processes: (1) microbial modification of biogenic precursors shortly after burial in sediment, (2) low-temperature diagenesis over a long period of time, or (3) high-temperature rearrangements of OM combustion products into polynuclear aromatic molecules (Meyers, 2003). Once formed, most PAHs are considered to be relatively robust and can provide source information in sediments (e.g. Jiang et al., 2000; Götze et al., 2001; Yunker and Macdonald, 2003; Muri and Wakeham, 2009; O'Dwyer and Taylor, 2009). In the nature reserve of the Macquarie Marshes, contaminant PAHs formed by spillage of unburnt petroleum are very unlikely to be present. The PAHs found in the sediments, if any, are likely formed by their biogenic precursors, pyrogenesis or the combination of the two. In this thesis, we are particularly interested in the third group of PAHs, which are usually referenced as pyrogenic (combustion-derived) PAHs and used as indicators of forest/wood fires, in particular to reveal if vegetation fires occurred naturally (commonly during droughts) or anthropogenically induced during land clearance campaigns (Killops and Massoud, 1992; Jiang et al., 2000; Gabos et al., 2001). These compounds mainly include:

(1) Retene is a unique marker for wood combustion, e.g., forest fires (Ramdahl, 1983; Gabos et al., 2001); but also a short-term diagenic product of abietic acid, abundant in resins of conifers and other higher plant lipids (Simoneit, 1977; Laflamme and Hites, 1978; Wakeham et al., 1980).

(2) Perylene is a diagenetic product derived from its natural precursors via post-deposition, indicating terrestrial input and transformation from the surrounding

environment to sediments (e.g. Ishiwatari et al., 1980; Wakeham et al., 1980; Venkatesan, 1988a; Jiang et al., 2000). It can also be produced by combustion (only trace or small amounts) (Jiang et al., 2000). It is also a palaeoenvironmental marker for syn-and post-depositional anoxia if the concentration is greater than 0.010 ppm (Silliman et al., 1998; Jiang et al., 2000).

(3) High molecular weight PAHs like benzofluoranthenes, indeno[1,2,3,cd]pyrene and benzo[ghi]perylene: They have a pyrolytic origin associated with soot particles delivered by long-range atmospheric transport, or by major contribution from anthropogenic or naturally occurring combustion (Dachs et al., 1997; Gabos et al., 2001).

The pyrogenic PAHs can be distinguished from those from other sources by:

(1) the predominance of higher molecular weight PAHs (three condensed rings or more) over the low molecular weight PAHs;

(2) the predominance of the unsubstituted parent PAHs over their corresponding alkylated homologues;

(3) a decrease in relative abundances with increasing levels of alkylation (Prahl and Carpenter, 1983; Wang et al., 1999; Gabos et al., 2001; Wilcke, 2007; Vergnoux et al., 2011).

The pyrogenic PAHs have been found recently and historically in sediments since the Middle Jurassic, however data on their occurrence in ancient sediments are far less than those in young sediments (e.g. Killops and Massoud, 1992; Jiang et al., 2000; Yunker and Macdonald, 2003; Conedera et al., 2009; O'Dwyer and Taylor, 2009; Vergnoux et al., 2011).

In this thesis 18 PAHs (Figure 5.3, Page 242) from 2 rings to 6 rings were analysed

including naphthalene, acenaphthylene, acenaphthene, fluorene, phenanthrene, retene, anthracene, fluoranthene, pyrene, benz[a]anthracene, chrysene, benzo[b]fluoranthene, benzo[k]fluoranthene, perylene, benzo[a]pyrene, indeno[1,2,3,cd]pyrene and benzo[ghi]perylene. The aim was to use these compounds to trace vegetation fires and, if possible, correlate to drought years or to anthropogenic combustion during land clearance campaign in the Macquarie Marshes.

5.1.5.3 Organochlorine pesticides (OCPs)

In addition to direct loss of wetland area, wetlands can be functionally lost due to contamination of the water supplies from agricultural pesticides and herbicides due to surface runoff from irrigated fields (Lemly et al., 2000). This leads to investigating the organochlorine pesticides (OCPs) − chlorinated hydrocarbons (Figure 5.4, Page 247) used extensively from the 1940s through the 1960s in agriculture and pest control. These compounds were introduced to Australia in the mid-1950s, widely used during the mid-1970s and phased out by 1990 (Connell et al., 2007). When large amounts were extensively used, the transport of OCPs from contaminated areas by water courses and atmosphere could also affect remote areas and be detected in sediments/soils/plants (e.g. Leonard et al., 1999; Haynes et al., 2000; Fu et al., 2001; Meijer et al., 2002).

The Macquarie Marshes are on the margin of 175,000 ha of cotton farming areas in northwestern New South Wales (Leonard et al., 1999). The release and transport of OCPs from surrounding cotton farming areas could have an impact on the wetlands and its ecosystem. In this thesis, compounds analysed include HCB (hexachlorobenzene), heptachlor, heptachlor epoxide, aldrin, γ-BHC (Lindane, γ-hexachlorocyclohexane), α-BHC, β-BHC, δ-BHC, trans-chlordane, cis-chlordane, dieldrin, pp-DDE

(dichlorodiphenyldichloroethylene), pp-DDD (dichlorodiphenyldichloroethane), pp-DDT (dichlorodiphenyltrichloroethane), endrin, endrin aldehyde, endrin ketone, α-endosulfan, β-endosulfan, endosulfan sulfate and methoxychlor (Figure 5.4), particularly focusing on the following compounds:

(1) Endosulfan, a mixture of α- and β-isomers, is an organochlorine pesticide registered for use on a wide range of crops to control chewing and sucking insects (e.g. Lee et al., 1997; Leonard et al., 1999). The most important use of endosulfan in Australia is to control *Helicoverpa* species, especially in cotton cropping (Leonard et al., 1999). Studies found that endosulfan runoff from cotton fields especially during storm events had an impact on freshwater fish, including immediate death or gene regeneration (Leonard et al., 1999).

(2) DDT, DDE and DDD. DDT was used very extensively in cotton-growing areas of Australia such as the Namoi and Gwydir valleys until being banned in 1982 (Leonard et al., 1999). The main residue observed after several years in these soils is DDE, although at the more heavily contaminated cattle-dip sites DDT itself is the major residue and DDD is also found (Leonard et al., 1999). The conversion of DDT to DDD is favoured by anaerobic conditions such as those encountered with soils that are periodically or permanently flooded (Shivaramaiah et al., 2002).

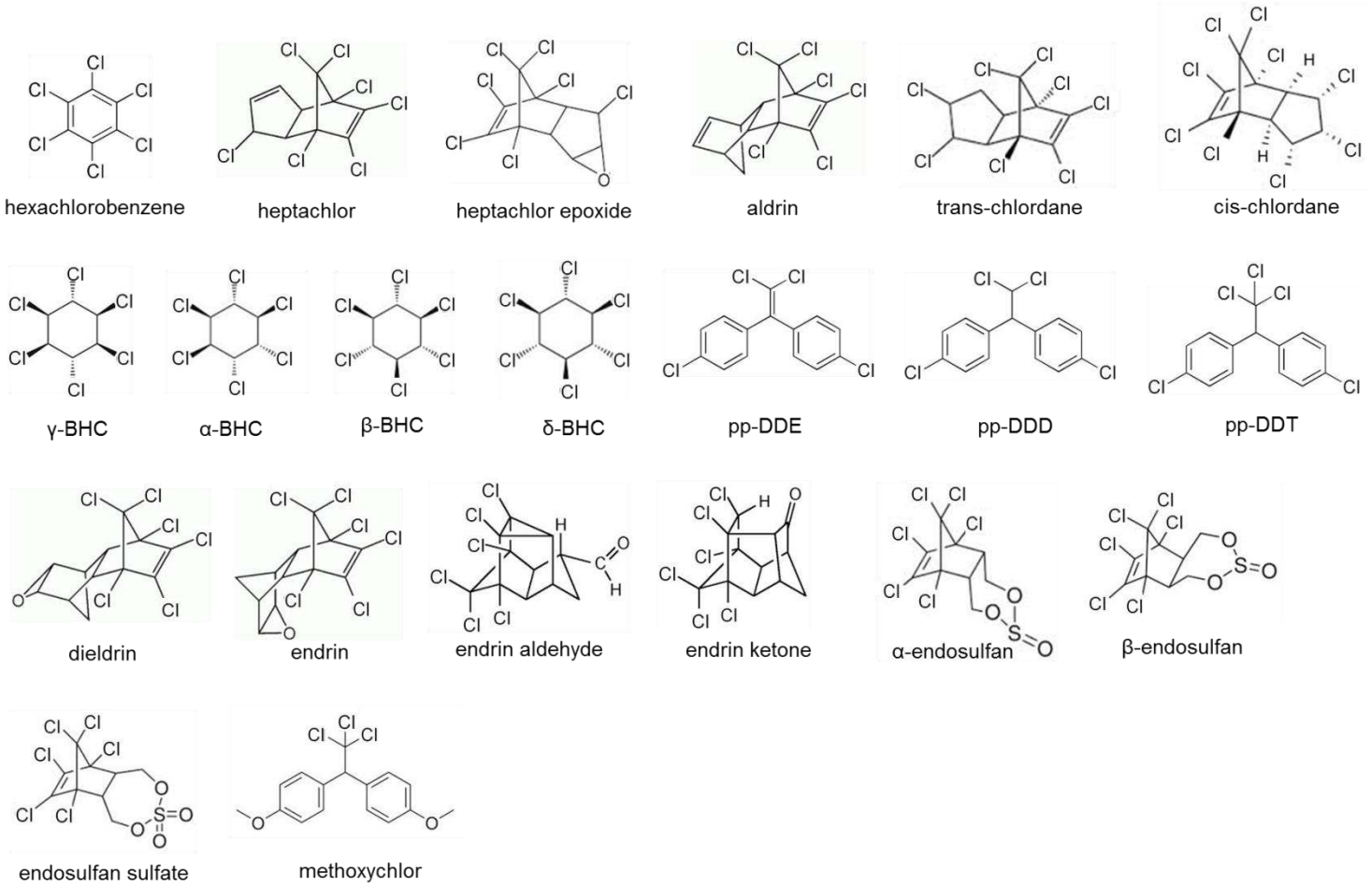

Figure 5.4. Structures of 21 organochlorine pesticides (OCPs) (source from Wikipedia).

5.2 Methodology

5.2.1 Sample preparation

All glassware used for the sample preparation was soaked in detergent overnight, rinsed with MilliQ water (18.2 MΩ cm^{-1} resistivity), heated in a muffle furnace (450 ºC, 24 h) and wrapped with aluminium foil. Prior to use, the glassware was rinsed with solvent (hexane or dichloromethane).

In this study, bulk sediments were used for organic geochemistry analysis, without sieving, as Fisher et al. (2003) found that lipid distributions in both fine and coarse sediment fractions were very similar in lacustrine sediments. Plant debris was handpicked and removed from these sediments to avoid contamination. Sediments were freeze-dried, ground to a fine powder and homogenised before extraction.

The target compounds include non-polar (*n*-alkanes) and polar (PAHs, *n*-alkanols, sterols and *n*-alkanoic acids), therefore a mixed solvent with dichloromethane:methanol (97:3 v:v) was used for extraction. About 10-20 g of dried and ground sample was extracted by Soxhlet apparatus with 200 mL mixed solvents for 24 hours. Copper chips were added to remove elemental sulfur from the extracts. The extracts were then concentrated to 1 mL by rotary evaporation at 40 °C and the solvent exchanged to hexane.

The chromatography columns used for separating the organic compounds were micro-columns (0.8 cm ID × 12 cm length) which are less solvent-consuming and more efficient in the separation performance (Xu and Sun, 2006). The column packing materials were silica gel (Sigma-Aldrich, 200-425 mesh) and alumina which have -OH functional groups on their surface to adsorb the compounds. All the compounds targeted can be obtained by the silica-alumina column while some compounds like aldehydes are

destroyed by alumina (Eglinton and Hamilton, 1967). Prior to packing, the column packing materials were combusted at 300 °C in a muffle furnace overnight and kept in desiccators prior to use. Silica gel was deactivated by adding 3 % (w/w) of distilled water. The dry silica gel and alumina (3cm: 3cm in length) were loaded in sequence into the micro-column. About 1 cm of anhydrous Na_2SO_4 was added on top of the alumina to remove moisture from the extracts (if any). The packed column was then rinsed and moisturised using hexane for pre-conditioning. The extracts were applied to the column before the column was completely dried.

In order to separate analytes the interference by their different chemical polarity, proper solvents should be chosen to elute the targeted compounds (Patnaik 1997, Loconto 2001, Pollard et al. 2007) —the interfering compound should be left adsorbed onto the column, while the targeted compounds are all eluted by the solvent. Depending on the compound of interest and its polarity, solvents/mixed solvents of different polarity are used. Alkanes, PAHs and OCPs are usually eluted by a solvent with less polarity such as hexane, toluene:hexane (5.6:9.4 v:v) or hexane:dichloromethane (1:1 v:v); while the more polar compounds including alcohols, sterols and fatty acids are eluted with more polar solvents such as dichloromethane:methanol (97:3 or 2:1 v:v) or acetic acid (e.g. Gogou and Stephanou, 2004; Hu et al., 2006; Hu et al., 2009). In this study, solvent/mixed solvents were used to collect the compound groups in the following sequence:

(1) Fraction 1 - 10 mL hexane

(2) Fraction 2 - 10 mL hexane:dichloromethane (1:1 v:v)

(3) Fraction 3 - 10 mL dichloromethane

(4) Fraction 4 - 10 mL dichloromethane:methanol (1:1 v:v)

(5) Fraction 5 - 10 mL methanol

The *n*-alkanes, PAHs and OCPs were eluted in fraction 1, the *n*-alkanols and sterols were eluted in fraction 3, and the *n*-alkanoic acids were eluted in fraction 4.

The fractions collected were concentrated to 0.5 mL under gentle N_2 flow and known amounts of internal standard were added. For the polar fractions (*n*-alkanols, sterols and *n*-alkanoic acids), an aliquot of 25 μL of sample was taken, dried and derivatised by bis-trimethyl silyl trifluoroacetamide (BSTFA) in a 50 °C oven for one hour before analysis. The reason for doing this is to replace the hydroxyl group with the less exchangeable trimethysilyl (TMS) group for GC analysis (Knapp, 1979).

The sample preparation procedure for sediments is summarised in the flowchart shown in Figure 5.5.

The plant samples were also freeze-dried and cut into small pieces with clean stainless scissors. The preparation procedures were similar to those used for sediments excepting that an extra step was added to the polar fractions. This is to remove the wax from the plants which would shorten the life of the capillary columns when introduced to the GC/GC-MS instrument. The micro-column was loaded with celite (diatomaceous earth composed of 80-90 % SiO_2, 2-4 % Al_2O_3 and 0.5-2 % Fe_2O_3) and pre-conditioned with 5 mL dichloromethane. The concentrated extracts containing *n*-alkanols, sterols and *n*-alkanoic acids were loaded into the micro-column with celite and eluted with dichloromethane/methanol.

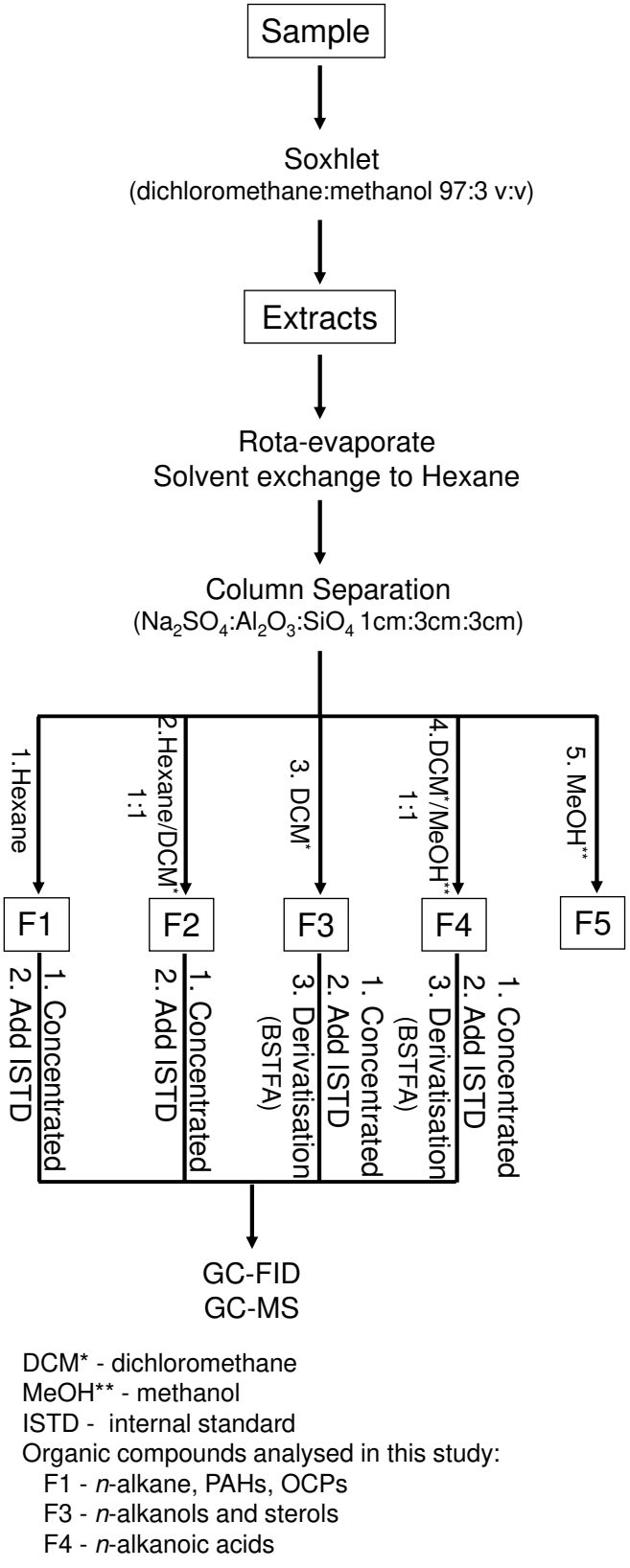

Figure 5.5. Flowchart of sample preparation procedures for organic geochemical analysis.

5.2.2 Instrumentation

An Agilent 6890N gas chromatography with flame ionisation detector (GC-FID) in the geochemistry laboratory of the University of Wollongong was used mainly for the quantification of the organic compounds. The GC column was a DB-5ms fused-silica capillary column (60 m × 0.25 mm × 0.25 μm film thickness). Injections (1 μL) were conducted mostly in the splitless mode except when running hexane to clean the column. The temperature ramping procedures were slightly different between each compound group (Table 5.4) as reported by other researchers (e.g. Patnaik, 1997; Gogou and Stephanou, 2004; Hu et al., 2006; Volkman et al., 2007; Hu et al., 2009). The carrier gas was helium (1.6 mL min^{-1}).

Table 5.4
GC-FID Instrumental analytical parameters.

Instrumental Setup \ Compound Groups		hexane	*n*-alkanes	PAHs	OCPs	*n*-alkanols, sterols & *n*-alkanoic acids
Column	length (m)	60				
	diameter (mm)	0.25				
	film thickness (μm)	0.25				
Carrier Gas	gas	helium				
	mode	constant flow				
Inlet	mode	split	splitless			
	initial Temp. (°C)	280				
	initial pressure (kPa)	1				
	split ratio	50	-			
	injection volumn (μL)	0.2	1			
	purge pressure (kPa)	-	50			
	purge time (min)	-	1.3			
	pre-wash solvent A	dicholomethane				
	number of pre-washes, Solvent A	5				
	pre-wash solvent B	hexane				
	number of pre-washes, Solvent B	5				
	wash solvent A	dicholomethane				
	number of washes, Solvent A	5				
	wash solvent B	hexane				
	number of washes, Solvent B	5				
GC Oven	initial Temp. (°C)	40	70	40	50	70
	time at initial Temp. (min)	2	2	4	1	2
	ramping Temp[1] (°C)	320	290	270	100	290
	hold Time[1] (mins)	40	30	60	0	30
	ramping rate[1] (°C/min)	10	3	10	25	3
	ramping Temp[2] (°C)				300	
	hold time[2] (min)				5	
	ramping rate[2] (°C/min)				5	
GC Pressure	initial pressure (kPa)	1.6				
FID	operation Temp (°C)	340				
	H_2 flow rate (mL/min)	40				
	air flow rate (mL/min)	300				

The chromatograms of some standards run by GC-FID are shown in Figures 5.6 to 5.10.

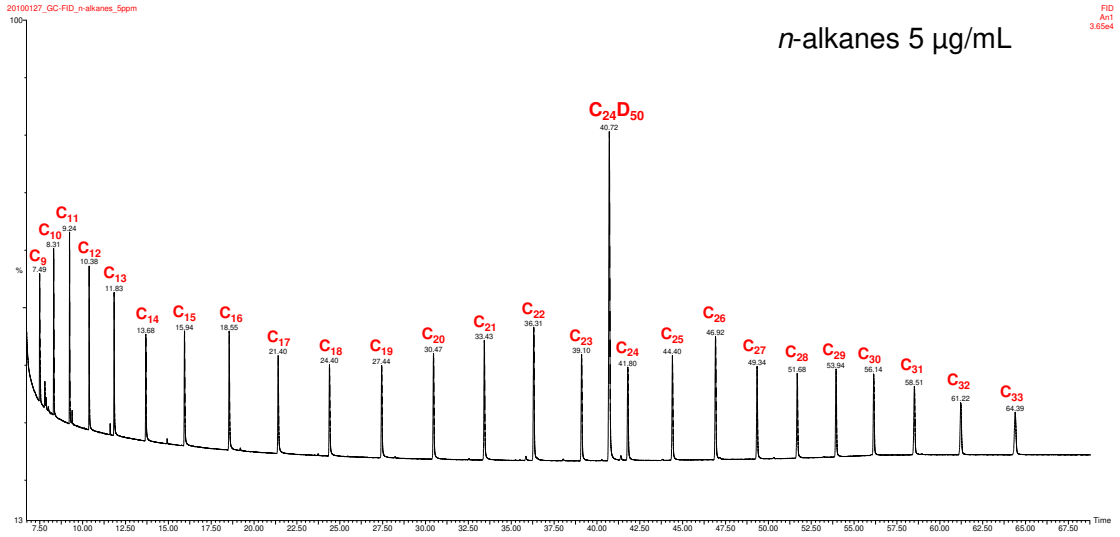

C_x: n-alkanes with carbon number $C_{24}D_{50}$: Tertracosane- d_{50}

Figure 5.6. Chromatogram of *n*-alkane compound group.

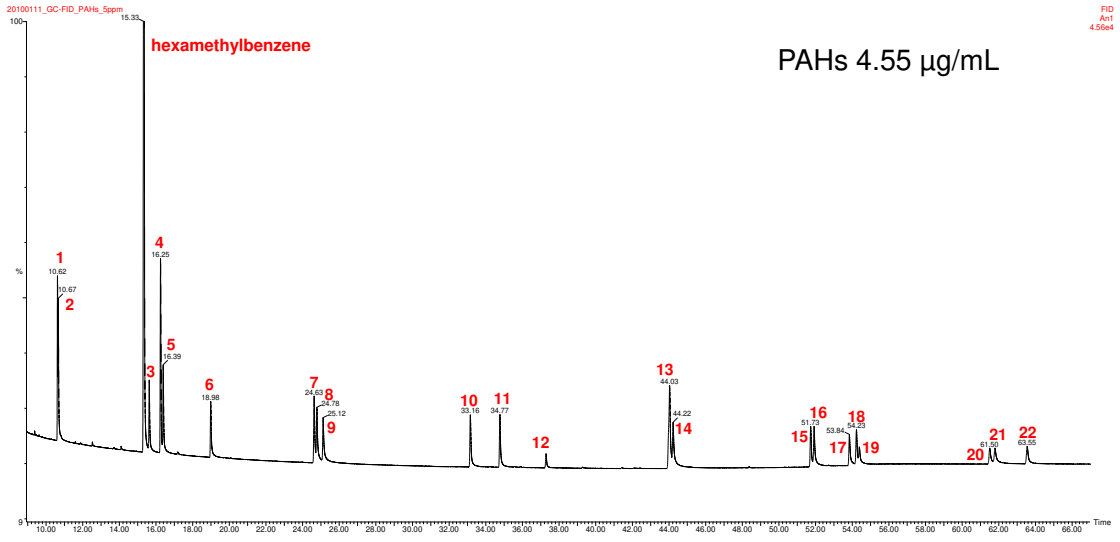

1. naphthalene-d_8 2. naphthalene 3. acenaphthylene 4. acenaphthene-d_{10} 5. acenaphthene
6. fluorene 7. phenanthrene-d_{10} 8. phenanthrene 9. anthracene 10. retene 11. fluoranthene
12. pyrene 13. chrysene-d_{12} 14. chrysene 15. benzo[b]fluoranthene 16. benzo[k]fluoranthene
17. benzo[a]pyrene 18. perylene-d_{12} 19. indeno[1,2,3-cd]pyrene 20. dibenzo[a,h]anthracene
21. benzo[ghi]perylene 22. perylene

Figure 5.7. Chromatogram of PAH compound group.

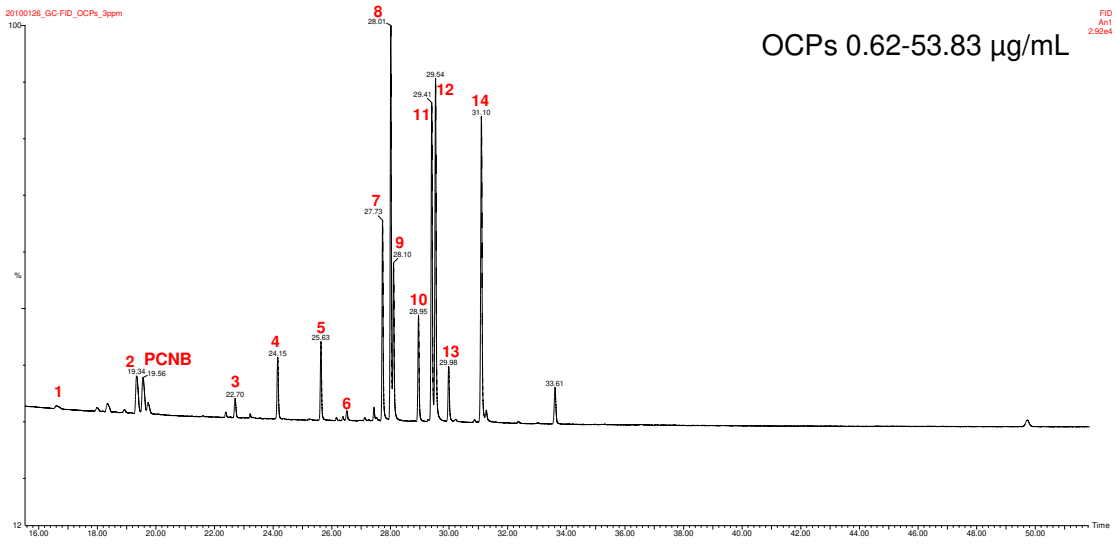

1. 2,4,5,6-tetrachloro-m-xylene 2. aldrin 3. α-BHC 4. β-BHC 5. 4,4'-DDE 6. γ-BHC 7. dieldrin
8. endrin 9. heptachlor epoxide 10. heptachlor 11. 2,4'-DDD 12. 2,4'-DDT 13. 4,4'-DDD 14. 4,4'-DDT

Figure 5.8. Chromatogram of OCP compound group.

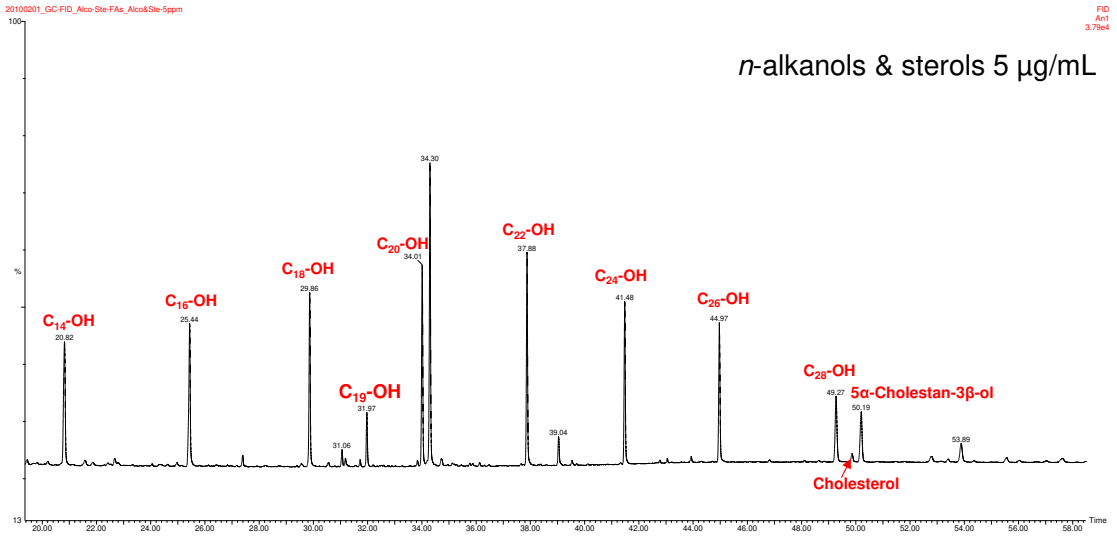

C_x: n-alkanols with carbon number

Figure 5.9. Chromatogram of *n*-alcohol and sterol compound groups.

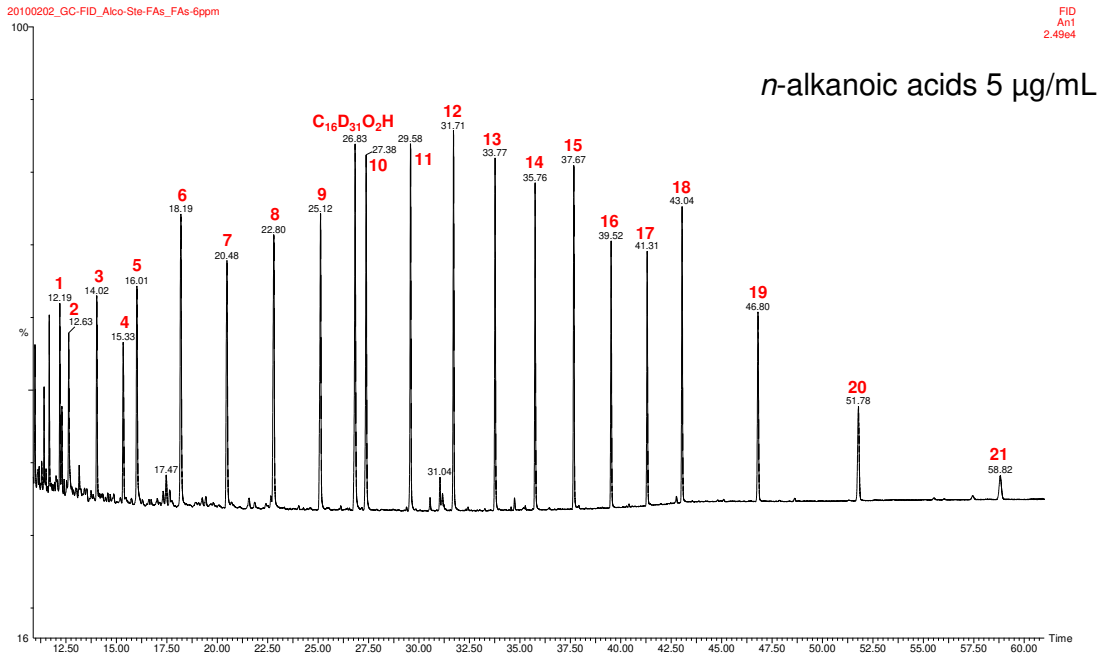

C_x: n-alkanoic acids with carbon number $C_{16}D_{31}O_2H$: palmitic-d_{31} acid

1. C_9 2. C_{10} 3. C_{11} 4. C_{12} 5. C_{13} 6. C_{14} 7. C_{15} 8. C_{16} 9. C_{17} 10. C_{18} 11. C_{19} 12. C_{20} 13. C_{21} 14. C_{22} 15. C_{23} 16. C_{24} 17. C_{25} 18. C_{26} 19. C_{27} 20. C_{28} 21. C_{30}

Figure 5.10. Chromatogram of *n*-alkanoic acid compound group.

The identification of some organic compounds with no reference standards was performed by gas chromatography mass spectrometry (GC-MS) in the organic geochemistry laboratory of The Australian National University. Samples were injected using a splitless mode on the same column used for GC-FID analysis, programmed at the same conditions as the GC-FID analysis, with ion source temperature at 300 °C, interface temperature at 310 °C, electron energy 70 eV, scanning from 40 to 600 a.m.u., 1.5 scan/s (Brocks and Schaeffer, 2008). Compounds were identified by interpretation of their characteristic mass spectral fragmentation patterns, gas chromatographic relative retention times, and by comparison with the software library and literature (e.g. Volkman et al., 2007; Castañeda et al., 2011; Andersson and Meyers, 2012). The retention times of these compounds in GC-FID were determined based on comparing their retention times to their two neighbouring compounds from the GC-MS.

Quantifications of the target compounds were made using the internal standard calibration procedure to correct for the variation of instrumental responses. The internal standards, different from the analytes, for each compound group were tetracosane-d_{50} for *n*-alkanes, hexamethylbenzene for PAHs, pentachloronitrobenzene for OCPs, 1-nonadecanol for *n*-alkanols and sterols, and palmitic-d_{31} acid for *n*-alkanoic acids. At least four mixed standards with sequential known concentrations from each compound group were run to build up a calibration curve. The response of the analyte in the calibration curve was the ratio of the signal of analyte and the internal standard. The response for the sample was compared with that of the standards within the linear range of the curve. Accordingly, the concentration of the analyte in the sample was calculated. In this study, peak identification and integrations were made under Ionvantage (Version 1.1) software

"Data Browser" window. Peak areas of the compounds were recorded and fitted into an excel spreadsheet established for building up the calibration curve from data of the standard series, calculating the parameters of the curve and assessing the concentration of the sample.

For the compounds without standards (e.g. α-phellandrene), semi-quantification was achieved by comparing their GC peak areas to that of the internal standard with known concentration and calculated from the ratio.

The compound-specific $^{13}C/^{12}C$ isotopes of *n*-alkanes were by gas chromatography-isotope ratio mass spectrometry (GC-IRMS) in the State Key Laboratory of Organic Geochemistry, Guangzhou Institute of Geochemistry, Chinese Academy of Science. A VG Instruments Isoprime mass spectrometer was used. The *n*-alkanes were separated on an HP-5 trace analysis fused silica capillary column (30 m × 0.32 mm × 0.25 μm film thickness). Helium was used as carrier gas. The GC oven temperature was programmed starting at 80 ºC for 2 min, from 80 ºC to 120 ºC at 15 ºC /min, from 120 ºC to 290 ºC at 4 ºC /min, then held isothermally at 290 ºC for 25 min. All carbon isotope ratios are expressed as per mil (‰) relative to the Pee Dee Belemnite (V-PDB) standard. Reported carbon-isotope values ($\delta^{13}C$) represent the averaged value of triplicate analysis. Standard deviations were generally $\leq \pm 0.5$ ‰.

5.2.3 Quality Assurance and Quality Control

To achieve precise and accurate results, good laboratory Quality Assurance and Quality Control (QA/QC) protocols are required. In this thesis, the QA/QC protocols include the following:

- All glassware was properly cleaned and stored as described in Section 5.2.1;

- Blank samples that contained no targeted analytes, surrogates, or matrix spikes were prepared in parallel in the same manner as sediments/plants to check for contamination during sample preparation. No target components or other substances with similar retention times were detected in the blanks;
- Matrix samples spiked with known amounts of standards were processed in the same manner as the sediment samples and analysed by GC-FID. The recoveries for the standards were all greater than 90 %, indicating that the sample preparation was efficient and that there was no contamination that would affect the analytical results;
- Three random sediment samples were prepared and analysed in duplicate in order to detect variations during sample preparation and analysis. Relative standard deviation was below 10 %;
- Samples were analysed by GC within 1 to 2 weeks of extraction. Prior to instrument analysis, samples were dark sealed and stored at 4 ºC to avoid evaporation and degradation;
- Analytical system performance was checked by injecting three hexane (1 μL) aliquots for cleaning the column and by running an analytical standard every 10 samples during each analysis sequence. Recalibration was conducted if the internal standard corrected response for an analyte varied by more than 15 % from the calibration standard of the analysis sequence. Duplicate analyses of samples by the GC-FID also indicated good analytical agreement; and,
- Eight surface sediment samples from eight sampling sites were freeze-dried and sent to the National Measurement Institute (NMI Australia) for OCPs analysis. Sample preparation and instrumental analysis were performed at NMI based on

USEPA 8081 method. Briefly, each sample was mixed with anhydrous sodium sulfate and extracted using hexane:acetone. The extract was cleaned up with alumina and analysed by gas chromatography with electron capture detector (GC-ECD) (dual column) for OC pesticides. Confirmation was made by gas chromatography - electronic ionization mode with selected-ion monitoring (GCMS-EI-SIM) and gas chromatography - negative chemical ionization with selected-ion monitoring (GCMS-NCI-SIM). The target compounds were HCB, heptachlor, heptachlor epoxide, aldrin, γ-BHC (Lindane), α-BHC, β-BHC, δ-BHC, trans-chlordane, cis-chlordane, dieldrin, pp-DDE, pp-DDD, pp-DDT, endrin, endrin aldehyde, endrin ketone, α-endosulfan, β-endosulfan, endosulfan sulfate and methoxychlor. The surrogates were TCMX, DF-DDE and DB-DDE. The detection limit for this method was 0.01 μg/g. None of the target compounds was detected (less than 0.01 μg/g) in the surface sediments.

5.3 Analysis of modern plants

In order to establish representative biomarkers from the plants and assist in understanding their contribution to the OM in the sediments, modern plant samples adapted to aquatic (emergent and submerged) and terrestrial habitats were collected and analysed. The plant samples analysed were *Phragmites australis* from the 2LOLA site (northern marshes) and the CT site (southern marshes), *Eucalyptus* sp., *Typha* sp. and *Chara australis* from the MC site (northern marshes), *Ranunculus* sp. from the 2LOLA site (northern marshes). *Eucalyptus* sp. and *Ranunculus* sp. represent the terrestrial plants; *Typha* sp. and *Phragmites australis* represent the emergent plants; *Chara australis* represents the submerged/floating plants/algae.

5.3.1 *n*-alkanes

The concentrations of total *n*-alkanes and some ratios are presented in Table 5.5. The total *n*-alkane (nC$_9$-nC$_{33}$) concentrations of the plant samples range from 10.6 to 432 µg/g (dry weight), and from 0.23 to 9.11 µg/g (TOC). The lowest values were observed in *Ranunculus* sp. (10.6 µg/g dry weight, 0.23 µg/g TOC) and then *Chara australis* (20.5 µg/g dry weight, 0.49 µg/g TOC); those in terrestrial plants and emergent plants were 20-40 times higher, with the highest values observed in *Typha* sp. (432 µg/g dry weight, 9.11 µg/g TOC). The concentration of the *n*-alkanes of the same species varied substantially between the sampling locations. For example, the concentrations of *n*-alkanes were 121 µg/g dry weight and 2.71 µg/g TOC in *Phragmites australis* from the 2LOLA site; and were 202 µg/g dry weight and 4.71 µg/g TOC in the same species from the CT site.

Table 5.5
TOC, *n*-alkane concentrations and proxy values of modern plants from the MM.

Type of sample	*Eucalyptus* sp. (Monkeygar Creek)	*Ranunculus* sp. (buttercup) (Loudens Lagoon)	*Typha* sp. (cumbungi) (Monkeygar Creek)	*Phragmites australis* (reeds) (Loudens Lagoon)	*Phragmites australis* (reeds) (Monkeygar Creek)	*Chara australis* (charophyte) (Monkeygar Creek)
TOC (%)	53.8	44.0	41.9	47.4	43.0	46.1
Σ *n*-alkanes ($C_{9\text{-}33}$ µg/g DW)	305	10.6	432	121.2	202.2	20.5
Σ *n*-alkanes ($C_{9\text{-}33}$ µg/g TOC)	5.67	0.23	9.11	2.71	4.71	0.49
CPI	15.9	12.9	10.2	6.94	5.30	1.75
OEP	7.56	8.51	9.80	5.15	3.77	1.68
ACL	27.5	29.0	26.9	28.4	28.6	27.9
P_{aq}	0.29	0.05	0.72	0.22	0.11	0.45
P_{wax}	0.84	0.96	0.45	0.84	0.92	0.65
C_{17}/C_{31}	0.04	0.00	0.02	0.00	0.00	4.80
C_{27}/C_{31}	31.8	0.64	10.6	3.45	2.77	1.42

Figure 5.11 shows the abundance of the *n*-alkanes (nC$_9$-nC$_{33}$) in plant samples. Higher plants consist mostly of high molecular weight *n*-alkanes (C$_{21}$ to C$_{33}$) with strong odd-to-even preference and generally the most dominant *n*-alkane is C$_{29}$ (except C$_{25}$ *n*-alkane in *Typha* sp. and C$_{27}$ *n*-alkane in *Eucalyptus* sp.), similar to the study by Ficken et al. (2000) and Wiesenberg et al. (2004) that emergent aquatic plants and terrestrial vegetation have similar *n*-alkane distributions dominated by the long-chain homologues. This finding is particularly significant in above-ground biomass (stems and leaves) rather than roots (Wiesenberg et al., 2004). The dominance of C$_{29}$ *n*-alkanes is also characteristic of C$_3$ plants, in agreement with the result of Wiesenberg et al. (2004). *Chara australis* contains *n*-alkanes of wider range (nC$_{12}$-nC$_{31}$) with less significant odd-to-even preference and maximised at C$_{17}$ *n*-alkanes, similar to an early study by Galpi et al. (1970).

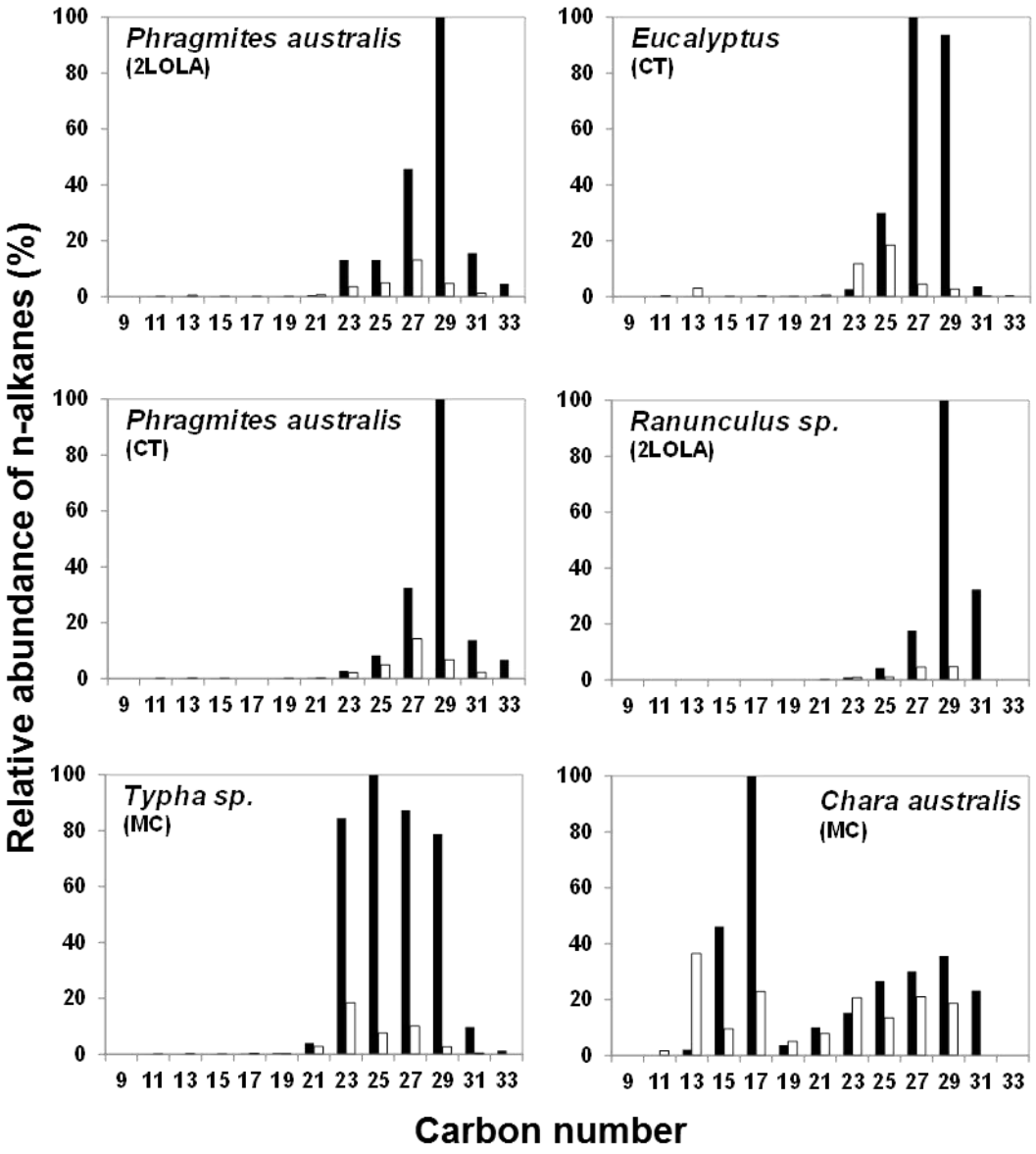

Figure 5.11. The distribution of *n*-alkanes (C_9-C_{33}) in modern plants from the MM. (The histograms portray relative abundance, with the mode set to 100. The white bar is even carbon numbers; the black bar is odd carbon numbers.)

As also shown in Table 5.5 (Page 262) and Figure 5.12 (Page 266), the CPI values are generally greater than 5.0 in higher plants and lowest (1.6) in *Chara australis*; the OEP values are greater than 5.0 in higher plants (except one of the *Phragmites australis* had OEP value of 3.8) and lowest (1.8) in *Chara australis*. The ACL values vary only slightly from 26.8 in *Typha* sp. to 29.0 in *Ranunculus* sp. with an average of 27.9 for the algae and

higher plants. The *n*-alkane composition and OEP varies greatly between higher plants and algae while the ACL values are less distinctive. The P_{aq} values in these modern plants were compared to those found by Ficken et al. (2000): *Ranunculus* sp. (0.05) was less than 0.10 as is commonly found in terrestrial plants while *Eucalyptus* sp. (0.29) was exceptionally higher; *Phragmites australis* (0.11 and 0.22) is within the range (0.10 - 0.40) for emergent macrophytes while *Typha* sp. (0.72) is higher than the range; *Chara australis* (0.45) was a little higher than the range (0.40 - 1.00) for submerged/floating aquatic macrophytes. The P_{wax} values range from 0.45 in *Typha* sp. to 0.96 in *Ranunculus* sp. and are generally high among higher plants (0.84 in *Eucalyptus* sp., 0.84 - 0.92 in *Phragmites australis*, 0.96 in *Ranunculus* sp.) and low in algae (0.65 in *Chara australis*). The C_{27}/C_{31} values are extremely high in *Eucalyptus* sp. (31.8) and *Typha* sp. (10.6); decreased to 2.77 - 3.45 in *Phragmites australis*, 1.42 in *Chara australis*, and 0.64 in *Ranunculus* sp.. Compared to the P_{aq}, P_{wax} and C_{27}/C_{31} values, the C_{17}/C_{31} values appear to be more indicative of higher plants and algae: C_{17}/C_{31} values were close to 0 in higher plants and 4.8 in *Chara australis*. Generally, except for the ACL value, the other *n*-alkane proxies are distinctive among various plant species.

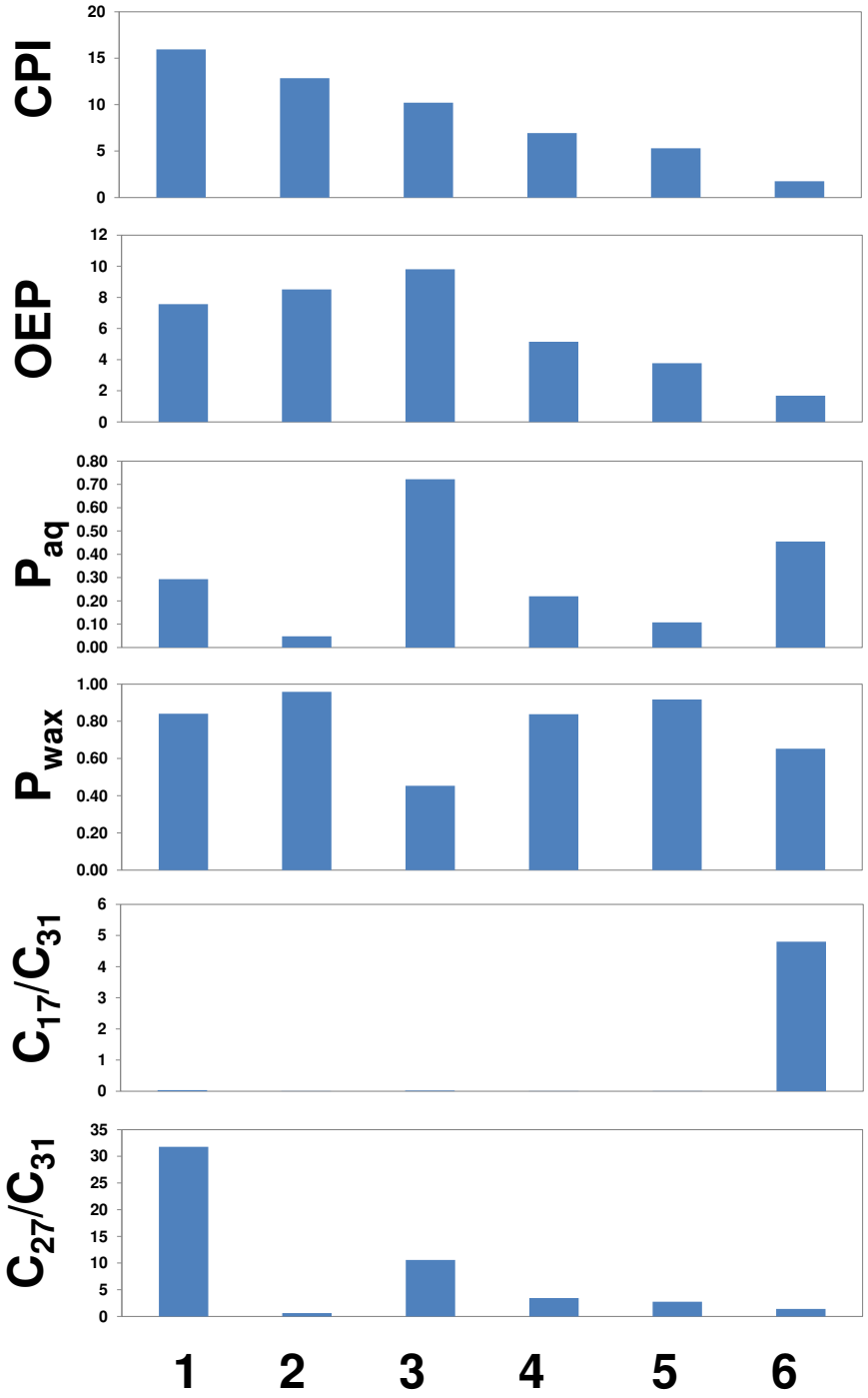

Figure 5.12. The *n*-alkane proxies for modern plants from the MM are distinctive between higher plants and algae. (1. *Eucalyptus* sp., 2. *Ranunculus* sp., 3. *Typha* sp., 4,5. *Phragmites australis*, 6. *Chara australis*)

5.3.2 *n*-alkanols

The concentrations of total *n*-alkanols and some proxy ratios are presented in Table 5.6. The total *n*-alkanol (nC$_{14}$-nC$_{32}$) concentrations of the plant samples range from 0.05 to 53.6 µg/g (dry weight), and from 0.001 to 1.13 µg/g (TOC). The highest value is in *Typha* sp. (53.6 µg/g dry weight, 1.13 µg/g TOC), followed by *Chara australis* (9.37 µg/g dry weight, 0.22 µg/g TOC); those in higher plants are generally 30- to 100- fold lower, with the lowest values observed in *Ranunculus* sp. (0.05 µg/g dry weight, 0.001 µg/g TOC).

Figure 5.13 (Page 269) shows the composition of *n*-alkanols (nC$_{14}$-nC$_{32}$) in plants. All the samples show strong even-to-odd number predominance (cf. Eglinton and Hamilton, 1967). The most abundant *n*-alkanol is C$_{32}$ in *Phragmites australis* and *Eucalyptus* sp.; C$_{26}$ in *Ranunculus* sp. and C$_{14}$ in *Typha* sp. and *Chara australis*. These findings correspond to those reported previously (summarised in Section 5.1.2 and reference therein) in algae, photosynthetic bacteria, submerged/floating macrophytes, vascular land plants and emergent macrophytes. In particular, the composition of *n*-alkanols in *Phragmites australis* and *Typha* sp. accord with data from the same species reported by Cranwell (1984).

As also shown in Table 5.6 and Figure 5.14 (Page 270), the CPI$_{OH}$ values were high in *Typha* sp. (20.3) and *Ranunculus* sp. (30.1), and low in *Chara australis* (1.9). The ratios of short-chain/long-chain *n*-alkanols range from 0.02 to 4.41. Higher plants (i.e. *Eucalyptus* sp., *Typha* sp. and *Phragmites australis*) show a predominance of long-chain *n*-alkanols whereas algae (*Chara australis*) are the opposite.

Table 5.6
TOC, *n*-alkanol concentrations and proxy values of modern plants from the MM.

Type of sample	*Eucalyptus* sp. (Monkeygar Creek)	*Ranunculus* sp. (buttercup) (Loudens Lagoon)	*Typha* sp. (cumbungi) (Monkeygar Creek)	*Phragmites australis* (reeds) (Monkeygar Creek)	*Chara australis* (charophyte) (Monkeygar Creek)
TOC (%)	53.8	44.0	41.9	43.0	46.1
Σ *n* - alkanols (C_{14-32} µg/g DW)	0.27	0.05	53.6	0.62	9.37
Σ *n* - alkanols (C_{14-32} µg/g TOC)	0.01	0.001	1.13	0.01	0.22
CPI_{OH}	-	30.14	20.27	-	1.94
$\Sigma C_{14-20}/\Sigma C_{21-30}$	0.02	0.31	1.24	0.03	4.41

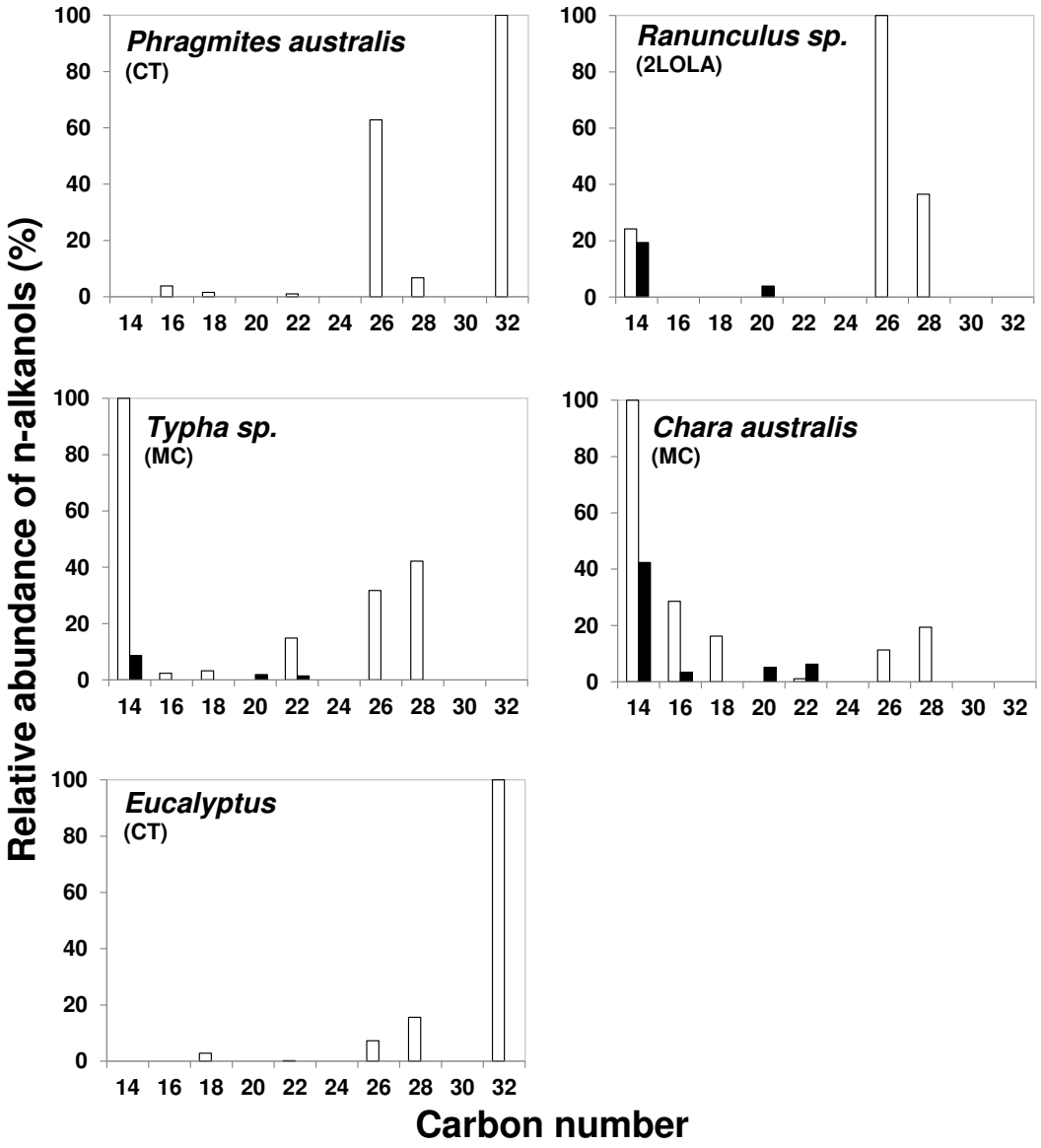

Figure 5.13. The distribution of *n*-alkanols (C_{14}-C_{32}) in modern plants from the MM. (The histograms portray relative abundance, with the mode set to 100. The white bar is even carbon numbers; the black bar is odd carbon numbers.)

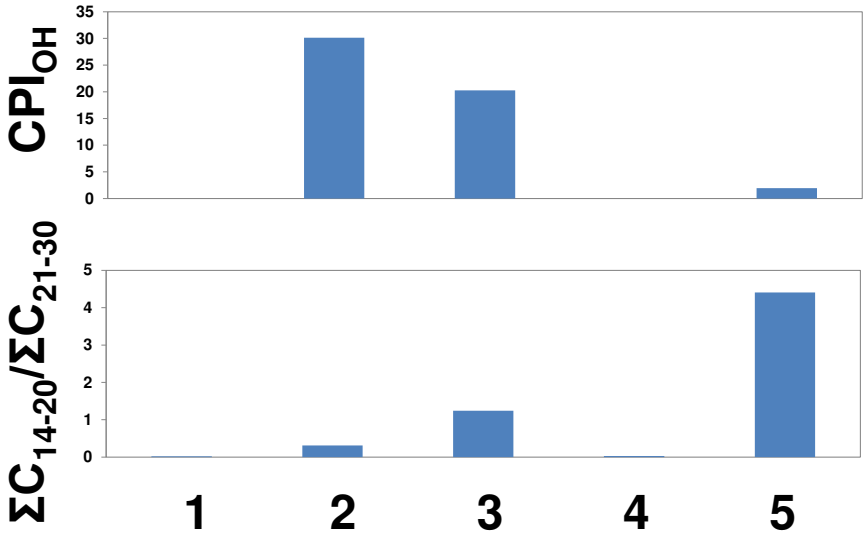

Figure 5.14. The *n*-alkanol proxies for modern plants from the MM are less distinctive between higher plants and algae. (1. *Eucalyptus* sp., 2. *Ranunculus* sp., 3. *Typha* sp., 4. *Phragmites australis*, 5. *Chara australis*)

5.3.3 *n*-alkanoic acids

The concentrations of total *n*-alkanoic acids and some ratios are presented in Figure 5.15 (Page 273). The total *n*-alkanoic acid (nC_9-nC_{30}) concentrations of the plants ranges from 0.64 to 287.4 µg/g (dry weight), and from 0.01 to 6.06 µg/g (TOC). As for the *n*-alkanols, the highest value is for *Typha* sp. (287.4 µg/g dry weight, 6.06 µg/g TOC), followed by *Chara australis* (184.9 µg/g dry weight, 4.41 µg/g TOC); the values in higher plants are generally 100- to 300- fold lower, with the lowest values in *Eucalyptus* sp. (0.64 µg/g dry weight, 0.01 µg/g TOC).

Figure 5.15 shows the composition of *n*-alkanoic acids (nC_9-nC_{30}) in modern plants. Similar to *n*-alkanols, all the samples show strong even-to-odd number predominance (cf. Eglinton and Hamilton, 1967). Odd number *n*-alkanoic acids are presented only in small amounts in some samples. The most abundant *n*-alkanoic acid is C_{16} in *Typha* sp.; C_{30} in *Phragmites australis* and C_{10} in the other plant samples. The composition of *n*-alkanoic acids in *Phragmites australis* and *Typha* sp. are similar to the early studies by Cranwell (1984) and Wiesenberg et al. (2004). However, the relative abundance of the high molecular-weight *n*-alkanols (C_{20}-C_{30}) found in higher plants in this study was slightly different from those found among leaf epicuticular waxes by Eglinton and Hamilton (1967), likely caused by species difference.

As also shown Table 5.7 and Figure 5.16 (Page 274), the ratios of short-chain/long-chain *n*-alkanoic acids range from 1.10 to 26.8. *Eucalyptus* sp. and *Ranunculus* sp. show a predominance of short-chain *n*-alkanoic acids whereas *Typha* sp., *Phragmites australis* and *Chara australis* contain *n*-alkanoic acids with a broader spectrum of chain lengths.

Table 5.7
TOC, *n*-alkanoic acid concentrations and proxy values of modern plants from the MM.

Type of sample	*Eucalyptus* sp. (Monkeygar Creek)	*Ranunculus* sp. (buttercup) (Loudens Lagoon)	*Typha* sp. (cumbungi) (Monkeygar Creek)	*Phragmites australis* (reeds) (Monkeygar Creek)	*Chara australis* (charophyte) (Monkeygar Creek)
TOC (%)	53.8	44.0	41.9	43.0	46.1
Σ *n* - alkanoic acids (C_{9-30} µg/g DW)	0.64	1.87	287.4	1.12	184.9
Σ *n* - alkanoic acids (C_{9-30} µg/g TOC)	0.01	0.04	6.06	0.03	4.41
$\Sigma C_{9-20}/\Sigma C_{21-30}$	11.9	26.8	1.10	1.10	2.97

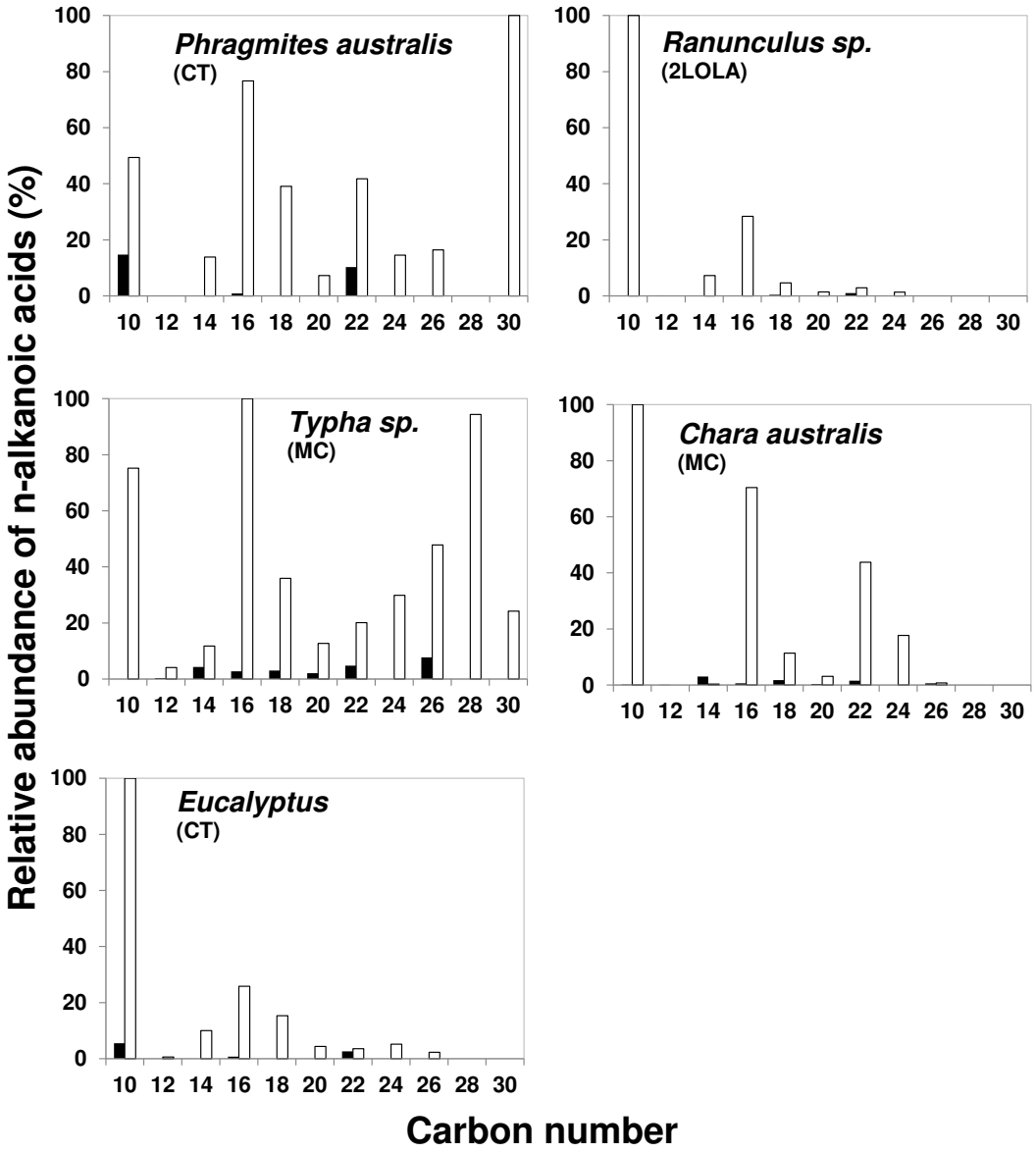

Figure 5.15. The distribution of *n*-alkanoic acids (C_9-C_{30}) in modern plants from the MM. (The histograms portray relative abundance, with the mode set to 100. The white bar is even carbon numbers; the black bar is odd carbon numbers.)

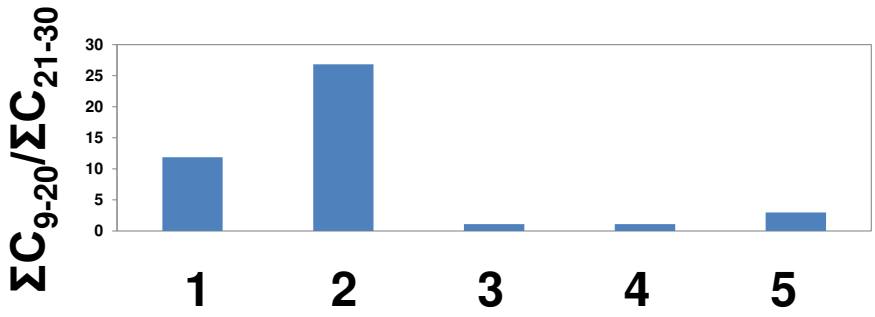

Figure 5.16. The *n*-alkanoic acid proxy of modern plants from the MM is less distinctive between higher plants and algae. (1. *Eucalyptus* sp., 2. *Ranunculus* sp., 3. *Typha* sp., 4. *Phragmites australis*, 5. *Chara australis*)

5.3.4 Sterols

As shown in Table 5.8 (Page 277), the total concentrations of sterols (C_{27} to C_{29}) in the modern plants studied here range from 0.65 μg g^{-1} (DW) and 0.01 μg g^{-1} TOC in *Eucalyptus* sp. to 80. 5 μg g^{-1} (DW) and 1.92 μg g^{-1} TOC in *Chara australis*. Among all samples, the concentrations of sterols decrease in the order C_{27}, C_{28} and then C_{29}. C_{29} sterols were only detected in *Ranunculus* sp., *Phragmites australis* and *Chara australis*.

The most abundant sterol in the plant samples is cholesta-5,22E-dien-3β-ol with a wide range of concentrations (from 0.65 μg g^{-1} DW in *Eucalyptus* sp. to 77.1 μg g^{-1} DW in *Chara australis*). Cholesta-5,22E-dien-3β-ol was only detected in *Eucalyptus* sp.. For *Ranunculus* sp., campesterol was also found in abundance (2.08 μg g^{-1} DW). For *Typha* sp., cholesterol is the second most abundant sterol (7.77 μg g^{-1} DW), followed by 5α-cholestan-3β-ol (2.69 μg g^{-1} DW) and 24-methylcholesta-5,6,22E-trien-3β-ol (1.32 μg g^{-1} DW). *Phragmites australis* collected from different sites showed very different compositions. In a sample from the LOLA site (northern MM) only cholesta-5,22E-dien-3β-ol (8.61 μg g^{-1} DW) was detected; whereas the sample from the MC site (southern MM) had a lower concentration of cholesta-5,22E-dien-3β-ol (1.28 μg g^{-1} DW) but contained 24-methylcholesta-5,6,22E-trien-3β-ol (0.40 μg g^{-1} DW) and stigmasterol (0.12 μg g^{-1} DW). The sterol composition of *Chara australis* was different from that of the higher plants, with the second most abundant compound 24-methylcholesta-5,6,22E-trien-3β-ol (2.59 μg g^{-1} DW) only 3 % of the cholesta-5,22E-dien-3β-ol (77.12 μg g^{-1} DW), followed by campesterol (0.45 μg g^{-1} DW), 5α-cholestan-3β-ol (0.15 μg g^{-1} DW) and 24-methyl-5α-cholesta-22E-en-3β-ol (0.10 μg g^{-1} DW). The major diversity of sterols in *Chara australis* found in this study contrasts with an earlier study of Chlorophyceae (*Chlorella minutissima*) by Volkman et al. (2003) in which campesterol, 24-methylcholesta-5,24

(28)-dien-3β-ol, 24-methylcholesta-7,22-dien-3β-ol, sitosterol and stigmasterol were found to be the most common sterols. However, the Chlorophyceae are unicellular green algae, not closely related to the plant-like macroalgae Charophyceae.

5.3.5 Summary

The concentrations and compositions of *n*-alkanes, *n*-alkanols, *n*-alkanoic acids and sterols show considerable variation among higher plants (i.e. *Eucalyptus* spp., *Ranunculus* sp., *Typha* sp., *Phragmites australis*) and the macroalgae (i.e. *Chara australis*), as recorded in some proxy formulae. Such proxies are distinctive among various plant types and offer promise in organic source identification for the sediments (containing plant matter) from the MM.

Table 5.8
The concentrations and compositions of sterols in modern biota samples from the MM.

Type of sample	*Eucalyptus* sp. (Monkeygar Creek)	*Ranunculus* sp. (buttercup) (Loudens Lagoon)	*Typha* sp. (cumbungi) (Monkeygar Creek)	*Phragmites australis* (reeds) (Loudens Lagoon)	*Phragmites australis* (reeds) (Monkeygar Creek)	*Chara australis* (charophyte) (Monkeygar Creek)
Coprostanol (µg/g DW)	0.00	0.00	0.00	0.00	0.00	0.00
Cholesta-5,22E-dien-3β-ol (µg/g DW)	0.65	3.00	25.49	8.61	1.28	77.1
Cholesterol (µg/g DW)	0.00	0.00	7.77	0.00	0.00	0.00
5α-Cholestan-3β-ol (µg/g DW)	0.00	0.00	2.69	0.00	0.00	0.15
24-methyl-5α-cholesta-22E-en-3β-ol (µg/g DW)	0.00	0.00	0.00	0.00	0.00	0.10
24-methylcholesta-5,6,22E-trien-3β-ol (µg/g DW)	0.00	0.03	1.32	0.00	0.40	2.59
Campesterol (µg/g DW)	0.00	2.08	0.00	0.00	0.00	0.45
Stigmasterol (µg/g DW)	0.00	0.00	0.00	0.00	0.12	0.00
Σ Sterols (µg/g DW)	0.65	5.11	37.3	8.61	1.84	80.4
Σ C_{27} Sterols (µg/g DW)	0.65	3.00	35.9	8.61	1.31	77.3
Σ C_{28} Sterols (µg/g DW)	0.00	2.11	1.32	0.00	0.40	3.18
Σ C_{29} Sterols (µg/g DW)	0.00	2.08	0.00	0.00	0.12	0.45
Σ Sterols (µg/g TOC)	0.01	0.11	0.79	0.19	0.04	1.92

5.4 Analysis of surface sediments from the northern and southern marshes

The 12 surface sediment samples analysed include: from the northern MM, MRI-S1 and MRI-S2 from a channel ridge parallel to the Macquarie River, LOLA-S1, LOLA-S2, LOLA-S3 and 2LOLA-S1 from Loudens Lagoon, LSW-S1, LSW-S2 and LSW-S3 from Longstowe station; and from the southern MM, MC-C6 from Monkeygar Creek, CT-S1 from east of Monkeygar Creek, and SL-C1 from South Lagoon. More detailed information of the sampling sites and sediment types is presented in the tables in the following sections.

5.4.1 *n*-alkanes

The total *n*-alkane (nC$_9$-nC$_{33}$) concentrations of the 12 surface sediment samples range from 2.74 to 23.1 µg/g (dry weight), and from 0.55 to 10.3 µg/g (TOC). The composition (Figure 5.17 Page 280) of these *n*-alkanes is dominated by long-chain compounds (nC$_{23}$-nC$_{33}$) with strong odd-to-even preference in the majority of the samples. The most abundant *n*-alkane is nC$_{29}$ in most of the samples, nC$_{33}$ in CT-S1, nC$_{31}$ in MC-C6 and exceptionally nC$_{30}$ in LSW-S3. The absolute concentration and composition of *n*-alkanes varies from site to site, and even differ in nearby sampling sites with different environmental settings. For example, samples collected within the floodplain of a small channel (MRI-S2) show a dominance of long-chain *n*-alkanes (nC$_{25}$-nC$_{33}$); whereas mud samples from the channel (MRI-S1) show bimodal peaks both in long-chain *n*-alkanes (nC$_{25}$-nC$_{33}$) and short-chain *n*-alkanes (nC$_{11}$-nC$_{19}$). In general, the *n*-alkane compositions of all the surface sediment samples can be divided into two groups – one with a dominant peak in the long-chain compounds with strong odd-to-even preference (including MRI-S2, 2LOLA-S1, LOLA-S1 and LOLA-S2); the other samples have additional peaks in short-

chain compounds with moderate odd-carbon predominance or even-carbon predominance in some sites (including MRI-S1, LSW-S1, LSdW-S2, LSW-S3, LOLA-S3, SL-C1, CT-S1 and MC-C6). The former samples indicate the contribution of macrophytes and vascular plants that grow within the watershed or nearby; the latter samples likely indicate the contribution of OM by microalgae and bacteria in samples collected from watercourses.

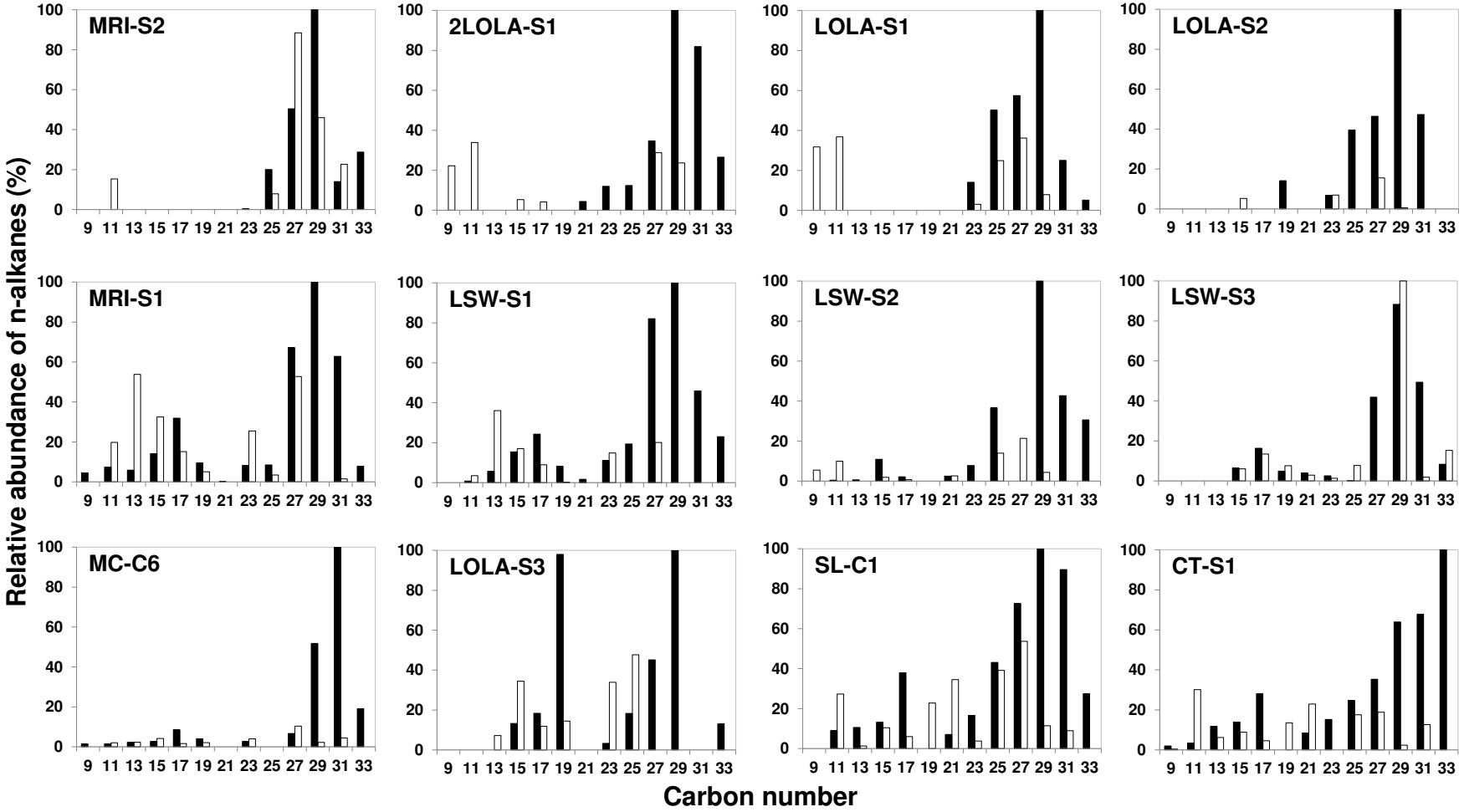

Figure 5.17. The relative abundance of *n*-alkanes (C_9-C_{33}) in surface sediments from the MM. (The white bar is even carbon numbers; the black bar is odd carbon numbers. The top row contains samples from dry sites, and the middle and bottom rows are samples from inundated sites.)

Table 5.9
TOC, *n*-alkane concentrations and proxies of the surface sediments from the MM.

Sample ID	Dry/Wet Sampling Site	Main Vegetation Cover	TOC (%)	Σ *n* - alkanes (C_{9-33} µg/g DW)	Σ *n* - alkanes (C_{9-33} µg/g TOC)	CPI	OEP	ACL	P_{aq}	P_{wax}	C_{17}/C_{31}	C_{27}/C_{31}
2LOLA-S1	Dry	*Phragmites australis*	3.91	9.88	2.53	4.87	2.78	29.6	0.12	0.90	0.00	0.42
MRI-S2	Dry	Woodland plants	2.00	4.56	2.28	1.29	1.10	28.8	0.15	0.89	0.00	3.60
LOLA-S2	Dry	*Phragmites australis* & *Ranunculus* sp.	3.93	4.15	1.06	12.3	6.72	28.3	0.24	0.81	0.00	0.98
LOLA-S1	Dry	*Phragmites australis* (dead)	2.07	4.69	2.27	3.37	2.03	28.0	0.34	0.74	0.00	2.30
MC-C6	Wet	Surrounded by *Typha* sp.	5.36	9.00	1.68	9.43	2.21	30.5	0.02	0.98	0.08	0.07
LSW-S3	Wet	Surrounded by woodland plants	5.18	10.07	1.95	1.56	0.85	29.3	0.02	0.99	0.33	0.85
MRI-S1	Wet	Woodland plants	1.36	6.42	4.72	3.62	2.28	29.0	0.09	0.93	0.51	1.07
LSW-S1	Wet	Woodland plants	1.61	6.33	3.93	10.6	7.61	28.8	0.17	0.88	0.53	1.79
LOLA-S3	Wet	*Phragmites australis*	2.25	2.47	1.10	2.93	2.04	28.4	0.18	0.87	-	-
CT-S1	Wet	Woodland plants & *Phragmites australis*	1.80	20.79	11.6	5.68	2.06	30.3	0.23	0.81	0.41	0.52
LSW-S2	Wet	Woodland plants & *Phragmites australis*	8.55	23.09	2.70	5.28	0.97	29.3	0.24	0.76	0.05	0.00
SL-C1	Wet	Wooldland plants & *Phragmites australis*	2.85	14.27	5.0	2.89	1.56	28.9	0.24	0.81	0.42	0.81

The CPI values of the surface sediment samples (Table 5.9, Page 281) range from 1.29 to 12.3. These surface sediments are considered to be deposited in relatively recent times and under climate conditions similar to present. The variation of the CPI values is mainly a result of the different organic sources (Matsumoto and Watanuki, 1990). Most of the samples with high CPI values (>5) and strong odd-to-even preference indicate *n*-alkanes that originate mainly from higher plants; the other samples with CPI values within the range 1-5 likely indicate *n*-alkanes originating from both higher plants, bacteria and algae (Cranwell et al., 1987). Comparatively, the OEP values were less variable and mostly around 1.0-2.0 in these surface sediment samples, except for two extremely high values found in LOLA-S2 (6.7) and LSW-S1 (7.6). The ACL values vary from 28.0 to 30.5 with an average of 29.1, generally higher than for algae (i.e. *Chara australis*) and closer to higher plants (i.e. *Ranunculus* sp. and *Phragmites australis*) analysed in the previous section, indicating a dominant contribution of OM from these higher plants. The very high values of CPI and OEP found in LOLA-S2, LSW-S1 and MC-C6 may be attributed to recent input of higher plants to the OM in these sites. Most of the surface samples show intermediate values of 0.1-0.4 corresponding to a mixture of inputs from terrestrial, emergent and submerged/floating aquatic macrophytes and charophytes as observed in the field. The variation of P_{aq} ratios among the several field sites indicates different proportions of plant species input to the OM in the sediments. The higher P_{aq} (e.g. LOLA-S1, LOLA-S2, LSW-S2, CT-S1 and SL-C1) reflects sediments from the lagoons/swamps which had abundant submerged/floating aquatic plants in their shallower parts and were bordered by a fringe of emergent macrophytes and terrestrial plants. The relative low P_{aq} (e.g. MC-C6, LSW-S3) corresponds to sediments from sites which had fewer submerged/floating and emergent plants. The P_{wax} ratio was applied to these surface

sediments to assess the relative proportion of waxy and terrestrial plants to total hydrocarbons (Zheng et al., 2007) and results show that the values range between 0.74 and 0.99. A low P_{aq} ratio and high P_{wax} ratio reflects the dominant contribution of higher plants to the surface sediments. Most of the C_{17}/C_{31} values are close to 0 except for a few high values (~0.50) found in MRI-S1, LSW-S1, LSW-S3, CT-S1 and SL-C1, indicating that algae and bacteria were not the main contributors to the sediment OM. Most of the low C_{27}/C_{31} values, indicative of the dominance of C_3 wetland grasses, were found in the sediments where the *Phragmites australis* and *Typha* sp. grew (e.g. LOLA-S2, 2LOLA-S1, MC-C6).

Most of the surface sediment samples analysed are very similar in the relative abundance of *n*-alkanes as found in modern plants (discussed previously in Section 5.3.1). Figure 5.18 (Page 285) and Figure 5.19 (Page 286) exemplify the distribution of *n*-alkane biomarkers extracted from sediments and modern plants. The surface sediments from the LOLA site (Figure 5.18 left graph) show the dominance of high molecular weight *n*-alkanes (nC$_{23}$-nC$_{31}$), with strong odd-to-even preferences; similar to the values obtained from *Phragmites australis* and *Ranunculus* sp. growing at this site indicating their contribution to the OM of the sediments. The *n*-alkane proxy values (Figure 5.18 right graph) for the sediments fall within the range of those from the two plant species. The surface sediment from the MC site (Figure 5.19 left graph) also shows odd-to-even carbon preference for all alkanes but with dominance in higher molecular weight *n*-alkanes (nC$_{27}$-nC$_{33}$). Extant *Typha* sp. from this site has *n*-alkanes with lower molecular weight *n*-alkanes (nC$_{23}$-nC$_{31}$), indicating that *Typha* sp. may not be the main contributor of OM to the sediment. *Chara australis*, which shows a bimodal carbon-number distribution with a mode at nC$_{17}$, may contribute to the small peaks in lower molecular weight *n*-alkanes in

the sediment. Thus, *Typha* sp. and *Chara australis* cannot be considered the main organic source for the sediments at the MC site. The high molecular-weight *n*-alkanes are likely to originate from other sources and very likely C_3 wetland grasses which are abundant in nC_{31} *n*-alkanes (Seki et al., 2010). The *n*-alkane proxies (Figure 5.19 right graph) also do not support a significant source of *Typha* sp. and *Chara australis* to the sediment. Only the CPI, OEP and C_{17}/C_{31} values of the sediments are within the range of the two plants. The very high ACL and P_{wax} and low P_{aq} and C_{27}/C_{31} may be attributed to C_3 wetland grasses. The dominant OM source for the MC site needs to be further investigated with more data from C_3 wetland grasses.

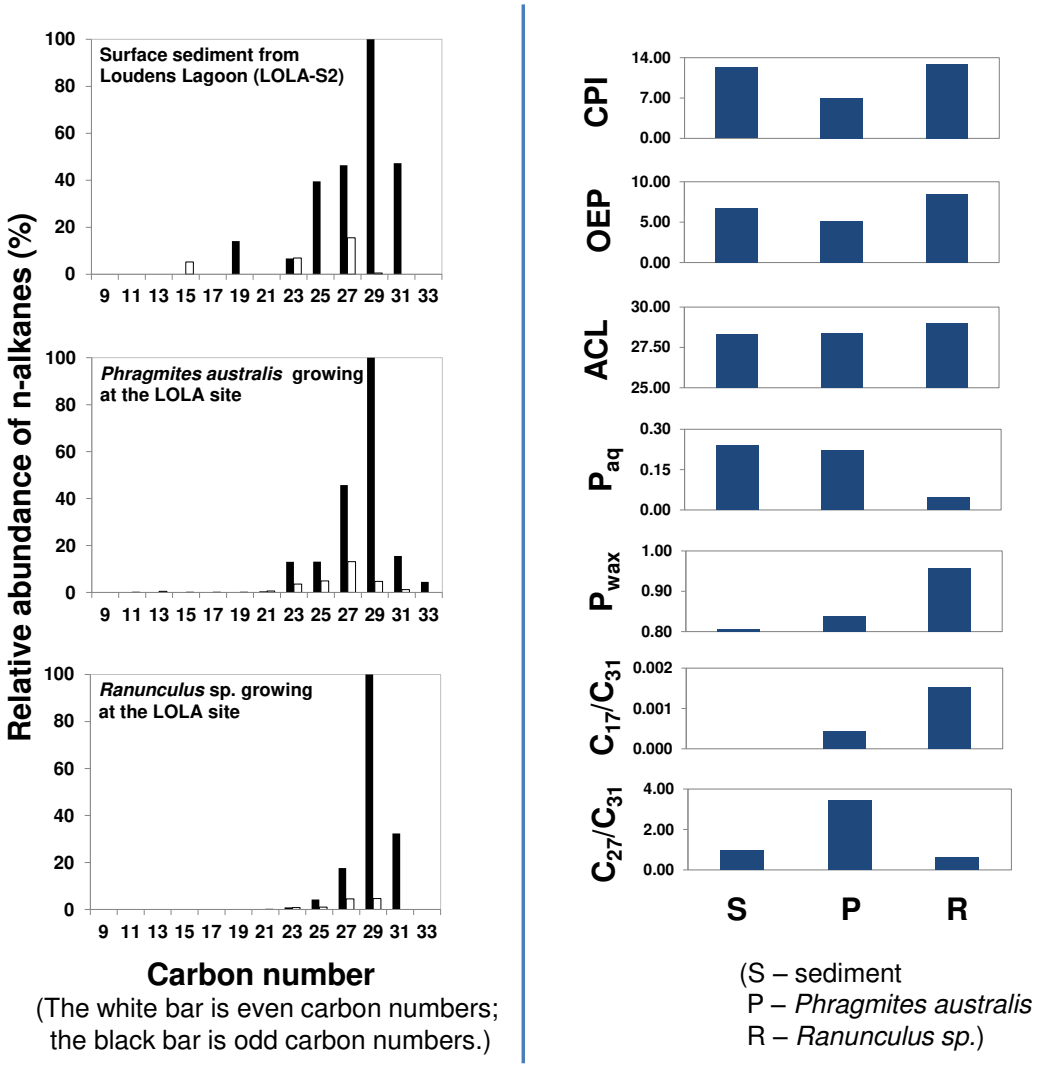

Figure 5.18. The distribution of *n*-alkanes (C_9-C_{33}) in surface sediments and plant samples from the LOLA site (left) and their *n*-alkane proxies (right).

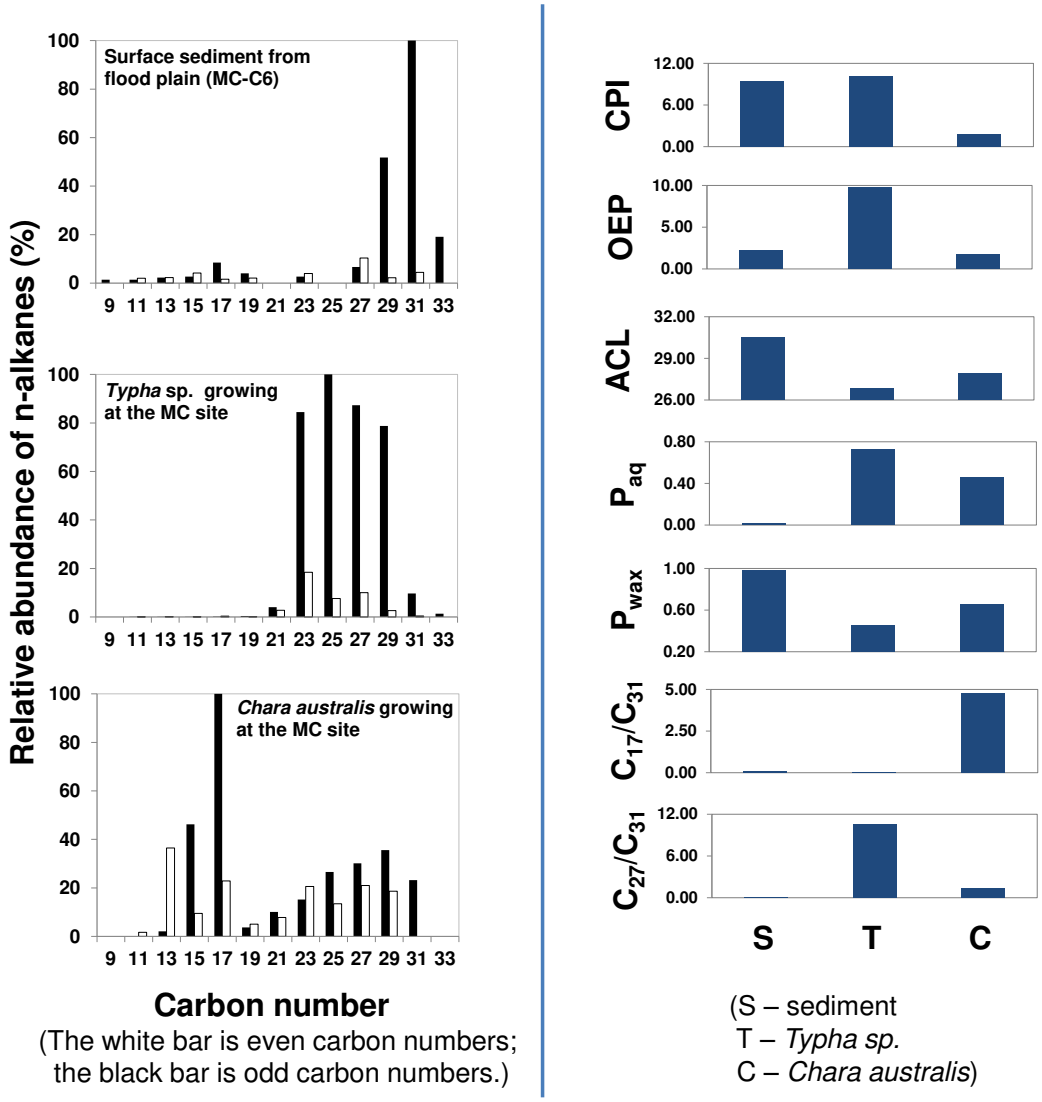

Figure 5.19. The distribution of *n*-alkanes (C_9-C_{33}) in surface sediments and plant samples from the MC site (left) and their *n*-alkane proxies (right).

Figure 5.20 shows a ternary diagram illustrating the relative abundance of the three most abundant *n*-alkanes (nC_{27}, nC_{29} and nC_{31}) in plants and surface sediments. *Eucalyptus* sp. and *Typha* sp. contain more C_{27} *n*-alkanes; *Phragmites australis* and *Ranunculus* sp. contain more C_{29} *n*-alkanes whereas *Chara australis* contains more C_{31} *n*-alkanes. The surface sediment samples mostly cluster close to the extant plant samples growing in these sites, again supporting the input of *n*-alkanes from plants to these surface sediments (Schwark et al., 2002; Wiesenberg et al., 2004).

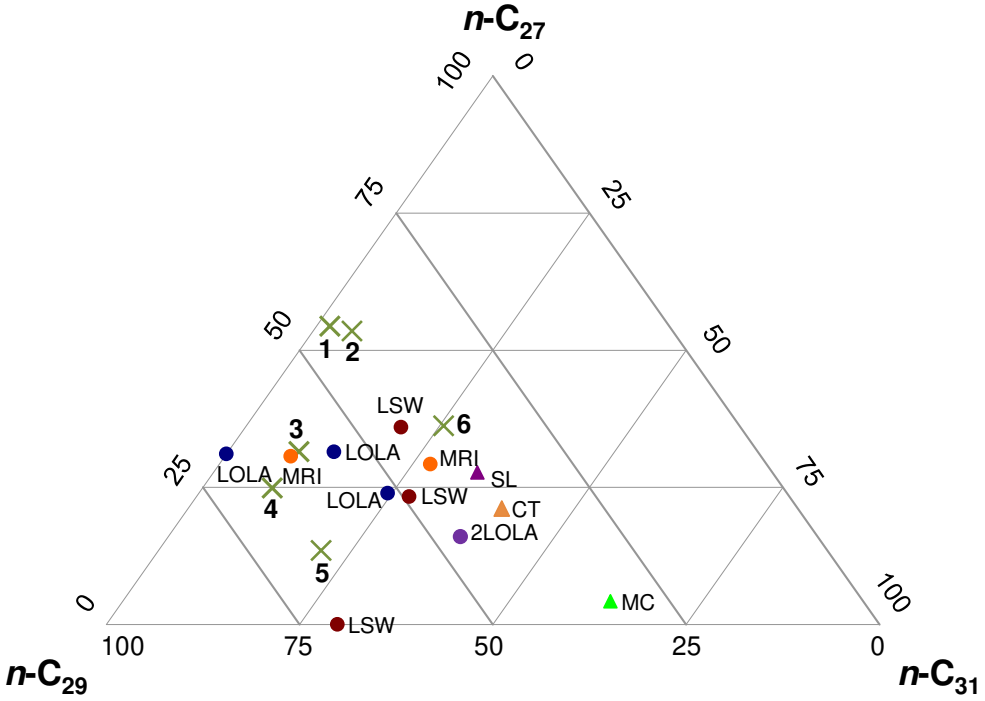

Figure 5.20. The relative abundance of the three most abundant *n*-alkanes (nC_{27}, nC_{29} and nC_{31}) in plants and surface sediments. (● surface sediments from the northern Macquarie Marshes; ▲ surface sediments from the southern Macquarie Marshes; × plant samples including 1. *Eucalyptus* sp., 2. *Typha* sp., 3, 4. *Phragmites australis*. 5. *Ranunculus* sp., 6. *Chara australis*)

5.4.2 *n*-alkanols

The total *n*-alkanol (nC$_{14}$-nC$_{30}$) concentrations (Table 5.10, Page 290) of the 12 surface sediment samples range from 1.67 to 15.2 µg/g (dry weight), and from 0.58 to 7.37 µg/g (TOC). The relative abundances (Figure 5.21, Page 291) of these *n*-alkanols are dominated by long-chain compounds (nC$_{22}$-nC$_{30}$) with strong even-to-odd preference in most of the samples. The most abundant *n*-alkanol is nC$_{28}$ in samples from MRI-S1, MRI-S2, LSW-S1, LSW-S2, LSW-S3 and MC-C6 and nC$_{26}$ in the remaining 6 samples. As for the *n*-alkanes, the concentration and relative abundances of *n*-alkanols varied depending on the environmental settings. In general, the *n*-alkanol composition of most of the surface sediment samples show a dominant peak in the long-chain compounds (nC$_{22}$-nC$_{30}$) with strong even-to-odd preference, indicating a strong contribution of terrestrial higher plants (Castañeda et al., 2011). There were also additional peaks in the short-chain compounds with moderate odd-carbon predominance or even-carbon predominance (nC$_{14}$-nC$_{21}$), probably due to the input of algae and photosynthetic bacteria (Volkman et al., 1999).

Unlike the *n*-alkanes, most of the surface sediments analysed differed in the composition and relative abundance of *n*-alkanols compared to the modern plants (Section 5.3.2). The reason for this needs to be further investigated.

The CPI$_{OH}$ values of the surface sediments (Table 5.10, Page 290) range from 3.51 to 9.41, generally lower than those reported in peat bogs (Andersson and Meyers, 2012). These values are lower than *Typha* sp. and *Ranunculus* sp. and higher than *Phragmites australis* and charophytes (discussed in the previous section), indicating probable mixed sources. The ratios of short-chain/long-chain *n*-alkanols ranges from 0.02 to 0.19,

indicating long-chain predominance which is likely a contribution of higher plants (Duan and Ma, 2001; Castañeda et al., 2011).

Table 5.10
TOC, *n*-alkanol concentrations and proxies of the surface sediments from the MM.

Sample ID	Dry/Wet Sampling Site	Main Vegetation Cover	TOC (%)	Σ *n* - alkanols (C_{14-30} µg/g DW)	Σ *n* - alkanols (C_{14-30} µg/g TOC)	CPI_{OH}	$\Sigma C_{14-20}/\Sigma C_{21-30}$
MRI-S1	Wet	Woodland plants	1.36	5.18	2.59	7.47	0.04
MRI-S2	Dry	Woodland plants	2.00	1.67	0.58	3.95	0.19
LOLA-S1	Dry	*Phragmites australis* (dead)	2.07	3.82	0.98	5.98	0.07
LOLA-S2	Dry	*Phragmites australis*	3.93	7.02	0.82	5.05	0.06
LOLA-S3	Wet	*Phragmites australis*	2.25	4.33	2.41	7.71	0.04
2LOLA-S1	Dry	*Phragmites australis*	3.91	15.2	7.37	6.98	0.12
LSW-S1	Wet	Woodland plants	1.61	8.65	2.20	7.24	0.08
LSW-S2	Wet	Woodland plants & *Phragmites australis*	8.55	14.2	6.30	6.47	0.12
LSW-S3	Wet	Surrounded by woodland plants	5.18	7.42	4.60	8.08	0.03
MC-C6	Wet	Surrounded by *Typha* sp.	5.36	9.25	1.79	9.41	0.02
CT-S1	Wet	Woodland plants & *Phragmites australis*	1.80	7.77	1.45	4.58	0.08
SL-C1	Wet	Wooldland plants & *Phragmites australis*	2.85	4.94	3.63	3.51	0.09

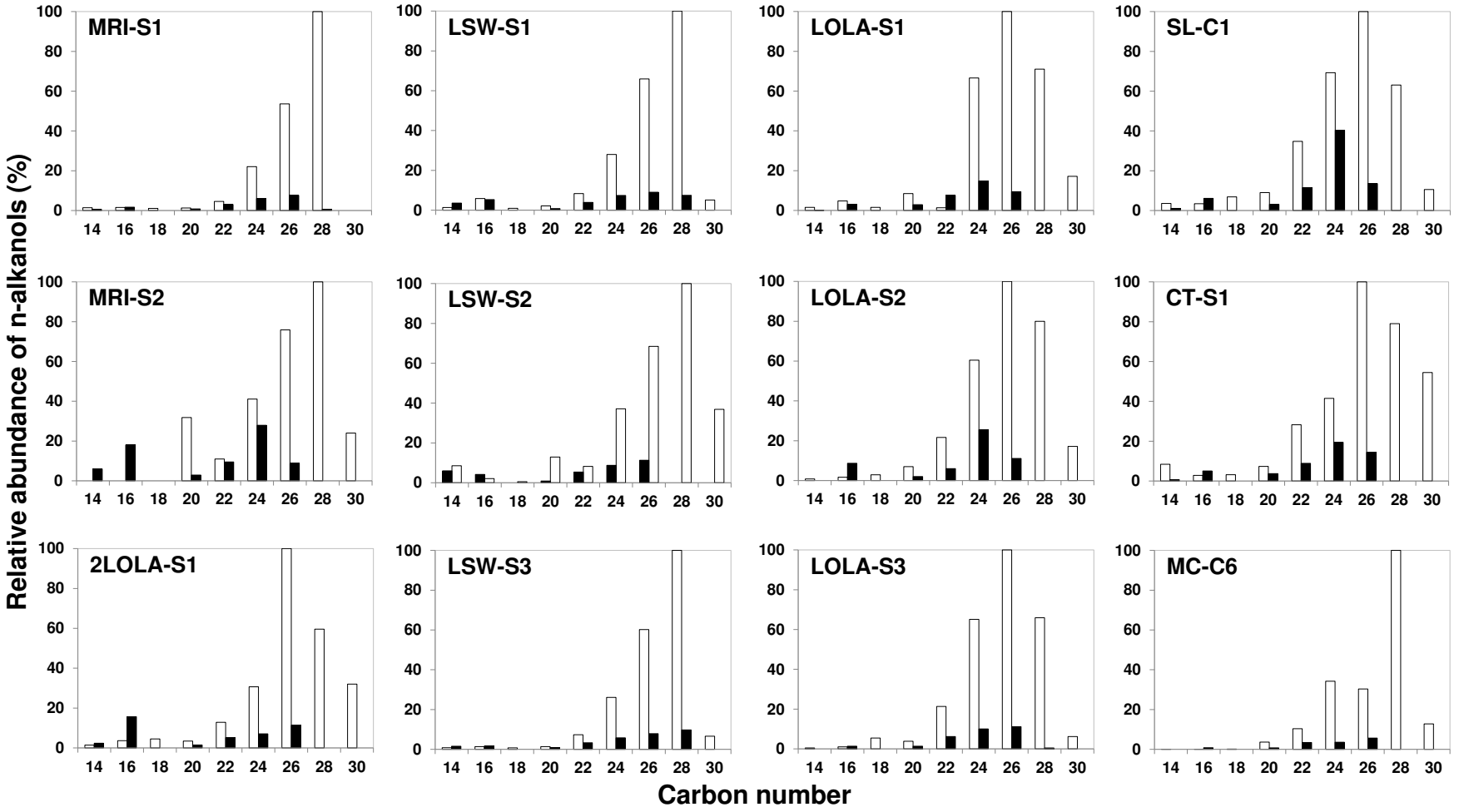

Figure 5.21. The relative abundance of *n*-alkanols (C_{14}-C_{30}) in surface sediments from the MM. (The white bar is even carbon numbers; the black bar is odd carbon numbers.)

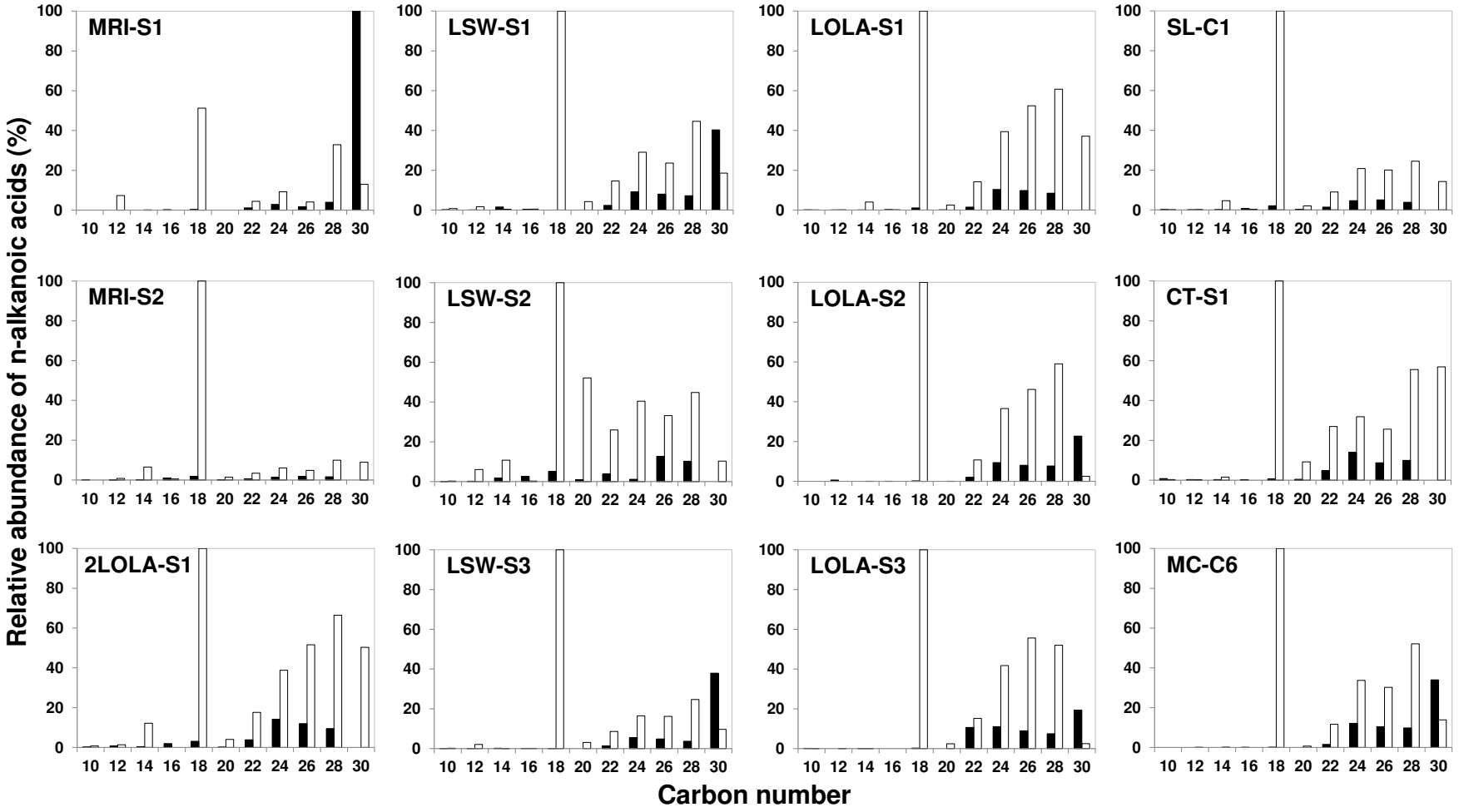

Figure 5.22. The relative abundance of *n*-alkanoic acids (C_{14}-C_{30}) in surface sediments from the MM. (The white bar is even carbon numbers; the black bar is odd carbon numbers.)

5.4.3 *n*-alkanoic acids

The total *n*-alkanoic acid (nC$_9$-nC$_{30}$) concentrations (Table 5.11, Page 295) of the 12 surface sediment samples range from 6.61 to 87.08 µg/g (dry weight), and from 2.52 to 38.68 µg/g (TOC). The most abundant *n*-alkanoic acid is nC$_{18}$ in most of the samples except nC$_{29}$ in MRI-S1, and likely originates from algae and photosynthetic bacteria (Robinson et al., 1984; Volkman et al., 1999). The relative abundances (Figure 5.22, Page 292) of *n*-alkanoic acids in most samples are dominated by long-chain compounds (nC$_{22}$-nC$_{30}$) with strong even-to-odd preference in most of the samples. This is similar to the results reported from Lake Wandakara, Uganda indicating that they are primarily derived from terrestrial plants (Eglinton and Hamilton, 1967; Russell et al., 2009). The absolute concentration and relative abundance of *n*-alkanoic acids varies from site to site with different environmental settings, depending on the organic input. Most of the surface sediment samples analysed also differ in composition and relative abundance of *n*-alkanoic acids compared to the plants (discussed Section 5.3.3), although generally closer to the higher plants (*Typha* sp., *Phragmites australis*, *Eucalyptus* spp.) than the algae (*Chara australis*). Degraded plant biomass is commonly depleted in mid-chain and enriched in long-chain *n*-alkanoic acids (Wiesenberg et al., 2004), so it is assumed that the composition of *n*-alkanoic acids in the surface sediments indicates the plant biomass input into OM of sediments.

The CPI_{FA} values of the surface sediment samples (Table 5.11) range from 0.57 to 6.86. Generally the samples from the watercourses (MRI-S1, LSW-S1, LSW-S3 and MC-C6) have lower CPI_{FA} values (<2.0). The reason for this still needs to be investigated. The ratios of short-chain/long-chain *n*-alkanoic acids are lower than 1.0 in the surface sediment samples except for one sample MRI-S2 (2.93), indicating long-chain predominance which

is likely due to contributions of terrestrial higher plants (Eglinton and Hamilton, 1967; Russell et al., 2009).

Table 5.11
TOC, *n*-alkanoic acid concentrations and proxies of the surface sediments from the MM.

Sample ID	Dry/Wet Sampling Site	Main Vegetation Cover	TOC (%)	Σ *n* - alkanoic aicds (C_{9-30} µg/g DW)	Σ *n* - alkanoic aicds (C_{9-30} µg/g TOC)	CPI_{FA}	$\Sigma C_{9-20}/\Sigma C_{21-30}$
MRI-S1	Wet	Woodland plants	1.36	6.61	3.31	0.57	0.34
MRI-S2	Dry	Woodland plants	2.00	22.4	7.86	6.72	2.93
LOLA-S1	Dry	*Phragmites australis* (dead)	2.07	54.0	13.8	6.86	0.46
LOLA-S2	Dry	*Phragmites australis*	3.93	21.5	2.52	3.12	0.49
LOLA-S3	Wet	*Phragmites australis*	2.25	19.0	10.6	3.40	0.46
2LOLA-S1	Dry	*Phragmites australis*	3.91	33.0	16.0	6.05	0.47
LSW-S1	Wet	Woodland plants	1.61	28.6	7.28	1.90	0.56
LSW-S2	Wet	Woodland plants & *Phragmites australis*	8.55	87.1	38.7	5.86	0.99
LSW-S3	Wet	Surrounded by woodland plants	5.18	23.1	14.3	1.37	0.82
MC-C6	Wet	Surrounded by *Typha* sp.	5.36	33.8	6.54	2.04	0.48
CT-S1	Wet	Woodland plants & *Phragmites australis*	1.80	47.3	8.82	5.60	0.49
SL-C1	Wet	Wooldland plants & *Phragmites australis*	2.85	51.8	38.1	6.22	1.07

Figure 5.23 shows a ternary diagram illustrating the relative composition of the three most abundant *n*-alkanoic acids (nC_{22}, nC_{24} and nC_{26}) in plants and surface sediments. *Chara australis*, *Ranunculus* sp. and *Phragmites australis* contain more C_{22} *n*-alkanoic acids; *Eucalyptus* sp. contains more C_{24} *n*-alkanoic acids while *Typha* sp. contains more C_{26} *n*-alkanoic acids. Unlike the *n*-alkanes, the *n*-alkanoic acids from the surface sediment samples tend to cluster close to the higher plants (*Phragmites australis*, *Eucalyptus* sp. and *Typha* sp., in particular the latter two), indicating more *n*-alkanoic acid input to the sediments from these plants than from *Chara australis* and *Ranunculus* sp..

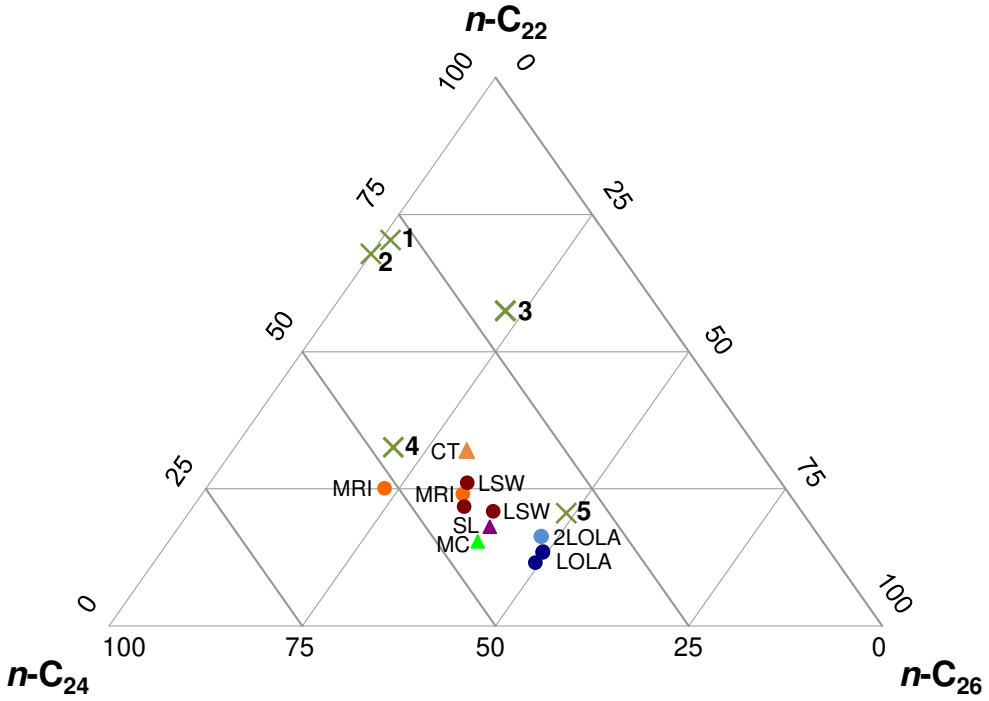

Figure 5.23. The relative abundance of the three most abundant *n*-alkanoic acids (nC_{22}, nC_{24} and nC_{26}) in plants and surface sediments. (● surface sediments from the northern Macquarie Marshes; ▲ surface sediments from the southern Macquarie Marshes; × plant samples including 1. *Chara australis*, 2. *Ranunculus* sp., 3. *Phragmites australis*, 4. *Eucalyptus* sp., 5. *Typha* sp.)

5.4.4 Sterols

The total concentrations of sterols (C_{27} to C_{29}) (Table 5.12, Page 299) range from 2.57 µg g^{-1} in Louden Lagoon (dry) in the northern MM (LOLA-S3) to 20.2 µg g^{-1} in a swamp bank in the northern MM (LSW-S2). The concentrations are comparable to those reported in shallow marine sediments (4 - 183 µg g^{-1}) (O'Leary et al., 1999) and lower than those in river sediments (28.9 - 63.9 µg g^{-1}) (Volkman et al., 2008) and creek sediments (22.8 - 148 µg g^{-1}) (O'Leary et al., 1999). In general, samples collected from a watercourse or nearby (i.e., samples from LSW, MC and CT sites) contain more sterols than those collected from sites where the vegetation cover was declining (samples from LOLA, MRI and SL sites). The lowest concentration occurs at the site (LOLA) that was dry at the time of collection. When the absolute concentration was calculated according to the relative contribution of OM in each sample, the ranking of total sterol abundance between the sampling sites was different. The higher concentration (10.1 µg g^{-1} TOC) was found in a bat colony site (LSW-S1) where there was fresh bat faecal input to the surface sediments. This was followed by samples from or nearby watercourses, and then samples from dry sites. Samples that had similar absolute sterol concentrations differed in their relative concentrations of OM due to the variation of organic content in the sediments. An example is LOLA-S2 (11.8 µg g^{-1}, 2.99 µg g^{-1} TOC) and CT-S1 (12.1 µg g^{-1}, 6.75 µg g^{-1} TOC). These two samples were collected from sites with different vegetation cover – LOLA-S2 was collected from dead reed beds (*Phragmites australis*) while CT-S1 was collected from a drier place where the reed beds had been replaced by more drought-tolerant species. As recorded in the sediments, the contributions of total OM and sterols to the sediments varied widely between those species.

Because many of the sterol biomarkers are not unique to just one species, examining the entire sterol profile may provide some information to distinguish the contribution of individual sources. Ratios calculated by the absolute amount of one particular compound or compound group may also assist in source identification. The most abundant sterols found in the surface sediments, identified by GC-MS (Figure 5.24, Page 300), were cholesterol, cholestanol, 24-methylcholest-5-en-3β-ol, campesterol, 24-methyl-5α-cholestanol, stigmasterol, stigmastanol, sitosterol, and sitostanol, in decreasing abundance order of C_{29}, C_{28} and C_{27} sterols. Sitosterol was the most abundant compound. None of the C_{30}-sterols, which are common in marine sediments (e.g. Fernandes et al., 1999; Duan 2000), was found in a recognisable amount. As shown in Figure 5.25 (Page 301), for most samples, the C_{27}, C_{28}, C_{29} sterols constituted about 15 %, 25 % and 60 % of the total sterols. A few exceptions include LSW-S1 and MC-C6 which contained more C_{27} sterols while samples from other sites contained more C_{28} sterols. Compared to the modern plant samples (Section 5.1.3), there were more sterols detected in surface sediments. Apart from the most common plants grown in/near where the sediments were collected, there were probably other sources of sterols. As the sterols are similar to those found in river sediments (Volkman et al., 2008), it is likely that higher plants and microalgae both contribute to the OM in the sediments (Volkman, 2003; Volkman et al., 2007; 2008).

Table 5.12
Sterol concentrations of the surface sediments.

	MRI-S1	MRI-S2	LOLA-S1	LOLA-S2	LOLA-S3	2LOLA-S1	LSW-S1	LSW-S2	LSW-S3	MC-C6	CT-S1	SL-C1
coprostanol (µg/g DW)	0.06	0.03	0.14	0.21	0.04	0.05	0.23	0.30	0.10	0.24	0.05	0.02
epicholestanol (µg/g DW)	0.02	0.01	0.07	0.11	0.03	0.05	0.05	0.01	0.03	0.07	0.02	0.01
epicoprostanol (µg/g DW)	0.01	0.01	0.08	0.09	0.02	0.03	0.06	0.05	0.02	0.06	0.01	0.02
cholesta-5,22E-dien-3β-ol (µg/g DW)	0.06	0.02	0.02	0.02	0.00	0.14	0.09	0.03	0.04	0.06	0.04	0.01
cholesterol (µg/g DW)	0.65	0.33	0.43	0.48	0.12	0.60	1.81	0.63	0.42	1.37	0.36	0.17
5α-cholestan-3β-ol (µg/g DW)	0.34	0.25	0.83	1.03	0.16	0.52	1.32	1.95	0.71	1.14	0.17	0.17
24-methylcholesta-5,22E-dien-3β-ol (µg/g DW)	0.49	0.34	0.29	0.40	0.09	0.35	0.70	0.57	0.37	1.14	0.37	0.10
24-methyl-5α-cholesta-22E-en-3β-ol (µg/g DW)	0.20	0.08	0.26	0.33	0.10	0.38	0.16	0.03	0.14	0.28	0.06	0.04
ergosterol (µg/g DW)	0.22	0.27	0.05	0.14	0.09	0.31	0.22	2.30	0.28	0.20	0.16	0.41
24-methylcholesta-5,24(28)-dien-3β-ol (µg/g DW)	0.22	0.15	0.76	0.71	0.11	0.69	0.39	0.74	0.29	0.98	0.34	0.21
campesterol (µg/g DW)	0.69	0.56	1.07	1.33	0.37	1.83	1.38	1.38	0.97	1.90	2.56	0.71
24-methyl-5α-cholestanol (µg/g DW)	0.00	0.00	0.00	0.00	0.00	0.00	0.00	0.00	0.00	0.00	0.00	0.00
stigmasterol (µg/g DW)	0.17	0.14	0.63	0.84	0.14	0.78	0.50	0.49	0.26	0.90	0.40	0.25
stigmastanol (µg/g DW)	0.02	0.00	0.00	0.15	0.02	0.00	0.04	0.12	0.02	0.04	0.08	0.00
β-sitosterol (µg/g DW)	4.46	3.40	3.16	3.53	0.85	3.79	7.81	10.1	5.44	4.25	6.52	1.56
sitostanol (µg/g DW)	0.65	0.51	1.92	2.37	0.42	1.49	1.52	1.52	0.96	1.96	1.02	0.60
Σ sterols (C_{27-29} µg/g DW)	8.26	6.09	9.71	11.8	2.57	11.0	16.3	20.2	10.0	14.6	12.1	4.29
Σ sterols (C_{27-29} µg/g TOC)	6.08	3.05	4.70	2.99	1.14	2.82	10.1	2.37	1.94	2.72	6.75	1.50

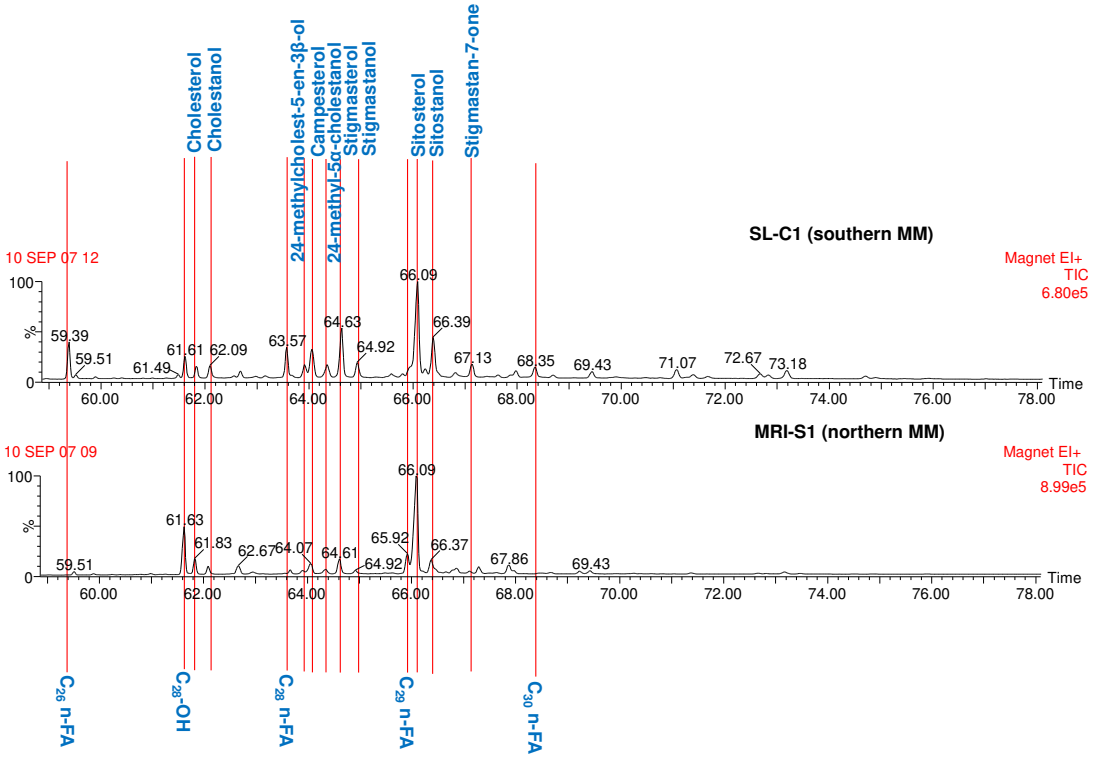

Figure 5.24. GC-MS chromatograph of two surface-sediment samples from the northern and southern MM.

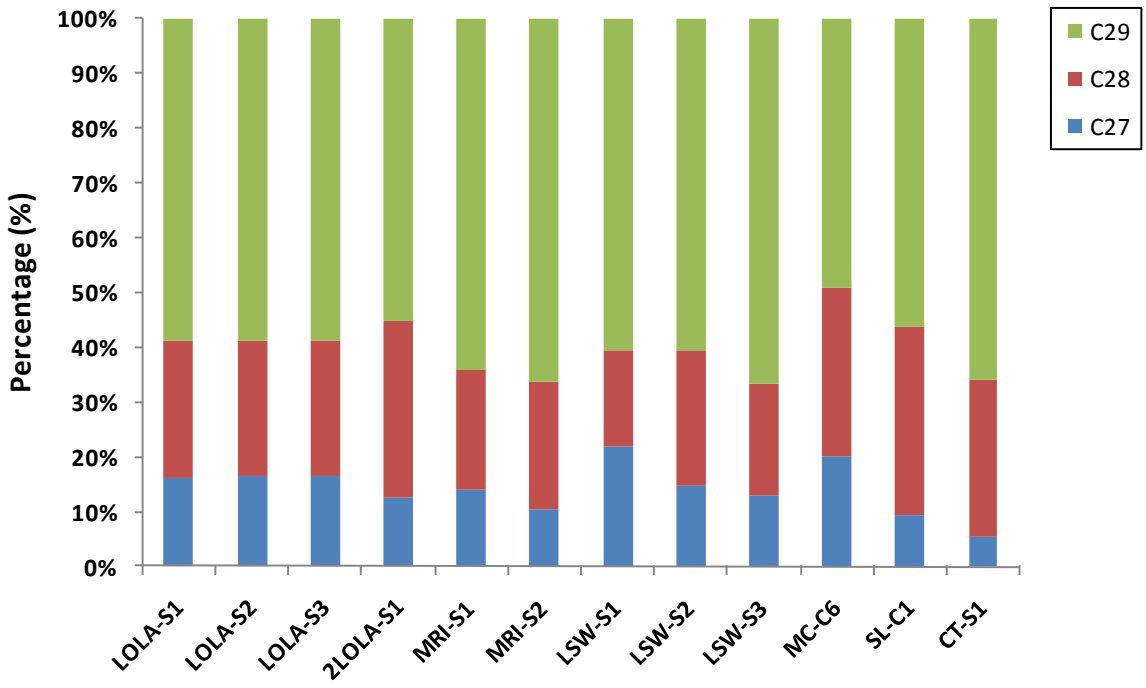

Figure 5.25. Relative-abundance sterol profiles (C_{27} to C_{29}) of the surface sediments in the MM.

Table 5.13 summarises the most abundant sterols (used as biomarker-sterols, relative abundance > 1 %) found among microorganisms, higher plants, animals and human faeces, indicated by '*'. The green areas are sterols found in surface sediment samples in this study. Potential sources of sterols in surface sediment samples can be interpreted by matching the data with biomarkers from known sources. As indicated in the table (the green shaded areas), there is a great variety of sterol sources including Bacillariophyceae (diatoms), Chlorophyceae (green algae, e.g. filamentous), Charophyceae (charophytes), Cyanobacteria (blue-green algae), higher plants (e.g. *Phragmites australis*, *Eucalyptus* spp.) and likely birds (e.g. duck, swan, rosella, magpie). However, the contributions of each individual source requires further investigation.

Table 5.13
Major sterols in various microorganisms, higher plants and animal faeces.

	5β-$C_{27}\Delta^0$	$C_{27}\Delta^{5,22}$	$C_{27}\Delta^5$	5α-$C_{27}\Delta^0$	$C_{28}\Delta^0$	$C_{28}\Delta^5$	$C_{28}\Delta^{5,22}$	$C_{28}\Delta^{22}$	$C_{28}\Delta^{5,7,22}$	$C_{28}\Delta^{5,24(28)}$	$C_{28}\Delta^{7,22}$	$C_{28}\Delta^7$	$C_{28}\Delta^{7,24(28)}$	$C_{29}\Delta^5$	$C_{29}\Delta^{5,22}$	5β-$C_{29}\Delta^{22}$	$C_{29}\Delta^{22}$	5α-$C_{29}\Delta^0$	5β-$C_{29}\Delta^0$	$C_{29}\Delta^{5,7}$	$C_{29}\Delta^{5,24(28)}$	$C_{29}\Delta^7$
Microorganism																						
bacillariophyceae		√	√				√			√				√								
chlorophyceae						√			√		√			√	√							
cyanobacteria			√	√										√				√				
yeasts & fungi									√			√	√									
euglenophyceae									√		√	√		√						√		
Methylotrophic bacteria																						
Plants														√	√							
seagrass			√			√	√							√	√							
angiosperms														√	√							
Animals faeces																						
duck	√		√	√	√	√								√	√			√	√		√	√
magpie			√	√	√	√								√	√			√				√
rosella			√			√								√	√			√			√	√
swan			√			√								√	√						√	
cow	√		√	√	√	√								√	√	√	√	√	√			
horse	√		√	√	√	√								√	√	√	√	√	√			√
sheep	√		√	√	√	√								√	√	√	√	√	√			√
possum	√		√	√	√	√								√	√	√		√	√			√
pig	√		√	√	√									√				√	√			√
human	√		√	√	√									√		√		√	√			√

√ Composition>1 %

Green areas indicate compounds found in surface sediments of the MM in this study. Accordingly, the green shaded areas indicate possible sources for the sterols in the surface sediments.

Sterol nomenclature: coprostanol (5β-$C_{27}\Delta^0$), ergosterol ($C_{27}\Delta^{5,22}$), cholesterol ($C_{27}\Delta^5$), cholestanol (5α-$C_{27}\Delta^0$), campestanol ($C_{28}\Delta^0$), campesterol ($C_{28}\Delta^5$), 24-methylcholesta-5,22E-dien-3β-ol ($C_{28}\Delta^{5,22}$), 24-methyl-5α-cholesta-22E-en-3β-ol ($C_{28}\Delta^{22}$), 24-methylcholesta-5,7,22-trien-3β-ol ($C_{28}\Delta^{5,7,22}$), 24-methylcholesta-5,24(28)-dien-3β-ol ($C_{28}\Delta^{5,24(28)}$), 24-methylcholesta-5,22-dien-3β-ol ($C_{28}\Delta^{7,22}$), 24-methylcholest-7-en-3β-ol ($C_{28}\Delta^7$), 24-methylcholesta-5,24(28)-dien-3β-ol ($C_{28}\Delta^{7,24(28)}$), sitosterol ($C_{29}\Delta^5$), stigmasterol ($C_{29}\Delta^{5,22}$), 5β-stigmasterol (5β-$C_{29}\Delta^{22}$), stigmastanol ($C_{29}\Delta^{22}$), sitostanol (5α-$C_{29}\Delta^0$), 24-ethylcoprostanol (5β-$C_{29}\Delta^0$), 24-ethylcholesta-5,7-dien-3β -ol ($C_{29}\Delta^{5,7}$), isofucosterol ($C_{29}\Delta^{5,24(28)}$), 24-ethylcholest-7-en-3β-ol ($C_{29}\Delta^7$)

References: Leeming et al., 1996; Volkman, 2003; Volkman, 2008; Sonibare, 2009

Coprostanol, a compound commonly biosynthesised by mammals has long been established as faecal biomarker (e.g. Leeming et al., 1996; Bull et al., 2003; Tindale et al., 2009), was found in very low amounts in almost all the surface sediment samples with exception of the sample collected near the bat colony site (concentration of coprostanol in LSW-S1 is 0.23 μg g^{-1} (DW) and 14.0 μg g^{-1} (TOC)). Although the Nature Reserve is surrounded by livestock grazing areas, coprostanol is unlikely to originate from faecal pollution, which can be confirmed by examining the relative abundance of other compounds or compounds groups. In this study, the ratio of coprostanol/(coprostanol+cholestanol) is 0.08 to 0.22, which is much lower than the reported value (0.7) of faecal matter from human or higher animals (Grimalt et al., 1990).

The relative abundance of coprostanol, cholestanol and cholesterol are presented in a triplot (Figure 5.26), showing that sterols from the surface sediment samples plot well away from the faecal values of herbivores (horse, cow, sheep), mammals (possum, pig) and humans, and are closer to birds (magpie, duck, rosella) in their composition of coprostanol but differ in cholesterol and cholestanol. Bird guano may have some contribution to the total coprostanol, and this contribution could be greater when large waterbird colony events occur in the marshes. However, this needs to be further confirmed by other proxies as coprostanol is not the major sterol in bird faeces and is either absent or present at very low levels (Leeming et al., 1996).

Another possibility is that coprostanol may be formed in anaerobic sediment from precursors (such as sitosterol) in these wetland environments as indicated by the ratio of coprostanol/total sterols (less than 0.02) (Leeming et al., 1996). It seems very unlikely that the potential runoff of faecal pollution from anthropogenic sources (e.g. humans or grazing animals) has had a significant impact on these natural reserve marshes.

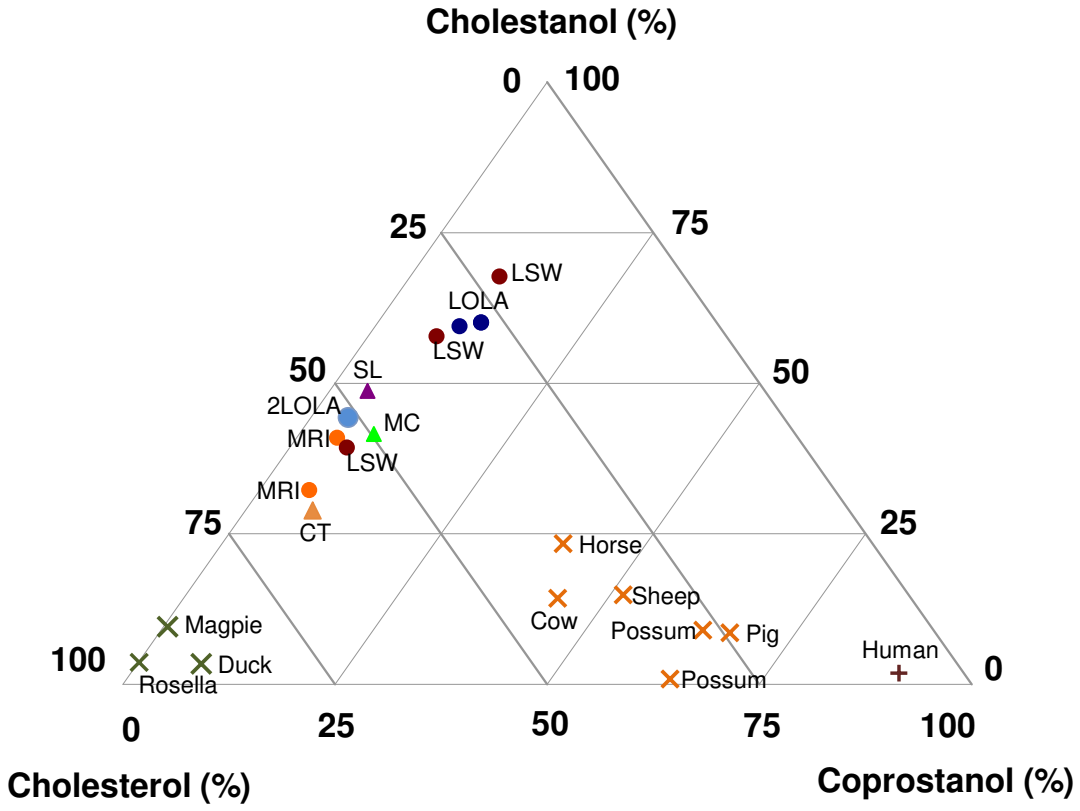

Figure 5.26. Relative abundance of coprostanol, cholestanol and cholesterol from various sources.

Despite the initial source contributions, the profiles of compounds may be altered in some environments after deposition and therefore can be used also as indicator of the post-depositional environment. Figure 5.26 shows the surface sediment samples are clustered in two groups – one with more cholestanol than cholesterol representing more anaerobic conditions with an abundance of water; the other with more cholesterol than cholestanol representing drier sediments.

5.4.5 Other organic markers in surface sediments

5.4.5.1 α-phellandrene

α-phellandrene, a biomarker from *Eucalyptus* sp. (Jacobs and Pickard, 1981), was detected in some of the surface sediments by GC-MS and the mass spectrum is shown in Figure 5.27. The presence of this compound is not a contaminant because it is not present in any of the blank samples. As is also shown in Figure 5.27, the peak of α-phellandrene was more significant in the surface sediments at the sites where *Eucalyptus* sp. was abundant. For example, the surface-sediment sample from a floodplain site (CT-S1) shows a distinctive α-phellandrene peak, in the GC-MS chromatogram, whereas there is no detectable α-phellandrene in the reed bed (*Phragmites australis*) site (2LOLA-S1). Therefore, we attempted to seek this particular compound in the core profiles and to use it as a specific biomarker for *Eucalyptus* sp. (see the following Section 5.5).

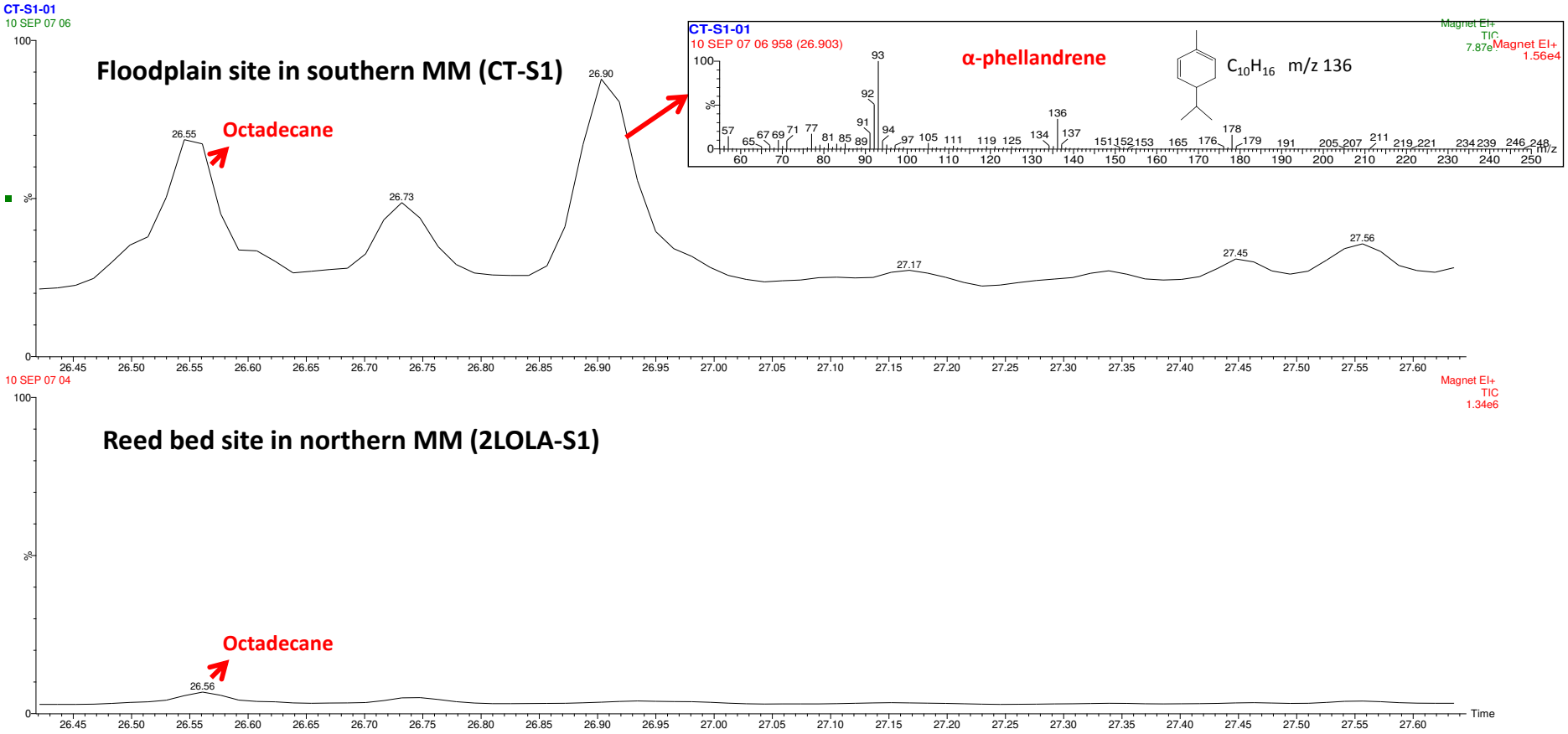

Figure 5.27. GC-MS total ion-current chromatogram of two surface-sediment samples and the mass spectrum of α-phellandrene (inset).

5.4.5.2 Polycyclic aromatic hydrocarbon (PAHs)

Among the 18 PAHs of interest (Figure 5.3, Page 242), perylene is the only one present in some of the surface sediments. It occurs in samples from the LSW site (LSW-S1 and LSW-S2), MRI site (MRI-S1), 2LOLA site (2LOLA-S1) and the SL site (SL-C1), and is more abundant in the northern MM than the southern MM. It is more likely of terrestrial origin rather than from fire/combustion origin. The reasons are: 1) perylene is the only compound present, and in very small amounts, while the other pyrogenic PAHs (e.g. benzofluoranthenes, indeno[1,2,3,cd]pyrene and benzo[ghi]perylene) are absent; 2) the northern marshes has more vegetation cover than the southern marshes and thus the input of terrestrial plants to the organic markers might be greater.

The PAHs formed during combustion of wild fires will remain in the gas phase at temperatures above 150 °C but rapidly condense onto fly-ash particles at lower temperatures (Harvey, 1991; Wilcke, 2000). Such ash deposited on the soil surface influences the soil chemistry (Kim et al., 2003). This ash can be easily removed by aeolian or fluvial processes unless incorporated in an anoxic environment (e.g. in the sediments of a lake) (O'Dwyer and Taylor, 2009, and references therein). Kim et al. (2003) found that five months after a forest fire occured, the concentrations of PAHs in burnt soils were similar to those in unburnt soils. In the semi-arid Macquarie Marshes, vegetation fires likely occurred during drier years when there was little water (Leblanc et al., 2012). Rainfall and/or wind erosion after the fire can be expected to remove the ashes with pyrogenic PAHs and erase their record in the sediments. This also indicates that the perylene found in some of the surface sediment samples is not from combustion but from terrestrial plants. Accordingly the use of pyrogenic PAHs as indicators for palaeofires is not ideal for studying sediments from semi-arid areas like the Macquarie Marshes.

5.4.5.3 Organochlorine pesticides (OCPs)

The surface sediment samples analysed for OCPs are "modern samples" that are less than 50 years old and from a time when cotton farming was established and pesticides and insecticides (e.g. DDT, DDE and DDD) extensively used in these areas (Cotton Australia, 2008). It is more likely that OCPs will be present in detectable amounts in these surface sediment samples rather than those from deeper core sections.

None of the target compounds was detected (less than 0.01 μg/g) in these surface sediments. Table 5.14 (Page 310) lists the concentrations of some of the commonly found OCPs in various locations, most of which are sediments from fluvial systems or wetland systems (Iwata et al., 1994; Burt and Ebell, 1995; Iwata et al., 1995; Mortimer, 1998; Doong et al., 2002; Marburger et al., 2002; Negoita et al., 2003; Imo et al., 2007; Minh et al., 2007; Hong et al., 2008; Liu et al., 2008; Leadprathom et al., 2009; Xiao et al., 2009; Zheng et al., 2009; Kim et al., 2010). The concentrations of OCPs in surface sediments from the Macquarie Marshes are within the low range of other background sites.

The MM samples were handled under strictly controlled laboratory procedures to ensure no contamination and high precision, and recoveries of the surrogates were high (> 80 %). Thus there are two possible interpretations: either the OCPs existed only at a very low level that could not be detected using standard methods (detection limit 0.01 μg/g); or they are not present in these surface sediments due to their loss by volatilisation, degradation and/or transportation after their deposition. Furthermore, OCPs have been banned for two or three decades (including in Australia), so that any concentration in the surface sediments would have been reduced by the processes mentioned above. Connell et al. (2002) found a decline of OCPs in Australian marine environments after their banning

in the period from the 1970s to 1980s, and observed a relatively low concentration (1.7 μg/g) in urban area sediments collected in the early 1990s, with a half-life of 1.1-3 years for various compounds. Assuming the concentration of DDT in the Macquarie Marshes sediment was 1.7 μg/g in 1990, when the sediment was collected in 2008, it would have degraded to 0.33 ng/g with a half-life of 2 years. Moreover, in the Macquarie Marshes wetlands system, the environmental setting is relatively unstable with alternating dry and wet periods. During dry periods, the surface sediment samples may be sub-aerially exposed, subjected to more intense sunlight and higher temperature, which would accelerate the degradation of OCPs.

Table 5.14
Concentration of OCPs in surface soils/sediments from various locations (unit: ng/g).

Sampling Site	Sampling Time	Sample Type	Concentration (ng/g dry weight)						Reference
			ΣDDTs	ΣHCHs	Dieldrin	HEP	Aldrin	HCB	
Macquarie Marshes, NSW Australia	Spring 2007/2008	surface soil/mud	<10	<10	<10	<10	<10	<10	this study
Southern Metropolitan Coastal Waters off Perth, WA Australia	1991	sediment	<1-2.2						Burt and Ebell 1995
Swan River, WA Australia	1990	sediment	3.4						Iwata et al. 1994
Sydney, NSW Australia	1990	sediment	6.3-1700						Iwata et al. 1994
Derwent River, Tasmania Australia	1990	sediment	1-58						Iwata et al. 1994
Brisbane River and Urban Creeks, Australia	1996	sediment	0.2-49						Mortimer 1998
South to middle parts of Lake Baikal, Russia	Summer 1992	sediment	0.014-2.7	0.019-0.12				0.005-0.16	Iwata 1995
Wetland restoration areas in central Florida, USA	1996	flooded soil	5463-8883		144-626				Marburger 2002
Wolong Natural Reserve, China	Spring & Autumn 2005	sediment	0.64 in Spring, 0.37 in Autumn	0.64 in Spring, 0.40 in Autumn				0.083 in Spring, 0.13in Autumn	Zheng 2009
Mengjin wetland, China		sediment	0-64.58						Xiao 2009
South coast of the Yangtze estuary, China	Autumn 2002	sediment	3.4-25.7	6.2-14.6					Liu 2008
Coastal wetland with high tidal ranges, Korea	Spring-Summer 1998	sediment (intertidal and subtidal)	0.0061-7.9 intertidal, 0.51-2 subtidal	0.11-0.84 intertidal, 0.68-1.8 subtidal	ND-0.22 intertidal, 0.014-0.023 subtidal			ND-3.1 intertidal, 0.24-10 subtidal	Kim 2010
Okinawa rivers of Okinawa wetland, Japan	Autumn 2005 to Summer 2006	surface sediment		12.3	2.6	ND	1.4		Imo 2007
Da-han River and Erh-jen River,Taiwan	Autumn 1997 to Spring 1998	sediment	0.21-8.81	0.57-14.1	0.12-5.8		0.05-0.15		Doong 2002
Chanthaburi River, eastern part of Thailand	Spring & Autumn 2006	surface sediment (0-5 cm)	0.1-28.2	0.5-49.5	0.1-8.3	0.4-13.0	0.1-8.3		Leadprathom 2009
Mekong River delta, South Vietnam	Autumn 2003, Summer 2004	sediment	<0.01-110	<0.02-1.3				<0.006-0.08	Minh 2007
Northeast coast of Vietnam	Spring 2003/2004	surface sediment	0.31-274	ND-0.85	ND-1.05		ND-0.03		Hong 2008
Eastern coast of Antarctica	Winter 1998	surface soil	0.11-1.22	0.86-4.69					Negoita 2003

* ΣDDTs - o,p'-DDD + o,p'-DDE + o,p'-DDT+ p,p'-DDE+ p,p'-DDT
ΣHCHs - (α- + β- + γ- + δ-) isomers
HEP - heptachlor
HEP-ox - heptachlorepoxide
HCB - hexachlorobenzene
** ND - Not detectable

5.4.6 Summary

The concentration and composition of *n*-alkanes, *n*-alkanols, *n*-alkanoic acids and sterols in surface sediments of the MM vary depending on the sampling site due to the various organic input and depositional environments. The organic compounds found in the modern plants are recognised in the surface sediments and can be used as proxies to reveal the source of OM. The analysis of concentration, composition and relevant proxies of *n*-alkanes, *n*-alkanols, *n*-alkanoic acids and sterols of the surface sediments all point to a mixed input of terrestrial plants (i.e., *Eucalyptus* spp.), aquatic plants (i.e. *Ranunculus* sp. and *Typha* sp.) and algae (i.e. *Chara australis*) to the OM; and comparatively, the higher plants have a greater input to the total OM.

Among all the compounds analysed, the *n*-alkane group seemed to be the most reliable and offered more information for discriminating various organic sources as well as the depositional environment. Their application can be summarised as: the CPI and OEP values allow the distinction between higher plants and algae; the ACL values may not vary much between samples but the small shift to a higher value is likely attributed to more terrestrial higher-plant input; the P_{aq} and P_{wax} are mainly indicative of the proportions of terrestrial, emergent and submerging plants; the C_{17}/C_{31} values indicate the abundance of algae and the C_{27}/C_{31} values indicate the relative abundance of trees/emergent plants and C_3 wetland grasses.

Coprostanol, a possible biomarker for bird guano was found in the surface sediments but its application is not promising, because it occurs in very low amounts and cannot be tracked uniquely to a source.

α-phellandrene, a biomarker from *Eucalyptus* spp., was detected in some of the surface sediments and will be applied to trace the vegetation change in the sediment cores.

Pyrogenic organic markers including PAHs were not found in detectable levels in the surface sediments and are not strong indicators of palaeofire. Perylene was the only one of the 18 PAHs analysed that is present in some of the surface sediments but it is considered to be derived from unburnt terrestrial higher plants.

OCPs, compounds that might indicate cotton-farming herbicide and pesticide residues, were not found in detectable levels in the surface sediments.

The analysis of organic markers in surface sediments showed that in the semi-arid Macquarie Marshes wetland system, the conventional organic marker *n*-alkanes worked well for studying the organic sources and their depositional environment. Accordingly, these are given prominence in the study of the MM sediment cores.

5.5 Analysis of sediment cores from the northern Marshes

Based on the results obtained from the study of surface sediments, the analysis of organic markers in the sediment cores will focus mainly on the northern marshes which has better vegetation cover and the sediments are more organic-rich.

The *n*-alkane data for core MMB3 was from a preliminary study and samples were analysed by Dr Jianfang Hu in the State Key Laboratory of Organic Geochemistry, Guangzhou Institute of Geochemistry, Chinese Academy of Science. The proxies of CPI, $(C_{27}+C_{29})/C_{31}$ and OEP (Figure 5.28) show a gradual change of vegetation in the watershed since the 1940s AD (when the construction of the Burrendong Dam occurred) – from algae and aquatic plant dominant to emergent and terrestrial plant dominant, suggesting a loss of wetland areas (Yu et al., 2011).

The other cores analysed in this thesis are LSW, LOLA and 2LOLA. Their *n*-alkane contents and relevant proxies (CPI, OEP, ACL, P_{aq}, P_{wax}, C_{17}/C_{31} and C_{27}/C_{31}) that may reflect the various vegetation types will be analysed to trace vegetation change. α-phellandrene, detected in some of the surface sediments as a specific biomarker for *Eucalyptus* spp., was also examined in the core profiles and its abundance was semi-quantified by GC.

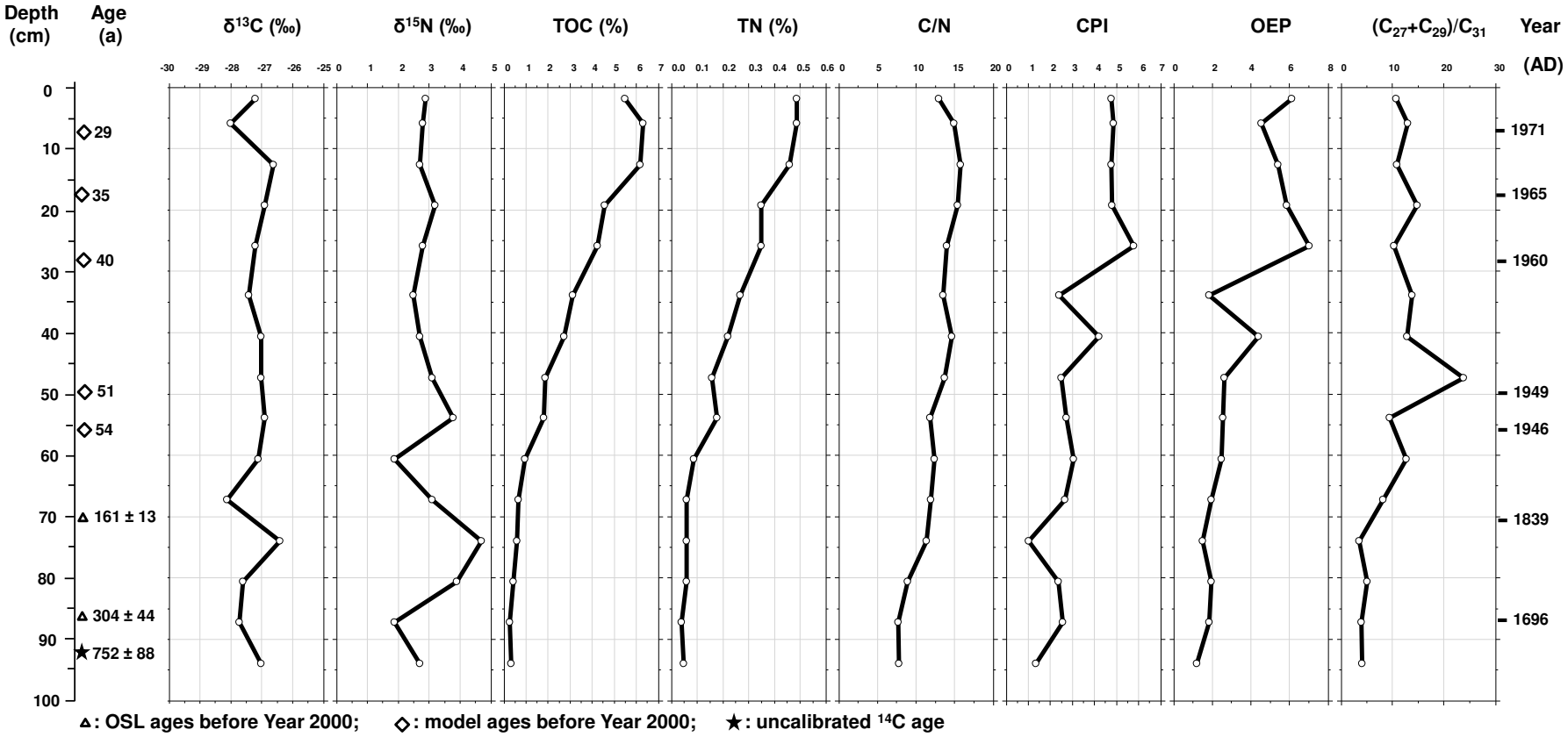

Figure 5.28. Bulk organic and *n*-alkane proxies for core MMB3.

5.5.1 Core LSW

The LSW profiles of the total *n*-alkanes and some proxies (Figure 5.29) show that the dry weight of total *n*-alkane (C_9-C_{33}) content increases towards the younger part of the core. However, when calculated based on the TOC values these *n*-alkanes reach a maximum at a core depth of ~ 53 cm (~1880 AD). Because this site had been inundated for a relatively long time, the *n*-alkane proxies will better reveal the OM source input. The CPI values are mostly between 1 and 5, indicating a mixed source of higher plants and algae in this site for a relatively long time (~ 1000 years). The OEP values are greater than 2 throughout the core, indicating odd over even carbon-number predominance. The highest CPI and OEP values occur at a depth of 15 cm (~2001 AD). The ACL values remain relatively constant around 26.5 from 82 cm to 45 cm and are greater than 28.0 above 30 cm in the core probably associated with greater input of terrestrial higher plants. The P_{aq} values generally increase from 82 cm to 77 cm, remain relatively stable, decrease sharply from 45 cm to 30 cm and remain relatively constant above 30 cm in the core. The trend of P_{wax} values appears to change antithetically to the P_{aq} values. The P_{aq} and P_{wax} values suggest a change from a submerged plant dominant ecosystem to an environment dominated by emergent and terrestrial plants, a shift likely driven by a change from wetter to drier conditions. The C_{17}/C_{31} and C_{27}/C_{31} values fluctuate along the core. Generally, the C_{17}/C_{31} values are higher in the older part of the core (53cm to 83 cm) while the C_{27}/C_{31} values are lower, indicating a larger input of aquatic and C_3 wetland grasses, indicating relatively wetter conditions for the pre-European period.

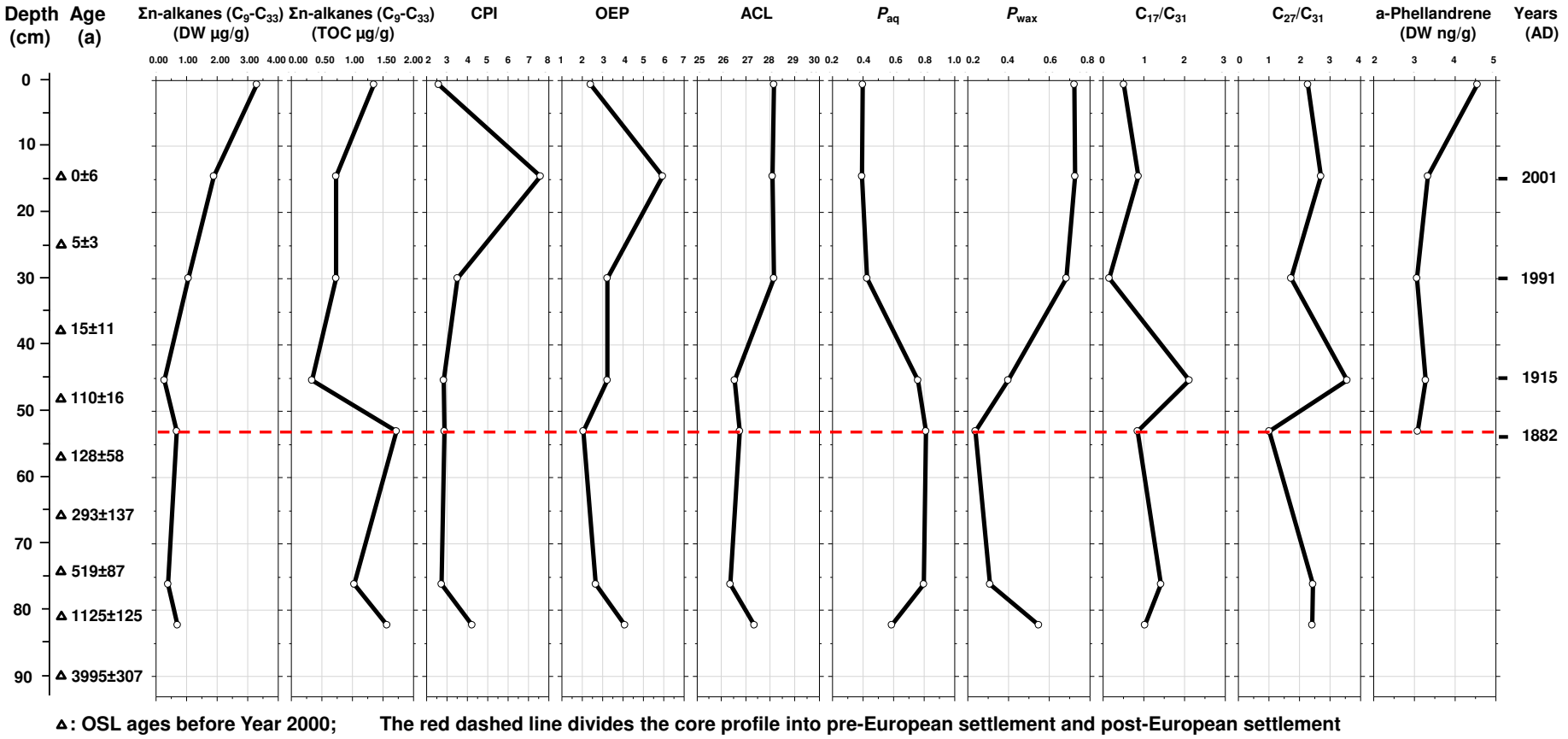

Figure 5.29. The *n*-alkane proxies for core LSW.

In general, the *n*-alkane proxies permit the distinction of two phases:

1) Pre-European settlement: Before European arrival (~ 1880 AD), the climate was relatively wet and this site was inundated with deep water which favoured the growth of aquatic plants/algae. This is shown by constant CPI, OEP values, relatively low ACL, P_{wax} and C_{27}/C_{31} values and high P_{aq} and C_{17}/C_{31} values. It also accords with the findings of the $\delta^{13}C$ and C/N values discussed in Chapter 3.

2) Post- European settlement: After European arrival (~ 1880 AD), there were more terrestrial higher plants (e.g. woodland vegetation like *Eucalyptus* spp.) growing in this site as indicated by shifts to higher ACL and P_{wax} values and lower P_{aq} values. The climate was relatively warmer and the water was shallower than before. It is likely that the frequency of inundation and the amount of water became less regular in the past ~100 years as recorded in the upper 45 cm of sediments. From 45 cm to 30 cm (~ 1915-1991 AD), a sharp decrease of P_{aq}, C_{17}/C_{31} and C_{27}/C_{31} values suggests a decrease of submerged (e.g. *Chara australis*) and emergent (e.g. *Phragmites australis*) plants; while the increase of P_{wax} values suggests the increase of drought-tolerant terrestrial higher plants (e.g. *Eucalyptus* spp.). Hogendyk (2007) described two dry phases in 1895-1946 AD and 1979 AD onwards that caused the decline of wetland vegetation and favoured the growth of drought-tolerant terrestrial plants. Despite the wet phase of 1947-1978 AD, the construction of upstream dams in the 1950s to 1970s greatly reduced the inflow of water to the Marshes (Kingsford and Johnson, 1998; Kingsford, 2000; Herron et al., 2002). From 30 cm to 15 cm (~ 1991-2001 AD), the slight increase of the C_{17}/C_{31} value is probably due to more aquatic plants resulting from three major floods, as recorded in 1990, 1998 and 2000 AD (Hogendyk, 2007). However, the terrestrial higher plants remained

dominant as shown by high P_{wax} and C_{27}/C_{31} values and low P_{aq} values. From 15 cm towards the younger part of the core (2001-2008 AD), the climate recorded is drier and there were fewer floods. The vegetation cover at this site is still dominated by terrestrial higher plants as shown by constant ACL, P_{aq} and P_{wax} values. The decrease of CPI, OEP, C_{17}/C_{31} and C_{27}/C_{31} values can probably be explained by accelerating degradation due to a lower water table during the dry years (Kvenvolden, 1970; Kuder and Kruge, 1998; Xie et al., 2004).

The compound α-phellandrene was not detected in the older part of the core (> 50 cm, i.e. older than ~ 1880 AD). Semi-quantification results (Figure 5.29, Page 316) showed this compound is present at this site since ~1880 AD, remained constant until 2000 AD and increasing in the most recent 10 years. The data reinforce the findings by *n*-alkane proxies discussed previously that terrestrial higher plants gradually replaced the wetland plants since ~ 1880s and were more dominant since the 1990s.

5.5.2 Core LOLA

Core LOLA profiles of the total *n*-alkanes and some proxies are shown in Figure 5.30 (Page 320). Similarly to core LSW, the total *n*-alkanes (dry weight) tended to increase from 0.17 to 3.57 μg/g (dry weight) towards the younger part of the core, in particular 7-fold from 18 cm to the surface. The total *n*-alkanes (TOC) also generally increased from 0.55 to 6.01 μg/g (TOC) towards the younger part of the core but fluctuated significantly along the core – two major peaks were found at depths of 185 cm and between 125 cm to 140 cm; followed by two small peaks at depths of 78 cm and 58 cm. The older sediments (>2 ka) have more organic input compared to the younger sediments (<2 ka). The trends of the CPI and OEP values are similar. The CPI values remain stable (1.50) from 183 cm

to 148 cm (~28.4 ka to 27.5 ka), then fluctuate between 2.36 to 5.47 up to 18 cm (~0.23 ka) and sharply increase to 7.64 near the core top. The OEP values remain relatively stable (1.17-1.42) from 183 cm to 148 cm (~28.4 ka to 27.5 ka), then fluctuate between 1.99 and 5.14 up to the top. The ACL values fluctuate between 25.8 to 29.1 along the core. The P_{aq} and P_{wax} values show opposed trends in the core profile. From 204 cm to 140 cm (> 27 ka) and 66 cm to 50 cm (~ 0.95 ka to 0.74 ka), the increase of the P_{aq} values and decrease of the P_{wax} values indicate more emergent, submerged and floating macrophytes to terrestrial plants. In contrast, from 140 cm to 66 cm (~27.5 ka to 0.95 ka) and 50 cm to the core top (~0.74 ka to present), the decrease of P_{aq} values and increase of P_{wax} values indicates more terrestrial plants to emergent, submerged and floating macrophytes. The C_{17}/C_{31} values fluctuate substantially along the core. Three high C_{17}/C_{31} values occur at 139 cm (0.80, age unknown), 123 cm (0.80, age unknown) and 2 cm (0.58, modern sediment) while there are two low values (0.06) at 51 cm (~0.74 ka) and 28 cm (~0.40 ka). The C_{27}/C_{31} fluctuates from 0.52 to 1.66 along the core.

Previous taxonomic study (APPENDIX B), inorganic geochemical and bulk C, N contents (Chapter 3) show the large hiatus between the Late Pleistocene and Late Holocene (~27.5 ka at 149 cm depth and ~ 2.29 ka at 108 cm) is barren of biological remains. The *n*-alkane proxies provide more information on the variation of the organic inputs to the sediments and allow the reconstruction of palaeovegetation change for the past ~ 50 ka in core LOLA, as follows.

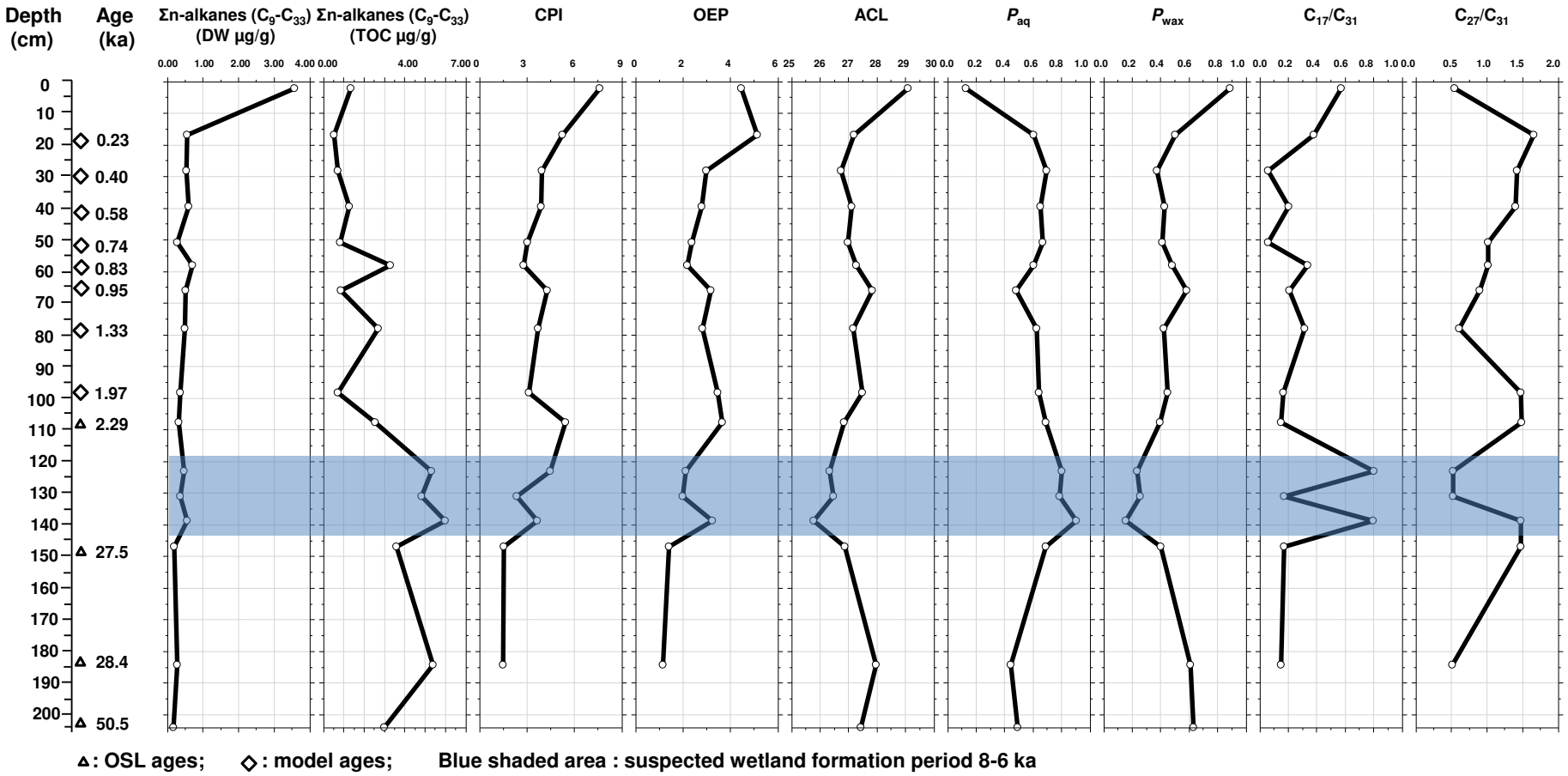

Figure 5.30. The *n*-alkane proxies for core LOLA.

From 208 cm to 185 cm (~50.5 to 28.4 ka), the P_{aq} and P_{wax} values indicate mixed vegetation types of submerged/emerging plants. Considering the modern marshes had not formed (Yonge and Hesse, 2009), it is likely this site used to be a deep-water lake inundated since ~ 50 ka. The active fluvial in MBD in this time span (Bowler, 1978) contributed to the high water level. However, the vegetation species may be different to modern ones as shown in the ACL values differentiating to the modern wetland plants and surface sediments.

From 185 cm to 146 cm (~28.5 to 27.5 ka), it is likely that a relatively warm and wet period was dominant as the P_{aq}, C_{17}/C_{31} and C_{27}/C_{31} values increased while the ACL and P_{wax} values decreased. The sediments are interpreted as being from palaeochannels (APPENDIX B), in agreement with the distinguishable fluvial history of the Macquarie catchment from 27-12 ka found by Watkins and Meakin (1996) and Young et al. (2002). This interpretation is also in agreement with studies from other Australian rivers which showed that more water was available during pre-Last Glacial Maximum time (~ 23 ka) (Magee et al., 1995). The vegetation types were likely mainly aquatic plants/algae. The shrub woodland vegetation type, modelled as predominant in the Last Glacial Maximum (LGM) for south-eastern Australia (Ray and Adams, 2001), may not have been present in this site.

Most of the proxies show distinctive peaks in the section from 146 cm to 108 cm where a hiatus in the sedimentation record occurs (from ~ 27.5 ka to 2.29 ka): the *n*-alkane contents (TOC) were at their highest; the ACL shifted to lower values (around 26.5) probably due to the input of algae/aquatic plants; the P_{aq} value reached very high values while the P_{wax} value was at its lowest; the C_{17}/C_{31} value reached its peaks with contributions from algae/aquatic plants; the C_{27}/C_{31} value also reached its lowest, likely

attributable to the input of C_3 wetland grasses (Seki et al., 2010). The wetland vegetation was probably different from the modern environment as the bulk $\delta^{13}C$ values (discussed in Chapter 3) were more negative and ACL values (around 26.5) were lower than the modern wetland plants and surface sediments. Flooding and blooming of aquatic plants/algae were probably at their highest of the whole record (dated back to 50.5 ka) as none of the proxies show similar values/trends in other parts of the core. The lithology (Chapter 3, Section 3.2.1) of this core also shows a change of sediment colour at ~ 123 cm. It is suspected the section between 140 to 120 cm represents the sediments deposited when the Macquarie Marshes were formed (8 to 6 ka) (Yonge and Hesse, 2009), and which were deposited on the palaeosediments. However this interpretation needs to be confirmed by more dating results and other proxies.

From 123 cm to 98 cm (unknown age to ~1.97 ka), it is estimated that the climate became relatively drier and there was less water available as indicated by the fluctuations of the *n*-alkane proxies. It is likely that the wetland plants/algae were largely replaced by drought-tolerant plants, which is also demonstrated by the shift of the bulk $\delta^{13}C$ value to the range of C_4 plants (discussed in Chapter 3). Desiccation is demonstrated by sub-aerial exposure via carbonate nodules, oxide mottling and organic debris. There is no similar record of dry climate in the MDB or southeastern rivers around 2 ka (e.g. Bowler, 1978; Tomkins and Hesse, 2004; Yonge and Hesse, 2009; Pietsch et al., 2013); however, a high salinity caused by the drought was recorded in the lake level work in western Victoria at 2.3 ka (Wilkins et al., 2013).

From 98 cm to 78 cm (~1.97 to 1.33 ka), a minor return to a relatively wet phase is shown by the increase of the *n*-alkane content (TOC), P_{wax} and C_{17}/C_{31} values as well as a decrease of OEP, ACL, P_{aq} and C_{27}/C_{31} values. This wet phase is also mirrored in the lake

level work in western Victoria (Wilkins et al., 2013). However, the wetland was not as prosperous as at 6-8 ka, as the ACL, P_{aq} and P_{wax} values are different from the wetland formation period.

From 78 cm to 17 cm (~1.33 to 0.23 ka), possible oscillations of dry and wet phases is recorded in the sediments by the fluctuation of the *n*-alkane proxies. It is likely that this site remained inundated during this period, as the P_{aq} values still indicate the dominance of aquatic plants. Because this lagoon functioned as lateral pondage receiving water only after other areas within the marshes had been inundated, the water table would fluctuate responding to the climate and affect the growth of different aquatic plant/algae species. Despite the oscillations of dry-wet phases, the vegetation types seemed to remain relatively constant as the CPI, OEP, ACL, P_{aq} and P_{wax} values were relatively constant. The relative abundance of various plants affected by the water table in this lagoon probably caused the variations of the *n*-alkane proxies. The fluctuation of the C_{17}/C_{31} values, in particularly two extremely low values (~ 0) observed at depths of 51 cm (~0.74 ka) and 28 cm (~0.40 ka), likely indicated the change of relative abundance of aquatic plants and terrestrial plants due to the sharp lowering of the water table during the dry period. The C_{27}/C_{31} values tend to increase upcore in this section, indicating the continuing decline of C_3 wetland grasses in this time interval.

From 17 cm to the core top (~0.23 ka to present), the increase of CPI, ACL and P_{wax} values and decrease of the P_{aq} values indicate more input of terrestrial higher plants to the OM during the last 100 years. As the climate was generally dry and warm in the past 100 years (Hogendyk, 2007), the increase of the C_{17}/C_{31} values was probably associated with the decline of C_3 wetland grass. The reason why the C_{27}/C_{31} values decreased in this time period still needs to be investigated.

5.5.3 Core 2LOLA

Compared to the neighbouring core LOLA, the organic profile of core 2LOLA is less variable (Figure 5.31). The total *n*-alkanes (dry weight) increase from 0.29 µg/g at 143 cm to 1.79 µg/g at 25 cm up core, with higher values to 27.0 µg/g at the top. The total *n*-alkane (TOC) profile is almost parallel, showing a relatively smaller range (0.41-3.76 µg/g TOC). Except for the two peaks at 100 cm and 15 cm, the CPI and OEP values are relatively stable. The ACL values decrease from 27.7 at 143 cm to 26.5 at 123 cm, fluctuate between 26.5 to 27.3 from 123 cm to 52 cm then increase to 28.7-29.6 in the upper 40 cm. The P_{aq} and P_{wax} values show the opposite trend in the core profile, generally indicating mixed non-emergent and emergent plants before 50-60 years ago and more terrestrial plants more recently. The C_{17}/C_{31} values show a peak of 0.80 at 123 cm and fluctuate between 0.02 and 0.34 in the other parts of the core. The C_{27}/C_{31} values range from 0.37 to 4.99 and show more fluctuation than the C_{17}/C_{31} values.

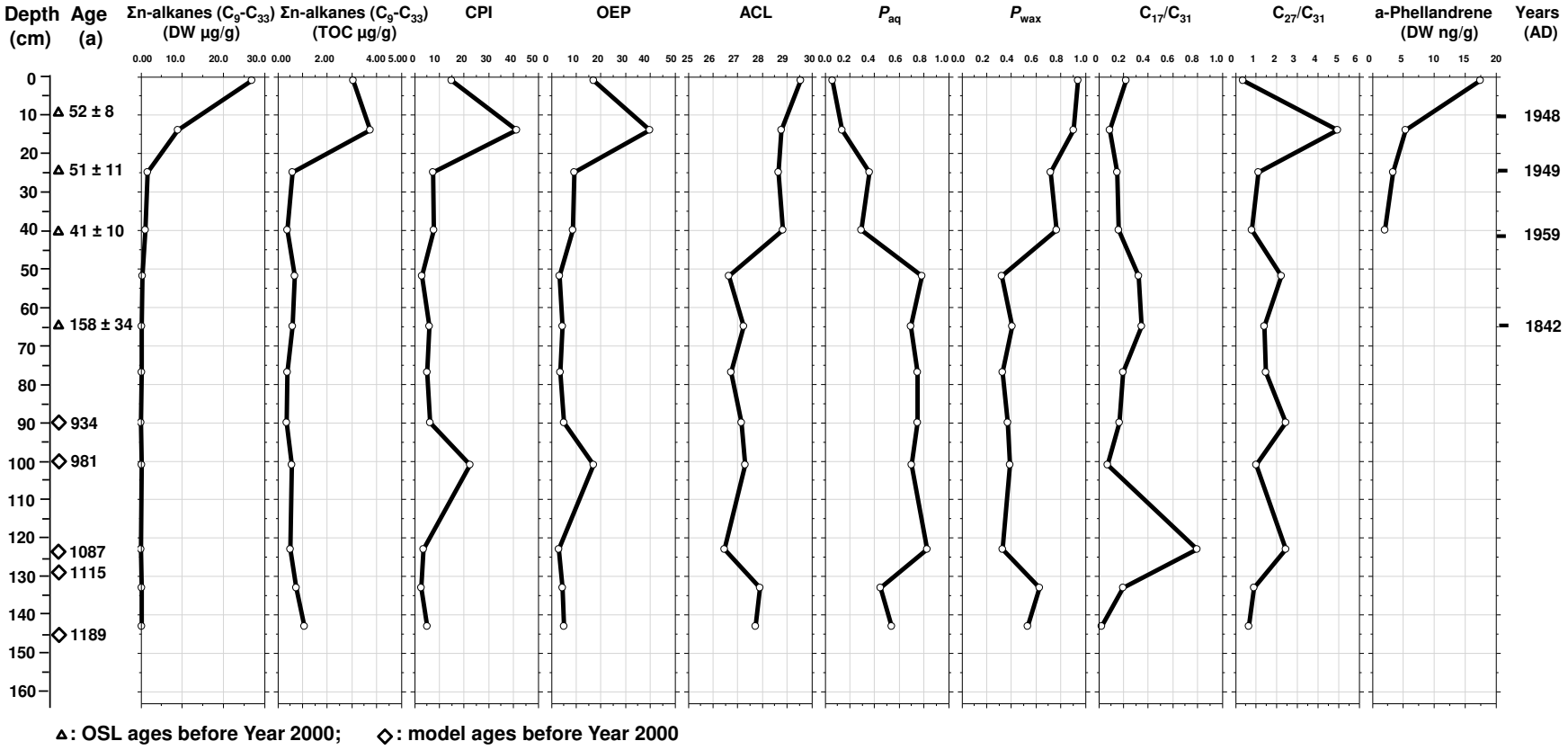

Figure 5.31. The *n*-alkane proxies for core 2LOLA.

Generally, the *n*-alkane profiles of core 2LOLA can be divided into two sections: from 143 cm to 52 cm represents a relatively wet phase when this site remained inundated; the upper 52 cm a relatively dry phase in the past 50-60 years with the invasion of higher terrestrial plants as indicated by an increase of the CPI, OEP, ACL, P_{wax} and C_{27}/C_{31} values;.

The profiles of the CPI, OEP, ACL, P_{aq} and P_{wax} proxies in core 2LOLA are similar to the upper 78 cm of core LOLA and the ages are comparable. The 143 cm to 90 cm section (~1.19 to 0.93 ka) in core 2LOLA resembles the relative wet phase in 80 cm to 60 cm section in core LOLA (~1.33 to 0.83 ka). From the hiatus section 90 cm to 65 cm (~0.93 to 0.16 ka), most of the *n*-alkane proxies are relatively constant indicating that this site has had a relatively constant vegetation mix. The sediments of core LOLA in this time period may provide a high-resolution record of the dry/wet phases. It is likely that there were significantly hydrological changes that caused the fluctuation of floods in the main water channel and of water tables of the lagoons in the margin depression areas of the marshes. However, these naturally occurring climate changes did not cause a severe decline of the wetland ecosystem as recorded in the sediments where the plant species remained relatively constant. Compared to core LOLA, core 2LOLA records more information for the past ~160 years in the upper 65 cm of its sediments. From 65 cm to 52 cm (~ 1840 AD to unknown year), most of the proxies remained relatively constant, indicating similar vegetation cover as those since ~ 1 ka. From 52 cm to 41 cm (unknown year - ~1960 AD), a change of wetland vegetation to more terrestrial plants is indicated by the large shift in *n*-alkane proxies. This is also demonstrated in core LSW. From 42 cm to 14 cm (1950s - 1960s), there was rapid sediment accumulation and an increase of the CPI, OEP and C_{27}/C_{31} values. These are indicative of a reduction in wetland plants which were

replaced by drought-tolerant terrestrial plants. For the upper 14 cm of sediments (~1950 AD onwards), the *n*-alkane proxies show various changes. The CPI, OEP and C_{27}/C_{31} values decrease sharply and the C_{17}/C_{31} values slightly increase, likely indicating a relative wetter environment. However the increase of ACL and P_{wax} values and decrease of P_{aq} values attributable to a larger input of terrestrial higher plants may be explained by the presence trees around the lagoon.

In the 2LOLA profiles (Figure 5.31, Page 325), α-phellandrene was completely absent below a core depth of ~ 40cm. This compound remained relatively constant from ~ 40 to 10 cm (~ 1950 AD) and increased significantly near the surface. It indicates that *Eucalyptus* spp. may only have started growing near this site in the 1950s. It reinforces the findings from the *n*-alkane proxies that this site had remained inundated with wetland plants since ~ 1 ka. Although terrestrial higher plants (e.g. *Eucalyptus* spp.) have been gradually replacing the wetland plants since European arrival (~ 1880s AD) as observed in other part of the marshes (cores MMB3 and LSW), they did not appear to be adjacent to this lagoon until the 1950s.

5.5.4 Carbon-13 compound-specific isotope analysis of the mid- to long-chain n-alkanes in core MMB3

Compound-specific isotope analysis generates isotopic data for individual compounds. Carbon compound-specific isotope analysis allows the separation of the isotopic signatures of various sources from the bulk OM, and thus discriminates C_3 or C_4 plant dominated ecosystems better and more precisely (Rieley et al., 1991b; Meyers, 1994; Lane et al., 2011). Identical $\delta^{13}C$ values of bulk OM could be interpreted as indicating a constant source for the sedimentary carbon, whereas the compound-specific $\delta^{13}C$ values

may indicate a difference in input over time (Rieley et al., 1991b). Analysing stable carbon-isotope of both bulk OM and specific organic compounds have been found to be particularly useful for reconstructing past terrestrial vegetation dynamics that may be responding to climate forcing (e.g. Meyers, 1994; Brincat et al., 2000; Lane et al., 2011). Moreover, stable carbon-isotopes can be used to detect increased drought stress in vegetation on a landscape scale if species assemblages remain fairly constant. The $\delta^{13}C$ value of terrestrial plant tissue typically increases by as much as 3-4 ‰ during periods of drought stress and leads to a shift in the average $\delta^{13}C$ value in OM in soils/sediments (Lane et al., 2011, and references therein).

In this thesis, the isotope composition of the mid-high chain *n*-alkane was analysed and discussed. As shown in Table 5.15, the $\delta^{13}C$ values of individual *n*-alkanes in the C_{23-33} range vary between -21.5 ‰ to -39.3 ‰, suggesting a mixed OM input, i.e. C_3 and C_4 plants, and algae (Rieley et al., 1991b; da Silva et al., 2008). This finding is also corroborated by the bulk $\delta^{13}C$, C/N values and the organic molecular markers discussed previously. The isotope values of the dominant *n*-alkanes (C_{23}-C_{33}) were more depleted in ^{13}C than those for the TOC, with offsets from 1.4 ‰ to 6.5 ‰ against the $\delta^{13}C_{TOC}$, probably due to biosynthetic fractionation (Hayes, 1993).

Table 5.15
Carbon-isotope data ($\delta^{13}C$ in ‰ vs V-PDB) for the bulk TOC and the individual mid to long-chain n-alkanes as a function of depth in core MMB3.

Depth (cm)	C_{TOC}	C_{23}	C_{24}	C_{25}	C_{26}	C_{27}	C_{28}	C_{29}	C_{30}	C_{31}	C_{32}	C_{33}
2	-27.2	-33.3	-31.9	-32.1	-32.6	-32.0	-32.2	-31.6	-31.5	-31.7		-26.2
6	-28.0	-32.5	-32.0	-31.1	-35.0	-31.4	-30.9	-31.5	-31.7	-31.3		-28.0
13	-26.6	-31.3	-30.4	-30.3	-30.6	-29.7	-30.3	-29.0	-31.3	-28.0	-26.7	-25.1
19	-26.9	-31.3	-30.4	-29.8	-30.8	-29.0	-29.1	-28.6	-30.5	-27.5	-31.2	-24.6
26	-27.2	-32.1	-30.8	-30.1	-30.3	-29.8	-32.4	-30.3	-31.9	-30.5	-39.3	-26.1
34	-27.4	-32.3	-29.7	-29.7	-29.7	-30.8	-34.8	-33.5	-32.5	-35.5		-33.5
41	-27.0	-32.6	-29.9	-29.8	-29.6	-30.9	-32.8	-32.9	-35.1	-35.0	-37.6	-33.2
47	-27.0	-32.8	-30.9	-30.3	-29.9	-30.8	-31.4	-32.5	-33.0	-34.4	-33.7	-32.1
54	-26.9	-34.2	-31.3	-30.8	-30.3	-30.9		-33.0				
61	-27.1	-35.8	-30.7	-30.0	-26.8	-30.5	-30.1	-32.9	-31.4	-34.1		
67	-28.1	-35.1	-30.3	-31.0	-30.4	-31.9	-32.5	-33.0		-34.2		
74	-26.4	-33.6	-31.7	-29.5		-29.8						
81	-27.6	-30.7	-29.1	-29.4	-21.5	-30.5						
87	-27.7	-34.3	-29.7	-27.8	-29.8	-30.7	-27.6	-31.0		-31.9		
94	-27.0	-31.0	-29.5	-30.0	-27.8	-29.0	-29.2	-31.8				
Average[a]	-27.2	-32.9	-30.5	-30.1	-29.6	-30.5	-31.1	-31.7	-32.1	-32.2	-33.7	-28.6
Δδ (‰)[b]	1.8	5.1	2.9	4.3	13.5	3.0	7.2	4.8	4.6	7.9	12.5	8.9

[a] Average=downcore averaged isotopic composition for individual n-alkanes.

[b] Δδ (‰)=maximum observed range of $\delta^{13}C$ values.

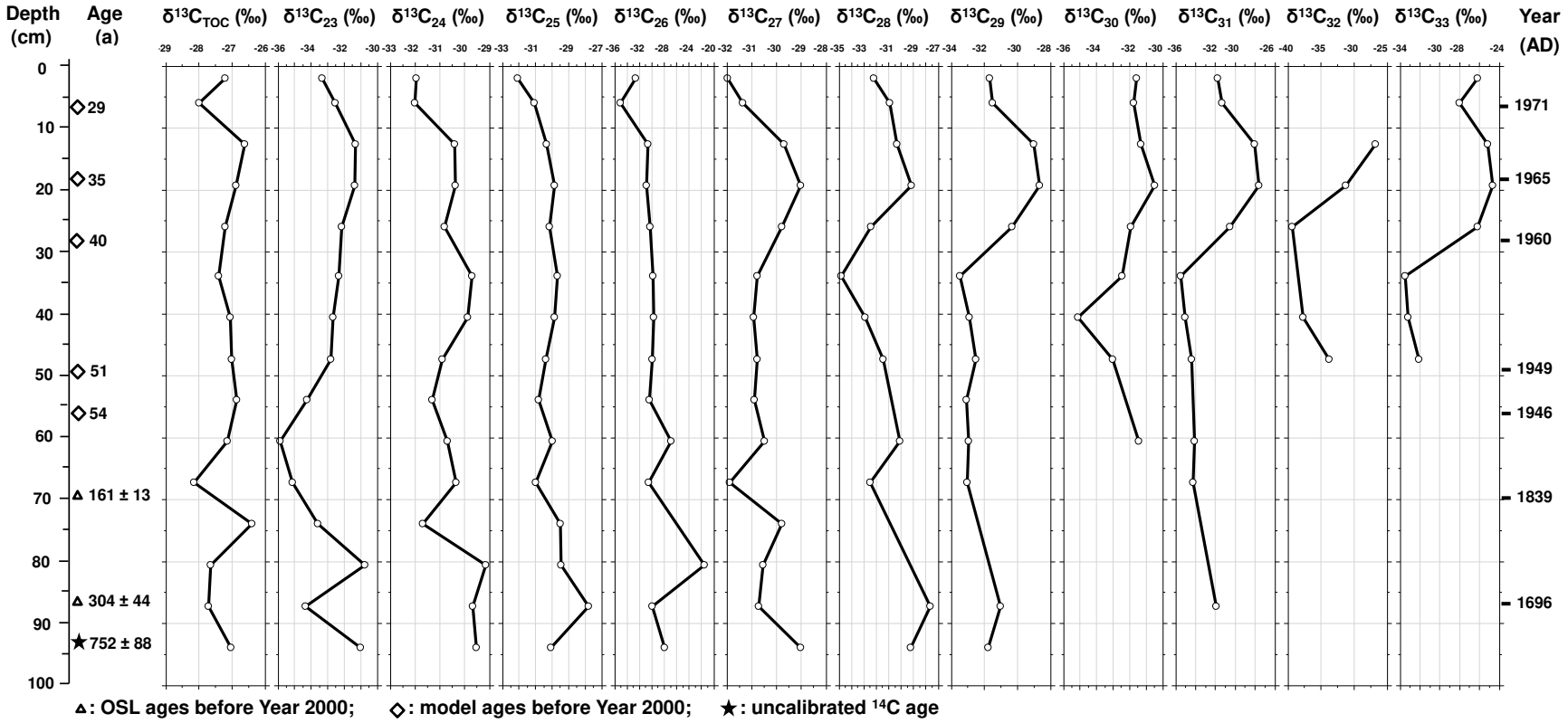

Figure 5.32. Carbon-isotope data ($\delta^{13}C$ in ‰ vs V-PDB) for the bulk TOC and the individual mid to long-chain *n*-alkanes as a function of depth in core MMB3.

The bulk $\delta^{13}C$ values (TOC) of core MMB3 display a range of 1.8 ‰, while those for each individual compound display ranges from 2.9 ‰ to 13.5 ‰ (Table 5.15, Page 329; Figure 5.32, Page 330). None of the individual compounds displays similar trends to each other, nor to the TOC $\delta^{13}C$ values, suggesting that they derive from more than one organic source. In the lower part from 93 cm to 20 cm (752 to 36 years old), the trend of C_{27}, C_{29} and C_{31} *n*-alkanes generally resemble that of the TOC. As the abundance of C_{27}, C_{29} and C_{31} *n*-alkanes reflects the input of vascular plants (Meyers, 2003), the resemblance of $\delta^{13}C$ values to TOC indicates their near-constant contributions to OM in the sediments before the construction of Burrendong dam (~ 50 years ago). In the upper 12 cm (<33 years old), the trend of C_{24} and C_{26} *n*-alkanes resembles that of the TOC.

From 93 to 26 cm, the decrease of $\delta^{13}C$ values (more ^{13}C depleted) with the increase of carbon chain length was only observed among C_{27} to C_{31} terrestrial-origin *n*-alkanes (Table 5.15, Page 329), a feature also noted in lake sediments (e.g. Rieley et al., 1991b; Brincat et al., 2000). In the upper 26 cm, the trend was opposite. This change also occurred around ~ 50 years ago at the construction of Burrendong Dam, indicating the impact of the dam to the deposition of OM.

The study by da Silva et al. (2008) found that the difference in isotope composition of odd to even *n*-alkanes in lacustrine sediments revealed different origins and occurred only during low lake levels, while no great difference was observed during high lake level. Here the $\delta^{13}C$ values of the long-chain *n*-alkanes ($C_{25\text{-}33}$) for some of the core sections (between 61 cm to 2 cm depth) are plotted in Figure 5.33. From 93-26 cm downward in the core, the *n*-alkane isotope patterns are irregular. The reason for that still needs to be investigated. In the upper 26 cm, the 'zig-zag' patterns is more apparent indicating that the odd carbon number *n*-alkanes are more enriched in ^{13}C than the even ones. According to

da Silva et al. (2008), this is probably due to low water levels and which, in the MM, corresponds to reduced water flow after the construction of Burrendong Dam.

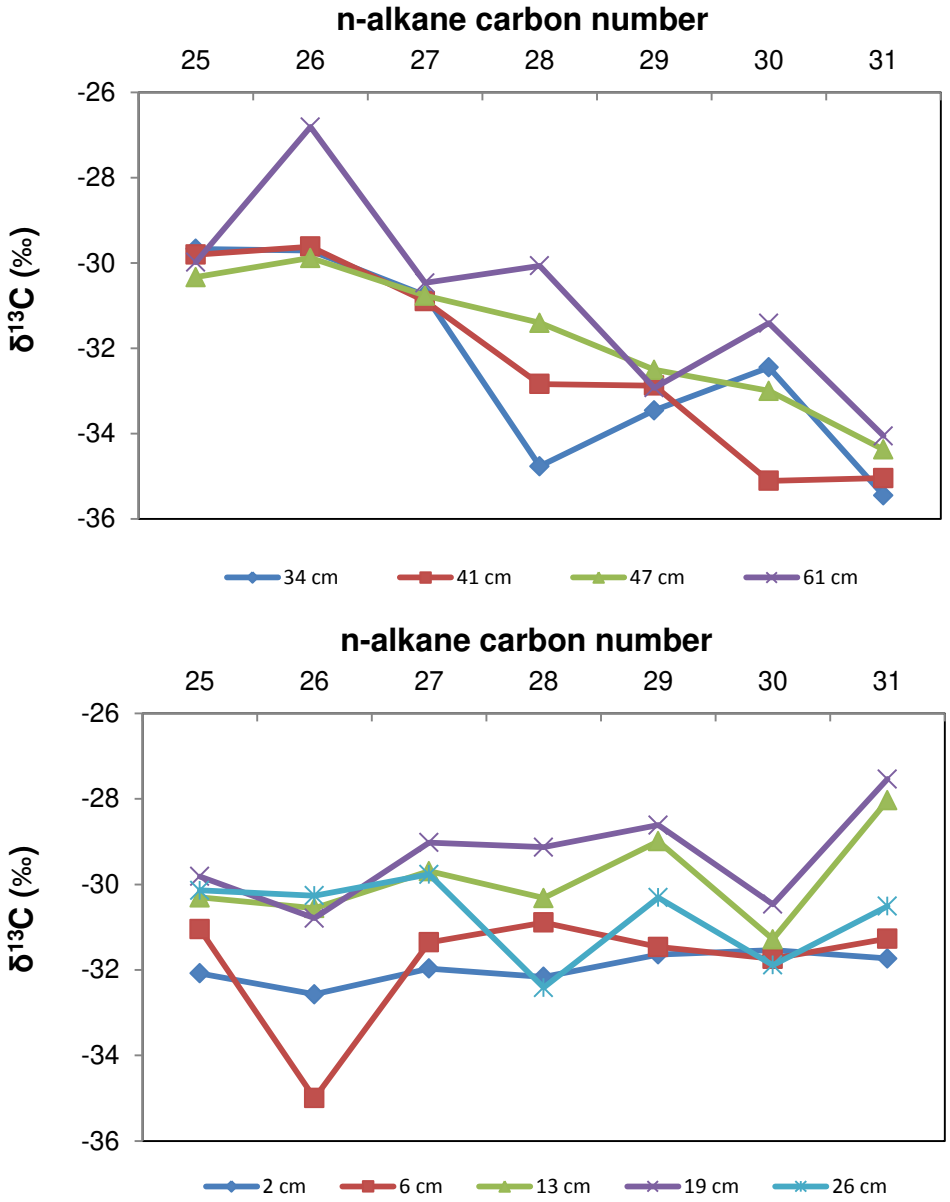

Figure 5.33. Long-chain *n*-alkane (C_{25-33}) $\delta^{13}C$ patterns in sediments from various depths within the core. (Top graph shows sediments from depths of 61-34 cm with irregular *n*-alkane $\delta^{13}C$ patterns; the lower graph shows sediments from depths of 26-2 cm with regular 'zig-zag' *n*-alkane $\delta^{13}C$ patterns)

A binary mixing model has been widely used where the plant community has undergone a change in the photosynthetic pathway of the dominant vegetation (Biedenbender et al., 2004 and reference therein):

$$\delta^{13}C_{meas}=x(\delta^{13}C_4)+(1-x)(\delta^{13}C_3)$$

where $\delta^{13}C_{meas}$ = measured $\delta^{13}C$ values, $\delta^{13}C_4$= $\delta^{13}C$ value for C_4 vegetation, $\delta^{13}C_3$= $\delta^{13}C$ value for C_3 vegetation, and x = proportion C_4 vegetation.

In this thesis, estimates of the relative abundance of C_3 and C_4 plants recorded in the sediment core were calculated based on the *n*-alkane compound-specific isotopic values. As the $\delta^{13}C$ value of *n*-alkanes in modern plants were not measured in this study, the endmenber values of -33.5 ‰ for C_3 vegetation and -24.9 ‰ for C_4 vegetation were chosen based on the data of C_4 grassland and C_3 woodland in central Queensland, Australia, with a semi-arid climate similar to the Macquarie Marshes (Krull et al., 2006). The $\delta^{13}C_{meas}$ value is the weighted average $\delta^{13}C$ values of the odd-numbered C_{27}-C_{31} *n*-alkanes, typical of terrestrial higher plants. For comparison, it was also calculated based on the bulk organic matter as the $\delta^{13}C_{meas}$ value, -35.2 ‰ for C_3 vegetation and -21.7 ‰ for C_4 vegetation (Rommerskirchen et al., 2006; Castañeda et al., 2009). The results are presented in Figure 5.34.

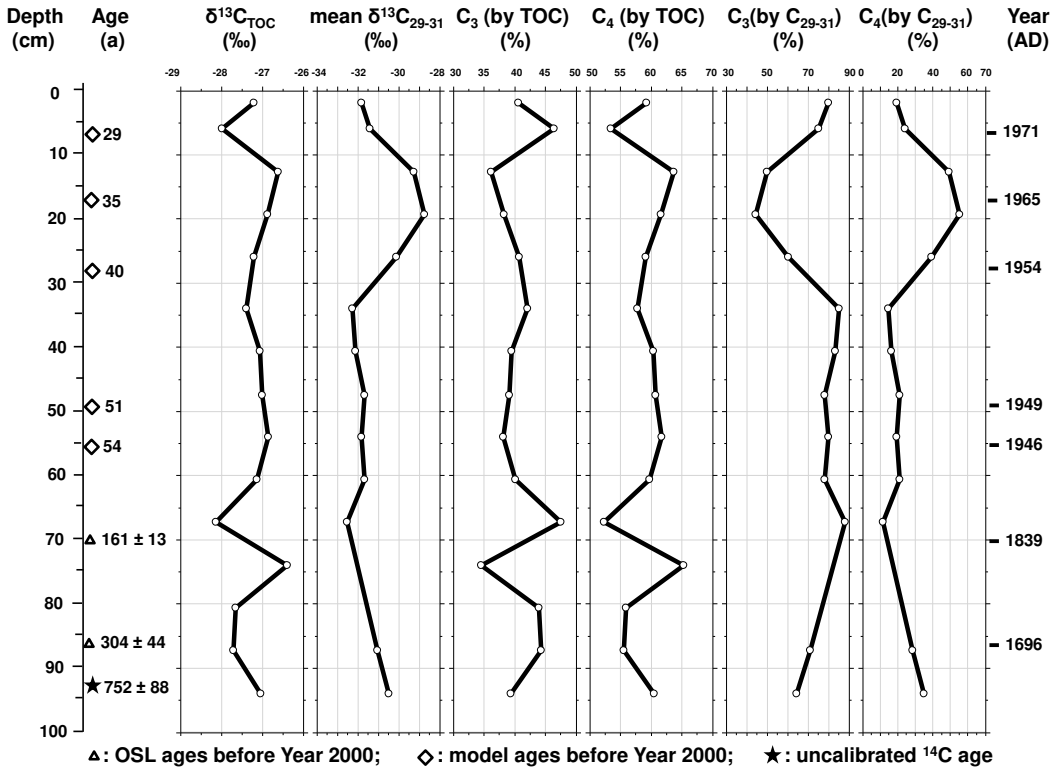

Figure 5.34. Core MMB3 profile of bulk organic isotope ($\delta^{13}C_{TOC}$), abundance-weighted average of $C_{29\text{-}31}$ *n*-alkanes (mean $\delta^{13}C_{29\text{-}31}$), the relative abundance of C_3 and C_4 calculated by TOC and by mean $\delta^{13}C_{29\text{-}31}$.

The trends of $\delta^{13}C_{TOC}$ and abundance-weighted mean $\delta^{13}C_{29\text{-}31}$ along core MMB3 are similar except for two sections. One is the top 6-2 cm where $\delta^{13}C_{TOC}$ increases and the mean $\delta^{13}C_{29\text{-}31}$ decreases; the other is in the interval 81-74 cm where the change of the mean $\delta^{13}C_{29\text{-}31}$ is unknown as two data points are missing. The similarity is probably due to the dominant input of *n*-alkanes from plants to the OM in the sediments. The proportion of C_3 plants calculated based on these two stable-isotope proxies show similar trends to each other and so does those of C_4 plants. However, the absolute abundances calculated by $\delta^{13}C_{TOC}$ and mean $\delta^{13}C_{29\text{-}31}$ values are offset by 14-44 % except at the depth of 19 cm where the values are similar (6 % offset). The proportion of C_3 plants calculated based on $\delta^{13}C_{TOC}$ value ranges from 35 % to 48 % (mean 41 %), indicating the dominance of C_4

plants over the ~300 years recorded in this core; the proportion of C_3 plants calculated based on abundance-weighted mean $\delta^{13}C_{29\text{-}31}$ values ranges from 45 % to 88 % (mean 72 %), suggesting a dominance of C_3 plants over the whole record. The dominant vegetation in the wetland ecosystems from historical records (Shelly, 2005) and present observations are C_3 wetland plants such as *Phragmites australis*, *Typha* sp., *Ranunculus* sp., and *Eucalyptus* spp.. Accordingly, the relative abundances of C_3 and C_4 plants calculated by the mean $\delta^{13}C_{29\text{-}31}$ are more reliable compared with those calculated by $\delta^{13}C_{TOC}$.

Based on the above analysis, the past C_3 and C_4 vegetation changes at this site can be interpreted as following. From 87 cm to 67 cm (~300 to 140 years ago), C_3 plants were increasing from 65 % to 88 % while C_4 plants were decreasing, indicating relatively more flooding of the marshes. From 67 cm to 34 cm (~140 to 43 years old), the C_3 plants reduced from ~ 90 % to ~ 80 % and fluctuated between ~ 80 % and 85 %. It indicated relatively more flooding of marshes. From 34 cm to 20 cm (~43 to 36 years old), the C_3 plants decreased sharply to 45 %. Because the climate was relatively wet during the past 30-62 years (Hogendyk, 2007), the reduction of C_3 plants and increase of C_4 plants is more likely affected by a drier depositional environment as the water flowing through the Marshes was greatly reduced after the construction of Burrendong dam ~ 50 years ago. The increase in C_3 plants in the upper 20 cm of the core did not explain a wet climate as it is recorded 'dry phase' in the past 30 years (Hogendyk, 2007). The reason for that needs to be further explored.

In conclusion, the specific carbon-isotope analysis of individual *n*-alkanes reinforces the findings by molecular biomarkers that wetland/woodland C_3 vegetation is the dominant contributor to the OM in the sediments, in particular using *n*-alkanes. The

variation of the individual *n*-alkane $\delta^{13}C$ values along core MMB3 indicate the variation of the wetland vegetation in response to natural dry/wet cycles as well as anthropogenic water regulation, which is associated with the construction of the Burrendong dam in the 1950s. Compared to the organic biomarkers, the specific carbon-isotope data permit semi-quantification of the relative abundances of C_3 and C_4 plants.

Studies of the hydrogen isotope composition (δD) of *n*-alkanes has the potential to indicate temperature, precipitation, relative humidity and hydrological cycles of the past, thus the combination of δD and $\delta^{13}C$ can provide better source information on biomarkers than single-element isotope analysis (Xie et al., 2004; Seki et al., 2010 and references therein). In future studies, it would be useful to obtain the δD values to better assess source and delivery processes of OM to the sediments.

It would also be useful in a future study to obtain compound-specific isotopic values on modern plants growing in the Marshes to assist in calculating their contributions to the OM.

5.5.5 Summary

The analysis of *n*-alkane proxies and α-phellandrene from the cores from the northern Macquarie Marshes provides a history of vegetation changes in the Marshes since ~ 50 ka. Despite variation in the modern environmental settings among these core sites, their data are complementary and permit generation of a history of the Marshes from before their formation, through to more detailed changes that occurred in the past 1000 years and in the post-European period.

The *n*-alkane proxies suggest that the site where the present Macquarie Marshes are had been inundated since ~ 50 ka and experienced dry/wet climate cycles during this time span. The high-resolution record obtained for the past 200 years provides information on the impact of both natural and anthropogenic changes in the Marshes and the response of vegetation associated with them.

- ~50.5 to 28.4 ka: The site was inudated and the vegetation was mainly submerged and emergent plants different to the modern species.
- ~28.4 to 27.5 ka: The relative warm and wet climate in particular in the pre-Last Glacial Maximum favoured the growth of aquatic plants/algae.
- ~27.5 to 2.29 ka: There is no clear record of this time interval due to the erosive (or non-depositional) hiatus in the sediments. However, the establishment of wetlands (8-6 ka) is suspected to be recorded in sections with the highest water table and the blooming of aquatic plants/algae, although the wetland plants were probably different from the modern ones.
- ~1.97 ka: A period of dryness as non-aquatic C_4 plants were observed in the sediments. It is likely that C_4 plants were introduced to the Marshes at this time.

- ~1.97 to 1.33 ka: There was a recovery with more water and associated aquatic plants. However, the wetland might not be as prosperous as at 8-6 ka.
- ~1.33 to 0.23 ka: There were oscillations s of dry-wet phases with variation of relative abundance of submerged and emergent plants. These naturally occurring climate or hydrological changes did not cause a decline of the wetland ecosystem as the record in the sediments shows that plant species abundance remained relatively constant.
- Post-settlement (~1880s AD): The introduction of terrestrial higher plants to the wetlands started about ~120 years ago (after European arrival in the 1880s) as recorded in the sediments in most of the cores. However, most of the wetland plants continued to survive (in particular in inundated depression areas like lagoons and swamps) until the 1950s. The proportions of C_3 plants calculated based on mean $\delta^{13}C_{29\text{-}31}$ *n*-alkane values in one core were ~ 80-90 %, indicating the dominance of C_3 plants after the European settlement.
- 1950s - 1970s AD: The construction of dams in the upper reaches of the Macquarie River have sharply reduced the water flowing into the wetlands and greatly accelerated the decline of wetland plants and animals. The wetland vegetation cover had been largely replaced by drought-tolerant terrestrial plants, as is seen today. The proportions of C_3 plants sharply reduced to 45%. Anthropogenic activities seemed to have a greater impact on the deterioration of wetlands than naturally occurring climate change.

CHAPTER 6 DISCUSSION, CONCLUSIONS AND FUTURE WORK

6.1 Discussion and conclusions

In this thesis, the combination of OSL dating results and several multi-proxy methods, in particular, lipid biomarkers, *n*-alkanes and α-phellandrene, have been successful in studying the sediments in the Macquarie Marshes. Results from four cores yield a coherent palaeoenvironmental history of the Marshes for the past ~ 50 ka.

1. Sedimentation

The age and lithology of the four cores are presented in Figure 6.1 (Page 341). The red lines divide the cores into 5 sections according to their ages (before Year 2000):

- section I (~ 50 ka to ~ 1 ka) representing the "palaeo-period";
- section II (~ 1 ka to ~ 180 a) representing the pre-European settlement period;
- section III (~ 180 a to ~ 50 a) representing the post-European settlement period;
- section IV (~ 50 a to ~ 30 a) representing the period after dam construction and water diversion; and,
- section V (~ 30 a and younger) representing the 'modern' environment.

Palaeoenvironmental information for section I is only available in core LOLA, a long-inundated lagoon away from the main watercourse; while those for sections II to V are better represented among the four cores and will generate a broader interpretation of the marshes.

The sedimentation rates estimated based on the ages vary depending on the environmental setting. In the lagoonal site (LOLA) which is less dynamic and tends to receive sediments only when flooded, the sedimentation rates are low and the ages are

older compared to sediments of other cores from the same depth. This is the case in the lower part of core LOLA with sediments older than ~ 1 ka. Although sedimentation rates vary at each sampling site, they generally decrease from section II to section III and to section V (Figure 6.1), probably due to reduction of floods. In section IV where the sediments were deposited during the construction of the dams and water diversion in the 1950s to 1970s, there is a higher sedimentation near the main watercourse (MMB3) compared to the lagoonal site (2LOLA and LOLA). As is well known, the flow into the marshes has been greatly reduced after the construction of the dam. The sediments deposited near the main watercourse are likely run-off from the construction sites upstream and the sites further from the main watercourse receive less sediment due to less frequent flood. There is an age hiatus in core LSW between ~ 118 a to 23 a so that information for section IV is missing.

The physical properties (i.e. colour, particle size) and geochemical parameters (i.e. C, N and major-/trace-elements) of the four cores also differ in each section, probably due to the different depositional environments. However, the OSL data show that the quartz extracted from these cores is typical of fluvial quartz that is not fully bleached before burial, indicating that this site has been inundated for much of the time since ~ 50 ka.

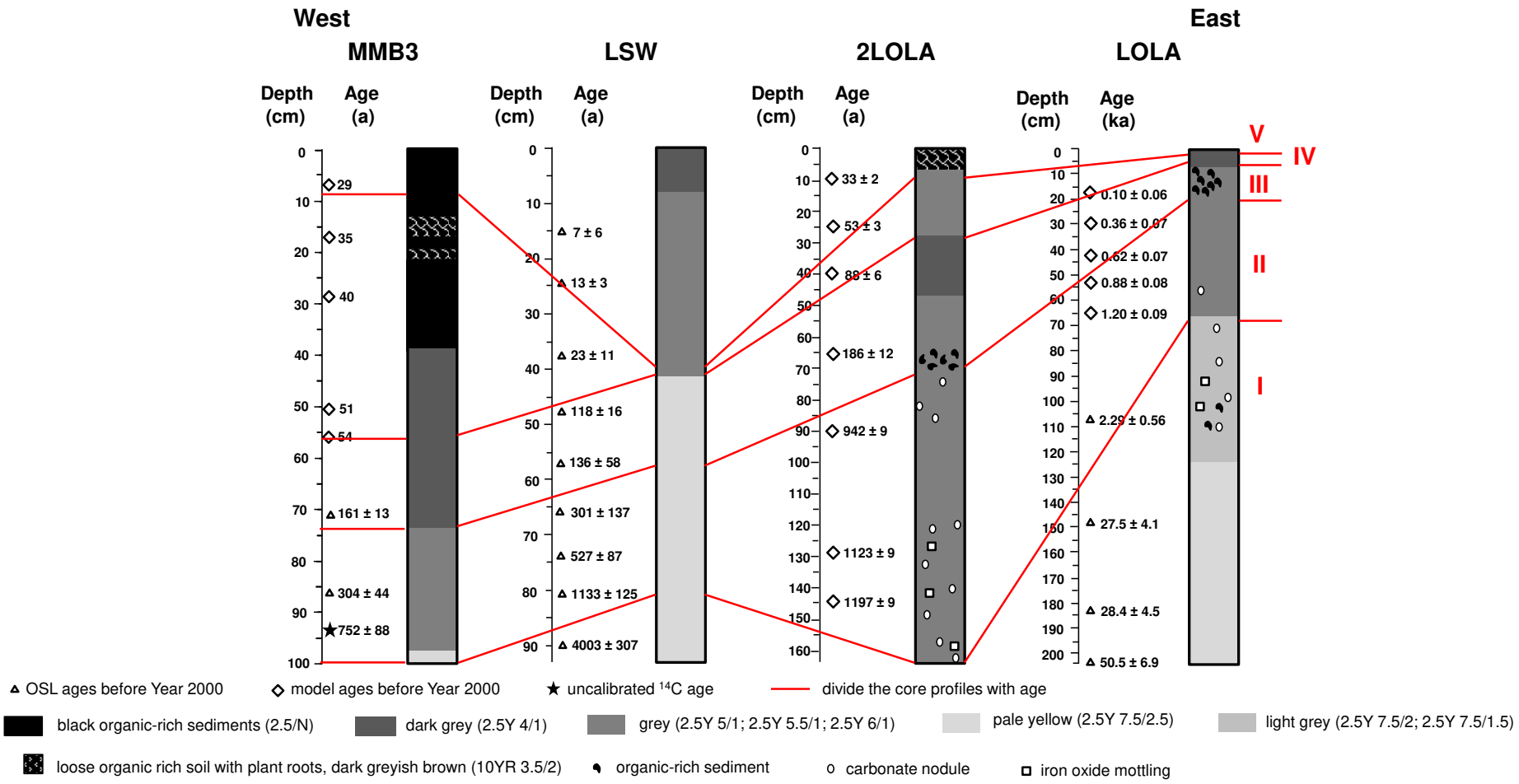

Figure 6.1. Lithology and ages of cores MMB3, LSW, 2LOLA and LOLA.

2. Vegetation

The n-alkane proxies CPI, OEP and ACL, which are indicative of vegetation types (i.e. algae/aquatic plants or terrestrial higher plants), are plotted for the four core profiles in Figure 6.2. The proxies in the palaeo-sediments (> ~ 1 ka) in section I of core LOLA generally indicate the abundance of algae and aquatic plants relative to inundation and wet environment. The fluctuation of the proxies in the age hiatus (~ 27.5 ka to 2.29 ka) is likely related to the formation of marshes. The presence of C_4 plants during the dry period around ~ 1.97 ka revealed by $\delta^{13}C$ values is also recorded here. The proxies in section II and the lower part of section III are similar among the four cores with CPI values less than 3, OEP ~ 2 to 3 and ACL ~ 26 to 27. It is likely that in this time period (~ 1 ka to ~ 180 a) the vegetation cover was mainly aquatic plants and algae and the marshes were inundated. The gradual shifts of the proxies to higher values were observed in most of the cores in section III indicating the introduction of higher plants after European arrival (~ 1880s AD). As shown in most of the cores, the most significant increase of these proxies occurred in section IV indicating that there were more terrestrial higher plants growing in the marshes in the 1950s – 1970s after the construction of the dams and water diversion. The vegetation cover after dam construction is variable in several sites in the marshes.

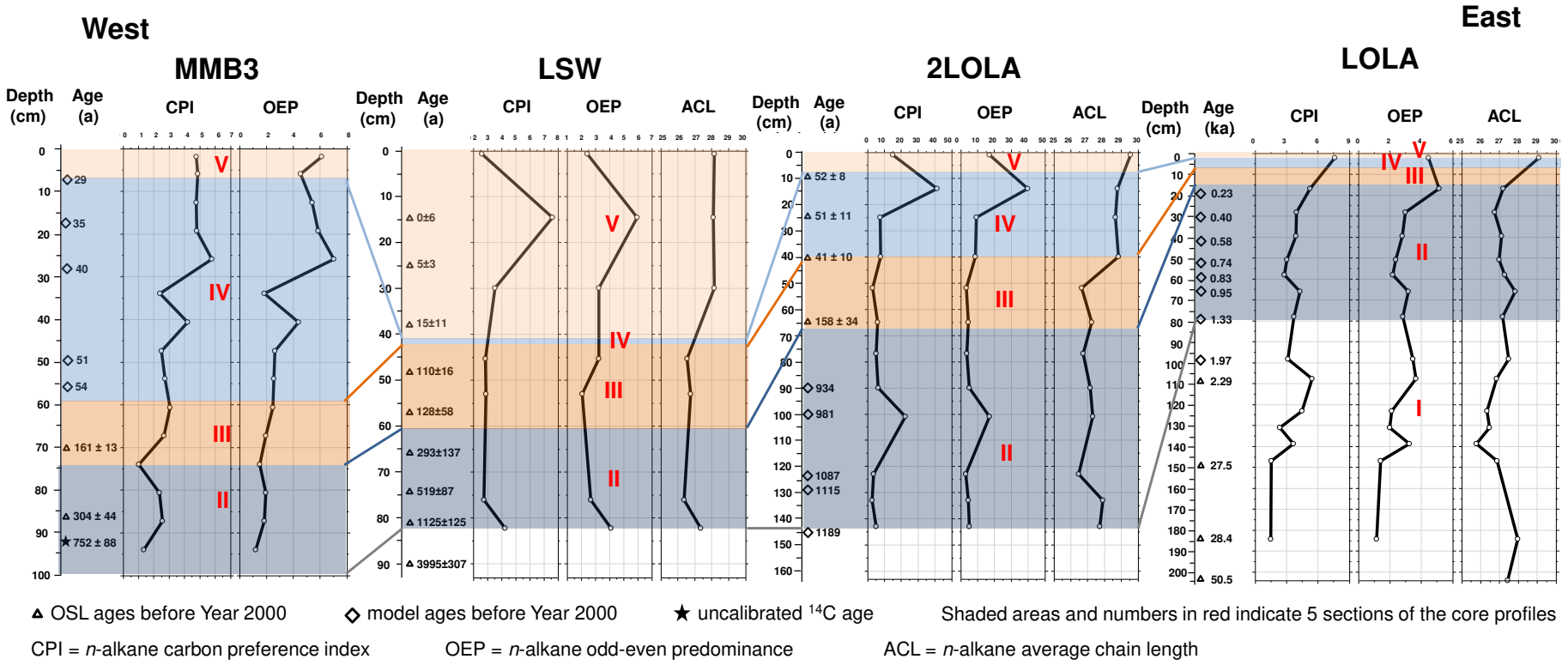

Figure 6.2. *n*-alkane proxy profiles for cores MMB3, LSW, 2LOLA and LOLA.

The *n*-alkane proxies P_{aq}, C_{17}/C_{31}, C_{27}/C_{31} and $(C_{27}+C_{29})/C_{31}$, which are indicative of the relative abundance of terrestrial, emergent and submerging plants, are plotted for the four core profiles in Figure 6.3 (Page 346). The profiles of α-phellandrene, indicative of *Eucalyptus* spp., are also plotted in the figure. These proxies in palaeo-sediments (> ~ 1 ka) in section I of core LOLA generally indicate the abundance of algae and aquatic plants relative to inundation and wet environment. The highest P_{aq} values and fluctuation of C_{17}/C_{31}, C_{27}/C_{31} values in the age hiatus (~ 27.5 ka to 2.29 ka) are likely related to the formation of marshes. The relatively high P_{aq} values (~ 0.6 to 0.8) in section II and in the lower part of section III are similar among the four cores while C_{17}/C_{31}, C_{27}/C_{31} and $(C_{27}+C_{29})/C_{31}$values fluctuated. It is likely that in this time period (~ 1 ka to ~ 180 a) the vegetation cover was mainly aquatic plants and algae and the marshes were inundated; however the relative abundance of algae, emergent and submerging plants differ in these sites depending on their environmental setting. The shifts of these proxies were observed in most of the cores in section III and the most significant changes are the decrease of P_{aq} values likely affected by the introduction of higher plants. It is also likely that the water level dropped after European arrival (~ 1880s AD). However, the wetland vegetation probably remained until the 1950s. In section IV, P_{aq} values sharply decreased to 0.2-0.4 in lagoonal sites away from the main stream, indicating a decrease in water levels and the shift away from dominant algae and submerged plants to emergent, terrestrial plants. This is likely driven by the changes from wetter to drier conditions due to the water diversion since the construction of the dams in the 1950s. The biomarker for *Eucalyptus* spp., is observed in the core collected near the main watercourse (core LSW) in section III (~ 1880s AD) but is only present in section IV in the core collected in the lagoon (core 2LOLA) away from the main stream since the 1950s. This reinforces the findings from the

n-alkane proxies discussed previously that terrestrial higher plants (i.e. *Eucalyptus* spp.) gradually replaced the wetland plants after European arrival (~ 1880s AD) and spread more broadly since the 1950s. The increase of this biomarker in section V is observed in both cores indicating the increasing abundance of terrestrial higher plants in the marshes in the 1990s.

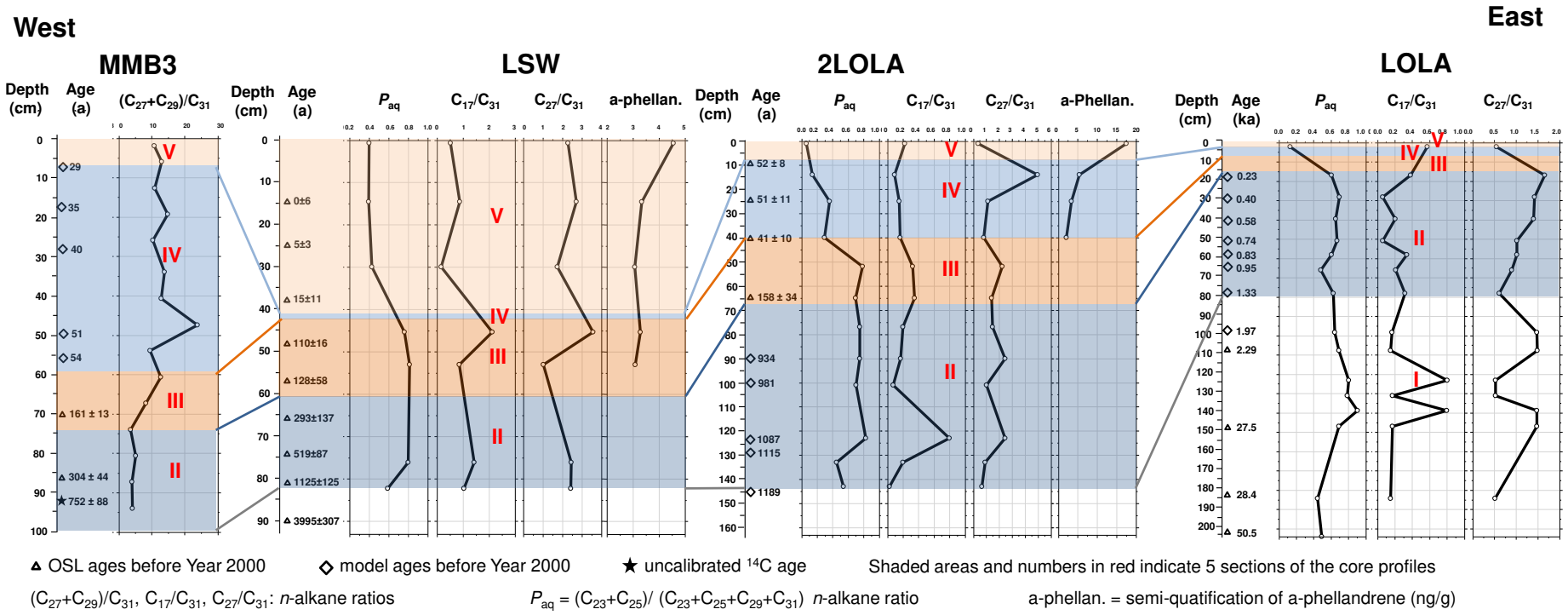

Figure 6.3. *n*-alkane proxies and α-phellandrene profiles of cores MMB3, LSW, 2LOLA and LOLA.

In general, the site where present Marshes are likely had been inundated since the late Pleistocene (prior to Aboriginal arrival, ~ 50 ka) and experienced dry/wet climate oscillations s during this time span. The vegetation types and their abundances varied with changes of water level responding to climate. There are several key milestones in the time span studied:

- 8 to 6 ka: Wetland plants did not appear in great abundance until the establishment of the Marshes in the mid-Holocene (Yonge and Hesse, 2009). The water level was highest, and the wetland plants (in particular aquatic plants/algae) probably different from the modern ones was also the most abundant in the record.
- ~ 1.97 ka: A period of dryness led to the introduction and growth of C_4 drought-tolerant plants in this area, similar to the findings of high salt and low lake level in western Victoria at 2.3 ka (Wilkins et al., 2013).
- ~1.33 to 0.23 ka: The wetlands experienced drastic climate fluctuations leading to the variation of water level and relative abundance of the vegetation types. However, these naturally occurring climate changes did not cause a severe decline of the wetland ecosystem and the wetland tended to self-recover.
- 1880s AD: After European arrival, terrestrial higher plants (i.e. *Eucalyptus* spp.) started growing with the wetland plants in the Marshes.
- 1950s to 1970s AD: Notable changes of vegetation occurred so that the wetland vegetation was largely replaced by drought-tolerant terrestrial plants as it appears today. As calculated by the *n*-alkane compound-specific isotope, C_3 plants reduced from ~ 80 % to ~45 %. The construction of the upstream dams have sharply reduced the water flowing into the wetlands and accelerated the decline of wetland

biota. Anthropogenic activities seem to have a much greater impact on the deterioration of wetlands than natural climate change.

- 1970s AD onwards: The wetlands were still declining due to the long-term drought (until 2011). The vegetation cover in the Marshes is dominated by terrestrial higher plants (woodland plants, e.g. *Eucalyptus* spp.) rather than wetland plants.

Although the Macquarie Marshes are still pristine regarding pesticides, the deterioration of the wetlands since European arrival (~ 120 years ago) is indicated by increasing terrestrial vegetation and diminishing aquatic biota.

To summarise, the three most important outcomes of this PhD project are:

1) Establishment of a very good chronology for environmental changes occurring in the MM during the last 50 ka (based on Optically Stimulated Luminescence);

2) Establishment of past vegetation changes based on organic geochemical proxies including TOC, *n*-alkanes and their numerical proxies, α-phellandrene, bulk and compound-specific *n*-alkane $\delta^{13}C$ stable isotope; and,

3) Assessment of natural and human-induced impacts on these wetlands.

6.2 Future work

Based on the results gathered, future work could be targeted:

- To collect and study more sediment cores from the perimeters of the Nature Reserve Marshes. This would allow a better coverage of the marshes and to 'map' the wetland areas responding to naturally occurring drought/flood in the long time scale. The anthropogenic impact (i.e. land clearing for agriculture usage) on the rapid shift of the primary organic producer in these cores will be more profound in the recent 200 years and will assist better underpin the direct human-induced changes.
- To collect and analyse more representative modern plant samples from the Macquarie Marshes. In particular, the analysis of compound-specific isotope data (e.g. *n*-alkane $\delta^{13}C$ stable isotope) will assist in the organic matter budgeting of various plant species.
- To obtain more detailed and direct information on palaeo-temperature, precipitation, relative humidity and hydrological variability by measuring the hydrogen isotope composition (δD) of *n*-alkanes combined with $\delta^{13}C$ data. These would allow a better assessment of the sources and delivery processes of organic matter to the sediments.

REFERENCES

Adamiec, G. & Aitken, M. 1998. Dose-rate conversion factors: update. *Ancient TL,* 16**,** 37-50.

Aitken, M. J. 1985. *Thermoluminescence Dating*, Academic Press.

Aitken, M. J. 1998. *An Introduction to Optical Dating: The Dating of Quaternary Sediments by the Use of Photon-Stimulated Luminescence*, Oxford University Press, USA

Aitken, M. J. & Smith, B. W. 1988. Optical dating: Recuperation after bleaching. *Quaternary Science Reviews,* 7**,** 387-393.

Andersson, R. A. & Meyers, P. A. 2012. Effect of climate change on delivery and degradation of lipid biomarkers in a Holocene peat sequence in the Eastern European Russian Arctic. *Organic Geochemistry,* 53**,** 63-72.

Armitage, S. J., Duller, G. a. T. & Wintle, A. G. 2000. Quartz from southern Africa: sensitivity changes as a result of thermal pretreatment. *Radiation Measurements,* 32**,** 571-577.

Arnold, L. J., Bailey, R. M. & Tucker, G. E. 2007. Statistical treatment of fluvial dose distributions from southern Colorado arroyo deposits. *Quaternary Geochronology,* 2**,** 162-167.

Arnold, L. J. & Roberts, R. G. 2009. Stochastic modelling of multi-grain equivalent dose (De) distributions: Implications for OSL dating of sediment mixtures. *Quaternary Geochronology,* 4**,** 204-230.

Arnold, L. J., Roberts, R. G., Galbraith, R. F. & Delong, S. B. 2009. A revised burial dose estimation procedure for optical dating of young and modern-age sediments. *Quaternary Geochronology,* 4**,** 306-325.

Arnold, L. J., Roberts, R. G., Macphee, R. D. E., Willerslev, E., Tikhonov, A. N. & Brock, F. 2008. Optical dating of perennially frozen deposits associated with preserved ancient plant and animal DNA in north-central Siberia. *Quaternary Geochronology,* 3**,** 114-136.

Bai, E., Boutton, T. W., Liu, F., Ben Wu, X. & Archer, S. R. 2012. Spatial patterns of soil $\delta^{13}C$ reveal grassland-to-woodland successional processes. *Organic Geochemistry,* 42**,** 1512-1518.

Bai, Y., Fang, X., Nie, J., Wang, Y. & Wu, F. 2009. A preliminary reconstruction of the paleoecological and paleoclimatic history of the Chinese Loess Plateau from the application of biomarkers. *Palaeogeography, Palaeoclimatology, Palaeoecology,* 271**,** 161-169.

Bailey, R. M. & Arnold, L. J. 2006. Statistical modelling of single grain quartz De distributions and an assessment of procedures for estimating burial dose. *Quaternary Science Reviews,* 25**,** 2475-2502.

Bailey, R. M., Smith, B. W. & Rhodes, E. J. 1997. Partial bleaching and the decay form characteristics of quartz OSL. *Radiation Measurements,* 27**,** 123-136.

Balek, C., L. 2002. Buried artifacts in stable upland sites and the role of bioturbation: A review. *Geoarchaeology,* 17**,** 41-51.

Ballarini, M., Wallinga, J., Murray, A. S., Van Heteren, S., Oost, A. P., Bos, A. J. J. & Van Eijk, C. W. E. 2003. Optical dating of young coastal dunes on a decadal time scale. *Quaternary Science Reviews,* 22**,** 1011-1017.

Ballarini, M., Wallinga, J., Wintle, A. G. & Bos, A. J. J. 2007. A modified SAR protocol for optical dating of individual grains from young quartz samples. *Radiation Measurements,* 42**,** 360-369.

Bateman, M. D., Boulter, C. H., Carr, A. S., Frederick, C. D., Peter, D. & Wilder, M. 2007a. Detecting post-depositional sediment disturbance in sandy deposits using optical luminescence. *Quaternary Geochronology,* 2**,** 57-64.

Bateman, M. D., Boulter, C. H., Carr, A. S., Frederick, C. D., Peter, D. & Wilder, M. 2007b. Preserving the palaeoenvironmental record in Drylands: Bioturbation and its significance for luminescence-derived chronologies. *Sedimentary Geology,* 195**,** 5-19.

Bender, M. M. 1971. Variations in the $^{13}C/^{12}C$ ratios of plants in relation to the pathway of photo-synthetic carbon dioxide fixation. *Phytochemistry,* 10, 1239-1244.

Bianchi, T. S. & Canuel, E. A. 2011. *Chemical Biomarkers in Aquatic Ecosystems,* New Jersey, Princeton University Press.

Biedenbender, S. H., McClaran, M. P., Quade, J. & Weltz, M. A. 2004. Landscape patterns of vegetation change indicated by soil carbon isotope composition. *Geoderma,* 119**,** 69-83.

Blatt, H., Middleton, G. & Murray, R. 1980. *Origin of sedimentary rocks*, Prentice-Hall, Inc.

Bond, W. J., Woodward, F. I. & Midgley, G. F. 2005. The global distribution of ecosystems in a world without fire. *New Phytologist,* 165**,** 525-538.

Bøtter-Jensen, L., Bulur, E., Duller, G. A. T. & Murray, A. S. 2000. Advances in luminescence instrument systems. *Radiation Measurements,* 32**,** 523-528.

Bøtter-Jensen, L., McKeever, S. W. S. & Wintle, A. G. 2003. *Optically Stimulated Luminescence Dosimetry*, Amsterdam; London Elsevier Science & Technology Books.

Bøtter-Jensen, L. & Mejdahl, V. 1985. Determination of potassium in feldspars by beta counting using a GM multicounter system. *Nuclear Tracks and Radiation Measurements,* 10**,** 663–666.

Boutton, T. W., Archer, S. R., Midwood, A. J., Zitzer, S. F. & Bol, R. 1998. δ13C values of soil organic carbon and their use in documenting vegetation change in a subtropical savanna ecosystem. *Geoderma,* 82**,** 5-41.

Bowler, J. M. 1978. Glacial and aeolian events in high and low latitudes: a Southern Hemisphere perspective. *Antarctic Glacial History and World Palaeoenvironments.* Balkema, Rotterdam, Taylor and Francis, pp. 149-172.

Bray, E. E. & Evans, E. D. 1961. Distribution of *n*-paraffins as a clue to recognition of source beds. *Geochimica et Cosmochimica Acta,* 22**,** 2-15.

Brereton, G. Salinity and watertables in the Macquarie Marshes. Macquarie Marshes Workshop 1994, Dubbo. Macquarie Marshes Total Catchment Management Subcommittee, 1-5.

Bridgham, S. D., Megonigal, J. P., Keller, J. K., Bliss, N. B. & Trettin, C. 2006. The carbon balance of North American wetlands. *Wetlands,* 26**,** 889-916.

Brincat, D., Yamada, K., Ishiwatari, R., Uemura, H. & Naraoka, H. 2000. Molecular-isotopic stratigraphy of long-chain *n*-alkanes in Lake Baikal Holocene and glacial age sediments. *Organic Geochemistry,* 31**,** 287-294.

Brock, F., Froese, D. G. & Roberts, R. G. 2010. Low temperature (LT) combustion of sediments does not necessarily provide accurate radiocarbon ages for site chronology. *Quaternary Geochronology,* 5**,** 625-630.

Brock, P. M. 1998. The significance of the physical environment of the Macquarie Marshes *Australian Geographer* 29**,** 71-90.

Brocks, J. J. & Schaeffer, P. 2008. Okenane, a biomarker for purple sulfur bacteria (Chromatiaceae), and other new carotenoid derivatives from the 1640 Ma Barney Creek Formation. *Geochimica et Cosmochimica Acta,* 72**,** 1396-1414.

Brodie, C. R., Casford, J. S. L., Lloyd, J. M., Leng, M. J., Heaton, T. H. E., Kendrick, C. P. & Yongqiang, Z. 2011. Evidence for bias in C/N, $\delta^{13}C$ and $\delta^{15}N$ values of bulk organic matter, and on environmental interpretation, from a lake sedimentary sequence by pre-analysis acid treatment methods. *Quaternary Science Reviews,* 30**,** 3076-3087.

Burt, J. S. & Ebell, G. F. 1995. Organic pollutants in mussels and sediments of the coastal waters off Perth, Western Australia. *Marine Pollution Bulletin,* 30**,** 723-732.

Castañeda, I. S., Mulitza, S., Schefuß, E., Lopes Dos Santos, R. A., Sinninghe Damsté, J. S. & Schouten, S. 2009. Wet phases in the Sahara/Sahel region and human migration patterns in North Africa. *Proceedings of the National Academy of Sciences*, USA.

Castañeda, I. S., Werne, J. P., Johnson, T. C. & Powers, L. A. 2011. Organic geochemical records from Lake Malawi (East Africa) of the last 700 years, part II: Biomarker evidence for recent changes in primary productivity. *Palaeogeography, Palaeoclimatology, Palaeoecology,* 303**,** 140-154.

Choudhary, P., Routh, J. & Chakrapani, G. J. 2009. An environmental record of changes in sedimentary organic matter from Lake Sattal in Kumaun Himalayas, India. *Science of The Total Environment,* 407**,** 2783-2795.

Conedera, M., Tinner, W., Neff, C., Meurer, M., Dickens, A. F. & Krebs, P. 2009. Reconstructing past fire regimes: methods, applications, and relevance to fire management and conservation. *Quaternary Science Reviews,* 28**,** 555-576.

Connell, D. W., Miller, G. & Anderson, S. 2002. Chlorohydrocarbon pesticides in the Australian marine environment after banning in the period from the 1970s to 1980s. *Marine Pollution Bulletin,* 45**,** 78-83.

Connell, D. W., Miller, G. J. & Anderson, S. M., 2007. Chapter 17 Persistent Organic Pollutants: Occurrence and Health Risks in Australia. *Developments in Environmental Sciences.* Elsevier, pp. 753-770.

Cotton Australia. 2008. *Australian Cotton History* [Online]. Cotton Australia. Available: http://www.cottonaustralia.com.au/facts/factsandfigures.aspx?id=21.

Craig, H. 1953. The geochemistry of the stable carbon isotopes. *Geochimica et Cosmochimica Acta*, 3, 53-92.

Cranwell, P. A. 1973a. Branched-chain and cyclopropanoid acids in a recent sediment. *Chemical Geology,* 11**,** 307-313.

Cranwell, P. A. 1973b. Chain-length distribution of *n*-alkanes from lake sediments in relation to post-glacial environmental change. *Freshwater Biology,* 3**,** 259-265.

Cranwell, P. A. 1974. Monocarboxylic acids in lake sediments: Indicators, derived from terrestrial and aquatic biota, of paleoenvironmental trophic levels. *Chemical Geology,* 14**,** 1-14.

Cranwell, P. A. 1984. Lipid geochemistry of sediments from Upton Broad, a small productive lake. *Organic Geochemistry,* 7**,** 25-37.

Cranwell, P. A., Eglinton, G. & Robinson, N. 1987. Lipids of aquatic organisms as potential contributors to lacustrine sediments-II. *Organic Geochemistry,* 11**,** 513-527.

Cull, V. 2007. *The Potential of Palaeogeological Techniques to investigate the use of the Macquarie Marshes by Colonial Breeding Waterbirds.* BSc (Hons) thesis, The University of New South Wales.

Cunningham, A. C. & Wallinga, J. 2009. Optically stimulated luminescence dating of young quartz using the fast component. *Radiation Measurements,* 44**,** 423-428.

da Silva, L. S. V., Piovano, E. L., Azevedo, D. D. A. & Aquino Neto, F. R. D. 2008. Quantitative evaluation of sedimentary organic matter from Laguna Mar Chiquita, Argentina. *Organic Geochemistry,* 39**,** 450-464.

Dachs, J., Bayona, J. M., Raoux, C. & Albaigés, J. 1997. Spatial, vertical distribution and budget of polycyclic aromatic hydrocarbons in the western Mediterranean seawater. *Environmental Science and Technology,* 31**,** 682-688.

David, B., Roberts, R., G. , Magee, J., Mialanes, J., Turney, C., Bird, M., White, C., Fifield, L. K. & Tibby, J. 2007. Sediment mixing at Nonda Rock: investigations of stratigraphic integrity at an early archaeological site in northern Australia and implications for the human colonisation of the continent. *Journal of Quaternary Science,* 22**,** 449-479.

DECC 2009. Draft Macquarie Marshes Adaptive Environmental Management Plan -- Synthesis of information projects and actions. Department of Environment and Climate Change NSW.

Delong, S. B. & Arnold, L. J. 2007. Dating alluvial deposits with optically stimulated luminescence, AMS ^{14}C and cosmogenic techniques, western Transverse Ranges, California, USA. *Quaternary Geochronology,* 2**,** 129-136.

Demuro, M. 2009. *Optically stimulated luminescence dating of tephra-bearing deposits from eastern Beringia.* PhD thesis, University of Wollongong.

DLWC 1996. A preliminary spatial assessment of current conditions and change within the Macquarie Marshes Wetland Subsystem. *The Macquarie Marshes Scientific Workshop 1996.* NSW Department of Land and Water Conservation.

DLWC 2000. A Review of Recent Studies Investigating Biological and Physical Processes in the Macquarie Marshes, NSW. Department of Land and Water Conservation.

DLWC & NPWS 1996. Macquarie Marshes Water Management Plan 1996, Sydney. Department of Land and Water Conservation and National Parks and Wildlife Service.

Dodd, A. N., Borland, A. M., Haslam, R. P., Griffiths, H. & Maxwell, K. 2002. Crassulacean acid metabolism: plastic, fantastic. *Journal of Experimental Botany* 53**,** 569-580.

Doong, R.-A., Sun, Y.-C., Liao, P.-L., Peng, C.-K. & Wu, S.-C. 2002. Distribution and fate of organochlorine pesticide residues in sediments from selected rivers in Taiwan. *Chemosphere,* 48**,** 237-246.

Driver, P. & Knight, C. 2007. Macquarie Marshes 2005 Environmental Flow Release. Report on observations and preliminary analyses of the responses of groundcover plants to environmental flows.

Duan, Y. 2000. Organic geochemistry of recent marine sediments from the Nansha Sea, China. *Organic Geochemistry*, 31, 159-167.

Duan, Y. & Ma, L. 2001. Lipid geochemistry in a sediment core from Ruoergai Marsh deposit (Eastern Qinghai-Tibet plateau, China). *Organic Geochemistry,* 32**,** 1429-1442.

Duller, G. A. T. 2003. Distinguishing quartz and feldspar in single grain luminescence measurements. *Radiation Measurements,* 37**,** 161-165.
DWR & NPWS 1986. Water Management Plan for the Macquarie Marshes, Sydney. Department of Water Resources and National Parks and Wildlife Service.
Eastwood, K. 2013. Flood of fortune. *Australian Geographic,* March-April**,** 30-34.
Eglinton, G. & Hamilton, R. J. 1967. Leaf epicuticular waxes. *Science,* 156**,** 1322-1334.
Erwin, K. L. 2009. Wetlands and global climate change: The role of wetland restoration in a changing world. *Wetlands Ecology and Management,* 17**,** 71-84.
Feakins, S. J., Eglinton, T. I. & Demenocal, P. B. 2007. A comparison of biomarker records of northeast African vegetation from lacustrine and marine sediments (ca. 3.40 Ma). *Organic Geochemistry,* 38**,** 1607-1624.
Feathers, J. 2008. Luminescence Dating. *Encyclopedia of Archaeology.* New York: Academic Press.
Fernandes, M. B., Elias, V. O., Cardoso, J. N. & Carvalho, M. S. 1999. Sources and fate of n-alkanols and sterols in sediments of the Amazon shelf. *Organic Geochemistry*, 30, 1075-1087.
Ficken, K. J., Street-Perrott, F. A., Perrott, R. A., Swain, D. L., Olago, D. O. & Eglinton, G. 1998. Glacial/interglacial variations in carbon cycling revealed by molecular and isotope stratigraphy of Lake Nkunga, Mt. Kenya, East Africa. *Organic Geochemistry,* 29**,** 1701-1719.
Ficken, K. J., Li, B., Swain, D. L. & Eglinton, G. 2000. An *n*-alkane proxy for the sedimentary input of submerged/floating freshwater aquatic macrophytes. *Organic Geochemistry,* 31**,** 745-749.
Finkel, E. & Normile, D. 2012. River Basin Management Plan Secures Water for the Environment. *Science,* 338**,** 1273-1274.
Fisher, E., Oldfield, F., Wake, R., Boyle, J., Appleby, P. & Wolff, G. A. 2003. Molecular marker records of land use change. *Organic Geochemistry,* 34**,** 105-119.
Folz, E., Bodu, P., Bonte, P., Joron, J.-L., Mercier, N. & Reyss, J.-L. 2001. OSL dating of fluvial quartz from Le Closeau, a Late Paleolithic site near Paris -- comparison with ^{14}C chronology. *Quaternary Science Reviews,* 20**,** 927-933.
Fu, S., Chu, S. & Xu, X. 2001. Organochlorine pesticide residue in soils from Tibet, China. *Bulletin of Environmental Contamination and Toxicology,* 66**,** 171-177.
Fuchs, M. & Owen, L. A. 2008. Luminescence dating of glacial and associated sediments: review, recommendations and future directions. *Boreas,* 37**,** 636-659.
Gabos, S., Ikonomou, M. G., Schopflocher, D., Fowler, B. R., White, J., Prepas, E., Prince, D. & Chen, W. 2001. Characteristics of PAHs, PCDD/Fs and PCBs in sediment following forest fires in northern Alberta. *Chemosphere,* 43**,** 709-719.
Galbraith, R. 2010. On plotting OSL equivalent dose estimates. *Ancient TL,* 28**,** 1-9.
Galbraith, R. F. 1988. Graphical display of estimates having differing standard errors. *Technometrics,* 30**,** 71-81.
Galbraith, R. F. & Green, P. F. 1990. Estimating the component ages in a finite mixture. *International Journal of Radiation Applications and Instrumentation. Part D. Nuclear Tracks and Radiation Measurements,* 17**,** 197-206.
Galbraith, R. F. & Laslett, G. M. 1993. Statistical models for mixed fission track ages. *Nuclear Tracks and Radiation Measurements,* 21**,** 459-470.
Galbraith, R. F., Roberts, R. G., Laslett, G. M., Yoshida, H. & Olley, J. M. 1999. Optical dating of single and multiple grains of quartz from Jinmium Rock Shelter, northern Australia: Part I, Experimental design and statistical models. *Archaeometry,* 41**,** 339-364.
Gale, S. J. 2009. Dating the recent past. *Quaternary Geochronology*, 4, 374-377.

Galpi, H., Schneider, J. & Mann, J. O. 1970. Hydrocarbons of geochemical significance in microscopic algae. *Phytochemistry,* 9**,** 603-612.

Gogou, A. & Stephanou, E. G. 2004. Marine organic geochemistry of the Eastern Mediterranean: 2. Polar biomarkers in Cretan Sea surficial sediments. *Marine Chemistry,* 85**,** 1-25.

Götze, J., Plötze, M. & Habermann, D. 2001. Origin, spectral characteristics and practical applications of the cathodoluminescence (CL) of quartz – a review. *Mineralogy and Petrology,* 71**,** 225-250.

Greenbaum, N., Schick, A. P. & Baker, V. R. 2000. The palaeoflood record of a hyperarid catchment, Nahal Zin, Negev Desert, Israel. *Earth Surface Processes and Landforms,* 25**,** 951-971.

Grimalt, J. O., Fernandez, P., Bayona, J. M. & Albaiges, J. 1990. Assessment of fecal sterols and ketones as indicators of urban sewage inputs to coastal waters. *Environmental Science and Technology,* 24**,** 357-363.

Håkanson, L. & Jansson, M. 1983. *Principles of Lake Sedimentology,* Berlin, Springer-Verlag.

Hall, K. C., Baldwin, D. S., Rees, G. N. & Richardson, A. J. 2006. Distribution of inland wetlands with sulfidic sediments in the Murray-Darling Basin, Australia. *Science of The Total Environment,* 370**,** 235-244.

Harvey, R. G. 1991. *Polycyclic Aromatic Hydrocarbons,* Cambridge, USA, Cambridge University Press.

Hatfield, R. G., Cioppa, M. T. & Trenhaile, A. S. 2010. Sediment sorting and beach erosion along a coastal foreland: Magnetic measurements in Point Pelee National Park, Ontario, Canada. *Sedimentary Geology,* 231**,** 63-73.

Hautevelle, Y., Michels, R., Malartre, F. & Trouiller, A. 2006. Vascular plant biomarkers as proxies for palaeoflora and palaeoclimatic changes at the Dogger/Malm transition of the Paris Basin (France). *Organic Geochemistry,* 37**,** 610-625.

Hayes, J. M. 1993. Factors controlling ^{13}C contents of sedimentary organic compounds: Principles and evidence. *Marine Geology,* 113**,** 111-125.

Haynes, D., Müller, J. & Carter, S. 2000. Pesticide and herbicide residues in sediments and seagrasses from the Great Barrier Reef World Heritage Area and Queensland coast. *Marine Pollution Bulletin,* 41**,** 279-287.

Hedges, J. I. & Prahl, F. G. 1993. Early diagenesis: consequences for appplications of molecular biomarkers. *Organic Geochemistry: principles and applications*, Plenum Press, New York, pp. 237-253.

Heimsath, A. M., Chappell, J., Spooner, N. A. & Questiaux, D. G. 2002. Creeping soil. *Geology,* 30**,** 111-114.

Herron, N., Davis, R. & Jones, R. 2002. The effects of large-scale afforestation and climate change on water allocation in the Macquarie River catchment, NSW, Australia. *Journal of Environmental Management,* 65**,** 369-381.

Hesse, P. P., Magee, J. W. & van der Kaars, S. 2004. Late Quaternary climates of the Australian arid zone: a review. *Quaternary International,* 118–119**,** 87-102.

Hjülstrom, F. 1935. Studies of the morphological activity of rivers as illustrated by the River Fyris. *Bulletin of the. Geological Institute University of Uppsala,* 25, 227-346.

Hogendyk, G. 2007. *The Macquarie Marshes: An Ecological History,* pp.11-36.

Hong, S. H., Yim, U. H., Shim, W. J., Oh, J. R., Viet, P. H. & Park, P. S. 2008. Persistent organochlorine residues in estuarine and marine sediments from Ha Long Bay, Hai Phong Bay, and Ba Lat Estuary, Vietnam. *Chemosphere,* 72**,** 1193-1202.

Hormes, A., Blaauw, M., Dahl, S. O., Nesje, A. & Possnert, G. 2009. Radiocarbon wiggle-match dating of proglacial lake sediments – Implications for the 8.2 ka event. *Quaternary Geochronology,* 4**,** 267-277.

Hu, G., Zhang, J.-F., Qiu, W.-L. & Zhou, L.-P. 2010. Residual OSL signals in modern fluvial sediments from the Yellow River (Huang He) and the implications for dating young sediments. *Quaternary Geochronology,* 5**,** 187-193.

Hu, J., Peng, P. A. & Chivas, A. R. 2009. Molecular biomarker evidence of origins and transport of organic matter in sediments of the Pearl River estuary and adjacent South China Sea. *Applied Geochemistry,* 24**,** 1666-1676.

Hu, J., Zhang, H. & Peng, P. A. 2006. Fatty acid composition of surface sediments in the subtropical Pearl River estuary and adjacent shelf, Southern China. *Estuarine, Coastal and Shelf Science,* 66**,** 346-356.

Hua, Q. 2009. Radiocarbon: A chronological tool for the recent past. *Quaternary Geochronology,* 4**,** 378-390.

Huang, X., Wang, C., Zhang, J., Wiesenberg, G. L. B., Zhang, Z. & Xie, S. 2011. Comparison of free lipid compositions between roots and leaves of plants in the Dajiuhu Peatland, central China. *Geochemical Journal,* 45**,** 365-373.

Huguet, A., Wiesenberg, G. L. B., Gocke, M., Fosse, C. & Derenne, S. 2012. Branched tetraether membrane lipids associated with rhizoliths in loess: Rhizomicrobial overprinting of initial biomarker record. *Organic Geochemistry,* 43**,** 12-19.

Huntley, D. J., Godfrey-Smith, D. I. & Thewalt, M. L. W. 1985. Optical dating of sediments. *Nature,* 313**,** 105-107.

Hütt, G., Jaek, I., Tchonka, J., 1988. Optical dating: K-feldspars optical response stimulation spectra. *Quaternary Science Reviews,* 7, 381-385.

Imo, S. T., Sheikh, M. A., Hirosawa, E., Oomori, T. & Tamaki, F. 2007. Contamination by organochlorine pesticides from rivers. *International Journal of Environmental Science and Technology,* 4**,** 1-9.

Ishiwatari, R., Ogura, K. & Horie, S. 1980. Organic geochemistry of a lacustrine sediment (Lake Haruna, Japan). *Chemical Geology,* 29**,** 261-280.

Iwata, H., Tanabe, S., Sakai, N., Nishimura, A. & Tatsukawa, R. 1994. Geographical distribution of persistent organochlorines in air, water and sediments from Asia and Oceania, and their implications for global redistribution from lower latitudes. *Environmental Pollution,* 85**,** 15-33.

Iwata, H., Tanabe, S., Ueda, K. & Tatsukawa, R. 1995. Persistent organochlorine residues in air, water, sediments, and soils from the Lake Baikal region, Russia. *Environmental Science and Technology,* 29**,** 792-801.

Jacobs, S. W. L. & Pickard, J. 1981. *Plants of New South Wales : a census of the cycads, conifers, and angiosperms*. Sydney, National Herbarium of New South Wales, Royal Botanic Gardens.

Jacobs, Z., Duller, G. A. T. & Wintle, A. G. 2003. Optical dating of dune sand from Blombos Cave, South Africa: II--single grain data. *Journal of Human Evolution,* 44**,** 613-625.

Jacobs, Z., Duller, G. A. T. & Wintle, A. G. 2006a. Interpretation of single grain De distributions and calculation of De. *Radiation Measurements,* 41**,** 264-277.

Jacobs, Z., Wintle, A. G. & Duller, G. A. T. 2006b. Evaluation of SAR procedures for De determination using single aliquots of quartz from two archaeological sites in South Africa. *Radiation Measurements,* 41**,** 520-533.

Jacobs, Z., Wintle, A. G., Roberts, R. G. & Duller, G. A. T. 2008. Equivalent dose distributions from single grains of quartz at Sibudu, South Africa: context, causes and consequences for optical dating of archaeological deposits. *Journal of Archaeological Science,* 35**,** 1808-1820.

Jain, M., Murray, A. S. & Botter-Jensen, L. 2004. Optically stimulated luminescence dating: How significant is incomplete light exposure in fluvial environments? *Quaternaire,* 15**,** 143-158.

Jain, M., Murray, A. S. & Bøtter-Jensen, L. 2003. Characterisation of blue-light stimulated luminescence components in different quartz samples: implications for dose measurement. *Radiation Measurements,* 37**,** 441-449.

Jeng, W.-L. 2006. Higher plant *n*-alkane average chain length as an indicator of petrogenic hydrocarbon contamination in marine sediments. *Marine Chemistry,* 102**,** 242-251.

Jenkins, K. M. 2005. A common parched future? Research and management of Australian arid-zone floodplain wetlands. *Hydrobiologia,* 552**,** 57-73.

Jiang, C., Alexander, R., Kagi, R. I. & Murray, A. P. 2000. Origin of perylene in ancient sediments and its geological significance. *Organic Geochemistry,* 31**,** 1545-1559.

Kennicutt, M. C. II, Barker, C., Brooks, J. M., Defreitas, D. A. & Zhu, G. H. 1987. Selected organic matter source indicators in the Orinoco, Nile and Changjiang deltas. *Organic Geochemistry,* 11**,** 41-51.

Killops, S. D. & Massoud, M. S. 1992. Polycyclic aromatic hydrocarbons of pyrolytic origin in ancient sediments: evidence for Jurassic vegetation fires. *Organic Geochemistry,* 18**,** 1-7.

Kim, E.-J., Oh, J.-E. & Chang, Y.-S. 2003. Effects of forest fire on the level and distribution of PCDD/Fs and PAHs in soil. *The Science of The Total Environment,* 311**,** 177-189.

Kim, S.-K., Kang, D.-J., Kim, K.-R. & Lee, D. 2010. Distribution of organochlorine pesticides in intertidal and subtidal sediments in coastal wetland with high tidal ranges. *Archives of Environmental Contamination and Toxicology,* 58**,** 514-522.

Kingsford, R. T. 2000. Ecological impacts of dams, water diversions and river management on floodplain wetlands in Australia. *Austral Ecology,* 25**,** 109-127.

Kingsford, R. T. & Auld, K. 2003. *Waterbird Breeding in the Macquarie Marshes-A Guide to River Health,* Hurstville, NSW, National Parks and Wildlife Service, NSW.

Kingsford, R. T. & Auld, K. M. 2005. Waterbird breeding and environmental flow management in the Macquarie Marshes, arid Australia. *River Research and Applications,* 21**,** 187-200.

Kingsford, R. T. & Johnson, W. 1998. Impact of water diversions on colonially-nesting waterbirds in the Macquarie Marshes of arid Australia. *colonial waterbirds,* 21**,** 159-170.

Kingsford, R. T. & Thomas, R. F. 1995. The Macquarie Marshes in arid Australia and their waterbirds: A 50-year history of decline. *Environmental Management,* 19**,** 867-878.

Kluge, M. & Ting, I. 1978. *Crassulacean Acid Metabolism*, New York, Springer-Verlag.

Knapp, D. R. 1979. *Handbook of Analytical Derifatization Reactions,* America, John Wiley & Sons, Inc.

Kobayashi, T., Ryder, D., Gordon, G., Shannon, I., Ingleton, T., Carpenter, M. & Jacobs, S. 2009. Short-term response of nutrients, carbon and planktonic microbial communities to floodplain wetland inundation. *Aquatic Ecology,* 43**,** 843-858.

Kobayashi, T., Ryder, D. S., Ralph, T. J., Mazumder, D., Saintilan, N., Iles, J., Knowles, L., Thomas, R. & Hunter, S. 2011. Longitudinal spatial variation in ecological conditions in an in-channel floodplain river system during flow pulses. *River Research and Applications,* 27**,** 461-472.

Krull, E., Sachse, D., Mügler, I., Thiele, A. & Gleixner, G. 2006. Compound-specific $\delta^{13}C$ and $\delta^{2}H$ analyses of plant and soil organic matter: A preliminary assessment of the effects of vegetation change on ecosystem hydrology. *Soil Biology and Biochemistry,* 38**,** 3211-3221.

Kuder, T. & Kruge, M. A. 1998. Preservation of biomolecules in sub-fossil plants from raised peat bogs - A potential paleoenvironmental proxy. *Organic Geochemistry,* 29**,** 1355-1368.

Kvenvolden, K. A. 1970. Evidence for transformations of normal fatty acids in sediments. *Advances in Organic Geochemistry 1966,* Pergamon Press, Oxford**,** 335-366.

Laflamme, R. E. & Hites, R. A. 1978. The global distribution of polycyclic aromatic hydrocarbons in recent sediments. *Geochimica et Cosmochimica Acta,* 42**,** 289-303.

Lane, C., Horn, S., Mora, C., Orvis, K. & Finkelstein, D. 2011. Sedimentary stable carbon isotope evidence of late Quaternary vegetation and climate change in highland Costa Rica. *Journal of Paleolimnology,* 45**,** 323-338.

Leadprathom, N., Parkpian, P., Satayavivad, J., Delaune, R. D. & Jugsujinda, A. 2009. Transport and deposition of organochlorine pesticides from farmland to estuary under tropical regime and their potential risk to aquatic biota. *Journal of Environmental Science and Health, Part B: Pesticides, Food Contaminants, and Agricultural Wastes,* 44**,** 249 - 261.

Leblanc, M., Tweed, S., Van Dijk, A. & Timbal, B. 2012. A review of historic and future hydrological changes in the Murray-Darling Basin. *Global and Planetary Change,* 80-81, 226-246.

Leeming, R., Ball, A., Ashbolt, N. & Nichols, P. 1996. Using faecal sterols from humans and animals to distinguish faecal pollution in receiving waters. *Water Research,* 30**,** 2893-2900.

Lemly, A. D., Kingsford, R. T. & Thompson, J. R. 2000. Irrigated agriculture and wildlife conservation: conflict on a global scale. *Environmental Management,* 25**,** 485-512.

Leonard, A. W., Hyne, R. V., Lim, R. P. & Chapman, J. C. 1999. Effect of endosulfan runoff from cotton fields on macroinvertebrates in the Namoi River. *Ecotoxicology and Environmental Safety,* 42**,** 125-134.

Li, Y.-H. 2000. *A Compendium of Geochemistry,* Princeton, Princeton University Press.

Lian, O. B., Hu, J., Huntley, D. J. & Hicock, S. R. 1995. Optical dating studies of Quaternary organic-rich sediments from southwestern British Columbia and northwestern Washington State. *Canadian Journal of Earth Sciences,* 32**,** 1194-1207.

Lian, O. B. & Roberts, R. G. 2006. Dating the Quaternary: progress in luminescence dating of sediments. *Quaternary Science Reviews*, 25, 2449-2468.

Lian, O. B. & Scott, A. E. 2007. Luminescence Dating. Optically-Stimulated Luminescence. *Encyclopedia of Quaternary Science.* Oxford: Elsevier.

Lin, T., Ye, S., Ma, C., Ding, X., Brix, H., Yuan, H., Chen, Y. & Guo, Z. 2013. Sources and preservation of organic matter in soils of the wetlands in the Liaohe (Liao River) Delta, North China. *Marine Pollution Bulletin,* 71**,** 276-285.

Liu, M., Cheng, S., Ou, D., Yang, Y., Liu, H., Hou, L., Gao, L. & Xu, S. 2008. Organochlorine pesticides in surface sediments and suspended particulate matters from the Yangtze estuary, China. *Environmental Pollution,* 156**,** 168-173.

Liu, X. D., Li, H.C., Sun, L. G., Yin, X.-B., Zhao, S. P. & Wang, Y. H. 2006a. $\delta^{13}C$ and $\delta^{15}N$ in the ornithogenic sediments from the Antarctic maritime as palaeoecological proxies during the past 2000 yr. *Earth and Planetary Science Letters,* 243**,** 424-438.

Liu, X. D., Zhao, S. P., Sun, L. G., Luo, H. H., Yin, X. B., Xie, Z. Q., Wang, Y. H., Liu, K. X., Wu, X. H., Ding, X. F. & Fu, D. P. 2006b. Geochemical evidence for the variation of historical seabird population on Dongdao Island of the South China Sea. *Journal of Paleolimnology,* 36**,** 259-279.

Loconto, P. R. 2001. Sample Preparation Techniques To Isolate And Recover Organics And Inorganics. *Trace Environmental Quantitative Analysis*, CRC Press.

Logan, G. A. & Eglinton, G. 1994. Biogeochemistry of the Miocene lacustrine deposit, at Clarkia, northern Idaho, U.S.A. *Organic Geochemistry,* 21**,** 857-870.

Long, H., Lai, Z., Wang, N. & Zhang, J. 2011. A combined luminescence and radiocarbon dating study of Holocene lacustrine sediments from arid northern China. *Quaternary Geochronology,* 6**,** 1-9.

Loomis, S. E., Russell, J. M. & Sinninghe Damsté, J. S. 2011. Distributions of branched GDGTs in soils and lake sediments from western Uganda: Implications for a lacustrine paleothermometer. *Organic Geochemistry,* 42**,** 739-751.

Lopes Dos Santos, R. A., Wilkins, D., De Deckker, P. & Schouten, S. 2012. Late Quaternary productivity changes from offshore Southeastern Australia: A biomarker approach. *Palaeogeography, Palaeoclimatology, Palaeoecology,* 363–364**,** 48-56.

Madsen, A. T. & Murray, A. S. 2009. Optically stimulated luminescence dating of young sediments: A review. *Geomorphology,* 109**,** 3-16.

Madsen, A. T., Murray, A. S., Andersen, T. J., Pejrup, M. & Breuning-Madsen, H. 2005. Optically stimulated luminescence dating of young estuarine sediments: a comparison with ^{210}Pb and ^{137}Cs dating. *Marine Geology,* 214**,** 251-268.

Magee, J. W., Bowler, J. M., Miller, G. H. & Williams, D. L. G. 1995. Stratigraphy, sedimentology, chronology and palaeohydrology of Quaternary lacustrine deposits at Madigan Gulf, Lake Eyre, south Australia. *Palaeogeography, Palaeoclimatology, Palaeoecology,* 113**,** 3-42.

Marburger, J., Johnson, W., Gross, T., Douglas, D. & Di, J. 2002. Residual organochlorine pesticides in soils and fish from wetland restoration areas in central Florida, USA. *Wetlands,* 22**,** 705-711.

Matsuda, H. & Koyama, T. 1977. Early diagenesis of fatty acids in lacustrine sediments—I. Identification and distribution of fatty acids in recent sediment from a freshwater lake. *Geochimica et Cosmochimica Acta,* 41**,** 777-783.

Matsumoto, G. I. & Watanuki, K. 1990. Geochemical features of hydrocarbons and fatty acids in sediments of the inland hydrothermal environments of Japan. *Organic Geochemistry,* 15**,** 199-208.

Mayya, Y. S., Morthekai, P., Murari, M. K. & Singhvi, A. K. 2006. Towards quantifying beta microdosimetric effects in single-grain quartz dose distribution. *Radiation Measurements,* 41**,** 1032-1039.

McKirdy, D. M., Thorpe, C. S., Haynes, D. E., Grice, K., Krull, E. S., Halverson, G. P. & Webster, L. J. 2010. The biogeochemical evolution of the Coorong during the mid- to late Holocene: An elemental, isotopic and biomarker perspective. *Organic Geochemistry,* 41**,** 96-110.

McLaren, R. G. & Cameron, K. C. 1996. *Soil Science--Sustainable Production and Environmental Protection*, Oxford University Press.

Meijer, S. N., Steinnes, E., Ockenden, W. A. & Jones, K. C. 2002. Influence of environmental variables on the spatial distribution of PCBs in Norwegian and U.K. soils: Implications for global cycling. *Environmental Science and Technology,* 36**,** 2146-2153.

Mejdahl, V. 1979. Thermoluminescence dating: beta-dose attenuation in quartz grains. *Archaeometry,* 21**,** 61-72.

Merck 1996. The Merck Index 12 ed.: the United States Pharmaceutical Company Merck & Co.

Meyers, P. A. 1994. Preservation of elemental and isotopic source identification of sedimentary organic matter. *Chemical Geology,* 114**,** 289-302.

Meyers, P. A. 2003. Applications of organic geochemistry to paleolimnological reconstructions: a summary of examples from the Laurentian Great Lakes. *Organic Geochemistry,* 34**,** 261-289.

Meyers, P. A. & Ishiwatari, R. 1993. Lacustrine organic geochemistry--an overview of indicators of organic matter sources and diagenesis in lake sediments. *Organic Geochemistry,* 20**,** 867-900.

Minh, N. H., Minh, T. B., Kajiwara, N., Kunisue, T., Iwata, H., Viet, P. H., Cam Tu, N. P., Tuyen, B. C. & Tanabe, S. 2007. Pollution sources and occurrences of selected persistent organic pollutants (POPs) in sediments of the Mekong River delta, South Vietnam. *Chemosphere,* 67**,** 1794-1801.

Mitsch, W. J. & Gosselink, J. G. 2007. *Wetlands,* New Jersey, John Wiley & Sons, Inc.

Morrison, T. N., Rayburg, S., Allery, C. & Atiquzzaman, M. D. 2011. Understanding the Flow Pathways Through the Macquarie Marshes. 34th IAHR World Congress -- Balance and Uncertainty, 33nd Hydrology & Water Resources Symposium, 10th Hydraulics Conference, Brisbane.

Mortimer, M. R. 1998. Organochlorine pesticide residues in Brisbane Waterways. Moreton Bay and Catchment, School of Marine Science, The University of Queensland, Brisbane. 241-246.

Mortimer, M. R. 2000. Pesticide and trace metal concentrations in Queensland estuarine crabs. *Marine Pollution Bulletin,* 41**,** 359-366.

Munsell 1971. Munsell soil color charts. revised washable edition ed.: GretagMacbeth.

Muri, G. & Wakeham, S. G. 2009. Effect of depositional regimes on polycyclic aromatic hydrocarbons in Lake Bled (NW Slovenia) sediments. *Chemosphere,* 77**,** 74-79.

Murray, A. S. & Clemmensen, L. B. 2001. Luminescence dating of Holocene aeolian sand movement, Thy, Denmark. *Quaternary Science Reviews,* 20**,** 751-754.

Murray, A. S. & Olley, J. M. 2002. Precision and accuracy in the optically stimulated luminescence dating of sedimentary quartz: a status review. *Geochronometria,* 21**,** 1-16.

Murray, A. S., Olley, J. M. & Caitcheon, G. G. 1995. Measurement of equivalent doses in quartz from contemporary water-lain sediments using optically stimulated luminescence. *Quaternary Science Reviews,* 14**,** 365-371.

Murray, A. S. & Roberts, R. G. 1997. Determining the burial time of single grains of quartz using optically stimulated luminescence. *Earth and Planetary Science Letters,* 152**,** 163-180.

Murray, A. S. & Roberts, R. G. 1998. Measurement of the equivalent dose in quartz using a regenerative-dose single-aliquot protocol. *Radiation Measurements,* 29**,** 503-515.

Murray, A. S. & Wintle, A. G. 2000. Luminescence dating of quartz using an improved single-aliquot regenerative-dose protocol. *Radiation Measurements,* 32**,** 57-73.

Murray, A. S. & Wintle, A. G. 2003. The single aliquot regenerative dose protocol: potential for improvements in reliability. *Radiation Measurements,* 37**,** 377-381.

Myers, S. C., Clarkson, B. R., Reeves, P. N. & Clarkson, B. D. 2013. Wetland management in New Zealand: Are current approaches and policies sustaining wetland ecosystems in agricultural landscapes? *Ecological Engineering,* 56**,** 107-120.

Negoita, T. G., Covaci, A., Gheorghe, A. & Schepens, P. 2003. Distribution of polychlorinated biphenyls (PCBs) and organochlorine pesticides in soils from the East Antarctic coast. *Journal of Environmental Monitoring,* 5**,** 281-286.

O'Leary, M. H. 1988. Carbon isotopes in photosynthesis. BioScience, 38, 328-336.

O'Leary, T., Leeming, R., Nichols, P. D. & Volkman, J. K. 1999. Assessment of the sources, transport and fate of sewage-derived organic matter in Port Phillip Bay, Australia, using the signature lipid coprostanol. *Marine and Freshwater Research,* 50**,** 547-556.

O'Dwyer, B. & Taylor, D. 2009. Paleolimnological evidence of variations in deposition of atmosphere-borne Polycyclic Aromatic Hydrocarbons (PAHs) in Ireland. *Chemosphere,* 77**,** 1374-1380.

Ohkouchi, N. & Eglinton, T. I. 2008. Compound-specific radiocarbon dating of Ross Sea sediments: A prospect for constructing chronologies in high-latitude oceanic sediments. *Quaternary Geochronology,* 3**,** 235-243.

Ollerhead, J., Huntley, D. J. & Berger, G. W. 1994. Luminescence dating of sediments from Buctouche Spit, New Brunswick. *Canadian Journal of Earth Sciences,* 31**,** 523-531.

Olley, J., Caitcheon, G. & Murray, A. 1998. The distribution of apparent dose as determined by Optically Stimulated Luminescence in small aliquots of fluvial quartz: Implications for dating young sediments. *Quaternary Science Reviews,* 17**,** 1033-1040.

Olley, J. M., Caitcheon, G. G. & Roberts, R. G. 1999. The origin of dose distributions in fluvial sediments, and the prospect of dating single grains from fluvial deposits using optically stimulated luminescence. *Radiation Measurements,* 30**,** 207-217.

Olley, J. M., De Deckker, P., Roberts, R. G., Fifield, L. K., Yoshida, H. & Hancock, G. 2004. Optical dating of deep-sea sediments using single grains of quartz: a comparison with radiocarbon. *Sedimentary Geology,* 169**,** 175-189.

Olley, J. M., Murray, A. & Roberts, R. G. 1996. The effects of disequilibria in the uranium and thorium decay chains on burial dose rates in fluvial sediments. *Quaternary Science Reviews,* 15**,** 751-760.

Olley, J. M., Roberts, R. G. & Murray, A. S. 1997. Disequilibria in the uranium decay series in sedimentary deposits at Allen's cave, Nullarbor Plain, Australia: Implications for dose rate determinations. *Radiation Measurements,* 27**,** 433-443.

Otto, A. & Simpson, M. 2005. Degradation and preservation of vascular plant-derived biomarkers in grassland and forest soils from western Canada. *Biogeochemistry,* 74**,** 377-409.

Page, K., Frazier, P., Pietsch, T. & Dehaan, R. 2007. Channel change following European settlement: Gilmore Creek, southeastern Australia. *Earth Surface Processes and Landforms,* 32**,** 1398-1411.

Paijmans 1981. The Macquarie Marshes of Inland Northern New South Wales, Australia. CSIRO Division of Land Use Research Technical Paper.

Patnaik, P. 1997. *Handbook of Environmental Analysis: Chemical Pollutants in air, water, soil and solid wastes*, CRC Press, Inc.

Perry, G. J., Volkman, J. K., Johns, R. B. & Bavor, H. J. Jr 1979. Fatty acids of bacterial origin in contemporary marine sediments. *Geochimica et Cosmochimica Acta,* 43**,** 1715-1725.

Peters, K. E., Walters, C. C. & Moldowan, J. M. 2005. *The Biomarker Guide,* Cambridge, Cambridge University Press.

Pietsch, T. J. 2009. Optically stimulated luminescence dating of young (<500 years old) sediments: Testing estimates of burial dose. *Quaternary Geochronology,* 4**,** 406-422.

Pietsch, T. J., Olley, J. M. & Nanson, G. C. 2008. Fluvial transport as a natural luminescence sensitiser of quartz. *Quaternary Geochronology,* 3**,** 365-376.

Pietsch, T. J., Nanson, G. C. & Olley, J. M. 2013. Late Quaternary changes in flow-regime on the Gwydir distributive fluvial system, southeastern Australia. *Quaternary Science Reviews,* 69, 168-180.

Pollard, M., Batt, C., Stern, B., Young, S. M.M. 2007. *Analytical Chemistry in Archaeology*. Cambridge, Cambridge University Press.

Porat, N., Wintle, A. G., Amit, R. & Enzel, Y. 1996. Late Quaternary earthquake chronology from luminescence dating of colluvial and alluvial deposits of the Arava Valley, Israel. *Quaternary Research,* 46**,** 107-117.

Prahl, F. G. & Carpenter, R. 1983. Polycyclic aromatic hydrocarbon (PAH) - phase associations in Washington coastal sediment. *Geochimica et Cosmochimica Acta,* 47**,** 1013-1023.

Prescott, J. R. & Hutton, J. T. 1994. Cosmic ray contributions to dose rates for luminescence and ESR dating: large depths and long-term time variations. *Radiation Measurements,* 23**,** 497–500.

Ralph, T. 2008. *Channel breakdown and floodplain wetland morphodynamics in the Macquarie Marshes, south-eastern Australia.* PhD thesis, Macquarie University.

Ralph, T. J. & Hesse, P. P. 2010. Downstream hydrogeomorphic changes along the Macquarie River, southeastern Australia, leading to channel breakdown and floodplain wetlands. *Geomorphology,* 118**,** 48-64.

Ralph, T. J., Kobayashi, T., García, A., Hesse, P. P., Yonge, D., Bleakley, N. & Ingleton, T. 2011. Paleoecological responses to avulsion and floodplain evolution in a semiarid Australian freshwater wetland. *Australian Journal of Earth Sciences,* 58**,** 75-91.

Ramdahl, T. 1983. Retene - a molecular marker of wood combustion in ambient air. *Nature,* 306**,** 580-582.

Ray, N. & Adams, J. M. 2001. A GIS-based Vegetation Map of the World at the Last Glacial Maximum (25,000-15,000 BP). *Internet Archaeology*, 11.

Ren, S. & Kingsford, R. 2011. Statistically integrated flow and flood modelling compared to hydrologically integrated quantity and quality model for annual flows in the regulated Macquarie River in arid Australia. *Environmental Management,* 48**,** 177-188.

Rhodes, E. J. 2011. Optically stimulated luminescence dating of sediments over the past 200,000 years. *Annual Review of Earth and Planetary Sciences,* 39**,** 461-488.

Rhodes, E. J., Fanning, P. C. & Holdaway, S. J. 2010. Developments in optically stimulated luminescence age control for geoarchaeological sediments and hearths in western New South Wales, Australia. *Quaternary Geochronology,* 5**,** 348-352.

Roberts, R., Bird, M., Olley, J., Galbraith, R., Lawson, E., Laslett, G., Yoshida, H., Jones, R., Fullagar, R., Jacobsen, G. & Hua, Q. 1998. Optical and radiocarbon dating at Jinmium rock shelter in northern Australia. *Nature,* 393**,** 358-362.

Rieley, G., Collier, R. J., Jones, D. M. & Eglinton, G. 1991a. The biogeochemistry of Ellesmere Lake, U.K.—I: source correlation of leaf wax inputs to the sedimentary lipid record. *Organic Geochemistry,* 17**,** 901-912.

Rieley, G., Collier, R. J., Jones, D. M., Eglinton, G., Eakin, P. A. & Fallick, A. E. 1991b. Sources of sedimentary lipids deduced from stable carbon-isotope analyses of individual compounds. *Nature,* 352**,** 425-427.

Rittenour, T. M. 2008. Luminescence dating of fluvial deposits: applications to geomorphic, palaeoseismic and archaeological research. *Boreas,* 37**,** 613-635.

Roberts, R. G., Galbraith, R. F., Yoshida, H., Laslett, G. M. & Olley, J. M. 2000. Distinguishing dose populations in sediment mixtures: a test of single-grain optical dating procedures using mixtures of laboratory-dosed quartz. *Radiation Measurements,* 32**,** 459-465.

Robertson, A. I., Bunn, S. E., Boon, P. I. & Walker, K. F. 1999. Sources, sinks and transformations of organic carbon in Australian floodplain rivers. *Marine and Freshwater Research,* 50**,** 813-829.

Robinson, N., Cranwell, P. A., Finlay, B. J. & Eglinton, G. 1984. Lipids of aquatic organisms as potential contributors to lacustrine sediments. *Organic Geochemistry,* 6**,** 143-152.

Rodnight, H., Duller, G. A. T., Wintle, A. G. & Tooth, S. 2006. Assessing the reproducibility and accuracy of optical dating of fluvial deposits. *Quaternary Geochronology,* 1**,** 109-120.

Rommerskirchen, F., Plader, A., Eglinton, G., Chikaraishi, Y. & Rullkötter, J. 2006. Chemotaxonomic significance of distribution and stable carbon isotopic composition of long-chain alkanes and alkan-1-ols in C4 grass waxes. *Organic Geochemistry,* 37**,** 1303-1332.

Roshier, D. A., Robertson, A. I. & Kingsford, R. T. 2002. Responses of waterbirds to flooding in an arid region of Australia and implications for conservation. *Biological Conservation,* 106**,** 399-411.

Roulet, N. T. 2000. Peatlands, carbon storage, greenhouse gases, and the Kyoto protocol: Prospects and significance for Canada. *Wetlands,* 20**,** 605-615.

Russell, J. M., McCoy, S. J., Verschuren, D., Bessems, I. & Huang, Y. 2009. Human impacts, climate change, and aquatic ecosystem response during the past 2000 yr at Lake Wandakara, Uganda. *Quaternary Research,* 72**,** 315-324.

Rustomji, P. & Pietsch, T. 2007. Alluvial sedimentation rates from southeastern Australia indicate post-European settlement landscape recovery. *Geomorphology,* 90**,** 73-90.

Sage, R.F., Monson, R.K., 1999. *C_4 Plant Biology*. Academic Press, San Diego, pp. 228-229.

Scalan, E. S. & Smith, J. E. 1970. An improved measure of the odd-even predominance in the normal alkanes of sediment extracts and petroleum. *Geochimica et Cosmochimica Acta,* 34**,** 611-620.

Schefuß, E., Ratmeyer, V., Stuut, J.-B. W., Jansen, J. H. F. & Sinninghe Damsté, J. S. 2003. Carbon isotope analyses of *n*-alkanes in dust from the lower atmosphere over the central eastern Atlantic. *Geochimica et Cosmochimica Acta,* 67**,** 1757-1767.

Schwark, L., Zink, K. & Lechterbeck, J. 2002. Reconstruction of postglacial to early Holocene vegetation history in terrestrial Central Europe via cuticular lipid biomarkers and pollen records from lake sediments. *Geology,* 30**,** 463-466.

Schwartz, D., Mariotti, A., Lanfranchi, R. & Guillet, B. 1986. $^{13}C/^{12}C$ ratios of soil organic matter as indicators of vegetation changes in the Congo. *Geoderma,* 39**,** 97-103.

Seki, O., Nakatsuka, T., Shibata, H. & Kawamura, K. 2010. A compound-specific *n*-alkane $\delta^{13}C$ and δD approach for assessing source and delivery processes of terrestrial organic matter within a forested watershed in northern Japan. *Geochimica et Cosmochimica Acta,* 74**,** 599-613.

Sheldon, N. D. & Tabor, N. J. 2009. Quantitative paleoenvironmental and paleoclimatic reconstruction using paleosols. *Earth-Science Reviews,* 95**,** 1-52.

Shelly, D. 2005. *Flora and Fauna of the Macquarie Marshes Region*, NSW Department of Infrastructure, Planning and Natural Resources.

Shivaramaiah, H. M., Odeh, I. O. A., Kennedy, I. R. & Skerritt, J. H. 2002. Mapping the distribution of DDT residues as DDE in the soils of the irrigated regions of northern New South Wales, Australia using ELISA and GIS. *Journal of Agricultural and Food Chemistry,* 50**,** 5360-5367.

Sifeddine, A., Meyers, P., Cordeiro, R., Albuquerque, A., Bernardes, M., Turcq, B. & Abrão, J. 2011. Delivery and deposition of organic matter in surface sediments of Lagoa do Caçó (Brazil). *Journal of Paleolimnology,* 45**,** 385-396.

Silliman, J. E., Meyers, P. A. & Eadie, B. J. 1998. Perylene: An indicator of alteration processes or precursor materials? *Organic Geochemistry,* 29**,** 1737-1744.

Simoneit, B. R. T. 1977. Diterpenoid compounds and other lipids in deep-sea sediments and their geochemical significance. *Geochimica et Cosmochimica Acta,* 41**,** 463-476.

Simoneit, B. R. T. 2002. Biomass burning - A review of organic tracers for smoke from incomplete combustion. *Applied Geochemistry,* 17**,** 129-162.

Singarayer, J. S. & Bailey, R. M. 2003. Further investigations of the quartz optically stimulated luminescence components using linear modulation. *Radiation Measurements,* 37**,** 451-458.

Singarayer, J. S. & Bailey, R. M. 2004. Component-resolved bleaching spectra of quartz optically stimulated luminescence: preliminary results and implications for dating. *Radiation Measurements,* 38**,** 111-118.

Smittenberg, R. H., Hopmans, E. C., Schouten, S. & Sinninghe Damsté, J. S. 2002. Rapid isolation of biomarkers for compound specific radiocarbon dating using high-performance liquid chromatography and flow injection analysis–atmospheric pressure chemical ionisation mass spectrometry. *Journal of Chromatography A,* 978**,** 129-140.

Soumana, S., Faïn, J., Miallier, D., Montret, M., Pilleyre, T. & Sanzelle, S. 1997. Alpha counting using scintillation techniques: Observations on TSAC calibration and gas cell use. *Radiation Measurements,* 27**,** 365-372.

Stuiver, M. & Polach, A. 1977. Reporting of ^{14}C data. *Radiocarbon*, 19, 355-363.

Sun, Q., Chu, G., Liu, M., Xie, M., Li, S., Ling, Y., Wang, X., Shi, L., Jia, G. & Lü, H. 2011. Distributions and temperature dependence of branched glycerol dialkyl glycerol tetraethers in recent lacustrine sediments from China and Nepal. *Journal of Geophysical Research,* 116**,** G01008.

Talbot, M. R. & Johannessen, T. 1992. A high resolution palaeoclimatic record for the last 27,500 years in tropical West Africa from the carbon and nitrogen isotopic

composition of lacustrine organic matter. *Earth and Planetary Science Letters,* 110**,** 23-37.
Thomas, R. F., Kingsford, R. T., Lu, Y. & Hunter, S. J. 2011. Landsat mapping of annual inundation (1979–2006) of the Macquarie Marshes in semi-arid Australia. *International Journal of Remote Sensing,* 32**,** 4545-4569.
Thomsen, K. J., Murray, A. & Jain, M. 2012. The dose dependency of the over-dispersion of quartz OSL single grain dose distributions. *Radiation Measurements***,** 47, 732-739.
Thorndycraft, V. R., Benito, G. & Gregory, K. J. 2008. Fluvial geomorphology: A perspective on current status and methods. *Geomorphology,* 98**,** 2-12.
Tissot, B. P. & Welte, D. H. 1984. *Petroleum Formation and Occurrence.* (2nd ed.) Springer-Verlag, Berlin pp. 699.
Tomkins, K. M. & Hesse, P. P. 2004. Evidence of Late Cenozoic uplift and climate change in the stratigraphy of the Macquarie River valley, New South Wales. *Australian Journal of Earth Sciences,* 51**,** 273-290.
Trendel, J. M., Schaeffer, P., Adam, P., Ertlen, D. & Schwartz, D. 2010. Molecular characterisation of soil surface horizons with different vegetation in the Vosges Massif (France). *Organic Geochemistry,* 41**,** 1036-1039.
Van Aarssen, B. G. K., Alexander, R. & Kagi, R. I. 2000. Higher plant biomarkers reflect palaeovegetation changes during Jurassic times. *Geochimica et Cosmochimica Acta,* 64**,** 1417-1424.
Venkatesan, M. I. 1988a. Occurrence and possible sources of perylene in marine sediments - a review. *Marine Chemistry,* 25**,** 1-27.
Venkatesan, M. I. 1988b. Organic geochemistry of marine sediments in Antarctic region: Marine lipids in McMurdo Sound. *Organic Geochemistry,* 12**,** 13-27.
Vergnoux, A., Malleret, L., Asia, L., Doumenq, P. & Theraulaz, F. 2011. Impact of forest fires on PAH level and distribution in soils. *Environmental Research,* 111**,** 193-198.
Vermeesch, P. 2009. RadialPlotter: A Java application for fission track, luminescence and other radial plots. *Radiation Measurements,* 44**,** 409-410.
Vesk, P. A. & Allaway, W. G. 1997. Spatial variation of copper and lead concentrations of water hyacinth plants in a wetland receiving urban run-off. *Aquatic Botany,* 59**,** 33-44.
Visher, G. S. 1969. Grain size distributions and depositional processes. *Journal of Sedimentary Petrology,* 39**,** 1074-1106.
Volkman 2003. Sterols in microorganisms. *Applied Microbiology and Biotechnology,* 60**,** 495-506.
Volkman, J. K., Barrett, S. M. & Blackburn, S. I. 1999. Eustigmatophyte microalgae are potential sources of C_{29} sterols, C_{22}-C_{28} *n*-alcohols and C_{28}-C_{32} *n*-alkyl diols in freshwater environments. *Organic Geochemistry,* 30**,** 307-318.
Volkman, J. K., Johns, R. B., Gillan, F. T., Perry, G. J. & Bavor, H. J. Jr 1980. Microbial lipids of an intertidal sediment—I. Fatty acids and hydrocarbons. *Geochimica et Cosmochimica Acta,* 44**,** 1133-1143.
Volkman, J. K., Revill, A. T., Bonham, P. I. & Clementson, L. A. 2007. Sources of organic matter in sediments from the Ord River in tropical northern Australia. *Organic Geochemistry,* 38**,** 1039-1060.

Volkman, J. K., Revill, A. T., Holdsworth, D. G. & Fredericks, D. 2008. Organic matter sources in an enclosed coastal inlet assessed using lipid biomarkers and stable isotopes. *Organic Geochemistry,* 39**,** 689-710.

Wait, D. A., Aubrey, D. P. & Anderson, W. B. 2005. Seabird guano influences on desert islands: soil chemistry and herbaceous species richness and productivity. *Journal of Arid Environments,* 60**,** 681-695.

Wakeham, S. G., Schaffner, C. & Giger, W. 1980. Polycyclic aromatic hydrocarbons in Recent lake sediments. II. Compounds derived from biogenic precursors during early diagenesis. *Geochimica et Cosmochimica Acta,* 44**,** 415-429.

Walker, M. J. C. 2005. *Quaternary Dating Methods*, Chichester, West Sussex, England : John Wiley & Sons, 2-16.

Wang, Z., Fingas, M., Shu, Y. Y., Sigouin, L., Landriault, M., Lambert, P., Turpin, R., Campagna, P. & Mullin, J. 1999. Quantitative characterization of PAHs in burn residue and soot samples and differentiation of pyrogenic PAHs from petrogenic PAHs − The 1994 Mobile Burn Study. *Environmental Science and Technology,* 33**,** 3100-3109.

Watanabe, T., Nakamura, T. & Kawai, T. 2007. Radiocarbon dating of sediments from large continental lakes (Lakes Baikal, Hovsgol and Erhel). *Nuclear Instruments and Methods in Physics Research Section B: Beam Interactions with Materials and Atoms,* 259**,** 565-570.

Watkins, J. J. & Meakin, N. S. 1996. Explanatory notes, Nyngan and Walgett 1:250 000 geological sheets, SH/55-15 and SH/55-11, Sydney: Geological Survey of New South Wales.

Wen, L., Yang, X. & Saintilan, N. 2012. Local climate determines the NDVI-based primary productivity and flooding creates heterogeneity in semi-arid floodplain ecosystem. *Ecological Modelling,* 242**,** 116-126.

Wetzel, R. 2001. *Limnology: Lake and River Ecosystems,* San Diego, Academic Press.

Wiesenberg, G. L. B. & Schwark, L. 2006. Carboxylic acid distribution patterns of temperate C_3 and C_4 crops. *Organic Geochemistry,* 37**,** 1973-1982.

Wiesenberg, G. L. B., Schwarzbauer, J., Schmidt, M. W. I. & Schwark, L. 2004. Source and turnover of organic matter in agricultural soils derived from *n*-alkane/*n*-carboxylic acid compositions and C-isotope signatures. *Organic Geochemistry,* 35**,** 1371-1393.

Wilcke, W. 2000. Polycyclic aromatic hydrocarbons (PAHs) in soil - A review. *Journal of Plant Nutrition and Soil Science,* 163**,** 229-248.

Wilcke, W. 2007. Global patterns of polycyclic aromatic hydrocarbons (PAHs) in soil. *Geoderma,* 141**,** 157-166.

Wilkins, D., Gouramanis, C., De Deckker, P., Fifield, L. K. & Olley, J. 2013. Holocene lake-level fluctuations in Lakes Keilambete and Gnotuk, southwestern Victoria, Australia. *The Holocene,* 1-12.

Wintle, A.G., 1973. Anomalous fading of thermoluminescence in mineral samples. *Nature*, 245, 143-144.

Wintle, A. G. & Murray, A. S. 1999. Luminescence sensitivity changes in quartz. *Radiation Measurements,* 30**,** 107-118.

Wintle, A. G. & Murray, A. S. 2006. A review of quartz optically stimulated luminescence characteristics and their relevance in single-aliquot regeneration dating protocols. *Radiation Measurements,* 41**,** 369-391.

Wolfe, D. J. H. & Ollerhead, J. 1995. Recent and late Holocene sand dune activity in southwestern Saskatchewan *current research, Geological Survey of Canada* 1995(B)**,** 131-140.

Woodroffe, C. D. 2002. *Coasts: Forms, Process and Evolution,* Cambridge, Cambridge University Press.

Xiao, C.-Y., Tai, C., Zhao, T.-Q., Wu, L., Zhou, T.-J. & Dong, J.-J. 2009. Distribution characteristics of organoclorine pesticides in surface water and sediments from the Mengjin wetland. *Huanjing Kexue/Environmental Science,* 30**,** 1614.

Xie, S., Nott, C. J., Avsejs, L. A., Maddy, D., Chambers, F. M. & Evershed, R. P. 2004. Molecular and isotopic stratigraphy in an ombrotrophic mire for paleoclimate reconstruction. *Geochimica et Cosmochimica Acta,* 68**,** 2849-2862.

Xu, S.-P. & Sun, Y.-G. 2006. Micro-column chromatography for the separation of compound-grouped fractions of sedimentary organic matter. *Geochimica,* 35**,** 681-688.

Young, R.W., Young, A.R.M., Price, D.M., Wray, R.A.L., 2002. Geomorphology of the Namoi alluvial plain northwestern New South Wales. *Australian Journal of Earth Sciences,* 49, 509-523.

Yonge, D. & Hesse, P. P. 2009. Geomorphic environments, drainage breakdown, and channel and floodplain evolution on the lower Macquarie River, central-western New South Wales. *Australian Journal of Earth Sciences,* 56**,** 35 - 53.

Yu, L., Chivas, A. R., García, A. & Hu, J. 2011. Decline of the Macquarie Marshes ecosystem, Australia, since European arrival recorded by organic geochemical proxies in sediments. AGU (American Geophysical Union) Fall Meeting, 2011 San Francisco USA.

Yum, J.-G., Takemura, K., Tokuoka, T. & Yu, K.-M. 2003. Holocene environmental changes of the Hwajinpo Lagoon on the eastern coast of Korea. *Journal of Paleolimnology,* 29**,** 155-166.

Yunker, M. B. & Macdonald, R. W. 2003. Alkane and PAH depositional history, sources and fluxes in sediments from the Fraser River Basin and Strait of Georgia, Canada. *Organic Geochemistry,* 34**,** 1429-1454.

Zedler, J. B. & Kercher, S. 2005. Wetland resources: Status, trends, ecosystem services, and restorability.

Zheng, X., Liu, X., Liu, W., Jiang, G. & Yang, R. 2009. Concentrations and source identification of organochlorine pesticides (OCPs) in soils from Wolong Natural Reserve. *Chinese Science Bulletin,* 54**,** 743-751.

Zheng, Y., Zhou, W., Meyers, P. A. & Xie, S. 2007. Lipid biomarkers in the Zoigê-Hongyuan peat deposit: Indicators of Holocene climate changes in West China. *Organic Geochemistry,* 38**,** 1927-1940.

APPENDIX A. OSL DATING

A1.1 Environmental dosimetry

A1.1.1 Determination of radionuclide concentrations by HRGS

A high-resolution gamma spectrometer (HRGS) was used to quantify the radio activities (in Bq/kg) of radionuclide and other daughter products from the sediment cores, providing information to assess the radioactive disequilibrium in these samples. If the sediment is in radioactive equilibrium, the activities of the parent (e.g., ^{238}U) and daughter (e.g., ^{226}Ra) should be the same (Aitken, 1998).

Selected samples from each core were analysed at the CSIRO Land and Water Radionuclide Laboratory at Black Mountain, Canberra. Details on instrumentation and calibration standards are described in Olley et al. (1996). The results are shown in Table A.1.1. The ^{232}Th decay chain appears to be in secular equilibrium as the ratios are compatible with unity for all the samples. In the ^{238}U series, the daughter to parent ratios are constant among samples from core MMB3 and core LSW except for the near-surface sediment samples (MMB3-01, LSW02_Dose). In these two samples, the ^{210}Pb concentrations exceed the ^{226}Ra concentrations, as commonly found in fluvial sediments and believed to have been caused by atmospheric fallout (Olley et al., 1996). This is particularly true for surface sediment samples buried at the time (late 1950 to mid-1960s) when atmospheric nuclear tests were conducted. For the core LOLA samples, except LOLA-DR_03 (145-151 cm), the other three samples show disequilibrium in the ^{238}U series with concentration of ^{226}Ra $>^{238}$U and ^{210}Pb $<^{226}$Ra. The concentration of ^{226}Ra exceeding ^{210}Pb can be explained by the escape of the intermediate gaseous nuclide ^{222}Rn (a critical nuclide in the U decay chain) (Olley et al., 1996). Except for the sediment sample LOLA-DR_04 (145-151 cm) which has a ^{226}Ra/^{238}U ratio of 1.53, the other two

deeply buried samples of core LOLA do not exceed 50 % disequilibrium. With the limitations of current analytical techniques, we would not be able to detect any ^{226}Ra excess after about 11,000 years since deposition (Olley et al., 1996). We could only assume the disequilibrium has prevailed throughout the entire period of burial. Also these two samples are buried relatively deep where the depositional environment is likely to be chemically closed, therefore the impact of disequilibrium for dose rate calculation could be assumed to be relatively small (<3 %) (Olley et al., 1996).

In addition to providing measures of the radionuclides contributing to the dose rate, HRGS also measures the activity concentration of ^{137}Cs, which is not expected to be found in sediments older than 50 years old (Pietsch, 2009) and can be used as an independent age control (discussed in Chapter 4).

Table A.1.1
Radionuclide concentrations determined by high-resolution gamma spectrometer.

Sample ID	Depth (cm)	^{238}U Series					^{232}Th Series			^{40}K (Bq/kg)
		^{238}U (Bq/kg)	^{226}Ra (Bq/kg)	^{210}Pb (Bq/kg)	^{226}Ra/^{238}U	^{210}Pb/^{226}Ra	^{228}Ra (Bq/kg)	^{228}Th (Bq/kg)	^{228}Th/^{228}Ra	
MMB3-01	0-5	24.3 ± 2.3	26.1 ± 0.4	39.9 ± 2.9	1.07	1.53	42.5 ± 0.9	42.9 ± 0.9	1.01	382.7 ± 9.5
MMB3-02	56-61	23.1 ± 1.9	27.2 ± 0.5	28.8 ± 2.6	1.18	1.06	42.1 ± 1.0	44.8 ± 0.9	1.06	392.5 ± 10.4
MMB3-03	87-89	22.7 ± 2.3	26.5 ± 0.5	27.0 ± 3.1	1.17	1.02	42.1± 1.0	42.9 ± 0.9	1.02	395.7 ± 10.2
LOLA-DR_04	105-111	20.4 ± 1.9	31.1 ± 0.5	27.8 ± 2.1	1.53	0.89	41.8 ± 0.9	41.9 ± 0.8	1.00	408.6 ± 9.7
LOLA-DR_03	145-151	21.7 ± 2.1	21.4 ± 0.5	22.8 ± 2.3	0.99	1.07	43.1 ± 1.1	43.9 ± 0.9	1.02	446.0 ± 11.7
LOLA-DR_02	181-186	23.2 ± 2.4	30.9 ± 0.6	24.8 ± 2.6	1.33	0.80	48.0 ± 1.2	51.9 ± 1.1	1.08	510.8 ± 13.3
LOLA-DR_01	201-207	19.6 ± 2.2	26.1 ± 0.5	25.4 ± 2.5	1.33	0.97	47.0 ± 1.0	47.0 ± 0.9	1.00	501.3 ± 11.7
LSW02_Dose	23-28	32.9 ± 2.2	27.2 ± 0.5	45.7 ± 2.6	0.82	1.68	44.9 ± 1.0	43.9 ± 0.9	0.98	381.8 ± 9.4
LSW04_Dose	65-68	19.3 ± 2.3	19.6 ± 0.4	19.2 ± 3.0	1.01	0.98	33.9 ± 1.0	33.2 ± 0.8	0.98	305.3 ± 8.4

A1.1.2 Determination of U, Th and K contents by XRF

The determination of U, Th and K was performed in the School of Earth and Environmental Sciences, University of Wollongong. Sample preparation was described in Section 3.2.2.1.

A1.1.3 Assessment of radionuclide concentrations by alpha and beta radiation counting

Beta counting was performed using a low-level Risø beta counter (GM-25-2) in the OSL laboratory at University of Wollongong. The equipment comprises a gas flow counter (99 % argon and 1 % butane), five individual Geiger-Mueller (GM) cylindrical detectors and a common guard counter that records the pulses derived from the beta emission from the sample (Bøtter-Jensen and Mejdahl, 1985). The detectors are mounted in a row facing downwards to the sample material. The whole instrument is placed inside 10 cm-thick lead bricks to reduce the background signal derived from cosmic rays. Triplicates of the dried and ground sample material are placed inside four different plastic cylindrical containers of 25 mm diameter. The other two of the five positions are used for calibration standard material (Nussloch Loess, called 'Nussi') and background material (MgO powder). The five positions are measured simultaneously in 24 ± 2 cycles of one hour each. The beta dose rate is calculated by the following equation

$$r_\beta = \left(\frac{C_{sample} - C_{MgO}}{C_{nussi} - C_{MgO}} \right) \times 1.49$$

r_β is the beta dose rate; C_{sample}, C_{nussi}, C_{MgO} are the counts of sample, Nussi and MgO; 1.49 Gy/ka is the known beta dose rate of Nussi.

Alpha counting is performed by thick-source alpha counting (TSAC). The measurements comprise a sealed background count of the ZnS screen and an unsealed count of the sample material, as described in Soumana et al. (1997). Two ZnS screens of 4.4 cm diameter are placed face to face (dull sides in, shiny sides out) in the sample cell, and counted for 24 hours prior to the measurement of the sample. Once completed, one of the two ZnS screens is removed from the cell and stored for the next measurement. The same finely milled sample materials are loaded on the dull side of the ZnS screen in Perspex sample holders. Though sealed with a rubber O-ring and screws, the cell is unsealed by placing fragments of toothpicks on the edge. The purpose of unsealing the samples is to allow the escape of radon from the sample. The sample is counted until at least 2,000 counts accumulate.

Beta counting (BC) determines the dose rate from U, Th and K while alpha counting determines the dose rate from U and Th; the radioactive contribution of K can be assessed by the results from those two procedures. The radionuclide concentration of U, Th and K are calculated by the conversion factors shown in Table A.1.2 below (Adamiec and Aitken, 1998).

Table A.1.2
Conversion factors.

Beta dose rate (Gy/ka)	1 ppm (or % for K)	Bq/kg	Gamma dose rate (Gy/ka)	1 ppm (or % for K)	Bq/kg
U	0.15	0.011	U	0.11	0.0088
Th	0.027	0.0067	Th	0.048	0.012
K	0.78	270	K	0.24	32.5

* These factors are used to convert radionuclide concentrations (ppm or %) and activities (Bq/kg) into dose rates (Gy/ka) for beta and gamma emissions.

A1.1.4 Comparison of radionuclide concentration results

Radionuclide U, Th and K concentrations of the three cores determined by the HRGS, XRF and TSAC&BC are listed in Table A.1.3.

For samples from core MMB3, bulk materials from several depths (from surface 5-8 cm, 27-29 cm, 48-51 cm, 55-57 cm, 85-88 cm) were used for XRF, alpha counting and beta counting (TSAC & BC). These bulk materials were collected from the sediment surrounding the core tubes, where quartz grains were extracted for OSL dating. Though the HRGS provides more reliable data and robust information to check the radionuclide disequilibrium in the samples, due to the limitation of core material and restriction of machine, only three samples were analysed by the HRGS. These three samples were taken from the adjacent layers (from the surface 0-5 cm, 56-61 cm, 87-89 cm) of the bulk material, to represent the surface layer, the median layer (which had obvious changes in colour, texture and other physical, chemical, biological factors) and the bottom layer. As shown in Table A.1.3, the results of K by HRGS, XRF and TSAC&BC show a good correspondence. The average ratios of $C_{TSAC\&BC}$:C_{HRGS} and C_{XRF}:C_{HRGS} for K concentrations are 1.07 and 1.05. The results of U are only comparable between the HRGS and TSAC&BC (with a $C_{TSAC\&BC}$:C_{HRGS} ratio of 0.97) , while the XRF gives relatively lower values (with a C_{XRF}:C_{HRGS} ratio of 0.72). The results of Th between the HRGS and XRF are similar (with a C_{XRF}:C_{HRGS} ratio of 0.96), while the ones by the TSAC&BC are relatively lower (with a $C_{TSAC\&BC}$:C_{HRGS} ratio of 0.67).

For samples from core LSW, bulk materials from several depths, which were selected for dating, were used for XRF, alpha counting and beta counting. Only two samples (24-26 cm, 65-67 cm) were selected for the HRGS analysis. Results show that the concentrations of K and U calculated by the alpha and beta counting are similar to those

determined by HRGS. The average $C_{TSAC\&BC}$:C_{HRGS} ratios of for K and U are 0.98 and 0.97; the concentrations of Th are more comparable between the XRF and HRGS, with an average C_{XRF}:C_{HRGS} ratio of 0.97 (compared to $C_{TSAC\&BC}$:C_{HRGS} ratio of 0.88).

For samples from core LOLA, bulk materials from the sections selected for dating, were analysed by HRGS, XRF, alpha counting and beta counting. One eception in the HRGS analysis is LOLA-DR_05 (63-69 cm). The concentrations of K are more comparable between the HRGS and TSAC&BC, with an average $C_{TSAC\&BC}$:C_{HRGS} ratios of 0.92. The concentrations of U and Th determined by the XRF are more comparable to the HRGS results, with average C_{XRF}:C_{HRGS} ratios of 0.92 and 0.94 individually.

Comparing the three methods, only K gave relatively similar concentrations while U and Th tended to vary among the several methods. The concentrations of U and Th presented in Table A.1.3 were determined by the TSAC – which explained why they (in particular Th) were lower than other methods. Ideally, HRGS is the best method to choose to determine radionuclide concentrations because it takes into consideration both the parent and daughter elements. Hence, in this study, we adopted the HRGS results where available and used the TSAC & BC results for other samples.

Table A.1.3
U, Th and ^{40}K concentrations determined by various methods.

Sample ID	Depth (cm)	Method	U (ppm)	Th (ppm)	K (%)
MMB3_DR-01	0-5	HRGS	3.06±0.22	10.51±0.15	1.26±0.03
MMB3-01	5-8	XRF	1.85±0.02	10.40±0.10	1.34±0.00
MMB3-01	5-8	TSAC&BC	2.34±0.11	6.33±0.39	1.45±0.09
MMB3-02	27-29	XRF	2.35±0.02	11.60±0.12	1.45±0.00
MMB3-02	27-29	TSAC&BC	1.39±0.10	7.69±0.33	1.82±0.09
MMB3-03	48-51	XRF	2.00±0.02	10.85±0.11	1.44±0.00
MMB3-03	48-51	TSAC&BC	2.66±0.12	6.62±0.42	1.66±0.10
MMB3-04	55-57	XRF	1.70±0.02	10.30±0.10	1.41±0.01
MMB3-04	55-57	TSAC&BC	2.27±0.12	8.33±0.43	1.39±0.09
MMB3_DR-02	56-61	HRGS	2.22±0.20	11.03±0.22	1.30±0.03
MMB3-05	85-88	XRF	1.65±0.02	10.05±0.10	1.31±0.01
MMB3-05	85-88	TSAC&BC	2.27±0.11	6.82±0.40	1.30±0.08
MMB3_DR-03	87-89	HRGS	2.08±0.23	10.57±0.21	1.31±0.03
LSW01_Dose	14-16	HRGS	-	-	-
LSW01_Dose	14-16	XRF	2.50±0.03	11.40±0.11	1.58±0.02
LSW01_Dose	14-16	TSAC&BC	2.31±0.32	9.38±1.56	1.16±0.10
LSW02_Dose	24-26	HRGS	2.66±0.18	10.84±0.22	1.26±0.03
LSW02_Dose	24-26	XRF	2.30±0.02	10.80±0.11	1.58±0.02
LSW02_Dose	24-26	TSAC&BC	2.46±0.33	8.68±1.46	1.34±0.10
LSW03_Dose	47-49	HRGS	-	-	-
LSW03_Dose	47-49	XRF	1.50±0.02	9.40±0.09	1.34±0.01
LSW03_Dose	47-49	TSAC&BC	1.83±0.23	9.75±1.52	1.11±0.09
LSW04_Dose	65-67	HRGS	1.56±0.18	8.21±0.20	1.01±0.03
LSW04_Dose	65-67	XRF	1.40±0.01	7.80±0.08	1.21±0.01
LSW04_Dose	65-67	TSAC&BC	1.58±0.17	7.81±1.23	0.91±0.07
LSW05_Dose	80-82	HRGS	-	-	-
LSW05_Dose	80-82	XRF	1.50±0.02	8.90±0.09	1.35±0.01
LSW05_Dose	80-82	TSAC&BC	3.23±0.44	7.06±1.25	0.97±0.10
LOLA-DR_01	201-207	HRGS	1.79±0.19	11.58±0.23	1.69±0.04
LOLA-DR_01	201-207	XRF	1.80±0.02	11.40±0.11	2.06±0.02
LOLA-DR_01	201-207	TSAC&BC	2.93±0.40	7.70±1.35	1.67±0.12
LOLA-DR_02	181-188	HRGS	1.878±0.19	12.79±0.26	1.69±0.04
LOLA-DR_02	181-188	XRF	1.70±0.02	11.90±0.12	2.11±0.02
LOLA-DR_02	181-188	TSAC&BC	3.23±0.51	8.85±1.63	1.57±0.13
LOLA-DR_03	145-151	HRGS	1.73±0.17	10.82±0.23	1.47±0.04
LOLA-DR_03	145-151	XRF	1.70±0.02	9.90±0.10	1.74±0.02
LOLA-DR_03	145-151	TSAC&BC	2.26±0.30	10.05±1.59	1.23±0.10
LOLA-DR_04	105-111	HRGS	1.92±0.15	10.32±0.21	1.35±0.03
LOLA-DR_04	105-111	XRF	1.50±0.02	9.80±0.10	1.67±0.02
LOLA-DR_04	105-111	TSAC&BC	2.82±0.37	8.76±1.38	1.27±0.10
LOLA-DR_05	63-69	HRGS	-	-	-
LOLA-DR_05	63-69	XRF	1.50±0.02	7.20±0.07	1.27±0.01
LOLA-DR_05	63-69	TSAC&BC	2.23±0.27	7.80±1.30	0.99±0.08

* TSAC&BC – U and Th concentrations were calculated by the TSAC, K concentration was calculated by the TSAC & BC

A1.1.5 Calculation of cosmic-ray dose rates

Cosmic rays are composed of a 'soft' component and a 'hard' component. The soft component affects only the uppermost 50 cm of sediment; while the hard component can penetrate much deeper. The intensity of cosmic rays decreases with increasing depth of penetration (Prescott and Hutton, 1994).

In this study, calculations were made following the standard procedure as described in Prescott and Hutton (1994). Parameters used in this procedure are the location of the sample in terms of its latitude, longitude and altitude (in metres), as well as the overburden thickness and density during the burial history of the sample. Considering the density of most mineral soils is 2.65 g cm^{-3} and that of organic matter is about 1.30 g cm^{-3} (Mclaren and Cameron, 1996), an assumed bulk density of 1.80 g cm^{-3} was used in the cosmic dose rate calculation for MM samples. It was assumed that the overburden thickness of the samples in this study had not changed significantly during the post-depositional burial period. Because for all the samples studied, the cosmic ray dose rate only made up a very small fraction of the total dose rate (<10 %), minor adjustments to the present-day overburden thickness would affect the OSL ages insignificantly. Figure A.1.1 shows the trend of decreasing cosmic dose rate with increasing depth applied to all the samples studied here, and the dose rate tends to decrease more sharply in the near-surface sediment samples (upper 50 cm) than those from deeper.

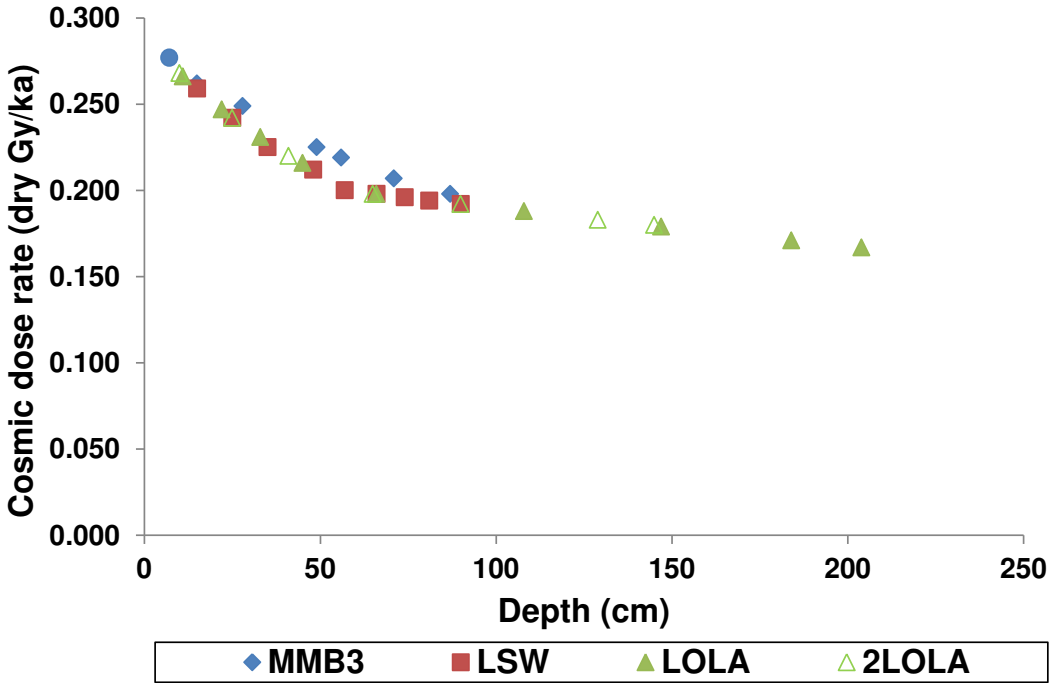

Figure A.1.1. Change of cosmic-ray dose rate according to depth.

A1.1.6 Assessment of water content and organic content

Due to absorption, water and organic matter attenuate ionising radiation arising from beta particles and gamma rays that would otherwise reach the quartz grains. For example, the absorption coefficient per unit mass of water is higher by 50 % for alpha particles, by 25 % for beta particles, and by 14 % for gamma radiation (Aitken, 1985). It is important to measure the water and organic content before conducting the total dose rate and age calculation.

Previous studies have shown that it is difficult to evaluate the representative water content of fluvial sediments, because the water table would have changed enormously during the burial time (Aitken, 1985; Olley et al., 1999; Folz et al., 2001). Most of the studies use laboratory (or "present day") water content; while others try to work out a representative value based on laboratory water content and measured saturated water

content (Olley et al., 1999; Rodnight et al., 2006). Aitken (1985) noted the use of an 80 % saturated water content is acceptable except in obviously dry environments. In cases like the Macquarie Marshes, to estimate the real water content of the samples becomes even harder, due to the alternating dry-wet periods. As is shown in Table 4.10 (Page 165), the laboratory measured water content values of MMB3 samples decrease with increasing depth of the core, with an extreme high value (155.85 %) on the top 4-6 cm layer. Typical saturated water content ranges from 20 % to 60 %, however it has been proved that in organic soils or volcanic soils, much higher water content values, over 100 %, are possible (Mclaren and Cameron, 1996). Considering the sampling site is a swamp, it is possible the surface sediments were saturated or over-saturated with water, which led to over 100 % water content. Laboratory experiments on measuring the saturated water contents of core LOLA materials, by measuring the weight change of drying and rewetting the sample, gave values mostly less than 50 % (range from 27.79 % to 50.55 %). Therefore, a value of 80±10 % was used for this particular top layer sample.

The organic matter is usually determined by measuring the LOI (Loss On Ignition) which is done by weighing the sample before and after it has been oxidised at 500 ºC to 550 ºC to produce carbon dioxide and ash, with carbonates being further oxidised at 900 ºC to 1000 ºC. In this study, directly determined TOC (Total Organic Carbon) acquired during $\delta^{13}C$ analysis was used to estimate the organic content.

An associated error of 10 % was used for the water and organic content values in calculating the errors of the dose rate.

A1.1.7 Calculation of total environmental dose rates

The total environmental dose rate (D_r) is calculated from the sum of the beta and gamma dose rates (corrected for attenuation of beta particles, water and organic content, and beta attenuation) and the cosmic ray dose rate (D_c, corrected for water content), as described in the following equation (Madsen et al., 2005; Demuro, 2009):

$$D_r = \frac{\left[\left(K_{\%} \cdot \beta_K \cdot K_{att}\right) + \left(Th_{ppm} \cdot \beta_{Th} \cdot Th_{att}\right) + \left(U_{ppm} \cdot \beta_U \cdot U_{att}\right)\right]}{1 + \left(1.25WF + 1.2OC\right)} + \frac{\left[\left(K_{\%} \cdot \gamma_K\right) + \left(Th_{ppm} \cdot \gamma_{Th}\right) + \left(U_{ppm} \cdot \gamma_U\right)\right]}{1 + \left(1.14WF + 1.1OC\right)} + \frac{D_c}{1 + 1.76WF}$$

Where $K_{\%}$, Th_{ppm} and U_{ppm} refer to the concentration of each element in ppm for Th and U and % for ^{40}K; β_K, β_U and β_{Th} are the beta dose rate conversion factors (Table A.1.2); γ_K, γ_U and γ_{Th} are the gamma dose rate conversion factors (Table 4.8); K_{att}, Th_{att} and U_{att} are the beta-dose attenuation factors from Mejdahl (1979); WF is the water content and OC is the organic content. For correcting beta and gamma dose attenuation, the value of 1.25 and 1.14 are used for correcting water content (Aitken, 1985) and the values of 1.2 and 1.1 are used for correcting the organic content (Lian et al., 1995).

Alpha radiation can be neglected due to the short penetration of alpha particles, and the very low internal radioactivity of quartz (Madsen et al., 2005). The outer layers of quartz grains, which could have been irradiated by externally derived alpha particles, are removed during the acid treatment in sample preparation (Aitken, 1985). For beta dose calculation, the concentrations of radionuclides are subsamples of the dating sections. For gamma dose calculation, the concentrations of radionuclides are subsamples collected from a distance of 30 cm from the dating sections (assuming the 30 cm sphere of the radius was homogeneous). We also correct for the deduction of gamma dose according to

the depth of the core sections, in particularly for those collected from depths less than 30 cm (Aitken, 1985).

The errors of final dose rate are calculated following the method reported in Demuro (2009). Results of dose rate and other parameters (water content and total organic carbon) are presented in

Table **4.3** in Chapter 4.

A1.2 Selection criteria for environmental dose determination

This section describes the seven selection criteria applied to both single aliquot and single grain dose determination.

A1.2.1 Signal intensity check

The signal intensity check is carried out to ensure that there is no interference of background noise to the target OSL signal. Aliquots/grains can pass this check if the test dose OSL signal is three times higher than the background signal. As reported by Jacobs et al. (2003), the failure proportion of samples can be as high as ~70 %. In this study, almost all the single-aliquot samples from core MMB3 were acceptable, except for one aliquot from MMB3-4 sample. The failure proportions among single grains vary from site to site and at different depth, but were all lower than the reported extreme high value (70 %). Generally, core LSW appeared to have higher proportions among all the sections compared with those from the other three cores. Even with two sampling sites which were close by, the signal intensity of the samples did not appear to be similar. These may indicate that the sources of grains were not the same or even if the grains originated from the same source, their exposure to sunlight differed to various extents.

A1.2.2 Recycling ratio check

Aliquots/grains were rejected if the recycling ratio exceeded 1.1 or was lower than 0.9. Our single-grain results showed a failure from 10-20 %, indicating there were certain grains where the sensitivity change could not simply be corrected by their test dose alone. Those grains could be excluded by this recycling ratio check. Comparatively, core MMB3 samples appeared to have greater failure proportions with one of the highest of 47 % (Table A.1.2).

A1.2.3 IR depletion ratio check

It has been shown that D_e analysis with the presence of feldspar will give rise to over-dispersion values (OD) (Jacobs et al., 2006a), therefore it is very important to reject the contamination by feldspars from the data set. This procedure checks if the IR OSL depletion ratios were between 0.9 and 1.1 as discussed in Chapter 4, Section 4.6.1.3.1. Aliquots/grains that failed in this examination were more likely to have feldspar contamination. Our results showed that all the aliquots passed this check while only a small proportion (less than 10 %) of single grains failed. This proved that the sample preparations had been quite successful in extracting pure quartz.

A1.2.4 Saturation and Monte Carlo fit check

In Chapter 4, Figure 4.6 and Figure 4.15 show the typical dose response curves. Figure A.1.2 and Figure A.1.3 show a typical case where the L_n/T_n ratio is well above the maximum L_x/T_x value. These results indicate an inability to obtain a D_e value because there was no intersection with the dose response curve. These D_e were considered to be over-saturated and were rejected.

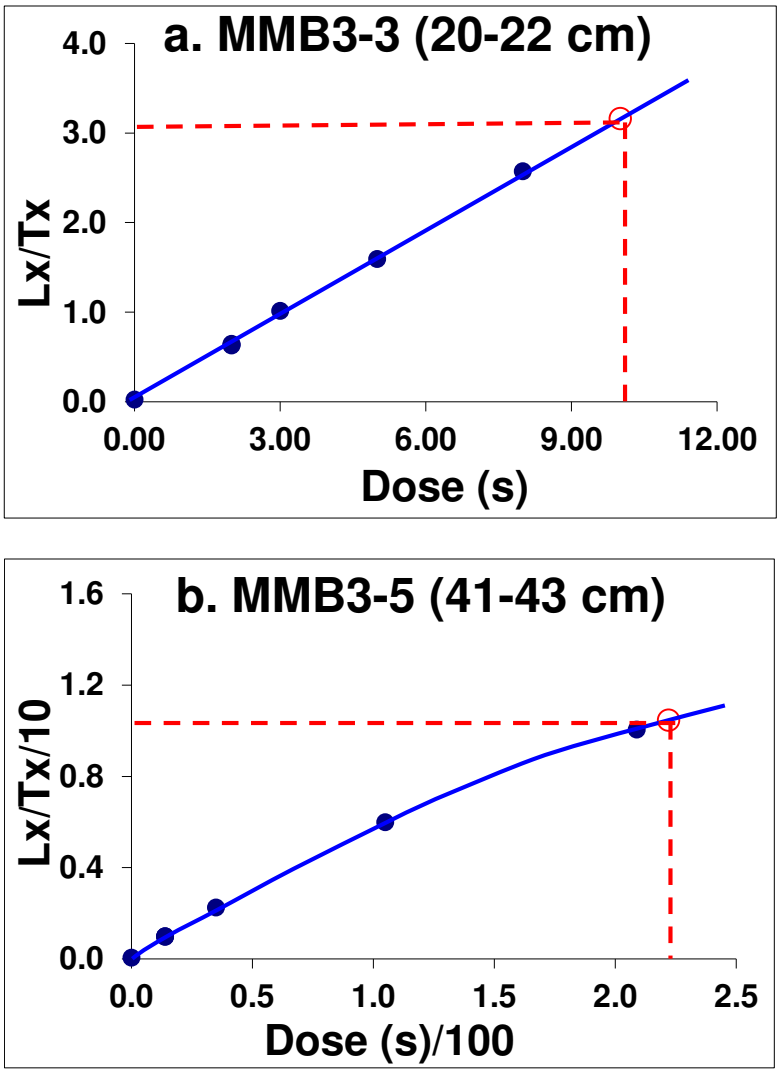

Figure A.1.2. Regeneration curve of the rejected single-aliquot data. (a. MMB3-3 linear fit; b. MMB3-5 exponential+linear fit)

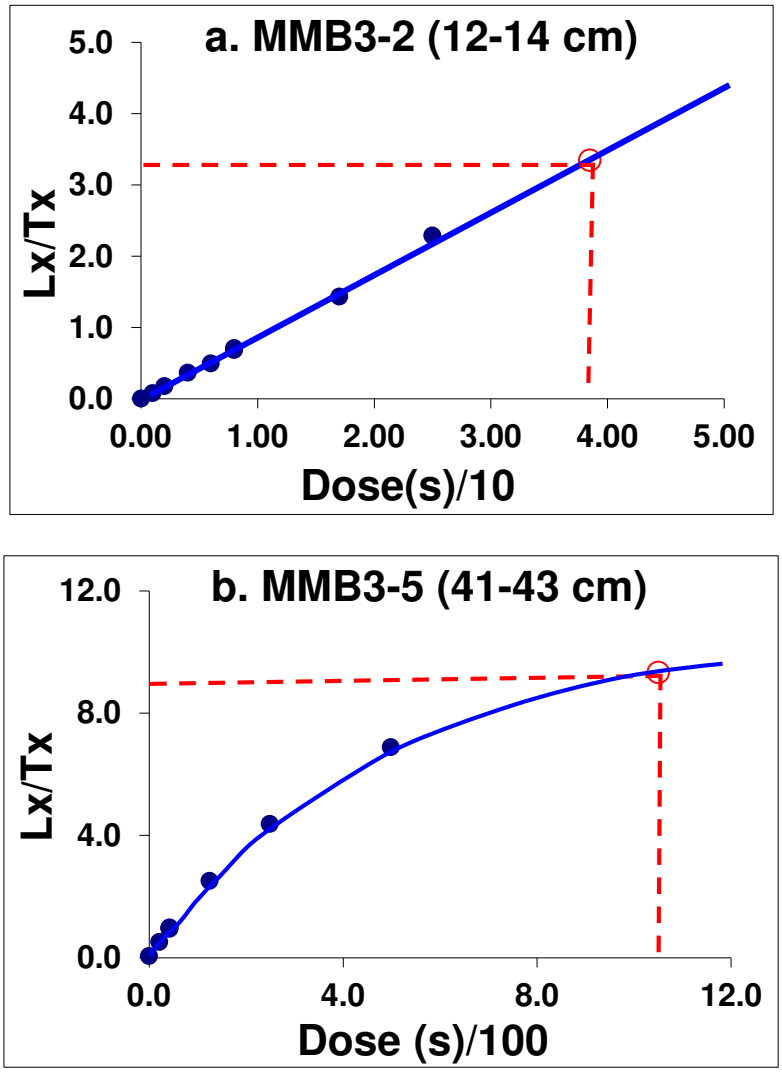

Figure A.1.3. Regeneration curve of single-grain data. (a. MMB3-2 linear fit; b. MMB3-5 exponential+linear fit)

A1.2.5 Tx/Tn curve check

Ideally, where no sensitivity changes occur, the T_x/T_n curve will appear to be linear. However, the thermal treatment and irradiation during the repeated regeneration procedures will inevitably cause the oscillation of the T_x/T_n curve. In order to derive the quartz that performs similar OSL behaviour, those with a flat T_x/T_n curve or at least similar to the curve from the dose recovery tests were accepted (Figure A.1.4 and Figure A.1.5). Very rarely, aliquots/grains failed this test. T_x/T_n curves of the aliquots/grains with

lower natural D_e tended to be more flat than those with higher natural D_e. This is similar to what was found in the dose recovery test. For the samples with relatively higher natural dose, the regeneration dose points were relatively higher. It is very likely that the beta irradiation might have caused the rise of the T_x/T_n curve.

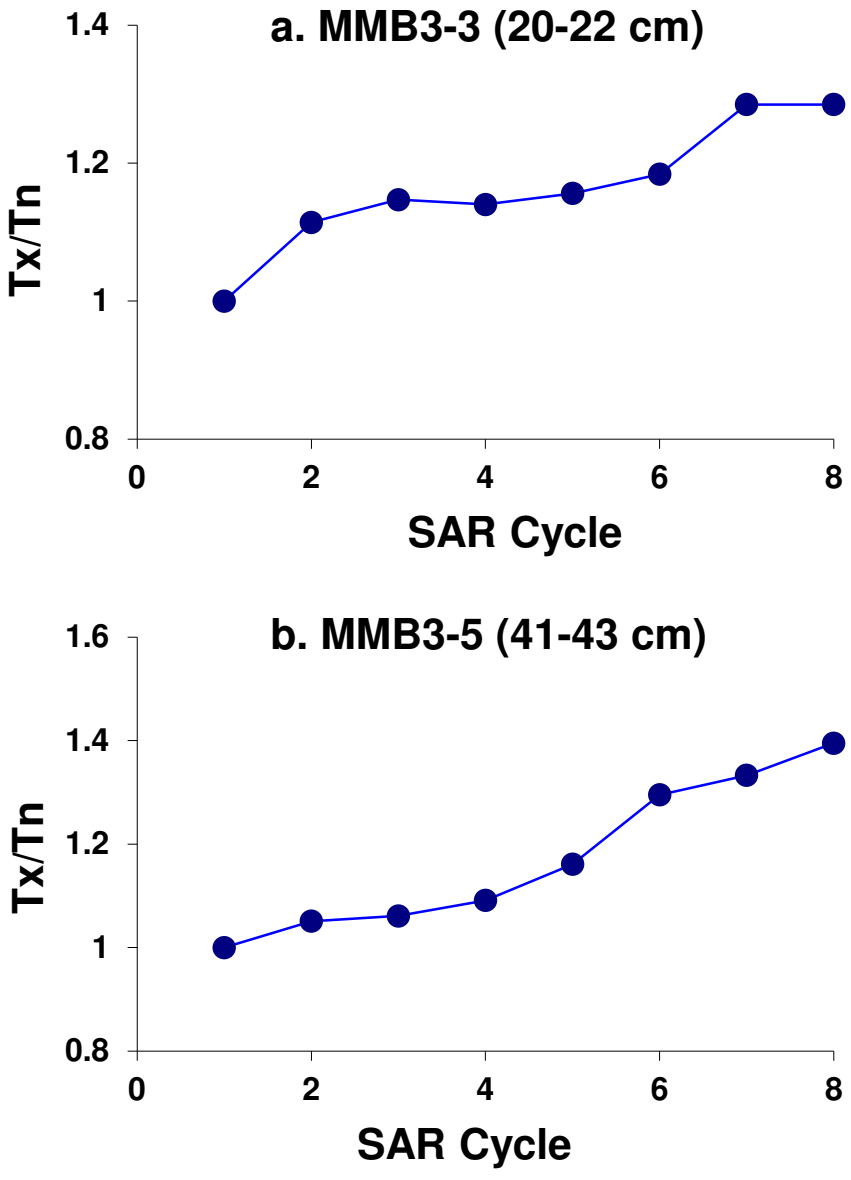

Figure A.1.4. T_x/T_n Curve of single-aliquot data. (a. sample MMB3-3 b. sample MMB3-5)

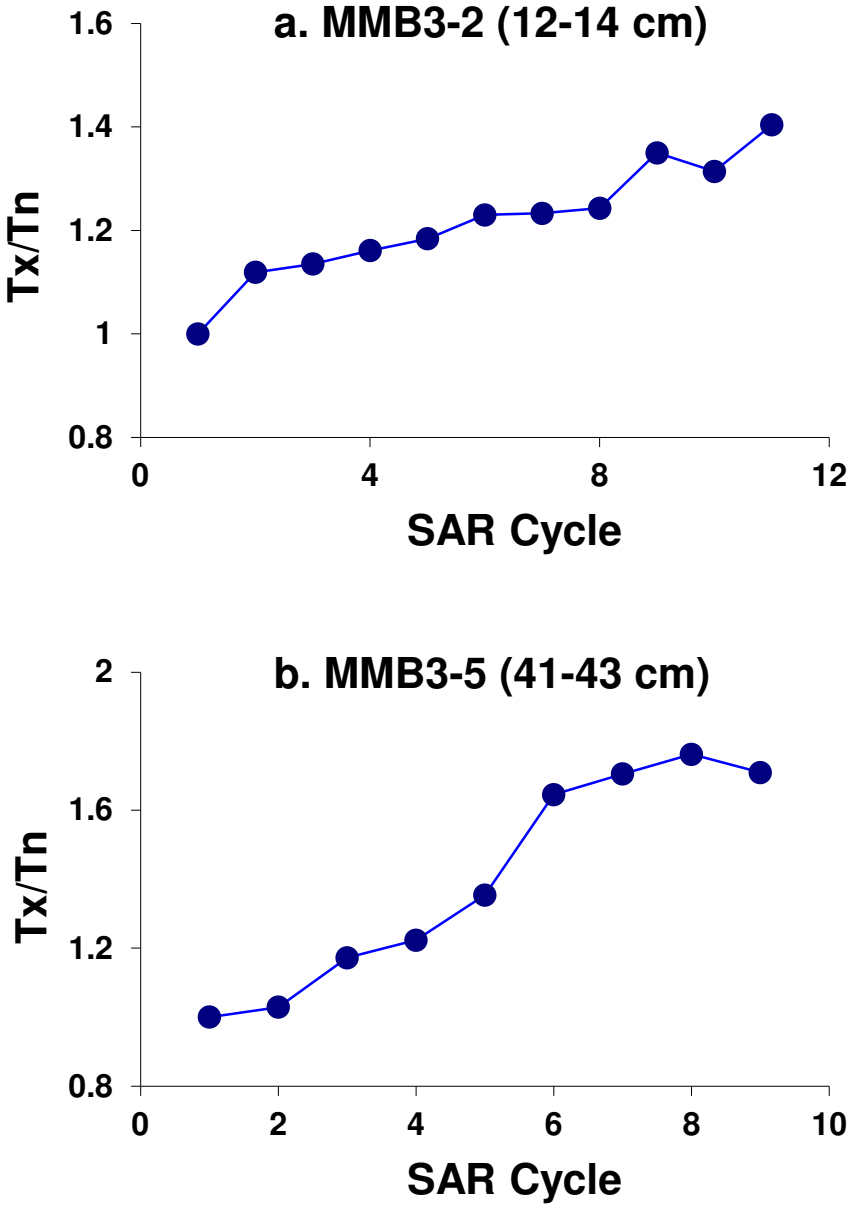

Figure A.1.5. T_x/T_n Curve of single-grain data. (a. sample MMB3-2 b. sample MMB3-5)

A1.2.6 Decay curve check

The decay curve provides insights into the optical behaviour of the quartz. A general observation made by Duller (2003) is that during measurement, the OSL signal from quartz tends to decrease rapidly and to a low residual level, while for feldspars the initial decrease in signal is slower and a significant 'tail' is observed even after prolonged optical stimulation.

In this step, the decay curves of the natural dose and regeneration dose, as well as the test dose were inspected. The decay curves of the natural dose were shown in Chapter 4, Figures 4.6 and 4.15. Variations of decay curves were observed in single grains among grains from different samples and even grains within the same sample. Grains were accepted when they showed a distinctive sharp peak within the 0.5 s of the decay curves and the signals in zero dose point were negligible (close to background signal). The samples with greater natural dose were more likely to have distinctive decay curves. Apart from those that did not have distinctive peaks, grains were strictly rejected when they showed more than one hump within 0.5 s of the decay curves, or their peaks tended to have noisy and long-lasting tails within 0.5 s of the decay curves. For samples with relatively lower natural dose, the criteria were basically the same except slightly less restricted for the natural dose decay curves as their signals were relatively lower, even though the failure proportions were relatively high.

A1.2.7 Recuperation check

As discussed in Chapter 4, a maximum of 5 % recuperation (Murray and Wintle, 2000) is set as one of the selection criteria to exclude the grains that might have undergone thermal transfer during the laboratory heating in the SAR protocol (Aitken and Smith, 1988). Such transfer can cause problems if it results in an OSL signal which is a significant fraction of

the natural signal, especially when dating young sediments (Madsen and Murray, 2009). Therefore it was necessary to check the recuperation for samples from the Macquarie Marshes.

In the dose recovery test, the proportion of grains that failed the recuperation selection criteria was relatively small (~6-8 %). A low proportion of failure was also found among most of the samples. Although most of the samples passed this check with recuperation values lower than 5 %, the absolute values were considerably higher (mostly with one decimal, some were close to 0.5 %). The recuperation values were calculated by dividing the sensitivity corrected dose at zero-dose point (L_x/T_x) by the sensitivity corrected natural dose (L_n/T_n). L_x/T_x values (close to 0) did not vary too much in most cases, so the recuperation values were more dependent on the L_n/T_n value. Where young surface sediment samples with natural values close to zero occurred, the lower L_n/T_n value was more likely to yield the greater recuperation value. Ballarini et al. (2007) also found higher recuperation values among their young samples with very low natural OSL response and they did not apply the rejection criterion of 5 % used in their study.

Madsen and Murray (2009) pointed out a rise in the D_e at higher temperature may be an indication of significant recuperation caused by the thermal transfer. In this study, the D_e seemed to be independent of the preheat temperatures used in the dose recovery test, and the failure proportion of recuperation checks were low in both the dose recovery tests. In this study, recuperations varied from sample to sample. Only samples from the deeper layers (more than 50 cm in depth) of the cores displayed recuperations values lower than 5 %. Young samples tend to have higher recuperation values as their T_n/L_n values were usually low. Of the core sections studied here, in particular for the young surface/near-surface sediment samples, we did not apply the strict criterion of 5 % and accepted

consistent recuperation values of grains from the same samples as long as they passed the other selection criteria.

A1.2.8 Summary of the selection criteria

From the above discussion, most of the single aliquots (more than 80 %) survived the seven selection criteria checks. Due to the inhomogeneity of the individual grains, a high proportion of failure was observed in signal intensity checks, recycling ratio checks and the decay curve checks among the single grain data (Table A.1.2).

Table A.1.2
Single-grain data selection results.

Sample ID	Grains analysed	Grains accepted	Passed Failed	Criterion 1 (%)	Criterion 2 (%)	Criterion 3 (%)	Criteria 4-7 (%)
MMB3-1	800	57	Failed	51	26	7	14
			Passed	49	23	16	**2**
MMB3-2	1000	37	Failed	44	29	6	18
			Passed	56	27	21	**3**
MMB3-3	800	45	Failed	22	36	9	27
			Passed	78	42	33	**6**
MMB3-4	600	37	Failed	12	47	7	30
			Passed	88	41	34	**5**
MMB3-5	1000	105	Failed	24	31	12	28
			Passed	76	46	33	**5**
MMB3-6	1000	100	Failed	41	29	4	18
			Passed	59	30	26	**8**
MMB3-7	1000	92	Failed	38	24	4	26
			Passed	62	38	34	**8**
LSW-1	24	800	Failed	69	23	2	4
			Passed	31	8	7	3
LSW-2	112	1000	Failed	52	24	5	9
			Passed	48	25	20	11
LSW-3	79	1000	Failed	59	19	4	10
			Passed	41	22	18	8
LSW-4	41	900	Failed	65	16	2	12
			Passed	35	19	17	5
LSW-5	72	1000	Failed	52	23	5	13
			Passed	48	25	20	7
LSW-6	93	1000	Failed	50	20	4	16
			Passed	50	30	26	9
LSW-7	99	1000	Failed	55	18	3	14
			Passed	45	27	24	10
LSW-8	68	500	Failed	45	14	3	24
			Passed	55	41	38	14
LSW-9	118	1000	Failed	45	17	5	22
			Passed	55	38	33	12
LOLA-1	182	1000	Failed	35	12	2	33
			Passed	65	53	51	**18**
LOLA-2	230	1000	Failed	21	19	5	32
			Passed	79	60	55	**23**
LOLA-3	164	1000	Failed	28	20	7	29
			Passed	72	52	46	**16**
LOLA-4	98	900	Failed	34	28	7	21
			Passed	66	38	31	**11**
LOLA-5	159	1000	Failed	52	11	2	20
			Passed	48	38	36	**16**
LOLA-6	111	1000	Failed	54	14	3	18
			Passed	46	32	29	**11**
LOLA-7	96	900	Failed	53	19	2	15
			Passed	47	28	26	11
LOLA-8	119	1000	Failed	45	19	5	19
			Passed	55	36	31	**12**
LOLA-9	120	1000	Failed	37	22	7	23
			Passed	63	42	35	**12**
2LOLA-1	107	1000	Failed	46	25	6	13
			Passed	54	29	23	**11**
2LOLA-2	144	1000	Failed	39	20	6	21
			Passed	61	40	35	**14**
2LOLA-3	175	1000	Failed	22	28	7	25
			Passed	78	50	43	**18**
2LOLA-4	145	1000	Failed	47	19	5	15
			Passed	53	35	29	**15**
2LOLA-5	137	1000	Failed	61	10	3	13
			Passed	39	30	27	**14**
2LOLA-6	150	1000	Failed	51	13	3	18
			Passed	49	35	33	**15**
2LOLA-7	159	1000	Failed	51	11	2	20
			Passed	49	38	36	**16**

Criterion 1-Signal intensity check (reject T_n<3XBG)
Criterion 2-Sensitivity correction-recycling ratios
Criterion 3-IR depletion ratio check
Criterion 4-Saturation and Monte Carlo fit check
Criterion 5- T_x/T_n curve
Criterion 6-Decade curve
Criterion 7-Recuperation (<5 %)

APPENDIX B. PUBLISHED PAPER

Yu, L., García, A., Chivas, A. R., Tibby, J., Kobayashi, T. and Haynes, D. 2015. Ecological change in fragile floodplain wetland ecosystems, natural vs human influence: The Macquarie Marshes of eastern Australia. *Aquatic Botany*, 120, 39-50.

Article in Appendix B removed for copyright reasons